MECHANISTIC CONSIDERATIONS IN RETROGRADE REACTION

Donald F. McMillen, and Ripudaman Malhotra
Chemistry and Chemical Engineering Laboratories, SRI International
333 Ravenswood Ave., Menlo Park, California, 94025

Key Words: Retrograde reaction, Coal liquefaction, Hydrogen transfer.

INTRODUCTION

The importance of retrogressive reactions has become obvious through the study of liquefaction kinetics and products, but the fundamental chemical reactions and their kinetics have remained more obscure. For instance, researchers such as Neavel recognized some time ago that soluble products could be generated *and consumed* very rapidly under coal liquefaction conditions.[1] Similar observations have been made for pyridine solubles under pyrolysis conditions, where there is no added solvent [2]. In a sense the whole technology of heavy oil conversion is bound up with retrograde reactions, in that thermal treatment of petroleum asphaltenes under a variety of conditions can produce similar amounts of distillate, but the amount of retrograde product (coke) generated in conjunction with these volatiles is critically dependent on conditions of catalyst, medium, and hydrogen pressure.[3,4] Thus the impact of retrograde processes has been quite obvious, but the detailed nature of the responsible bond forming reactions has remained unclear.

Similarly, hydrogen transfer has been acknowledged for many years to play a key role in coal liquefaction, though not until more recently was it recognized as a prerequisite to the cleavage of strong bonds in both liquefaction and pryolysis.[5,6] The extension of the induced strong-bond scission picture and the consideration of its microscopic reverse provides new insights for bond-forming processes. Thus, the reverse of H-atom displacement of C-C or O-C linkages to aromatic clusters is the addition of a C-centered or O-centered radical *to* an aromatic ring system, to displace an H-atom. When the adding radical is resonance stabilized, the addition is highly reversible. Just as the key step in the de-substitution (cleavage) reaction is H-atom transfer to the coal linkage, the key step in the microscopic reverse (the substitution reaction) is H-atom transfer *from* the substitution adduct.

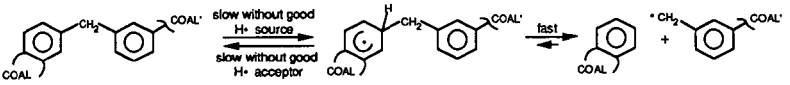

In this paper we extend some earlier qualitative discussion[7] of these aspects of bond formation with the quantitative results of a numerical model. This model was originally assembled to fit and help interpret experimental data for bond cleavage in model systems;[8] however, since it includes the reverse of essentially all of the fundamental reaction steps incorporated, it is equally suitable for exploring bond formation, or retrograde reaction. We use it here to illustrate limits on the ability to scavenge radicals, the relative importance of recombination and addition, and the key role of H-atom removal from retrograde intermediates.

MODELING CONSIDERATIONS AND PROCEDURES

Chemical Constituents. We chose the addition of stabilized radicals, as indicated in Scheme 1 above, as the major retrograde reaction type on which to focus, not because we believe it to necessarily be always the most important class of retrograde reaction, but as a highly reversible reaction, its outcome is quite sensitive to changing hydrogen-transfer conditions. However, since for completeness the model necessarily incorporates the possibility of recombination of resonance stabilized radicals, that route to retrograde products is also examined. Retrograde reaction by recombination of course also depends on H-transfer to "lock in" a stable product, since otherwise the weak bond formed by recombination will not represent a permanent retrograde linkage.

The mechanistic numerical model we have used incorporates a single surrogate "coal" structure [1,2-(1,1'-dinaphthy)lethane] in a reaction medium consisting of aromatic/hydroaromatic mixture (phenanthrene/dihydrophenanthrene) of various compositions, with and without H_2 overpressure. This four starting-component reaction system provides for both weak-bond- and strong-bond scission, H-transfer by H-atom abstraction, free H-atom addition, reverse radical-disproportionation, and RHT, retrograde reaction by radical addition, radical recombination, and radical displacement. When limited to only the more important reactions, including virtually all of the reverse reactions, this provides a set of more than 40 species and 150 reactions. Thus the model is very detailed in that it that incorporates all relevant fundamental chemical reactions (non-ionic) of essentially all species, both closed shell and free radical, in the reaction system. Because of this mechanistic detail, the model, of necessity, is very simple in that it includes only a very limited set of starting structures. To limit the complexity, we have confined the model to a pure hydrocarbon system, though the same general considerations will also apply to systems containing phenolics, where the presence of the -OH groups will in all likelihood further promote radical addition (as well as promoting attack of electrophilic fragments and the subsequent loss of hydrogen as a proton).

Mechanistic Considerations. The model is homogeneous; it consists of relatively low-molecular-weight species assumed to be miscible in all proportions. We have made the simplifying assumptions that the system is free of concentration gradients and requires no mass- or heat-transport.* The activity of H_2 in solution is taken to equal that provided by presumed equilibrium with the gas-phase H_2 pressure.

We emphasize that this model was *not* intended in any way to actually simulate the conversion of a real coal, or even, in the present case, to match exactly the experimental retrograde behavior of model systems, but to provide a general illustration of how chemical factors influence certain classes of retrograde reactions under different circumstances. However, because the strength of the weak central bond in 1,2-dinaphthylethane (55 kcal/mol) leads to a 400°C-half-life of about 12 minutes at 400°C, it was previously chosen by other researchers[9] as a prototypical linkage type that would give coal linkages lifetimes similar to those observed for actual coals during liquefaction, *assuming* the dominant bond cleavage reaction is weak-bond scission. We subsequently subjected a polymeric version of 1,2-dinaphthylethane to donor solvent liquefaction conditions, and observed a product mixture that strikingly revealed some of the shortcomings of the then-accepted weak-bond scission picture of coal liquefaction.[10] As it happens, the numerical modeling results presented here reproduce some of the experimental observations on bond scission, notwithstanding the fact that nothing has been done to force such a correspondence, except to use the best available experimental or estimated rate parameters for each of the individual reactions included in the numerical model. We therefore expect the model to provide valid illustrations, in general terms, of the relative importance of retrograde reaction types under various circumstances.**

As reflected by the total number of reactions, the scheme that follows from even the limited set of starting structures used here appears rather complex, but is based on relatively few reaction types. These reaction types and the products in which they result are shown below in Scheme 2. In the figures that follow, we generally have grouped together all of a common product that follows from several different examples of a given reaction type, and have identified them by a generic heading, rather than individual acronyms used in the integration program.

Scheme 1. Categories of Bond Cleavage and Bond Formation

"Strong-bond cleavage-1"

This category includes all H-atom displacements, or hydrogenolyses, from 1,2-dinaphthylethane (producing naphthalene and ethylnaphthalene), from all sources of H-atoms: free H•, RRD, and RHT, coming from either solvent or substrate species.

"Strong bond cleavage-2"

This category also generates ethylnaphthalene, but results instead from displacement (i.e., addition-elimination) by radical species other than H-atom. "Strong-bond cleavage-2 " is not a *net* cleavage, in that whenever the displacing radical is a naphthylmethyl radical, one aryl-aryl coupling is simply being traded for another.

"True retrograde product"

In the present work, dinaphthylmethane is the dominant coupling product that, as indicated above, is companion to the cleavage product generated in strong-bond cleavage-2. This coupling product is formed from attack of a naphthylmethl radical on the starting substrate 1,2-dinaphthylethane, or on the other products naphthylmethane or naphthyl ethane. It is also formed in a "net" retrograde reaction by addition of naphthylmethyl radical to naphthalene, followed by successful removal of the ipso hydrogen from the initial adduct. The term "true retrograde product" is used here because the bond is about 87 kcal/mol, with a homolytic half-life of more than 10 years even at 500°C.

"Weak bond cleavage"

The "weak-bond cleavage" product is of course the naphthylmethane that results from scavenging of the naphthylmethyl radicals that are generated by homolysis of the weak (ca. 55 kcal/mol) central bond in dinaphthylethane.

---

* Limits on miscibility are of course very important in retrograde reactions, as evidenced by the importance of micelle formation during coke formation in heavy-oil upgrading. However, covalent bond formation is both a *cause* of, and a *result* of, phase separation. Therefore it is probably not possible to find a simple partisan answer to the question of which of these most controls coke formation and other retrograde processes.

** Since this model was originally used with a more limited set of reactions to address the competition in cleavage processes between H-transfer by free H-atoms, the reverse of radical-disproportionation (RRD), and radical hydrogen-transfer (RHT), and since the outcome of such attempts at deconvolution of parallel, competing H-transfer processes is still a matter of dispute, it is reasonable to ask whether that dispute should cast doubt on the illustrations and conclusions provided below. The answer to this question is no. Just as the functional form of overall cleavage dependence does not allow one to easily assign exact proportions of the transferred H to free H•, RRD, and RHT, when they are in competition, so also any error that may exist in the assigned parameters for RHT will not result in any gross miss-statement of bond formation outcomes that we are addressing here.

"Recombination product"

The "recombination product" is simply the dinaphthylmethane that results from recombination of the initial weak-bond scission product, naphthylmethyl radical. In reality it is indistinguishable from the starting material itself, but in the numerical integration simulations is distinguished by nomenclature from the original molecules of the starting material. The recombination product undergoes all of the reactions that the original starting material does. Since this recombination product is itself just as fragile as the starting material, in the area graphs that follow, the amount of the recombination product that survives is so small that it cannot be seen on the scale of the figures.

"Stilbene product"

The fragility of the recombination product of course does not apply to the "stilbene product," which is the naphthalene analog of stilbene resulting from loss by various processes of 2(H) from either the original dinaphthylethane substrate or the recombination product that comes from the reversal of the weak-bond cleavage. The central double bond of this stilbene analog is very strong, and represents one of the ways that weakly bonded recombination products can be converted to more refractory retrograde products.*

Integration Procedure. The conversion simulations using this model were performed on a VAX 11/750 computer using a numerical integration routine based on the Gear algorithm. Some of the results are shown below using area graphs to depict the evolution of various products as a function of time, or bar graphs to show product distributions at a fixed time for different starting compositions. The time-steps used in the integration were very much smaller than the time steps output by the program and used to construct the area graphs shown here.

RESULTS AND DISCUSSION

Figure 1 shows the evolution of the computed product distribution for the "bibenzylic" starting material in a system of minimal H-donor content . There is of course rapid loss of substrate, but not all to desired products: about 2/3 of the mass after 2 hours, consists of uncleaved or retrograde products. The recombination product itself is not visible on the scale of the figure: it has either re-homolyzed, or lost 2(H) to form the "stilbene" product. The weak-bond cleavage product is substantial, but accounts for slightly less than 15% of the mass of starting material. The two strong-bond cleavage products (displacement by H• and by R•) are almost as prominent as the weak-bond cleavage product, even though the original donor content of the system was quite low (ca. 15 m% of substrate). In an actual coal, the stilbene retrograde product would not persist, owing to the thermodynamic driving force for unsaturation to be grouped in aromatic systems.

For comparison, Figure 2 shows the effects of added H_2 at 400°C. Strong-bond cleavage product 1 (displacement by free H• *and* solvent-mediated H•) has increased about five-fold, and is now more important than strong-bond cleavage product 2, which has actually declined. Weak-bond cleavage product has increased substantially, and the stilbene product has declined. Interestingly, the "true retrograde" product (dinaphthylmethane from H• and R• displacement reactions) has increased substantially, so that the sum of stilbene and true retrograde product is essentially unchanged by the addition of H_2. The important observation here is that while the presence of 1000 psi H_2 has markedly increased the strong-bond cleavage that results from displacement by H•, there has been essentially *no* suppression of the true retrograde products. That is, H_2 in a purely thermal system clearly does indeed react with resonance stabilized radicals in the system (as Vernon showed experimentally some years ago[11]) to substantially increase strong-bond cleavage, but the "scavenging" aspect of this reaction has essentially no effect retrograde reaction by addition-elimination reactions of resonance-stabilized radicals. Clearly, there is a large increase in H-atom activity, but no significant fractional decrease in resonance-stabilized radical concentration.

The result of the inability to fully scavenge stabilized radicals, is that at long reaction times such radicals will continue to form retrograde products through addition-elimination reactions, particularly in the present case, through displacement of methyl radical from the weak-bond cleavage product, methylnaphthalene. The consequence of this factor is that long reaction times or higher temperatures tend to be beneficial *only* in the presence of H_2 or a H-donor, as illustrated in Figure 3, which shows the sum of cleavage products with and without H_2 at several different sets time/temperature conditions.

Comparisons of the effectiveness of two different H-donors, dihydrophenanthrene and 9,10-dihydroanthracene leads to additional interesting observations of short-term vs long-term behavior. At short reaction times, where there is a large generation of fragment radicals from homolysis of the weakly bonded coal surrogate, modeling indicates that dihydroanthracene, as the better scavenger, indeed maximizes the yield of capped fragment radicals, and minimizes the yield of recombination products and radical displacement retrograde products.

* Although the double bond in stilbene is "very strong," this refers to the enthalpy input required to break the double bond directly, forming two naphthylcarbene moeities. As a non-aromatic double bond, there will be a great tendency for any stilbene-like double bond to undergo rearrangements such that all unsaturation comes to reside in aromatic structures. Such "tertiary" reactions are not included in the present model.

However, at long reaction times, the "better" scavenger actually *enhances* the yield of retrograde product. This is because, at longer reaction times when the burst of radicals from the decomposing coal has largely died away, the principal source of fragment radicals is abstraction of hydrogen atoms from the previously capped fragment species by the pool of scavenger radicals generated by the scavenger itself. Thus, the model appears to further explain a trend which has been noted previously, namely that coal conversion tends to be better in the presence of hydroaromatics that are not the best scavengers, and is evidently better because these latter scavengers tend to be better hydrogenolysis reagents, while being poorer radical initiators.

The origin of the effects of H_2 can be seen more clearly with the help of Figures 4 and 5. Figure 4 shows that hydrogen pressure (at a somewhat higher temperature where they occur more strongly in these uncatalyzed systems) serves, as expected, to partially maintain the H-donor (dihydrophenanthrene) level in the reaction medium. Figure 5 shows that the percent increase in hydrogenolysis rates is much higher than the percent increase in donor concentration. In other words, the total new H-atom activity resulting from the presence of H_2 is much larger than the increase in H-donor. Thus, in the short term, the steady-state concentration of H• and ArH• has increased more than the steady-state concentration of ArH_2.

Returning to the observation that scavenging increases hydrogenolysis, but does not, through its "scavenging" action, decrease the rate of formation of retrograde products, Figure 6 shows the computed ratios of scavenger concentration ($[H_2]/[PhenH_2]$), the ratios of scavenging by these two components, and the percent of recombination that occurs (for H_2 = 0 and 1000 psi.) for the naphthylmethyl radicals produced by homolysis of the original weak bond. Clearly, not only is the scavenging ability of H_2 inconsequential, compared even to a small concentration of H-donor (as expected because of their greatly different bond strengths), but the ability of H_2 to limit recombination is barely observable, even at 600°C.

Perhaps more surprising are the computed effects of H_2 or added H-donor on stabilization of the "true retrograde" intermediate (the removal of H-atom from the ipso-substituted radical addition intermediate). Figure 7 shows the instantaneous net rate of stabilization at by each of the major H-transfer processes for three different starting conditions: no added H_2 and 0.1 M $PhenH_2$, 1000 psi H_2 and 0.1 M $Phen_2$, and 0 H_2 and 0.5 M $PhenH_2$. In all three cases, H-removal by radical disproportionation with 9-hydrophenanthryl- naphthylmethyl- and dinaphthylethyl-ethyl radicals gives a net formation rate for the dinaphthylmethane retrograde product. Either added H_2 or increased starting H-donor actually serve to *increase* the net rate of formation of the true retrograde product by radical addition and H-atom removal in disproportionation processes. This increased formation by the first three categories is more than compensated for by large negative rates of retrograde product formation by free H-atoms and RHT. That is, free H-atoms transfer much more H to dinaphthylmethane than they take away from ipso-H-substituted dinaphthylmethane, and are net destroyers, not net formers, of retrograde product. Thus, addition of H_2 or H-donor does *not* actually prevent retrograde product formation (it in fact increases it), but serves to cleave such products more effectively *after* they are formed!

This finding makes somewhat moot earlier discussions of whether coal linkages are dominated by strong or by weak bonds: Even if coal starts out with many of most of its linkages connected by weak bonds, there will very shortly be many strong bonds formed, whose subsequent cleavage will likely by critical to the ultimate conversion yield from the coal. The findings here also serve to articulate and explain our earlier experimental observations with a polymeric version of the dinaphthylethane substrate[10] we have computationally studied here: even when a substrate has a weak bond between every pair of asromatic clusters, as in 1,2-diarylethane linkages, there will be much cleavage not only of the weak bond between the two aliphatic carbons in the linkage but also of the strong aryl-alkyl bonds at either side. This cleavage will result not only from hydrogenolysis, but also from displacement by carbon-centered radicals to form retrograde products with new, strong linkages that can only be cleaved by hydrogenolysis. Thus in many cases, coal liquefaction may be as much about cleaving retrograde bonds as it is about cleaving linkages that are original to the coal structure.

SUMMARY AND CONCLUSIONS

In some cases the results presented here are a quantitative illustration of what can be qualitatively anticipated from thermochemical considerations, while in other cases the results were qualitatively surprising. The major conclusions and points to be emphasized from the modeling results are the following.

- All scavengers that operate via a radical capping process have a dual role—they also act as initiators.
- Higher temperatures provide more reaction, but if there is not something to mitigate retrograde reactions, higher temperatures tend to cause the retrograde reactions to increase as fast or faster than the bond-cleavage reactions. This modeling result appears to be completely in accord with the common observation that increasing liquefaction temperature beyond about 440°C tends to lower coal conversion, and similarly in pyrolysis, that higher heating rates tend

to decrease char yields, *primarily* when the higher heating rates are associated with more rapid removal of volatile products.

- The presence of H_2 does *not* inhibit retrograde product formation as much as it hydrogenolyzes retrograde products faster after they are formed. In fact, modeling indicates that H_2 can, at certain reactions times, *increase* the yield of retrograde products.
- The impact of added H_2 on hydrogenolysis (at least in the short term) does *not* come primarily through its maintenance of a useful hydroaromatic content, as has often been postulated in coal liquefaction, but through a higher steady state concentration of H• that is established long before the hydroaromatic content can be substantially affected.

ACKNOWLEDGMENT

The authors wish to acknowledge the Support of the U.S. Department of Energy in various projects whose goals have included an improved understanding of the chemistry responsible for coal liquefaction.

REFERENCES

1. McMillen, D. F.; Malhotra, R.; Nigenda, S. E. *Fuel*, **1989**,*68*, 380.
1. Neavel, R. C. *Fuel*, **1976**, *55*, 237.
2. Fong, W. S.; Peters, W. A.; Howard, J. B. *Fuel*, **1986**,*65*, 251.
3. Savage, P. E.; Klein, M. T.; Kukes, S. G. *Fuel*, **1988**,*2*, 619.
4. Khorasheh, F.; Rangwala, H. A.; Gray, M. R.; Dalla Lana, I. G. *Energy &Fuels*, **1989**, *3*, 716.
5. McMillen, D. F.; Malhotra, R.; Chang, S.-J., Ogier, W. C.; Nigenda, S. E.; Fleming, R. H. *Fuel*, **1987**, *66*, 1611.
6. Malhotra, R.; McMillen, D. F. *Energy &Fuels*, **1993**, *7*, 227.
7. McMillen, D. F.; Malhotra, R. *Am. Chem. Soc. Div Fuel Chem. Preprints* **1992**, *37(1)*, 385.
8. Malhotra, R.; McMillen, D. F. *Energy &Fuels*, **1990**, *4*, 184.
9. Squire, K. R.; Solomon, P. R.; Carangelo, R. M.; DiTaranto, M. B. *Fuel* **1986**, *65*, 833.
10. Malhotra, R.; McMillen, D. F.; Tse, D. S.; St.John, G. A. *Energy & Fuels* **1989**, *3*, 465.
11. Vernon, L. W. *Fuel*, **1980**, *59*, 102.

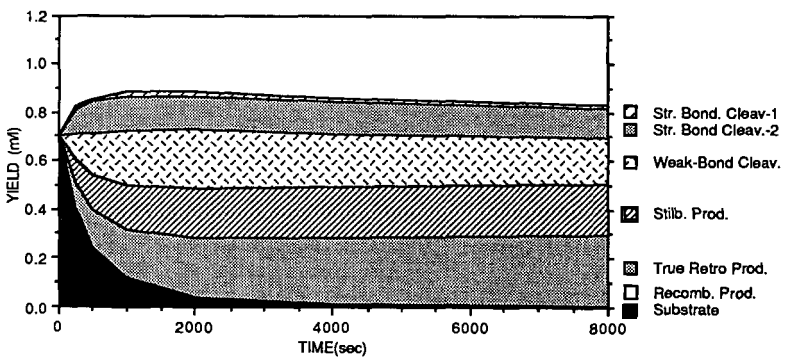

Figure 1. Computed product distribution at 400°C with minimal H-donor content. [PhenH2] = 0.1M, P (H_2) = 0.

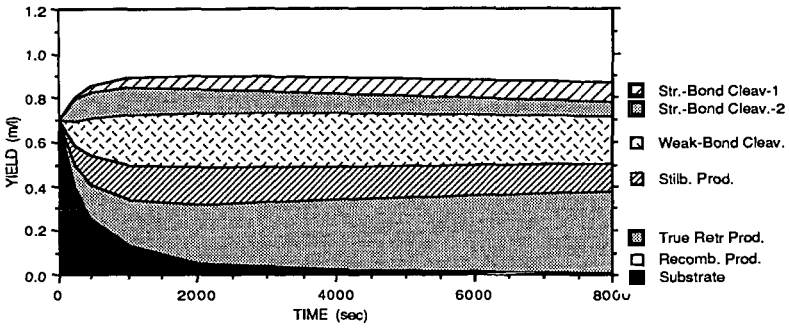

Figure 2. Computed product distribtuion at 400°C with minimal donor content but added H_2. [PhenH2] = 0.1M, P (H_2) = 1000 psi.

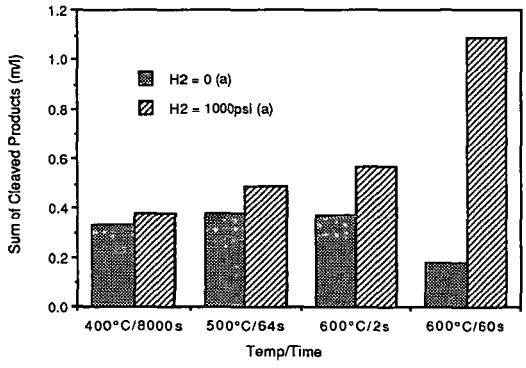

Figure 3. Sum of cleavage products for different time and temperature conditions. [PhenH2] = 0.1M.

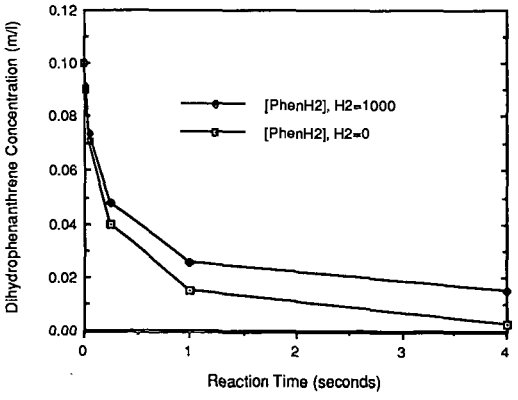

Figure 4. Computed H-donor concentration at 500°C as a function of time with and without 1000 psi added H_2. [PhenH2] = 0.1M.

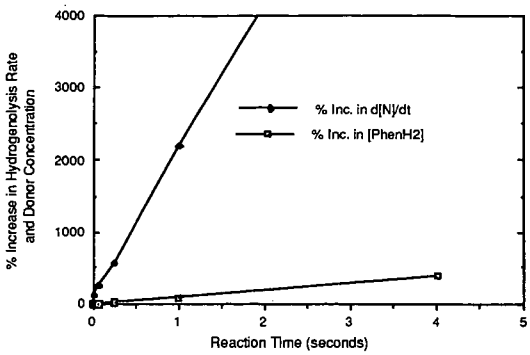

Figure 5. Comparison of percent increase in hydrogenolysis rate and donor concentration as a result of 1000 psi added H_2. 500°C; [$PhenH_2$] = 0.1M.

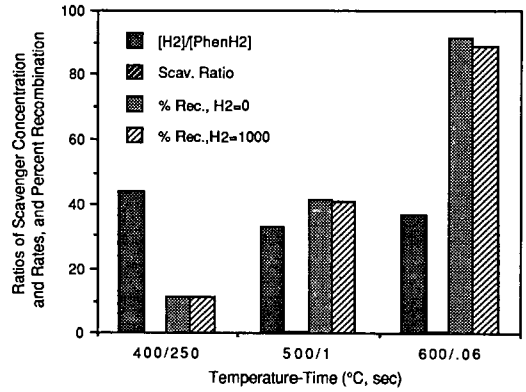

Figure 6. Computed ratios of scavenger concentration, scavenging rates for H_2 and H-donor, and the percent recombination of homolysis fragments with and without 1000 psi H_2. [$PhenH_2$] = 0.1 M.

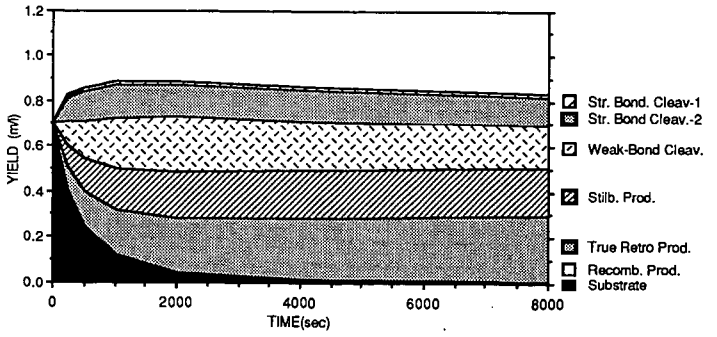

Figure 7. Computed net rates of H-removal from diarylmethane retrograde intermediate for various H-tran

PYROLYSIS KINETICS AND MECHANISMS FOR POLYCYCLIC PERHYDROARENES BEARING LONG N-ALKYL CHAINS

Phillip E. Savage
University of Michigan
Department of Chemical Engineering
Ann Arbor, MI 48109-2136

keywords: hydrocarbons, pyrolysis, mechanisms

ABSTRACT

A set of long-chain polycyclic n-alkylperhydroarenes was pyrolyzed neat at temperatures between 400 and 475°C. The disappearance of these compounds typically followed first-order kinetics. The pyrolysis of a perhydroarene with an n-carbon containing n-alkyl chain generated numerous primary products. The primary products with the highest initial selectivities were generally the perhydroarene plus an α-olefin with n carbon atoms, the methylene perhydroarene plus an n-alkane with n-1 carbon atoms, and a polycyclic mono-olefin plus an n-alkane with n carbon atoms. The kinetics data from this investigation were used to test a structure-reactivity correlation in the literature for the pyrolysis of saturated cyclic compounds and to update it so that it becomes consistent with the kinetics of long-chain n-alkylperhydroarenes.

INTRODUCTION

Naphthenic (perhydroarene) moieties decorated with n-alkyl substituents exist in heavy hydrocarbon resources such as coal, heavy oils, and asphaltenes. Additionally, these types of chemical structures are present in the endothermic jet fuels being developed for the next generation of high-performance jet aircraft. Given the presence of these structures in these materials, which experience elevated temperatures of around 400°C during their processing or use, it is clear that information about the thermal decomposition of saturated cyclic compounds with alkyl substituents at temperatures around 400°C would be useful.

Until very recently, the literature was limited to kinetics data at a single temperature (700K) for 28 saturated cyclic compounds (six were polycyclic), most of which bore short chains (Fabuss et al., 1964) and more extensive kinetics data and mechanistic information for a single one-ring compound, tridecylcyclohexane (Savage and Klein, 1988; Mushrush and Hazlett, 1984). Indeed, prior to the publication of our group's recent work (Humburg and Savage, 1996; Mizan et al., 1997), the literature provided no information about the pyrolysis kinetics, pathways, or mechanisms for any polycyclic perhydroarenes bearing a long (> C4) n-alkyl chain. This lack of information about the behavior of polycyclic n-alkylperhydroarenes and previous results showing that the pyrolysis of other polycyclic hydrocarbons led to products that differed from those of their single ring analogs (Savage et al., 1989; Virk et al., 1979) motivated the investigations with n-alkyl-substituted polycyclic perhydroarenes.

EXPERIMENTAL

The model compounds were obtained from the Thermodynamics Research Center at Texas A & M University, Pfaltz and Bauer, TCI Organics, and Wiley Organics. All chemicals were used as received. All pyrolyses were conducted neat in batch microreactors fashioned from a nominal 1/4 inch stainless steel Swagelok port connector and two caps. We loaded between 10 and 40 mg of the reactant and about 10-15 mg of biphenyl (an internal standard) into each reactor, and these quantities were weighed to within ± 0.1 mg. The loaded reactors were placed in a fluidized sand bath maintained at the desired pyrolysis temperature. When the desired batch holding time had elapsed, the reactors were removed from the sand bath, and the reaction was quenched by immersing the reactors in water at room temperature. The reactors were then opened and their contents retrieved by repeated additions of methylene chloride. The reaction products were identified and quantified via capillary-column gas chromatography with either a mass spectrometric or flame-ionization detector. Product molar yields, calculated as the number of moles of product formed divided by the number of moles of reactant initially loaded into the reactor, were obtained from the chromatographic analysis using experimentally determined detector response factors. Additional details about the experimental methods appear in the literature (Humburg and Savage, 1996; Mizan et al., 1997).

RESULTS AND DISCUSSION

This section summarizes the experimental results obtained from n-alkylperhydroarene pyrolysis. These results were used to determine the reaction rate law and to develop the reaction network for neat pyrolysis.

Pyrolysis Kinetics

The objectives of the kinetics analysis were to determine the global reaction order (m) and Arrhenius parameters (A, E) for the power-law rate expression in Equation 1 that best describes n-alkylperhydroarene disappearance.

$$rate = kC^m = A\exp\left(\frac{-E}{RT}\right)C^m \qquad (1)$$

The parameters in the rate law were determined by examining the results of numerous experiments at different temperatures, holding times, and initial concentrations. First order kinetics

gave an adequate description of the kinetics for each compound examined in detail. Our previous reports (Humburg and Savage, 1996; Mizan et al., 1997) provide the experimental data and the details of the kinetics analysis for 9-dodecylperhydroanthracene (DDPA) and 1-undecylperhydronaphthalene (UPN). Additionally, Table 1 provides new kinetics data for the pyrolysis of nine other n-alkylperhydroarenes.

Structure-Reactivity Relations

The reaction kinetics for compounds in a single family can often be correlated using a structure-based reactivity index. Such structure-reactivity correlations are useful in computer models of the reactions of complex materials such as fossil fuels and for predicting the reactivity of compounds that have not been investigated experimentally. One needs a large set of reliable kinetics data to develop structure-reactivity correlations. Fabuss et al. (1964) provide data for the pyrolysis kinetics at 800°F (700K) of 28 saturated cyclic compounds that were either unsubstituted or bore short ($\leq C_4$) alkyl substituents. They correlated the disappearance kinetics using a "characterization number", n, as the reactivity index. The Fabuss et al. (1964) correlation is

$$k\,(hr^{-1}) = 0.044 - 0.0114n + 0.0008n^2 \qquad (2)$$

The characterization number can be determined by inspection of the structure of the compound, and it is based on group-additivity. The characterization number for decylcyclohexane, for example, is 49 (12 for the cyclohexane ring, plus 4 for each of the nine CH_2 group in the alkyl chain, plus 2 for the terminal methyl group in the chain, and minus 1 for the one C-H bond in the ring structure replaced by an alkyl substituent). We note that the equation above shows 0.0114 as the coefficient for the second term, whereas the equation that appears in Fabuss et al. shows 0.114. We believe the equation in Fabuss et al. contains a typographical error because using 0.114 in Equation 2 leads to negative values for the rate constants.

In this report, we expand the existing database by providing new kinetics data (see Table 1) for the pyrolysis of long-chain and polycyclic perhydroarenes at 427°C. We can use the data in Table 1, along with that previously reported for tridecylcyclohexane, TDC, (Savage and Klein, 1988; Mushrush and Hazlett, 1984), undecylperhydronaphthalene, UPN (Mizan et al., 1997), and dodecylperhydroanthracene, DDPA, (Humburg and Savage, 1996) to assess the predictive ability of the Fabuss et al. (1964) structure-reactivity relation.

Figure 1 shows the correlation of Fabuss et al. along with our experimental data for 11 different long-chain n-alkylperhydroarenes. It is clear that the correlation fails to predict the kinetics for these compounds. Fabuss et al., to their credit, anticipated that the performance of their correlation would deteriorate as the length of the alkyl substituent exceeded four carbon atoms. Indeed, none of the compounds they pyrolyzed had characterization numbers that exceeded 40, and Figure 1 shows that the correlation performs poorly when extrapolated to these higher characterization numbers.

We next combined the kinetics data provided by Fabuss et al. with our more recent data for long-chain compounds to develop a new structure-reactivity relation that uses the characterization number as the sole correlating parameter. We fit the experimental kinetics data in Fabuss et al. along with our data for long-chain perhydroarenes to a quadratic equation of the form originally used by Fabuss et al. (Equation 2). The results from the non-linear regression showed that the uncertainty in the second parameter exceeded the value of the parameter itself. In fact, a value of zero was contained within the 95% confidence interval for this parameter. Consequently, we repeated the non-linear regression of the kinetics data, but with the statistically insignificant term set equal to zero. The resulting correlation is

$$k\,(hr^{-1}) = -0.041 + 0.00035n^2 \qquad (3)$$

The level of agreement between the new correlation and the experimental data is apparent upon inspection of Figure 2. We expect that the correlation of Equation 3 will provide reasonable estimates of the rate constants for long-chain alkylperhydroarenes. The only compound for which the correlation performs poorly is decylperhydropyrene. The reason for this failure is not clear, and additional experiments with other polycyclic compounds are required to address this issue.

The structure-reactivity relation of Fabuss et al. qualitatively incorporates some fundamental aspects of hydrocarbon pyrolysis kinetics in their characterization number. For example, a CH_2 group adds more to the characterization number than does a CH_3 group, which is consistent with secondary C-H bonds being weaker and hence more reactive than primary C-H bonds. This correlation is empirical, however, because the relative contributions of the different structural groups were determined by fitting data rather than by building squarely upon the foundation of the governing reaction mechanism. The mechanism for the pyrolysis of saturated cyclic hydrocarbons is reasonably well established, and closed-form analytical rate expressions are available (Savage, 1990). A mechanism-based structure-reactivity relation has already appeared for n-alkylbenzenes (Savage and Korotney, 1990). Thus, the stage is now set for progress toward a mechanism-based structure-reactivity relation for long-chain n-alkylperhydroarenes.

Pyrolysis Products, Network, and Mechanism

The neat pyrolysis of n-alkylperhydroarenes led to numerous reaction products, and the product spectrum comprised n-alkanes, 1-alkenes, perhydroarenes substituted with alkyl or alkenyl chains, and partially hydrogenated arenes. Our work with these compounds showed that a perhydroarene with an n-carbon-containing alkyl substituent pyrolyzed to form three pairs of major

primary products and numerous minor primary products. This network is illustrated in Figure 3 for UPN. The major primary product pairs are the perhydroarene plus a C_n olefin (decalin plus undecene for UPN), the methylene perhydroarene plus a C_{n-1} alkane (methylene decalin plus decane for UPN), and a cyclic olefin plus a C_n alkane (octahydronaphthalene plus undecane for UPN).

Although the identities of the three major primary product pairs are analogous for the different n-alkylperhydroarenes, the relative abundances of these products differ for the different compounds. The ring-containing products from the neat pyrolysis of the 2- and the 3-ring compounds were, in order of decreasing selectivity, the cyclic olefin, the methylene perhydroarene, and the perhydroarene. The pyrolysis of DPP, a 4-ring compound, on the other hand, led to the perhydroarene being the most abundant product, followed by the methylene perhydroarene and the cyclic olefin. The product spectrum from DPP more closely resembled that of an alkylcyclohexane, wherein the major primary pyrolysis products are cyclohexane, methylene cyclohexane, and lesser amounts of cyclohexene and methylcyclohexane. This comparison of the major primary products from neat pyrolysis of 1-, 2-, 3-, and 4-ring n-alkylperhydroarenes shows that an analogous set of three major product pairs forms in all cases. The compound-to-compound differences involve only the relative abundance of these different product pairs. This similarity in the reaction network suggests a corresponding similarity in the underlying reaction mechanism. Thus, the free-radical reaction steps advanced previously for 1-, 2-, and 3-ring alkylperhydroarenes (Savage and Klein, 1988; Humburg and Savage, 1996; Mizan et al., 1997) appear to be general.

SUMMARY AND CONCLUSIONS

This paper provides a summary of results from the pyrolysis of long-chain polycyclic n-alkylperhydroarenes. The neat pyrolysis typically follows first-order kinetics. The reaction network for n-alkylperhydroarenes includes parallel primary reactions to form an α-olefin plus the perhydroarene, an n-alkane plus the methylene perhydroarene, and an n-alkane plus a polycyclic mono-olefin. The numerous minor primary products were other n-alkanes, α-olefins, alkylperhydroarenes, and alkenylperhydroarenes. The arene and methylarene appeared as products at the more severe reaction conditions.

Kinetics data for the pyrolysis of n-alkylperhydroarenes revealed that the correlation of Fabuss et al. (1964) cannot be extrapolated to predict the reactivity of long-chain and polycyclic perhydroarenes. Equation 3 provides a new correlation, based on the Fabuss et al. characterization number, that is consistent with both their data and that reported herein. This correlation can be used to predict the kinetics of a wide variety of saturated cyclic compounds.

REFERENCES

Fabuss, B. M.; Kafesjian, R.; Smith, J. O.; Satterfield, C. N. Thermal Decomposition Rates of Saturated Cyclic Hydrocarbons. *Ind. Eng. Chem. Proc. Des. Dev.* **1964**, *3*, 248.

Humburg, R. E.; Savage, P. E. Pyrolysis of Polycyclic Perhydroarenes 1. 9-n-Dodecylperhydroanthracene. *Ind. Eng. Chem. Res.* **1996**, *35*, 2096.

Mizan, T. I.; Savage, P. E.; Perry, B. Pyrolysis of Polycyclic Perhydroarenes 1. 1-n-Undecylperhydronaphthalene. *Energy Fuels* **1997**, 11, in press.

Mushrush, G. W.; Hazlett, R. N. Pyrolysis of Organic Compounds Containing Long Unbranched Alkyl Groups. *Ind. Eng. Chem. Fundam.* **1984**, *23*, 288.

Savage, P. E. Pyrolysis of a Binary Mixture of Complex Hydrocarbons: Reaction Modeling. *Chem. Eng. Sci.* **1990**, *45*, 859.

Savage, P. E.; Jacobs, G. E.; Javanmardian, M. Autocatalysis and Aryl-Alkyl Bond Cleavage in 1-Dodecylpyrene Pyrolysis. *Ind. Eng. Chem. Res.* **1989**, *28*, 645.

Savage, P. E.; Klein, M. T. Asphaltene Reaction Pathways: 4. Pyrolysis of Tridecylcyclohexane and 2-Ethyltetralin. *Ind. Eng. Chem. Res.*, **1988**, *27*, 1348.

Savage, P. E.; Klein, M. T. Asphaltene Reaction Pathways: 5. Chemical and Mathematical Modeling. *Chem. Eng. Sci.* **1989**, *44*, 393.

Savage, P. E.; Korotney, D. J. Pyrolysis Kinetics for Long-Chain n-Alkylbenzenes: Experimental and Mechanistic Modeling Results. *Ind. Eng. Chem. Res.* **1990**, *29*, 499.

Virk, P. S.; Korosi, A.; Woebcke, H. N. Pyrolysis of Unsubstituted Mono-, Di-, and Tricycloalkanes. In ACS Advances in Chemistry Series; Oblad, A. G., Davis, H. G., Eddinger, R. T., Eds.; American Chemical Society: Washington, DC, 1979; Vol. 183, p. 67

Table 1: Rate Constants (in sec^{-1}) for Neat Pyrolysis of Long-Chain n-Alkylnaphthenes at 427°C

Compound	k x 10^4	95% C.I.
2-Octylperhydrochrysene (OPC)	2.97	1.64
9-Dodecylperhydrophenanthrene (9DPPh)	4.22	0.38
1-Dodecylperhydrophenanthrene (1DPPh)	3.73	0.78
1-Decylperhydropyrene (DPP)	1.28	0.56
Tridecylcyclohexane (TDC)	2.90	0.86
Dodecylcyclohexane (DDC)	2.75	0.70
Decylcyclohexane (DC)	2.57	0.96
Heptylcyclohexane (HPC)	1.63	0.30
Hexylcyclohexane (HXC)	1.01	0.49

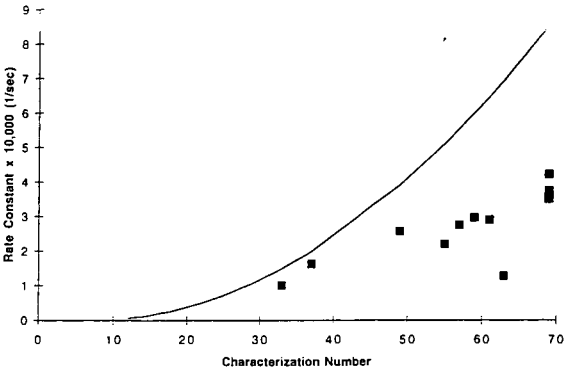

Figure 1: Structure-reactivity relation of Fabuss et al. (solid curve) and experimental data for long-chain n-alkylperhydroarenes (discrete points).

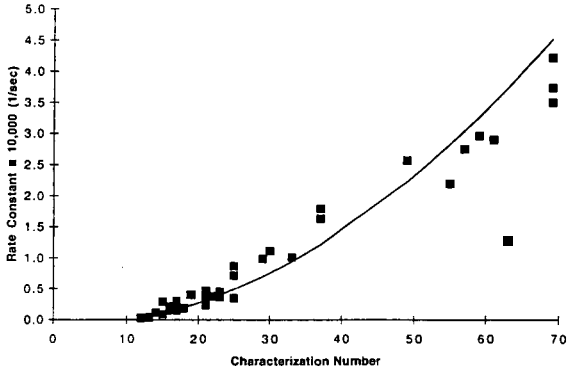

Figure 2: Updated structure-reactivity relation for saturated cyclic compounds.

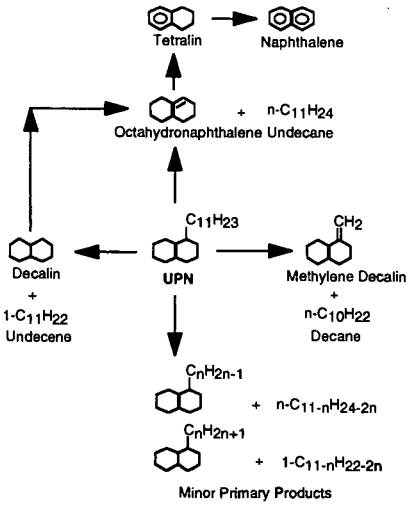

Figure 3: General reaction network for alkylperhydroarene neat pyrolysis.

RAPID CLEAVAGE OF DIARYL ETHERS IN FUEL PROCESSING INDUCED BY *ortho*-BENZYLIC RADICAL FORMATION: KINETICS OF REARRANGEMENT OF THE 2-PHENOXYBENZYL RADICAL

James A. Franz, John C. Linehan, Anne E. Crump, Lauren Kaune, Mikhail S. Alnajjar, Donald M. Camaioni, and Tom Autrey

Pacific Northwest National Laboratory
P.O. Box 999
Richland, WA 99352

Keywords: Kinetics, Radical Rearrangements, Aryl Ether Cleavage

INTRODUCTION

Recently we reported the cleavage of the aryl ether bond of 2-benzyldiphenyl ether in reactions with an iron sulfide nanocatalyst in dihydrophenanthrene at 400 °C (1). In that work, the rearrangement of 2-benzyldiphenylether to 2-(diphenylmethyl)phenol and the subsequent rapid scission of 2-diphenylmethylphenol to give diphenylmethane and phenol (eq.1, X = H) was found to occur not

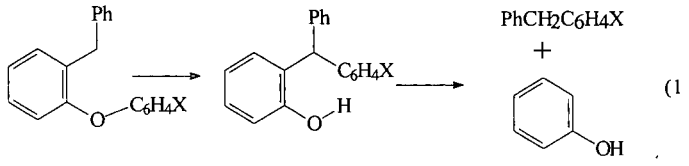

by a direct ether C-O bond scission pathway, but rather by stepwise formation of a benzylic radical followed by phenyl migration from oxygen to the carbon radical center (Scheme 1). Substitution of a methyl group on the phenyl ether ring confirmed that diphenylmethane was formed in a rearrangement reaction (eq 1, X = *p*-CH_3). Thus, alkyl substituents adjacent to aromatic ether linkages provide a pathway for enhanced thermal cleavage of the relatively inert ether C-O bond. Note that the alternate pathway to eq. 1 is cleavage of the benzyl group to form a diphenyl ether. As shown by the first two entries in Table 1, direct benzyl cleavage is the slow, but favored pathway for the 4-benzyl-substituted diphenylethers. To further explore and quantitate this pathway for strong bond scission in fuels processing, we have determined rate constants for the rearrangement of the 2-phenoxybenzyl radical to the 2-benzylphenoxy radical. We present global rate constants for conversion of substituted diphenyl ethers by nanophase FeS catalysts that illustrate that *ortho* alkyl substitution of a diaryl ether leads to an enhanced rate of scission of the aryl ether bond under hydrocarbon processing conditions.

EXPERIMENTAL

Kinetics of Rearrangement of the 2-Phenoxybenzyl Radical. 2-Phenoxybenzyl radical (**2**, Scheme 1) was formed either by the reaction of 2-phenoxybenzyl chloride and Bu_3SnH or by the photolysis of ketone **1**, Scheme 1, which was prepared by the method of Sasaki and Kitagawa(2). The rearrangement kinetics were performed by photolysis of reagents sealed in quartz tubes in a specially modified GC oven equipped with a quartz photolysis window. The tubes were placed in an aluminum block in the GC oven at reaction temperature through a hole on top of the oven and allowed to equilibrate for 5 minutes prior to photolysis. Solutions containing the ketone 1 (10^{-2} M), tributyltin hydride (1×10^{-4} to 5×10^{-3} M), and eicosane (an internal GC standard) in dodecane were made up in an inert atmosphere box. The solutions were syringed in 100 ul portions into 4 mm o.d. quartz tubes. The tubes were placed on a vacuum line and degassed in three freeze-pump-thaw cycles prior to sealing. Analysis by GC of tubes sealed in this manner showed no evidence of reaction during preparation and sealing. The samples were photolyzed, through a quartz window in the GC oven door, with a 150-watt deuterium/mercury lamp. The reactions were run between 190°C and 270°C to 20% or less consumption of Bu_3SnH. GC analyses were performed on a J&W Scientific 15-m DB-5 column using a Hewlett-Packard model 5890 GC with FID detection. The rate constants were calculated by computer solution of the integrated rate expression relating unrearranged product (**4**) , rearranged product (**5**), initial tributyl tin hydride concentration (B_0), and the relative rate $r = k_{re}/k_{abs}$:

$$[4 + 5] = (B_0 + r)*(1-\exp(-[5]/r) \quad (2)$$

The relative rate constants (r) were combined with an absolute rate expression for abstraction of hydrogen from Bu_3SnH by benzyl radical (3): $\log(k_{abs}/M^{-1}s^{-1}) = 8.65 - 5.58/\theta$, $\theta = 2.3RT$ kcal/mol, to yield the rearrangement rate constants k_{re}.

Kinetics of Reactions of Diaryl Ethers With FeS Catalysts. Samples of diaryl ethers (15-20 mg) were sealed in glass ampules in the presence of dihydrophenanthrene (100 mg), FeS catalyst precursor (3 mg), and sulfur (3 mg), and heated in a fluidized sand bath at 390°C. Products were analyzed by GC using authentic products. Detailed procedures for FeS/substrate reactions have been published (4-6).

RESULTS AND DISCUSSION

The 1,4-aryl migration of 2-phenoxybenzyl radical, **2**, to form the 2-benzylphenoxy radical, **3**, follows the Arrhenius rate expression $\log(k_{re}/s^{-1}) = (10.8 \pm .8) - (20.2 \pm 1.8)/\theta$, $\theta = 2.3$ RT kcal/mol. These Arrhenius parameters suggest that the rearrangement occurs efficiently at coal liquefaction temperatures ($k_{re} = 3 \times 10^4\ s^{-1}$ at 700K). The controlling factor for this category of rearrangement will be the efficiency of radical formation and the unimolecular lifetime of the radical relative to bimolecular reaction with available hydrogen donors. With efficient radical initiation, such as in the presence of sulfur-derived thiyl radicals, regeneration of benzylic radicals will occur through many cycles. Once the radical has undergone rearrangement, subsequent trapping by available hydrogen donors produces an ortho-hydroxydiphenylmethane, which undergoes rapid unimolecular homolysis (7).

Rate constants for the disappearance of methyl substituted 2- and 4-benzyldiphenylethers (Table 1) reveal that benzyl substitution at the 2-position enhances the rate of "uncatalyzed" ether conversion by a factor of 30 compared to substitution at the 4-position. For the catalyzed cases, the 2-benzyl-substituted diphenyl ether is about 10 times more reactive than the 4-benzyl-substituted diphenyl ether. Table 1 shows that for the cases of 4-benzyl-substituted diphenylmethanes, catalyzed cleavage of the benzyl-aromatic ring C-C bond occurs exclusively, illustrating the regiochemical requirements for C-O cleavage leading to diphenylmethane formation. These results demonstrate a pattern of enhancement of cleavage of diaryl ethers consistent with the participation of the 1,4- oxygen-to-carbon aryl migration reaction.

ACKNOWLEDGMENT

This work was supported by the U. S. Department of Energy, Office of Energy Research, Office of Basic Energy Sciences, Chemical Sciences Division, Process and Techniques Branch. This work was conducted at Pacific Northwest National Laboratory, which is operated by Battelle Memorial Institute for the U. S. DOE under contract DE-AC06-76-RLO 1830. Support for LK was provided through AWU-NW under grant DE-FG06-89ER-75522 from the U. S. Department of Energy.

REFERENCES

(1) Autrey, T.; Linehan, J.C.; Camaioni, D. M.; Powers, T. R.; McMillan, E. F. And Franz, J. A. *Fuel Preprints*, **1995**, 973-977.
(2) Sasaki, H. And Kitagawa, T. *Chem. Pharm. Bull.* **1983**, 31, 2868.
(3) Franz, J.A.; Suleman, N.K.; and Alnajjar, M.S. *J. Org. Chem.* **1986**, *51*, 19-25.
(4) Autrey, T.; Linehan, J.C.; Camaioni, D.M.; Kaune, L.E.; Watrob, H.M.; and Franz, J.A *Catalysis Today*, **1996** *31* , 105-111.
(5) Matson, D.W., J.C. Linehan, J.G. Darab, D.C. Camaioni, S.T. Autrey, and E. Lui. **1995**, "New Nanopohase Iron-Based Catalysts for Hydrocracking Applications" MRS Symposium Proceedings #368, Synthesis and Properties of Advanced Catalytic Materials, E. Iglesia, P.W. Lednor, D.A. Nagaki, L.T. Thompson, eds. pp.243-248.
(6)Linehan, J. C.; Matson, D. W.; and Darab, J. G. *Energy & Fuels* **1994**, 56.
(7) McMillen,D.F; Ogier, W. C.; and Ross, D. S. *J. Org. Chem.* **1981**, 46, 3322.

Table I
Rate Constants for the Disappearance of Benzyldiphenyl Ethers with Iron-Sulfide Catalysts

Substrate[a] DPM/DPE	Catalyst Precursor[b]	Rxn Temp	k (1 x $10^4 s^{-1}$)	% Consumed[c]	
(4'Me)-4-BzDPE	none	390°C	0.04 ± .005	3	d
(4'Me)-4-BzDPE	6-line	390°C	0.40 ± .08	25	0.02[e]
(4'Me)-2-BzDPE	none	390°C	1.3 ± .2	50	70[f]
(4'Me)-2-BzDPE	6-line	390°C	3.8 + .3	90	23[f]

a) DPM = diphenylmethane, DPE = diphenylether, 4-BzDPE = 4-benzyldiphenylether, 2-BzDPE = 2-benzyldiphenylether, (4'Me)-2-BzDPE = 4'-methyl-2-benzyldiphenylether, (4'Me)-4-BzDPE = 4'-methyl-4-diphenylether. b) 6-line = 6-line ferrihydrite, see refs. 4-6. c) Percent consumed in 90 minutes. d) No DPM observed. e) MeDPM/MeDPE. f) 4-methyldiphenyl -methane and 4-methyldiphenylether.

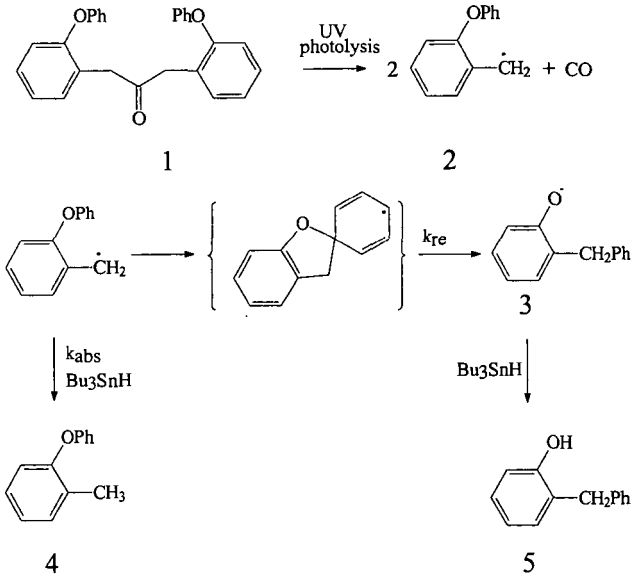

Scheme 1. Photolysis of Ketone **1** provides radical **2**, which undergoes irreversible rearrangement, k_{re}, in competition with hydrogen abstraction, k_{abs}, from Bu_3SnH.

CONTRASTING RETROGRESSIVE REARRANGEMENT PATHWAYS DURING THERMOLYSIS OF SILICA-IMMOBILIZED BENZYL PHENYL ETHER

A. C. Buchanan, III, Phillip F. Britt, and J. Todd Skeen

Chemical & Analytical Sciences Division
Oak Ridge National Laboratory
P.O. Box 2008, MS-6197
Oak Ridge, Tennessee 37831-6197

Keywords: Retrogressive reactions, rearrangements, restricted diffusion, ether linkages

INTRODUCTION

Many coal model compound studies have focused on the mechanisms of bond *cleavage* reactions, and the means to alter reaction conditions to promote such reactions. However, there has become increasing interest in elucidating mechanisms associated with retrogressive or retrograde reactions in coal processing, which involve the *formation* of refractory bonds.[1-3] Retrograde reactions inhibit efficient thermochemical processing of coals into liquid fuels, which has been particularly well-documented for low rank coals where abundant oxygen-containing functional groups are thought to play a key role in the chemistry. For example, the decarboxylation mechanism of carboxylic acids is being investigated because of the correlation between CO_2 evolution and cross-linking in low rank coals.[4,5] In addition, phenols have been investigated because of their ability to undergo condensation reactions.[6,7]

Much less is known about retrogressive reactions for ether-containing model compounds. Radical recombination through ring coupling of phenoxy radicals in benzyl phenyl ether (BPE) is known to lead to more refractory diphenylmethane linkages to a limited extent.[2,8-11]

$$PhOCH_2Ph \rightarrow PhO\bullet + \bullet CH_2Ph \rightarrow o\text{-}, p\text{-}HOPhCH_2Ph$$

Since this chemistry may be attributed at least in part to cage recombination, it could be promoted in a diffusionally constrained environment such as in the coal macromolecule. Using silica-immobilization to simulate restricted diffusion in coal, we have found that retrogressive reactions can be promoted for certain hydrocarbon model compounds.[12,13] We have now begun an examination of the thermolysis behavior of silica-immobilized benzyl phenyl ether (≈BPE, where ≈ represents the Si-O-C linkage to the surface as shown in Table 1) at 275-325 °C. Our initial results indicate that *two retrogressive reaction pathways*, radical recombination as shown above and molecular rearrangement through ≈PhOCH•Ph, are promoted by restricted diffusion. Remarkably, the retrograde products typically account for 50 mol % of the thermolysis products.

EXPERIMENTAL

The precursor phenol, *m*-$HOC_6H_4OCH_2C_6H_5$ (HOBPE), was synthesized by the reaction of benzyl bromide with the sodium salt of resorcinol (NaH in DMF). Following addition of water and acidification, the organics were extracted into toluene. Ether was added to the toluene solution, and the desired phenol was separated from the dibenzylated byproduct by extraction with 2 M NaOH. The basic layer was acidified and extracted with diethyl ether, which was then washed with brine, dried over Na_2SO_4, filtered, and the solvent removed under reduced pressure to produce a brown oil. The product was eluted twice from silica gel columns, once with toluene and then with toluene:hexane (75:25). Multiple recrystallizations from hot toluene:hexane (1:1) gave the desired phenol in 99.9 % purity by GC.

Chemical attachment of the precursor phenol to the surface of a nonporous silica (Cabosil M-5, Cabot Corp.; 200 m^2g^{-1}; ca. 1.5 mmol SiOH per g) was accomplished as described below. HOBPE (2.715g; 13.6 mmol) was dissolved in dry benzene (distilled from $LiAlH_4$) and added to a benzene slurry of silica (9.00g; 13.5 mmol SiOH) that had been dried at 225 °C for 4 h under vacuum. Following stirring and benzene removal on a rotovap, the solid was added to a Pyrex tube which was evacuated to 2 x 10^{-6} torr and flame sealed. The attachment reaction was performed at 200 °C for 1 h. Unattached HOBPE was removed by Soxhlet extraction (6h) with dry benzene under argon. The silica-attached BPE (≈BPE) was then dried under vacuum.

Surface coverage analysis was accomplished by dissolution of the solid (ca. 130 mg) in 30 mL of 1N NaOH over night. 3,4-Dimethylphenol and 4-phenylphenol in 1N NaOH were added as internal standards. The solution was acidified with HCl (pH ~ 4) and extracted with diethyl ether (3x). The ether layer was washed with 20 mL of brine, and the emulsion separated by centrifugation. The ether phase was dried over $MgSO_4$, filtered, and the solvent was removed under reduced pressure. Silylation with *N,O*-bis-(trimethylsilyl)trifluoroacetamide (BSTFA) in pyridine (2.5 M) produced the corresponding trimethylsilyl ether, which was analyzed by GC (HP 5890) on a J&W Scientific 30 m x 0.25 mm i.d. (0.25 μm film thickness) methyl silicone column with flame ionization detection. GC analysis of multiple assays gave a surface coverage of 0.245 (± 1%) mmol g^{-1} with a purity of 98.3 %.

Thermolyses were conducted at 275-325 °C (± 1 °C) in sealed, evacuated (2 x 10^{-6} torr), T-shaped Pyrex tubes in a temperature controlled tube furnace. Volatile products were trapped as they were produced in liquid nitrogen, and subsequently analyzed by GC and GC-MS (HP 5972A/5890 Series II) with the use of internal calibration standards. Surface-attached products were similarly analyzed after separation by digestion of the silica in aqueous base and silylation of the resulting phenols to the corresponding trimethylsilyl ethers as described above for the surface coverage analysis procedure. Independent recovery studies show that resorcinol, a major product from the thermolysis, is quantitatively recovered by this work-up procedure. The identities of nearly all the products in Table 1 were confirmed with authentic commercial materials. Two isomers of benzyl resorcinol were identified by GC-MS, and the 4-benzyl- isomer was confirmed with a commercial sample. 3-Hydroxybenzhydrol was synthesized from 3-hydroxybenzophenone by reduction with $LiAlH_4$ in ether. The benzylated ≈BPE isomers were identified solely by GC-MS.

RESULTS AND DISCUSSION

Thermolysis of ≈BPE proceeds readily at 275 °C to afford a complex array of products. A linear plot of conversion (%) *vs.* reaction time (6-runs from 2.5-13.3 % conversion) yields a rate for ≈BPE conversion of 17 x 10^{-4} % s^{-1} or 6.1 % h^{-1} (r=0.998). The principal products are shown in Table 1, and typically account for 98-99% of the products at 275 °C. Small amounts (≤ 0.2 mol % each) of bibenzyl, stilbene, and 3-hydroxydiphenylmethane are also detected. As observed from the data in Table 1, the product distributions do not exhibit a marked dependence on conversion or temperature. Mass balances are typically ≥ 97 % at 275 °C.

Typically, thermolysis of BPE in fluid phases has been reported to yield phenol, toluene, and benzylphenols as major products along with minor amounts of bibenzyl, diphenylmethane, and benzylated aromatics.[8-11] Clearly, for surface-immobilized BPE, a much more rich chemistry exists that produces numerous new thermolysis products. A plausible reaction scheme for the formation of these products is shown in Figure 1. Homolysis of the weak O-C bond (*ca.* 54 kcal mol^{-1}) generates phenoxy and benzyl radicals (Eq. 1), which can abstract hydrogen from ≈BPE to generate the ≈PhOH and $PhCH_3$ products (Eqs. 3-4). However, these radicals can also recouple prior to hydrogen abstraction at the ring carbons of the phenoxy radical to produce, following tautomerization, isomers of benzylphenol (Eq. 2). Benzyl radicals are also lost through adduction to aromatic rings to form higher molecular weight products as illustrated in Eq. 7 for addition to ≈BPE (addition to only one ring is shown in the table and figure for convenience). In fluid phases, the retrograde radical coupling reaction analogous to Eq. 2, which generates a more refractory diphenylmethane linkage as well as a reactive phenol functionality, can account for as much as 15 mol % of the thermolysis products. However, the restricted mass transport experienced by ≈BPE (and ≈PhO•) apparently results in a substantially enhanced probability of recoupling, and the isomeric benzylphenols (analyzed as benzylresorcinols after cleavage from the surface) account for 27-31 mol % of the products.

In addition to enhanced benzylphenol production, two major new products, surface-attached benzophenone and benzhydrol, were formed in comparable amounts and totaled 21-24 % of the products. Although there are numerous studies of BPE thermolysis in fluid phases, we have found only one report of analogous compounds identified in trace amounts amongst the products.[9] Formation of these products under restricted diffusion can be explained by reactions of the ≈PhOCH•Ph radical intermediate (Eq. 5), which is formed in Eqs. 3-4 by hydrogen abstraction. This radical can undergo a 1,2-phenyl shift to form ≈PhCH(Ph)O• followed by loss of hydrogen (Eq. 5a) to form the benzophenone, or hydrogen abstraction (Eq. 5b) to form the benzhydrol. The 1,2-phenyl migration from oxygen to carbon proposed in Eq. 5 has been detected previously in the thermolysis of other aryl alkyl ethers.[14] The retrograde molecular rearrangement process shown in Eq. 5 is clearly promoted by the restrictions on molecular diffusion, and a similar rearrangement pathway was observed previously to be the dominant reaction in the thermolysis of surface-immobilized

bibenzyl {≈$PhCH_2CH_2Ph$ → ≈$PhCH(Ph)CH_3$}.[12] For ≈BPE, the benzophenone and benzhydrol products also contain reactive functional groups that can also become involved in additional retrograde reactions (reduction to diphenylmethane linkages, adduction to aromatics, formation of complex cyclic ethers, etc.) under coal processing conditions.[6,7,15] Finally, the hydrogen required for formation of the unexpected hydrocracked products (Eq. 6) likely arises from the formation of the aldehyde and ketone products (principally the benzophenone (Eq. 5a)) and the benzylation of aromatics such as ≈BPE (Eq. 7).

CONCLUSIONS

Thermolysis of benzyl phenyl ether under conditions of restricted mass transport has been found to produce a dramatically different product distribution compared with fluid phases. Two significant retrograde, free-radical reaction pathways are found to be promoted for ≈BPE under these conditions. Radical coupling at phenolic ring positions is observed to be substantially enhanced as a consequence of restricted diffusion for ≈PhO• radicals compared with fluid phases. A second, kinetically competitive retrograde reaction not observed in fluid phases involves rearrangement *via* ≈PhOCH•Ph intermediates to form benzophenone and benzyhydrol products in significant yields. The sum of these two retrograde processes accounts for a remarkable 50-54 mol % of the products at 275 °C. In addition to forming more stable diphenylmethyl-type bridges, these two processes also generate reactive hydroxyl and keto functionalities that can be involved in secondary retrograde reactions. Current research is exploring the effect of surface coverage and reaction temperature on the rate of ≈BPE thermolysis and on the selectivity for these two retrograde pathways.

ACKNOWLEDGEMENTS

Research sponsored by the Division of Chemical Sciences, Office of Basic Energy Sciences, U.S. Department of Energy under contract DE-AC05-96OR22464 with Oak Ridge National Laboratory, managed by Lockheed Martin Energy Research Corp.

REFERENCES

1. Buchanan, III, A. C.; Britt, P. F. *Prepr. Pap., Am. Chem. Soc., Div. Fuel Chem.* **1994**, *39*, 22.
2. Malhotra, R.; McMillen, D. F. *Energy Fuels* **1993**, *7*, 227.
3. McMillen, D. F.; Malhotra, R. *Prepr. Pap., Am. Chem. Soc., Div. Fuel Chem.* **1992**, *37*, 385.
4. Eskay, T. P.; Britt, P. F.; Buchanan, III, A. C. *Energy Fuels* **1996**, *10*, 1257.
5. Manion, J. A.; McMillen, D. F.; Malhotra, R. *Energy Fuels* **1996**, *10*, 776.
6. Poutsma, M. L.; Dyer, C. W. *J. Org. Chem.* **1982**, *47*, 3367.
7. McMillen, D. F.; Chang, S.-J.; Nigenda, S. E.; Malhotra, R. *Prepr. Pap., Am. Chem. Soc., Div. Fuel Chem.* **1985**, *30*, 414.
8. Meyer, D.; Nicole, D.; Delpuech, J. J. *Fuel Proc. Technol.* **1986**, *12*, 255.
9. Sato; Y.; Yamakawa, T. *Ind. Eng. Chem. Fundam.* **1985**, *24*, 12.
10. King, H.-H.; Stock, L. M. *Fuel* **1984**, *63*, 810.
11. Korobkov, V. Y.; Grigorieva, E. N.; Bykov, V. I.; Senko, O. V.; Kalechitz, I. V. *Fuel* **1988**, *67*, 657.
12. Buchanan, III, A. C.; Dunstan, T. D. J.; Douglas, E. C.; Poutsma, M. L. *J. Am. Chem. Soc.* **1986**, *108*, 7703.
13. Britt, P. F.; Buchanan, III, A. C.; Malcolm, E. A.; Biggs, C. A. *J. Anal. Appl. Pyrol.* **1993**, *25*, 407.
14. Britt, P. F.; Buchanan, III, A. C.; Malcolm, E. A. *J. Org. Chem.* **1995**, *60*, 6523.
15. Choi, C.-Y.; Stock, L. M. *J. Org. Chem.* **1984**, *49*, 2871.

Products From Pyrolysis of Silica-Immobilized Benzyl Phenyl Ether

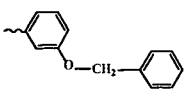

(0.25 mmol/g)

where

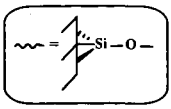

PRODUCT (mol %)	275 °C, 90 min 9.7 % convn. 99.4 % mass bal.	275 °C, 360 min 25.5 % convn. 97.8 % mass bal.	300 °C, 30 min 17.9 % convn. 101.1 % mass bal.	325 °C, 10 min 22.7 % convn. 92.6 % mass bal.
	21.6	24.3	24.0	25.6
	11.0	11.1	11.0	11,9
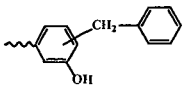	29.0	26.7	28.5	27.7
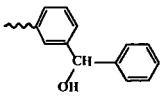	12.5	12.2	10.0	10.4
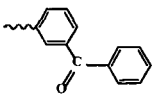	11.6	12.4	10.2	9.6
	2.6	2.4	3.0	4.0
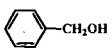	3.6	3.4	3.1	2.5
	1.9	1.5	1.8	2.1
	1.8	1.5	2.0	2.5
	1.5	1.3	2.0	2.5
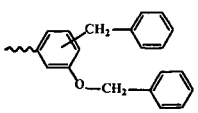	1.6	0.9	1.5	0.6

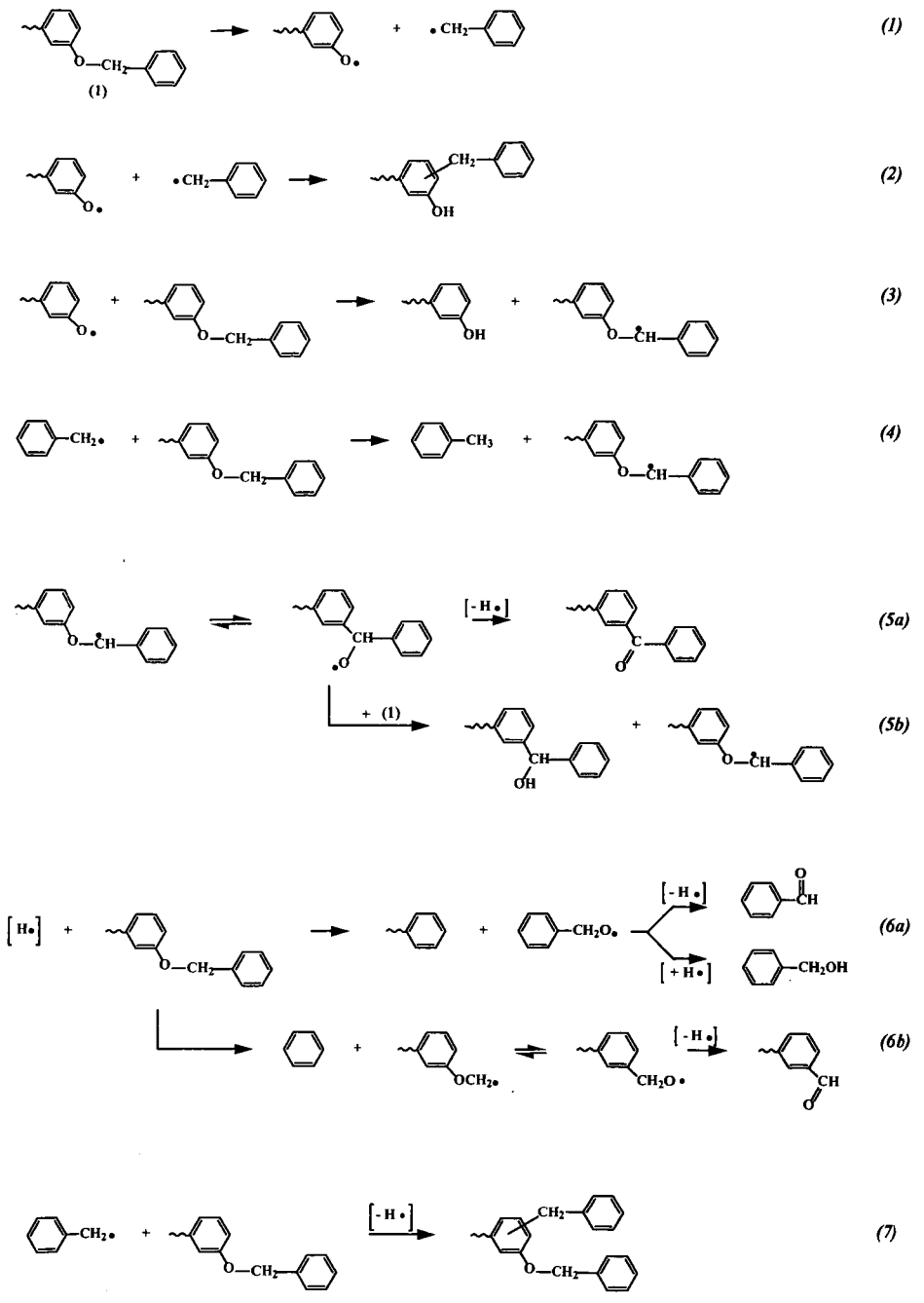

Figure 1. Proposed Reaction Mechanism For Principal Product Formation

INVESTIGATION OF THE ROLE OF AROMATIC CARBOXYLIC ACIDS IN CROSS-LINKING PROCESSES IN LOW-RANK COALS.*

Thomas P. Eskay, Phillip F. Britt, and A. C. Buchanan, III
Chemical and Analytical Sciences Division, Oak Ridge National Laboratory
P.O. Box 2008, MS-6197, Oak Ridge, Tennessee 37831-6197

Keywords: Carboxylic acids, Cross-Linking, Decarboxylation

INTRODUCTION

In recent years, oxygen functional groups in low-rank coals have clearly been shown to be the major actors in retrograde reactions that inhibit efficient thermochemical processing of low-rank coals. In the pyrolysis and liquefaction of low-rank coals, low-temperature cross-linking reactions have been correlated with the loss of carboxyl groups and the evolution of CO_2 and H_2O [1,2]. Pretreatments such as methylation, demineralization, or ion-exchange of the inorganic cations reduce cross-linking and CO_2 evolution in pyrolysis [2a,3a]. In pyrolysis and liquefaction, the exchange of Na^+, K^+, Ca^{++}, or Ba^{++} into demineralized coal increases cross-linking and CO_2 evolution [3,4]. Solomon et al. has modeled cross-linking in coals by including one cross-link for every CO_2 evolved [2a], while Niksa has modeled the evolution rates and yields of oxygen-containing species by including char links when non-condensable gases are expelled [5]. These results suggest that decarboxylation may occur by a pathway that initiates retrograde (cross-linking) reactions in the coal polymer. However, the mechanism by which decarboxylation occurs in low-rank coals is not known. Hence, it is not clearly understood how decarboxylation leads to cross-linking beyond the suggestion that decarboxylation could be a radical process that involves radical recombination or radical addition reactions. However, the role of decarboxylation in cross-linking processes has been brought into question by Manion et al. by their observation that the decarboxylation of benzoic acid derivatives in tetralin yielded only small amounts of aryl-aryl coupling products [6]. Further, we have recently conducted a study of the pyrolysis of 1,2-(3,3'-dicarboxyphenyl)ethane (**1**) and 1,2-(4,4'-dicarboxyphenyl)ethane (**2**) and found that decarboxylation occurs readily between 350-425 °C with no evidence of coupling products or products representative of cross-links [7]. We proposed that decarboxylation occurred primarily by an acid-promoted cationic pathway, and the source of acid was a second carboxylic acid (eq 1). The possible involvement of decarboxylation by a free-radical pathway was ruled out with our finding that no deuterium (<5 mol %) was incorporated into the aryl ring following decarboxylation of 1,1,2,2-tetradeuterio-1,2-(3,3'-

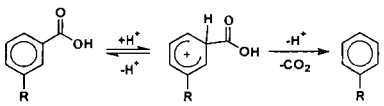

(1)

dicarboxyphenyl)ethane at 400 °C [7a,b]. The decarboxylation of **1** and **2** was also investigated in diphenyl ether and naphthalene as inert diluents. In each solvent, the rate of decarboxylation dropped by roughly a factor of 2 upon dilution from the neat liquid to *ca.* 0.4 mole fraction of acid, but further dilution had no effect on the rate, which is contrary to a bimolecular reaction mechanism. This could be a consequence of hydrogen bonding or an intramolecular protonation. Molecular mechanics calculations indicated that **1** and **2** can adopt an appropriate conformation for internal proton transfer from a carboxy group on one ring to the second aryl ring without a significant energy penalty. In addition, the dicarboxylic acid could internally hydrogen bond, which may further complicate the reaction mechanism. Therefore, we have conducted a study of the pyrolysis of a monocarboxybibenzyl, 1-(3-carboxyphenyl)-2-(4-biphenyl)ethane (**3**), to determine if decarboxylation occurs by an ionic pathway in the absence of intramolecular pathways.

---

* Research sponsored by the Division of Chemical Sciences, Office of Basic Energy Sciences, U.S. Department of Energy, under Contract DE-AC05-96OR22464 with Oak RidgeNational Laboratory, managed by Lockheed Martin Energy Research Corp. T.P.E. was supported in part by an appointment to ORNL Postdoctoral Research Associate program administered jointly by Oak Ridge Institute for Science and Education and ORNL.

EXPERIMENTAL

1-(3-carboxyphenyl)-2-(4-biphenyl)ethane (**3**) was synthesized as described previously [7d]. The anhydride of **3** was synthesized via dicyclohexylcarbodiimide (DCC) coupling of **3** in THF. 1-(3-carboxaldehydephenyl)-2-(4-biphenyl)ethane (**7**) was synthesized by reduction of **3** to the benzyl alcohol with $LiAlH_4$ followed by oxidation to the aldehyde with pyridinium chlorochromate (PCC). 1-(3-(1-naphthyl)phenyl)-2-(4-biphenyl)ethane (**5**) was synthesized by $Pd(PPh_3)_4$ coupling of 1-naphthylboronic acid and 1-(3-bromophenyl)-2-(4-biphenyl)ethene followed by hydrogenation to the bibenzyl with Pd/C. Full details of these syntheses will be reported later. Naphthalene (Aldrich, 99.9 %) was used without further purification. Gas chromatography analysis was performed using a Hewlett-Packard 5890 Series II gas chromatograph equipped with a J&W Scientific 30 m x 0.25 mm id, 0.25 μm film thickness DB-1 column and a flame ionization detector. Mass spectra were obtained at 70 eV on a Hewlett-Packard 5972 GC/MS equipped with a capillary column identical to that used for GC analysis. Reverse phase HPLC was obtained using a Water's 600E System equipped with a Nova-Pak C18 3.9 mm x 150 mm column (4μm particle size), and a Water's 996 Diode Array detector using a solvent mixture of 50:50 CH_3CN:H_2O for 10 min then a linear gradient to 90:10 CH_3CN:H_2O at 25 min. Analysis of HPLC data was performed using Water's Millenium software.

Pyrolyses. Pyrolyses in naphthalene were performed by loading pyrex tubes with the appropriate amounts of carboxylic acid and naphthalene and conducting 3 freeze-pump-thaw cycles prior to sealing the tube at 10^{-5} Torr. Neat pyrolyses were performed in an analogous manner with the omission of naphthalene.The pyrolyses were performed in a Carbolite tube furnace, which maintained a temperature of 400 $\pm$ 1 °C. Following the pyrolysis, the samples were quickly removed from the furnace and cooled in liquid N_2. The tubes were cracked open, and the solid products were removed with a 2:1 mixture of pyridine:N,O-bis(trimethylsilyl)trifluoroacetamide (BSTFA). Internal standards (2-phenylbenzoic acid and 3,5-dimethylbenzoic acid) were added and the reaction mixtures analyzed by GC and GC-MS. The identities of products from the thermolysis of **3** were determined by GC-MS analysis and were further confirmed by comparison with commercially available or synthesized authentic materials.

RESULTS AND DISCUSSION

Thermolyses of **3** were conducted in sealed, evacuated pyrex tubes at 400 °C. The products identities were determined by GC-MS and comparison with authentic materials, either commercially available or independently synthesized, and the reaction products were quantitated by GC. The major products from the thermolysis of neat **3** are shown in equation 2, and a typical

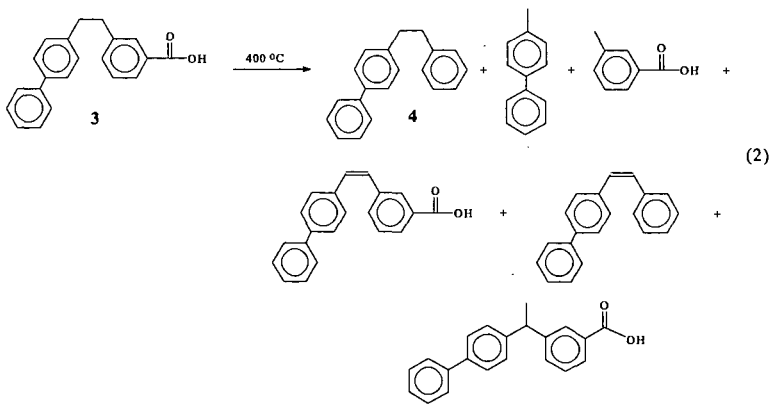

(2)

product distribution for a 1 h pyrolysis is given in Table 1, entry 1. Product distributions were similar at higher conversions and mass balances were good (97 % at 40 % conversion). Several other products are formed in the pyrolysis that have not been identified, but based upon the GC

peak area and the good mass balance, the amount of these products are small (<2 mol %).

As observed with diacids **1** and **2** (see Introduction [7]), decarboxylation is the dominant process in the pyrolysis of **3**. The excellent mass balances establish that the decarboxylation pathway does not lead to any significant amounts of coupling or cross-linking products not detected by our analysis. The apparent first-order rate constant for decarboxylation of **3** to 1-(phenyl)-2- (4-biphenyl)ethane (**4**) at 400 °C was 2.8 ● 0.7 x 10^{-5} s^{-1}, which is similar to the rate constant for decarboxylation of **1** (3.7 ± 0.2 x 10^{-5} s^{-1}). Based on the similar rate constants for decarboxylation and the similar products distributions of the monoacid and diacids, we propose that the decarboxylation of neat **3** is occuring primarily by the acid-promoted cationic mechanism as previously proposed for the decarboxylation of **1** and **2** (eq 1).

The study of the thermolysis of **3** was extended to dilution (10-fold) in a non-donor solvent, naphthalene, to better mimic the environment of carboxylic acids in coal. The major products from the thermolysis at 400 °C were the same as in the neat pyrolysis (see Table 1, entries 2 and 3), and the mass balances were excellent indicating that we are not missing any significant amount of unidentified products. In naphthalene, there is a small shift in the product distribution as a consequence of a decrease in the rate for the bimolecular decarboxylation reaction while the rate of C-C homolysis remained roughly constant. In addition, two new minor products (< 3 mol %), **5** and **6**, were identified in which naphthalene was grafted onto **4**. The identity of these new products was determined from MS, and the point of attachment to the

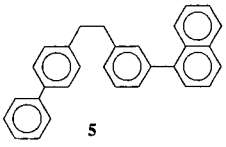

5

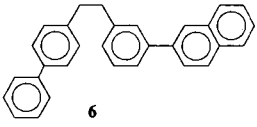

6

aromatic ring was confirmed by independent synthesis of **5**. Similar arylated products were also observed in the thermolysis of **1** diluted in naphthalene (10-fold). Specifically, the major product from the thermolysis of **1** at 400 °C for 45 min was monoacid (59 %), but a small amount of naphthylated products was found (2.7 %). The yield of **5** and **6** was reduced 2-fold by the thermolysis of **3** in a mixture of naphthalene:tetralin (1:1), when compared to a pyrolysis in naphthalene:biphenyl (1:1), indicating the pathway for arylation may involve the formation of an aryl radical as shown in equation 3. Stein has studied the free-radical reaction of aryl radicals, formed from the decomposition of aromatic aldehydes, with aromatic rings in the gas phase at

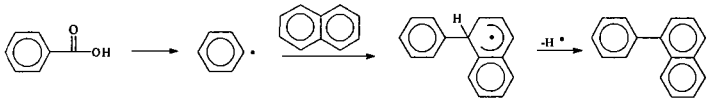

(3)

400 and 450 °C [8]. To investigate if **5** and **6** could arise from a free-radical pathway, we studied the pyrolysis of 1-(3-carboxaldehydephenyl)-2-(4-biphenyl)ethane, (**7**). The aryl radical can be produced by homolysis of the benzylic C-C bond of **7** to form benzyl radicals, hydrogen abstraction from the aldehydic hydrogen, followed by rapid decarbonylation. Pyrolysis of **7** under the same dilution conditions used for the acid (10:1, naphthalene:**7**) produced 4:**5**:**6**, as the major products in a ratio of 1.0:1.1:1.0, respectively (eq 4), showing that **5** and **6** can arise via a

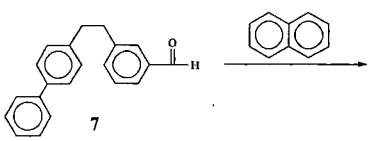

7

4 + 5 + 6 (4)

free-radical pathway. On the basis of the product distribution, the ratio of arylation to hydrogen abstraction by the aryl radical is 2:1. However, in the pyrolysis of **3** in naphthalene, >8 times more **4** is produced than arylated products (**5** and **6**) indicating that the majority of the decarboxylation (>80%) can not be produced by a radical pathway, which is consistent with our proposal that an ionic decarboxylation mechanism is dominant.

Formation of **5** and **6** from pyrolysis of **3** suggests that aryl radicals are formed during the pyrolysis. On the basis of bond strengths, it is unlikely that abstraction of hydrogen from the carboxylic acid (O-H 101 kcal/mol [9]) by benzylic radicals (from C-C homolysis of **3**) would be competitive with hydrogen abstraction from the benzylic hydrogens of **3** (86 kcal/mol [10]). At this point, it was unclear how aryl radicals could arise in the pyrolysis of **3**. However, it was later shown that water could affect the yields of **5** and **6**. The results of two runs in which 1.6 and 3.5 eq of H_2O:**3** were added are shown in Table 1, entries 4 and 5. These results show that there is *ca.* 2-3-fold reduction in the rate of formation of these coupled products with H_2O present. Water did not have any influence on the ratio of **4**:**5**:**6** in the pyrolysis of **7**:naphthalene:H_2O (1:10:1.5 molar ratio), indicating that the water does not inhibit the arylation reaction. Therefore, the reduction of products **5** and **6** with the addition of H_2O demands that their formation must come from a pathway that is inhibited by H_2O. One possible route to the formation of an aryl radical that would be sensitive to water is through the decomposition of an anhydride formed from the coupling of two carboxylic acids. Anhydrides are known to be formed if carboxylic acids (such as benzoic acid) are heated under conditions that remove H_2O [11]. As shown in equation 5, homolysis of the C-O bond of the anhydride would produce fragments that could decarboxylate and decarbonylate to form two aryl radicals. Although thermochemical estimates predict that

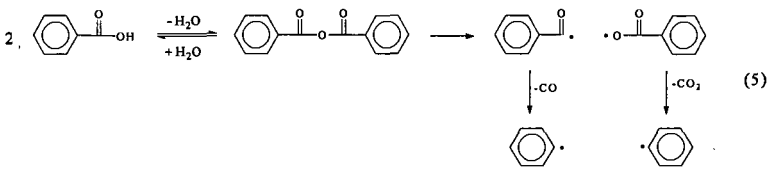

(5)

benzoic anhydride should not decompose by this pathway to any significant extent at 400 °C, we investigated the pyrolysis of benzoic anhydride diluted in naphthalene to determine if the reaction pathway outlined in equation 5 can occur at a reasonable rate at 400 °C (Table 2). Suprisingly, benzoic anhydride decomposed at an average rate of 12 %/h to benzene and 1-and 2-phenylnaphthalene, which is consistent with the formation of aryl radicals from the anhydride decomposition. Furthermore, the radical nature of the anhydride decomposition is supported by the formation of small amounts of binaphthyls in the pyrolysis: i.e. naphthyl radicals are formed by abstraction of hydrogen by an aryl radical or hydrogen atom, followed by coupling with a second naphthalene. Hence, if an anhydride could be formed in the pyrolysis of the acids, it appears it could produce phenyl radicals by its decomposition under these reaction conditions.

Because it is unlikely that the anhydride would be detectable by GC, we investigated whether the anhydride of **3** was formed during the pyrolysis of **3** in naphthalene by HPLC. In the pyrolysis of **3**:naphthalene (1:4), at 400 °C for 1.5 h, a small amount of anhydride was found. The amount of anhydride is currently unquantified but most likely its formation is ~1% of the starting amount of **3** based on peak area. This is supported by the excellent mass balances obtained in these pyrolyses (Table 1), which do not include the anhydride. The identity of the anhydride was confirmed by comparison of the HPLC retention time of the product formed in the pyrolysis with an authentic sample of the anhydride prepared by independent synthesis. While the anhydride was detected without H_2O added, the addition of H_2O (1.5 eq to **3**), inhibited the formation of the anhydride. These results show that the anhydride can be formed in the pyrolysis of **3**, its formation is inhibited by H_2O, and benzoic anhydride decomposes at a reasonable rate to produce arylated products. More importantly, if we estimate that the conversion of the anhydride of **3** will be the same as benzoic anhydride, only ~1-3 % of the starting acid needs to be converted to the anhydride to produce the amount of coupling products observed in the pyrolysis as shown in Table 1. This calculation does not take into account any chain chemistry that may also be operating as a result of anhydride decomposition in the presence of carboxylic acids that could potentially lower the amount of anhydride needed to produce the coupling products.

SUMMARY AND CONCLUSION

The pyrolysis of **3** was studied both neat and diluted in naphthalene to determine the role of thermal decarboxylation in the thermal processing of low-rank coal. The mechanism of decarboxylation proceeds primarily by an acid-promoted ionic pathway that does not lead to cross-linking or coupling products. However, with a 10-fold dilution in naphthalene, 10-15 % of

the carboxylic acid lost can result in a cross-link by a pathway involving the formation of an aryl radical at the ring position of the carboxylic acid. The radical pathway can be reduced by a factor of 2 either by tetralin (in 1:1 mixtures with naphthalene) or H_2O. These preliminary results indicate that the radical pathway, in part, arises as a result of the formation and decomposition of the anhydride of **3**. Further studies on the mechanism of the anhydride decomposition pathway and the influence of the anhydride decomposition in the presence of aromatic carboxylic acids are currently in progress. In addition, we are investigating further why the cross-linking is not evident in the pyrolysis of neat **3**.

In reference to the behavior of low-rank coals, the results of this study suggest that carboxylic acids may lead to a small amount of cross-linking; however, it appears unlikely that the majority of acid decarboxylations produce a cross-link. If it is true that a cross-link is made in coal for every CO_2 evolved, there must be additional chemistry other than decarboxylation involved in cross-link formation. In addition, it is likely that the aromatic carboxylic acids in low-rank coals are contained on rings that contain electron donating groups, such as methoxy groups. The presence of these electron-donating substituents should increase the rate of decarboxylation by the ionic pathway, which could further minimize the amount of cross-linking observed from carboxy groups. However, while the results of this paper and our previous papers have established a framework for understanding the thermal chemistry of carboxylic acids, it should be realized that the results from our model compounds do not consider the restricted mass transport that would exist in coal. In addition, the carboxylic acids in low-rank coal may be present as carboxy salts and not as free carboxylic acids. These features need to be further explored before the role of decarboxylation and cross-linking can be fully evaluated.

REFERENCES

1. Suuberg, E.M.; Lee, D.; Larsen, J.W. *Fuel* **1985**, *64*, 1668.
2. (a) Solomon, P.R.; Serio, M.A.; Despande, G.V.; Kroo, E. *Energy Fuels* **1990**, *4*, 42. (b) Ibarra, J.V.; Moliner, R.; Gavilan, M.P. *Fuel* **1991**, *70*, 408.
3. (a) Serio, M.A.; Kroo, E.; Chapernay, S.; Solomon, P.R. *Prepr. Pap.-Am. Chem. Soc. Div., Fuel Chem.* **1993**, *38(3)*, 1021. (b) Serio, M.A.; Kroo, E.; Teng, H.; Solomon, P.R. *Prepr. Pap.-Am. Chem. Soc., Div. Fuel Chem.* **1993**, *38(2)*, 577.
4. Joseph, J.T.; Forria, T.R. *Fuel* **1992**, *71*, 75.
5. Niksa, S. *Energy Fuels* **1996**, *10*, 173.
6. (a) Manion, J.A.; McMillen, D.F.; Malhotra, R. *Prepr. Pap.-Am. Chem. Soc., Div. Fuel Chem.* **1992**, *37(4)*, 1720. (b) Manion, J.A.; McMillen, D.F.; Malhotra, R. *Energy Fuels* **1996** *10*, 776.
7. (a) Eskay, T.P; Britt, P.F.; Buchanan, III, A.C. *Prepr. Pap.-Am. Chem. Soc., Div. Fuel Chem.* **1996**, *41(2)*, 739. (b) Eskay, T.P; Britt, P.F.; Buchanan, III, A.C. *Energy Fuels* **1996**, *10*, 1257. (c) Britt, P.F.; Buchanan, III, A.C., Hoenigman, R.L. *Coal Science* Pajares, J.A. andTascon, J. M. D. Eds.; Coal Science and Technology 24; Elsevier Science B.V.: Amsterdam, Netherlands, 1995, 437. (d) Eskay, T.P; Britt, P.F.; Buchanan, III, A.C. *Prepr. Pap.-Am. Chem. Soc., Div. Fuel Chem.* **1996**, *41(3)*, 1084.
8. (a) Fahr, A.; Stein, S.E. *J. Phys. Chem.* **1988**, *92*, 495. (b) Chen, R.H.; Kafafi, S.A.; Stein, S.E. *J. Am. Chem. Soc.* **1989**, *111*, 1418.
9. The bond strength for the O-H bond was calculated using additivity Tables in Benson, S, *Thermochemical Kinetics, Second Edition,* John Wiley and Sons, New York, 1976 and heat of formation of $PhCO_2^{\cdot}$ (-21 ± 2 kcal/mol) In Mortimer, C.T., *Reaction Heats and Bond Strengths,* Pergamon Press, New York, 1962, p. 142.
10. McMillen, D.F.; Golden, D.M. *Ann. Rev. Phys. Chem.* **1982**, *33*, 493.
11. Davison, D.; Newman, P. *J. Am. Chem. Soc.* **1952**, *74*, 1515.

Table 1. Product Distributions from the Pyrolysis of 1-(3-carboxyphenyl)-2-(4-biphenyl)ethane (**3**) at 400 °C for One Hour Under Various Conditions.

Entry	1	2	3	4	5
Product (mole %)[a]	Neat	10 :1 Naph:**3**	10 :1 Naph:**3**	10 :1:1.6 Naph:**3**: H_2O	10 :1: 3.5 Naph:**3**: H_2O
$PhCO_2H$	0.3	0.2	0.2	0.2	nd
3-CH_3PhCO_2H	13.6	24.6	27.0	26.5	26.0
3-$CH_3CH_2PhCO_2H$	0.6	0.9	1.0	0.9	0.6
4-Ph-$PhCH_3$	14.9	25.7	28.0	27.4	27.2
4-Ph-$PhCH_2CH_3$	0.5	0.8	0.9	0.7	0.4
4-Ph-$PhCH(CH_3)Ph$	0.2	0.2	nd	0.1	Nd
4-Ph-$PhCH_2CH_2Ph$ (4)	44.9	27.0	20.2	21.9	25.2
4-Ph-PhCH=CHPh	1.1	0.5	0.5	0.4	0.7
4-Ph-$PhCH_2PhCO_2H$	0.8	0.4	0.4	0.5	nd
4-Ph-$PhCH(CH_3)PhCO_2H$	7.8	4.7	5.0	5.0	3.6
4-Ph-PhCH=CH$PhCO_2H$	15.0	12.3	14.0	15.0	15.2
4-Ph-$PhCH_2CH_2Ph$-3-(1-naphthyl) (**5**)	nd	1.4	1.4	0.6	0.5
4-Ph-$PhCH_2CH_2Ph$-3-(2-naphthyl) (**6**)	nd	1.5	1.4	0.7	0.4
Conversion[b]	12.6	10.8	9.5	10.35	10.0
Mass Balance	98.1 %	100.1	99.7	99.8	100.0

a-Based on products detected and quantified.
b-Conversion based on products recovered.
Naph=naphthalene
nd-not detected

Table 2. Product Distributions from the Pyrolysis of Benzoic Anhydride in Naphthalene (1:10 molar ratio) at 400 °C for 50 min.

Product[a]	Run # 1	Run # 2
Benzene	31 %	30 %
1-Phenylnaphthalene	43 %	39 %
2-Phenylnaphthalene	26 %	31 %
Conversion[b]	14 %	9 %

a-Small amounts of phenyl benzoate and 1- and 2-naphthylphenyl ketone were also formed.
b-Conversion based on products detected.

THERMOLYSIS OF A POLYMER MODEL OF AROMATIC CARBOXYLIC ACIDS IN LOW-RANK COAL

William S. Mungall[†], Phillip F. Britt[‡], A. C. Buchanan, III[‡]
[†]Department of Chemistry, Hope College, Holland, Michigan 49423
[‡]Chemical and Analytical Sciences Division, Oak Ridge National Laboratory
P. O. Box 2008, Oak Ridge, Tennessee 37831-6197

Keywords: cross-linking reactions, pyrolysis mechansisms, polymer pyrolysis

ABSTRACT

To compliment our current investigation into the role that decarboxylation of aromatic carboxylic acids plays in the low-temperature cross-linking of low-rank coals, we are investigating the thermolysis of a polymeric coal model compound to determine if the polymeric network structure of coal can alter the decarboxylation pathways. In this investigation, a bibenzylic polymer, poly-(*m*-xylylene-*co*-5-carboxy-*m*-xylylene), **1**, was synthesized containing 2.3 carboxylic acids per 100 carbons, which is similar to that found in Zapp lignite. The pyrolysis of **1** was compared to poly-*m*-xylylene, **2**, and the methyl ester of **1**, **3**, to determine if the carboxy group enhances cross-linking reactions. The major product from the pyrolysis of **1** at 375 °C or 400 °C for 1 h was a THF insoluble residue (60-75 wt%), while pyrolysis of **2** or the methyl ester of **1** produced only a THF soluble product. The mechanistic pathways leading to cross-linking will be discussed.

INTRODUCTION

In recent years, it has been proposed that oxygen functional groups (i.e. carboxylic acids, phenols, and ethers), prevalent in low rank coals, are major contributors to retrograde reactions that inhibit the efficient conversion of low-rank coals to liquid fuels and chemicals. In the pyrolysis and liquefaction of low rank coals, low-temperature ($T \leq 400$ °C) cross-linking reactions (measured by the solvent swelling technique) have been correlated with the loss of carboxyl groups in the char and the evolution of CO_2 and H_2O [1,2]. The pyrolytic loss of solvent swelling in coal has also been modeled by including one cross-link for every CO_2 evolved [1]. Cross-linking can be reduced by methylation, demineralization, or a hydrogen donor solvent and increased by oxidation or ion-exchanging Na^+, K^+, or Ca^{2+} into a demineralized coal [1]. These results suggest that the reaction pathways that lead to decarboxylation may play an important role in cross-linking. However, the reaction pathways for decarboxylation and cross-linking in low-rank coals are not known. Therefore, to gain a better understanding of the reaction pathways that lead to decarboxylation at temperatures relevant to coal processing, we have studied the pyrolysis of 1,2-(3,3′-dicarboxyphenyl)ethane ($HO_2CC_6H_4CH_2CH_2C_6H_4CO_2H$) neat and diluted in naphthalene or tetralin at 400 °C as a model of free carboxylic acids in low rank coal [3]. In these studies, decarboxylation did not produce any significant amount of coupling or other high molecular weight products that might be indicative of cross-linking reactions. However, recent pyrolysis studies of a monoacid, 1-(3-carboxyphenyl)-2-(4-biphenyl)ethane, diluted in naphthalene have shown the formation of small amounts (<3 mol %) of coupled products. It was proposed that decarboxylation occurred predominantly by an acid promoted ionic pathway. However, it is realized that simple model compounds may not be able to completely portray the complex chemistry and physical environment found in coal. Moreover, a small amount of cross-linking chemistry (1-5%) could go undetected in a simple model compound study (showing up as mass balances slightly less than 100% or a series of small unidentified peaks in a GC or GC-MS trace), but a small amount of cross-linking could have a profound impact on the solvent swelling properties of a complex macromolecule. For example, polystyrene (an organic polymer highly soluble in organic solvents) can be made insoluble by cross-linking with only 1-2 mol % divinylbenzene. Therefore, to determine if a polymeric network can alter the reaction pathways, we have incorporated aromatic carboxylic acids into a polymeric network and studied the pyrolysis of the polymer under a variety of conditions.

In this investigation, we have synthesized poly(*m*-xylylene-*co*-5-carboxy-1,3-xylylene), **1**, as a polymeric model for aromatic carboxylic acids in low-rank coal. The density of carboxylic acid in the polymer, 2.3 carboxylic acids per 100 carbons, is similar to that reported for Beulah-Zap coal, 2.2 acids per 100 carbons [4]. To determine if the carboxy functional group enhances cross-linking reactions, the pyrolysis of **1** will be compared to the unsubstituted homopolymer,

2. Our previous studies on the pyrolysis of carboxy-substituted bibenzyls will also provide useful insights into interpreting the pyrolysis results for **1** [3].

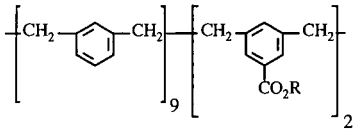

1: R = H
3: R = CH_3

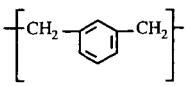

2

EXPERIMENTAL

The synthesis of **1** and **2** has been previously described [5]. The methyl ester of the carboxy polymer, **3**, was prepared by methylation of **1** with an excess of diazomethane. Molecular weight distributions were determined by gel permeation chromatography (GPC) using a Waters chromatography system consisting of a 600E system controller and pump, 717 autosampler, and 410 differential refractometer interfaced to a computer running Waters Millennium 2010 software for GPC analysis. A bank of three columns (Waters Styragel HR1, HR3 and HR5E) were calibrated using six narrow molecular weight standards (polystyrene, Mw 89,300; 25,400; 12,600; 4,000; 687 and bibenzyl, Mw 182) at 32 °C in THF at a flow rate of 1.00 mL/min. The molecular weight, M_N, and polydispersity (M_w/M_N) of **1** and **2** were 11,300 (2.8) and 9900 (2.5), respectively. A similar molecular weight was obtained for the methyl ester **3**. The polymers were characterized by ^{13}C-NMR, FTIR, and elemental analysis. By CP/MAS ^{13}C-NMR, there is one acid per 5.4 ± 0.5 aromatic rings or 2.3 acids per 100 carbons. Similar results were obtained by elemental analysis.

In a typical pyrolysis experiment, the polymer (ca. 45 mg) and a small plug of glass wool was loaded into a T-shaped tube (8 mm), the tube was pumped down, and sealed under vacuum (<10^{-5} Torr). One end of the tube was place in a liquid nitrogen trap and the polymer was placed in a Carbolite three zone tube furnace (38 mm ID). The pyrolysis temperature was measured by a RTD thermocouple placed beside the sample, and the temperature was held ±1.0 °C over the sample length. After the reaction, the tube was opened, the glass wool plug was rinsed with THF, and THF (2.0 mL) was added to the pyrolysis residue. The tube was capped and heated to 60-70 °C for 18-24 h. The THF layer was removed and the insoluble residue was washed with THF (2x). The combined washings were concentrated, dried under vacuum, weighed, redissolved in THF, filtered, and analyzed by GPC, GC, and GC-MS. The insoluble residue was dried under vacuum and weighed. The volatile products that collected in the cold trap were dissolved in CH_2Cl_2 (1.0 mL) containing an internal standard (pentamethylbenzene), and analyzed by GC and GC-MS.

Infrared spectra were recorded on a Bio-Rad FTS-60 FT-IR in a KBr matrix or as a thin film formed by pressing the polymer melt between Teflon sheets. TGA was performed on a Sinku-Riko differential thermal-galvimetric analyzer TGD 7000 and TGA-MS was performed on a TGD 7000 interfaced to a VG mass spectrometer. The heating rate for the TGA and TGA-MS experiments was 5 °C min^{-1} and the experiments were run under argon. Samples sizes were typically 10-25 mg for these experiments.

RESULTS AND DISCUSSION

Figure 1 show the weight loss curves for **1**, **2**, and **3** at a heating rate of 5 °C min^{-1} under argon. The thermograms for the three polymers are very similar: weight loss starts at ca. 400 °C with the major degradation occurring between 425 - 500 °C. However, the carboxylated polymer forms ca. 2.5 times more char than the unsubstituted polymer. Methylation of the carboxylic acid decreases char formation. A similar trend has been observed in the pyrolysis of lignite coal in which methylation increased tar yield and reduce cross-linking [1]. Figure 2a shows the evolution of volatile materials from the depolymerization of the homopolymer, **2**, by monitoring the benzyl fragment *m/e* 91 ($C_7H_7^+$) from the fragmentation of the pyrolysis products in the mass spectrometer. From the sealed tube pyrolysis of **2** and **1** (see below), the major volatile products identified by GC-MS were monomer (*m*-xylene), dimer, trimer, and tetramer (which contain *m/e* 91 in their mass spectral fragmentation patterns). A similar TGA-MS evolution profile was found for **2** by monitoring the xylylene fragment (*m/e* 105). Figure 2b shows that the evolution of CO_2 (*m/e* 44) from **1** precedes depolymerization of the polymer backbone (by monitoring the benzyl fragment, *m/e* 91). For low-rank coals, a similar trend in gas evolution,

measured by TGA-FTIR, has been reported [1] in which CO_2 evolution precedes tar evolution. To our delight, these simple bibenzylic polymers reproduce many of the qualitative trends found in the pyrolysis of low-rank coals, but in a much simpler matrix such that it may be possible to gain mechanistic insight into specific reaction pathways that lead to cross-linking.

Much of the experimental data on the cross-linking behavior of low-rank coals has been obtain in pyrolysis experiments in which the volatile materials are swept away (sometimes for additional analysis) from the char by an inert gas. To investigate the pyrolysis of **1**, **2**, and **3** under conditions in which the volatile products are removed, the pyrolysis was performed in sealed T-shaped tubes (see experimental) under vacuum in which one leg of the tube was place in a liquid nitrogen trap to remove the volatile products. After pyrolysis, the tubes were broken, THF was added, and the solutions were heated to 60-70 °C overnight (16 h). The soluble and insoluble fractions were separated (if present) and the molecular weight distribution of the soluble fraction was determined by GPC. The results from the pyrolysis of the polymers are summarized in Table 1. Pyrolysis of **1**, **2**, and **3** at 375 °C for 1 h produced very small amounts of volatile products (as anticipated from the TG analysis and the low reactivity of bibenzyl at 375 °C). Analysis by GC and GC-MS found monomer, dimer, trimer, and tetramer as the major products. The residue from the pyrolysis of **2** and **3** was soluble in THF, but a large fraction of the residue from the pyrolysis of **1** was still insoluble in THF. As shown in entries 1, 2, 5-8 in Table 1, pyrolysis of **1** for <60 min at 375 or 400 °C typically produced 60-75 wt% of an insoluble polymer. The reactions that lead to a loss of solubility occur quickly at 400 °C because the yield of insoluble polymer is established after 15 min and does not change significantly except for long reaction times. However, the molecular weight of the THF soluble fraction decreases as the longer reaction times increase as a consequence of C-C homolysis. At very longer reaction times (60 h) at 400 °C, the yield of volatile products increased and some of the insoluble residue was converted to lower molecular weight products, but a significant fraction of the polymer still remained insoluble in THF. In contrast, no insoluble residue was found in the pyrolysis of **2** or **3** at 375 °C or 400 °C even at long reaction times (60 h, see entry 9 Table 1).

These results indicate that cross-linking reactions can occur in the bibenzyl polymer as a consequence of the carboxyl group to produce an insoluble polymer. This is in stark contrast to the results previously obtained in the pyrolysis of simple model compound (1,2-(3,3'-dicarboxyphenyl)ethane) in which no cross-linking was observed [3]. This highlights the importance of the polymeric network in influencing reaction chemistry. When the carboxylic acid is removed or methylated, the pyrolysis residue is completely soluble in THF and the yield of char decreases. The reaction pathways leading to the cross-linking reaction are currently under investigation and the results will be discussed in the presentation.

ACKNOWLEDGMENTS

Research sponsored by the Division of Chemical Sciences, Office of Basic Energy Sciences, U.S. Department of Energy, under contract DE-AC05-96OR22464 with Oak Ridge National Laboratory, managed by Lockheed Martin Energy Research Corp.

REFERENCES

1. (a) Solomon, P. R.; Serio, M. A.; Despande, G. V.; Kroo, E. *Energy Fuels* **1990**, *4*, 42 and references therein. (b) Serio, M. A.; Kroo, E.; Chapernay, S.; Solomon, P. R. *Prep Pap.-Am. Chem. Soc., Div. Fuel Chem.* **1993**, *38(3)*, 1021.
2. Suuberg, E. M.; Lee, D.; Larsen, J. W. *Fuel* **1985**, *64*, 1668.
3. (a) Eskay, T. P.; Britt, P. F.; Buchanan, III, A. C. *Energy Fuels* **1996**, *10*, 1257. (b) Eskay, T. P.; Britt, P. F.; Buchanan, III, A. C. *Prep. Pap.-Am. Chem. Soc., Div. Fuel Chem.* **1996**, *41(2)*, 739. (c) Eskay, T. P.; Britt, P. F.; Buchanan, A. C. III *Prep. Pap.-Am. Chem. Soc., Div. Fuel Chem.* **1996**, *41(3)*, 1084.
4. Jung, B.; Stachel, S. J.; Calkins, W. H. *Prep. Pap.-Am. Chem. Soc., Div. Fuel Chem.* **1991**, *36(3)*, 869.
5. (a) Britt, P. F.; Buchanan, III, A. C.; Hoenigman, R. L. *Coal Science* Pajares, J. A.; Tascon, J. M. D. Eds.; Coal Science and Technology 24; Elsevier; Amsterdam, Netherlands, 1995, 437. (b) Mungall, W. S.; Britt, P. F.; Buchanan, III, A. C. manuscript in preparation.

Table 1. Thermolysis of **1**, **2**, and **3** in sealed tubes under vacuum.

Entry	Polymer[a]	Temp °C	Time min	Volatile Products	THF Soluble	M_w x10^3 [b]	THF Insoluble	Mass Balance
1	**1**	375	60	1 %	41 %	10.8	60 %	102 %
2	**1**	375	60	1 %	31 %	23.2	67 %	99 %
3	**3**	375	60	1 %	93 %	74.7	–[c]	94 %
4	**2**	375	60	1 %	95 %	19.0	–[c]	96 %
5	**1**	400	15	2 %	24 %	7.3	73 %	99 %
6	**1**	400	30	4 %	18 %	4.4	76 %	98 %
7	**1**	400	60	7 %	21 %	3.5	73 %	101 %
8	**1**	400	3600	49 %	7 %	1.3	39 %	95 %
9	**2**	400	3600	26 %	70 %	7.6	–[c]	97 %

[a] M_w of **1**, **2** , and **3** is 31,500, 24,700, and 33,100, respectively. [b] Weight averaged molecular weights determined by GPC vs. polystyrene standards. [c] No insoluble material was detected.

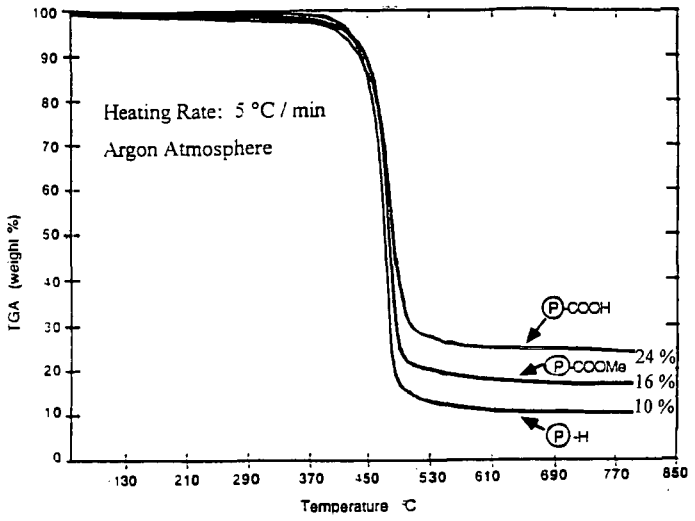

Figure 1. TG curves for polymers **1** (P-COOH), **2** (P-H), and **3** (P-COOMe).

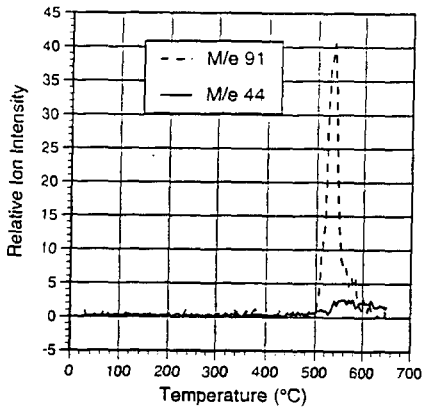

Figure 2a. TG-MS of **2** (P-H) monitoring *m/e* 91 (benzyl fragment) and *m/e* 44 (CO_2).

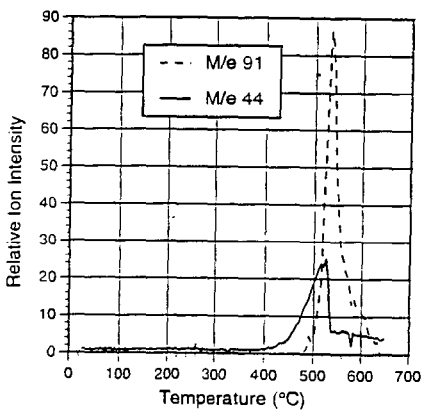

Figure 2b. TG-MS of **1** (P-COOH) monitoring *m/e* 91 (benzyl fragment) and *m/e* 44 (CO_2).

DECARBOXYLATION AND COUPLING REACTIONS OF PHENYLACETIC ACID UNDER COAL-LIQUEFACTION CONDITIONS

Jeffrey A. Manion, Donald F. McMillen, and Ripudaman Malhotra
Molecular Physics Laboratory, SRI International
333 Ravenswood Ave., Menlo Park, California, 94025

INTRODUCTION

The conversion of low-rank coals to liquids or volatile hydrocarbons is known to be substantially hindered by retrograde reaction, and oxygen functional groups in the coal structure are strongly correlated with these retrograde reactions. Carboxyl functions have been implicated in the crosslinking of coals during heating at relatively low temperatures,[1,2] and Solomon et al.[3] have been able to model the pyrolytic loss of solvent swelling by including one additional crosslink in the network for every CO_2 evolved. However, carboxyl groups are not the dominant oxygen-containing moeties, even in low-rank coals, and we suspected hydroxyl functions may play just as large a role, particularly since phenolic -OH in polyhydroxy systems are known to lead to furanic systems under coal liquefaction conditions.[4] Therefore we have examined the rates of decarboxylation some prototypical carboxylic acids to see if crosslinking results directly from decarboxylation, as well as how crosslinking is affected by H-donors, electron transfer reagents, the addition of water, and other conditions relevant to pretreatment and liquefaction of coals.

We have previously reported the decarboxylation and coupling reactions of aromatic carboxylic acids and their calcium salts,[5] and found that little coupling generally followed from these decarboxylations. Generally, fewer than one in ten decarboxylations led to a crosslinking reaction, except in the presence of 1-electron oxidants where, under some non-reducing conditions, one coupling reaction occurred for every two decarboxylations of benzoic acid. Recently Eskay, et al. prepared and studied polymers containing unactivated aromatic carboxylic acids to test whether the presence of a polymeric structure would significantly enhance crosslinking reactions, but they also observed little coupling resulted from decarboxylation of unactivated benzoic acid structures.[6]

For activated aromatic acids, we found that coupling by direct reactions of radical fragments is very low, but coupling as an indirect result of decarboxylation can be very substantial. Loss of the electron-withdrawing carboxyl group from, for example, 2-hydroxybenzoic acid, allows the hydroxy group to exert its full activating effect toward any subsequent subsitution by electrophiles. Thus we showed that by this route, decarboxylation of activated aromatic acids can lead to ring coupling and even to subsequent ring-closure, though not by the radical-coupling routes that are often cited.

Because it is likely that some carboxyl groups in low-rank coals are not attached directly to an aromatic ring, we have extended our examination to the thermal behavior of phenylacetic acid, a prototypical structure with an aliphatic acid side chain. In addition to a very early report on the thermolysis of the neat liquid,[7] there are more recent gas phase studies at high temperature.[8] A recent study of PAA decomposition at 250°C reported that a major pathway for phenylacetic acid decomposition at 250°C involves net elimination of H_2O and CO_2 to form the coupling product dibenzyl ketone (DBK) and proposed a four-membered ring rearrangement of the anhydride to the unstable ß-keto acid, which then easily decarboxylates.[9] The presence of water completely inhibits the ketone formation.

EXPERIMENTAL

Reactions were performed in fused silica ampoules, heated inside a stainless steel pressure jacket, as described previously.[5] Products were analyzed by GC (FID) and GC-MS. The estimated overall accuracy was ±2% in most cases, ±5% for some polar products, and ±12% for phenylacetic acid itself. Phenylacetic acid (99+% by GC analysis), naphthalene (Aldrich 99+%), tetralin (Aldrich, 99%), pyridine (Mallinckrodt, AR grade, 99+% by GC analysis), and Fe_3O_4 powder (particle size ~0.2 µm) were used without further purification.

RESULTS AND DISCUSSION

Decarboxylation Rates and Major Products. Table 1 shows the major thermal decomposition products of PAA in naphthalene/tetralin mixtures. In 1 hour at 400°C, 28 to 43% decarboxylation is observed. The primary products were toluene and dibenzyl ketone (DBK), as described in the literature,[7-9] along with one isomer of tetralylbenzyl ketone (TBK), bibenzyl, and trans-stilbene. Also found were small quantities of benzylnaphthalenes, dihydro-benzylnaphthalenes, phenylnaphthalenes, and an isomer of benzyltetralin. Benzene accounted for less than 0.5% of the PAA that was consumed. We also found coupling products formed entirely from solvent: binaphthyls, bi-tetralyls, their cross products, and partially hydrogenated versions of these compounds. Together, these solvent coupling products accounted for less than 0.5% of the starting acid. Mass balances were generally >97%, except in the two experiments with naphthalene-only solvent, where only 91% of the PAA was accounted for.

Figure 1 shows the changes in the distribution of the main products as the solvent was shifted from naphthalene to tetralin. Decarboxylation of PAA, as measured by toluene formation, decreased by about 25%, but the proportions of toluene and total ketones were not changed significantly.

Mechanism of Decarboxylation. Although the mechanism of the condensed phase thermal decarboxylation of phenylacetic or other aliphatic acids has not, to our knowledege, been fully elucidated, the thermal reaction in the gas phase has been reported to proceed via reactions (1) and (2) at temperatures between 587 and 722°C.[8] Reaction 1 would give toluene in two steps, but its parameters, as selected in a critical review of the work,[10] would dictate a half-life for PAA of about 10,000 h at 400°C.

$$PAA \rightarrow C_6H_5CH_2\bullet + \bullet CO_2H \quad (1)$$

$$PAA \rightarrow C_6H_5CH{=}C{=}O + H_2O \quad (2)$$

This projected half-life is orders of magnitude longer than that actually observed here, and therefore the liquid phase reaction must proceed via another mechanism. Similarly, four-center elimination of water from the phenylacetic acid, as implied by Reaction 2 as written, is unlikely under our conditions because the analogous elimination from acetic acid, for instance, has a very high activation energy (68 kcal/mol[11]). It is more likely that reaction proceeds through an anhydride intermediate, which can eliminate PAA and generate phenyl ketene in a favorable 6-center transition-state (Reaction 3). Radical addition to ketene could then give the observed ketone products. The parameters reported[12] for acetic acid anhydride decomposition, $k/s^{-1} = 10^{12.0 - 7540/T}$, would lead to a half-life of only about a tenth of a second at 400°C, easily fast enough to give the required ketene, provided that the formation of the anhydride is itself facile.

(3)

The anyhydride could be formed via either a concerted or an acid- or base-catalyzed elimination of water. While the formation of toluene is consistent with reaction via $PhCH_2^-$, as previously suggested,[9] the observation of small amounts of 1,2-diphenylethane (1,2-DPE), trans-stilbene, benzylnaphthalenes, and dibenzyl ketone (see below) appear more consistent with the presence of benzyl radicals. Similarly, decomposition of the anhydride to ketene is not limited to a concerted reaction. Since H-atom chain reactions are often, at high temperatures, close competitors to electrocyclic eliminations, the ketene could also be formed from the anhydride by an H-abstraction, ß-scission process to yield phenylacetoxy radical as the companion product. This radical would decarboxylate extremely rapidly, possibly leading to some reaction of its product benzyl radical with ketene before they left the solvent cage. If benzyl radical and ketene are formed exclusively by an H-abstraction, ß-scission process chain process, then the presence of substantial cross products indicates escape from the cage is competitive with cage addition of benzyl radical.

Effect of Donor Solvent on Ketone Formation. As the reaction medium was shifted from naphthalene to tetralin, a gradual four-fold drop in formation of dibenzyl ketone was observed, while a new species, tetralylbenzyl ketone, became a prominent product. This result, shown graphically in Figure 2, suggests that benzyl radicals are increasingly scavenged by tetralin. The formation of cross-products certainly means that DBK does not form exclusively by the sequence of concerted rearrangement to a ß-keto acid, followed by facile decarboxylation, as has been suggested previously.[9] Cross products also mean that radical reaction is not limited to recombination within a cage. Therefore, we suggest instead that dibenzyl ketone is formed in reactions (5) and (6). No rate parameters for (5) have been reported, but the reaction would be expected to be rapid.

$$C_6H_5CH_2CO\bullet \rightarrow C_6H_5CH_2\bullet + CO \quad (4)$$

$$C_6H_5CH_2\bullet + C_6H_5CH{=}C{=}O \rightarrow C_6H_5CH_2(C{=}O)CH\bullet C_6H_5 \quad (DBK\bullet) \quad (5)$$

$$DBK\bullet + RH \rightarrow DBK + R\bullet \quad (6)$$

$$C_6H_5CH_3\bullet + \text{tetralin} \rightleftarrows C_6H_5CH_3 + \text{1-tetralyl}\bullet \quad (7)$$

As tetralin is added to the system, benzyl radicals will be partly scavenged by tetralin, and tetralyl radicals will replace benzyl radicals in Reaction 5 to give tetralyl benzyl ketone, as reflected in the data in Figure 2. Because the 1-tetralyl radical is ~12 kcal/mol more stable than the 2-isomer,[13] the TBK product should be almost entirely 1-tetralyl benzyl ketone, as observed. However, even in pure tetralin, only about 2/3 of the dibenzyl ketone was replaced with tetralylbenzyl ketone. The inability of tetralyl radicals to intercept a greater proportion of the presumed intermediate phenyl ketene needs to be considered carefully because it bears on the hypothesis that this radical addition is the route to benzylphenyl ketone.

Because the equilibrium constant[14] for Reaction 7 is ≥ 10, and because the tetralin was in substantial excess over toluene, it is apparent from the ratio of DBK/TBK (Table 1), that either Equilibrium 7 has not been established, or k_5/k_7 is very large. Estimation of the rates of reactions 5 and 7, based on measured rates of analogous reactions and thermochemical data, suggests that indeed, scavenging of benzyl radical is simply not fast enough to completely outpace its addition to ketene.

The Effect of Added Water. A rationale involving reaction through the anhydride and the corresponding ketene suggests that the addition of water to the reaction mixture should slow the formation of ketones, both through hydrolysis of the proposed anhydride intermediate and by the rapid reaction of phenylketene with water [15] to re-form phenylacetic acid (Reaction -2, above). In partial accord with this expectation, and as Katritzky et al. have reported[9] for lower temperatures, we found that the addition of 34 mol% of water to a mixture of naphthalene and PAA led to more than a seven-fold drop in dibenzyl ketone formation (Table 1). Curiously, however, there is *no* decrease in the rate of decarboxylation: the decrease in ketone formation corresponds almost exactly to the increase in toluene formation. Added water does *not* simply send anhydride or ketene back to acid. Since water with its very strong HO–H bond is a terrible radical scavenger but a good acid, the diversion of ketone to toluene suggests an anhydride-like intermediate whose benzyl fragment can act as a carbanionic species. This reaction would be similar to hydrolysis of the anhydride, except that the $CO–CH_2$ bond would act as the electrophile, rather than the C=O double bond, as occurs in a normal hydrolysis.

Water also caused a three-fold decrease in benzylnaphthalenes and a six-fold decrease in the sum of bibenzyl and stilbene. The system containing water had the lowest coupling/(total reaction) ratio at 0.024. Because bibenzyl and stilbene can plausibly result only from benzyl radical recombination, and because water is a poor radical scavenger, this observation provides additional evidence that water shifts decomposition of PAA more towards ionic pathways, so that fewer radicals are generated in the first place. This explanation would require an intermediate X that decomposes either via radical production or via an ionic pathway: by increasing the rate of the ionic pathway, the steady state concentration of X (and the consequent generation of radicals) is reduced, though the overall decarboxylation rate remains unchanged. Water, acting as an acid, captures an anionic benzyl fragment from the intermediate, increasing the toluene yield and decreasing those products that result from radical reactions.

Non-Ketone Coupling Products. In pure naphthalene solvent, traces of benzylnaphthalenes were observed. When tetralin was added to the naphthalene, we observed increased levels of benzylnaphthalenes, as well as dihydrobenzylnaphthalenes and a single isomer of benzyltetralin [identified by mass spectometry as α-benzyltetralin (1,2,3,4-tetrahydro-1-benzylnaphthalene)]. The absence of significant amounts of benzylnaphthalenes in pure naphthalene presumably reflects the fact that addition of benzylic radicals to aromatic systems forms an initial cyclohexadienyl adduct radical having a very weak C-C bond, and is therefore a highly reversible process. The initial adduct cannot be stabilized unless the ipso-hydrogen is rapidly removed, in a bimolecular fashion, by some H-acceptor species. However, when tetralin is present, a-tetralyl radicals will constitute a significant part of the radical population and can provide additional routes to benzylnaphthalenes.

The marked increase in benzylnaphthalene formation with added tetralin is accompanied by a similar increase in the ratio of 1-benzylnaphthalene/2-benzylnaphthalene. As the reaction medium is shifted from naphthalene to pure tetralin, the yield of benzylnaphthalenes increases by 20X, and the ratio of the 1-isomer to the 2-isomer increases from near 1 to almost 40 (Figure 3). This predominance of 1-benzylnaphthalene, together with the observation that only the α-isomer of benzyltetralin was observed, suggests that in tetralin, 1-benzylnaphthalene is formed predominantly by recombination of benzyl radical with the dominant α-tetralyl radical, followed by dehydrogenation of the α-benzyltetralin. In pure naphthalene, on the other hand, the benzylnaphthalenes are evidently formed only by radical addition to naphthalene, which should show more limited selectivity, though still favoring the 1- position of naphthalene.

The Effect of an Amine Base. The addition of 10 mol% of pyridine to the naphthalene/PAA mixture (Table 1) did *not* increase decarboxylation, but did increase toluene yield by about 20%. The effect is thus different than that observed with benzoic acid, where 10% pyridine increased decarboxylation fourfold.[5] The effect of base on ketone formation was minor, decreasing formation of dibenzylketone by about 10%. More surprising was its effect on the other coupling products. The sum of 12DPE and trans-stilbene was increased a factor of 2.5, and new products appeared, including diphenylmethane (DPM, 0.47%), an isomer of phenylpyridinylethane (0.17%), phenylnaphthalenes (0.12%), pyridinylnaphthalenes (0.13%), and various unidentified coupling products of higher molecular weight. The precise sources of these products are unclear: DPM has been identified by Miller and Stein[16] as a significant product in the *later* stages of neat 1,2-DPE pyrolyis, but they were unable to identify the route to this product. It is not likely to arise from addition of benzyl radicals to benzene, since the formation of the initial adduct would be even more readily reversed than in the benzylnaphthalene case discussed above. Similarly, the formation of phenylnaphthalenes and pyridinylnaphthalenes suggests that the generation of aryl radicals from the solvent components is somehow being promoted by pyridine. Although we

observed similar coupling products in the case of decarboxylation of aromatic acids,[5] in that case the addition of pyridine actually resulted in a *lower* total yield of products most easily attributable to radicals.

The Effect of Fe_3O_4. In the previous study of aromatic acids, we had found that under some conditions the addition of electron transfer agents, which may be present in coals as inorganic components, increased the rates of decarboxylation and coupling. Fe_3O_4 was the most effective of these agents at promoting coupling, and therefore we examined its effect on the decarboxylation and coupling of PAA. The effects of iron oxide on the course of the reaction were somewhat different, depending on whether the solvent was pure naphthalene, or contained a donor component. When the solvent was naphthalene only, addition of 10 mol% Fe_3O_4 doubled the total conversion of PAA, but resulted in little or no increase in the "major" products: dibenzyl ketone was unchanged, and toluene increased only 25%. Most of the additional conversion resulted in various "minor" coupling products, which were increased to the point where they constituted, in total, about half of the coupling products. The sum of bibenzyl and t-stilbene was increased by a factor of nearly 25 when compared to the case without added Fe_3O_4. Benzylnaphthalenes were increased by a factor of 45, with both isomers now found in similar quantities. Perhaps most surprising was the presence of phenylnaphthalenes, not formed at all without added Fe_3O_4, but now found at about 75% of the level of the benzylnaphthalenes. A new ketone, benzylphenyl ketone, was found at about 10% of the level of dibenzyl ketone.

When the solvent contained tetralin, Fe_3O_4 roughly doubled the fractional conversion of PAA, as it had in pure naphthalene solvent, but with the donor present, dibenzyl ketone was increased by 300%! Toluene and most of the minor coupling products, such as benzylnaphthalene and phenylnaphthalene, decreased significantly. This effect can also be stated in terms of tetralin addition: in the absence of Fe_3O_4, tetralin addition suppresses dibenzyl ketone by ~70% (essentially replacing it with tetralylbenzyl ketone), but when Fe_3O_4 is present, tetralin addition increases dibenzyl ketone by 300%.

Evidently, Fe_3O_4 increases the number of decomposition intermediates, or complexes, regardless of whether tetralin is present. If tetralin isn't present, then most of these decomposition intermediates go on to generate radicals that are distributed in the bulk of the solvent, and therefore primarily give coupling products that involve one or two solvent molecules. However, when tetralin is present, it evidently can prevent escape of benzyl radicals from the "cage" of decomposition intermediates, and send most of the intermediates to dibenzylketone. If the last step in ketone formation from PAA is indeed radical addition to phenyl ketene, then stabilization of the adduct requires transfer of a hydrogen *to* that adduct; tetralin would clearly help to provide this hydrogen. This case is in curious contrast to the "normal" case of retrograde reaction, where addition to an aromatic ring system requires H-removal *from* the initial adduct in order to achieve a stable, aromatic coupling product. In that case, formation of a stable adduct is most facilitated by a hydrogen *acceptor*, rather than a hydrogen *donor*.

Implications for Coal Liquefaction and Gasification. Because of its ca. 1-h half life at 400°C, phenylacetic acid, and by extension, other short chain fatty acids, are probably not related to the coal species that undergo rapid decarboxylation below ca. 400°C. Thus, barring substantial promotion of decarboxylation rates by indigenous coal substances, these aliphatic acids appear unlikely to account for the crosslinking at mild conditions that has been observed for low-rank coals. Such decarboxylation would appear to be limited to aromatic acids activated by hydroxy substitution. On the other hand, the primary coupling reactions of PAA, which lead to ketones, and the secondary coupling reactions, which lead to alkyl-aryl and aryl-aryl coupling products through addition of substrate- and solvent-derived radicals, could well contribute to retrograde reactions that occur between 400 and 450°C. Such ketone formation is expected to be quite general for other fatty acids possessing α-hydrogens. In coal structures, these reactions that require two acid groups may be restricted by limited availability of other acid functionalities in the nearby coal matrix. In fact, the opportunity to form retrograde products via anhydride intermediates could help to explain how such products are enhanced when divalent metal cations are ion-exchanged into low-rank coals, forming di-acid salts. The observed diversion by water of dibenzyl-ketone-forming intermediates to toluene could also help to explain some of the reported benefits[17,18] of added water on coal liquefaction.

Decarboxylation to generate radical species which then undergo simple recombination reactions or addition to aromatic rings appears to be directly responsible for only a limited amount of coupling, with generally less than one crosslink for every ten decarboxylations of PAA. These radical-recombination or addition routes can be partially controlled through the use of H-donors. As the solvent composition is shifted from pure aromatic to hydroaromatic, the dominant route to alkyl-aryl coupling products can be seen to shift from radical addition to radical recombination, where the bulk of initial recombination products survive at 400°C only because aromatization enormously increases adduct bond strength.

The electron transfer agent Fe_3O_4 caused a two-fold enhancement of decarboxylation, but because it seems to primarily enhance radical pathways, resulted in a four-fold enhancement of coupling products. In the presence of Fe_3O_4, added tetralin caused a dramatic enhancement of dibenzyl

ketone formation rates. This unexpected effect, presumably a result of enhanced trapping of a cage addition product, provides yet another illustration of fact that "hydrogen transfer" is not always good for liquefaction, in that it is equally necessary for both the formation and the scission of strong bonds.

SUMMARY AND CONCLUSIONS

Phenylacetic acid in naphthalene at 400°C undergoes about 25% decarboxylation in one hour, intermediate to the rates of the activated and unactivated aromatic acids. The rate decreases about 25% as the solvent medium is switched to tetralin, but is essentially unchanged by the addition of amine base or water. The major coupling products of PAA are dibenzylketone (DBK) and, when tetralin was present, tetralylbenzyl ketone (TBK), probably formed from reaction of phenylketene with benzyl and tetralyl radicals, respectively. Smaller amounts of 1,2-diphenylethane, trans-stilbene, benzylnaphthalenes, and benzyltetralins are also formed. Total coupling is between 14-23% of reaction except in the presence of added water, where the coupling was reduced to about 2%. The ketones account for 40-90% of the coupling products, with the percentage decreasing as tetralin is added. Only ~2 to 15% of the total retrograde products result from actual recombination of the parent benzyl radicals, the commonly invoked retrograde reaction.

Water inhibits the formation of the ketones without decreasing the extent of decarboxylation, presumably by diverting intermediates that could have led to anhydride or ketene formation. Other coupling products evidently result from radical recombination or addition/elimination reactions. The one-electron oxidant Fe_3O_4 caused a two-fold increase in decarboxylation and a more substantial increase in products expected from radical reactions. Fe_3O_4 added to naphthalene had little effect on DBK formation, but Fe_3O_4 added in the presence of tetralin markedly increased the formation of DBK and increased the ratio of coupling/(total reaction) to about 0.5, independent of the amount of tetralin present (at tetralin > 10%). In the presence of tetralin and Fe_3O_4, about 80% of the total coupling was due to formation of DBK.

REFERENCES

1. Suuberg, E. M.; Lee, D.; Larsen, J. W.; *Fuel* **1985**, *64*, 1668.
2. Serio, M. A.; Hamblen, D. A.; Markham, J. R.; Solomon, P. R. *Energy Fuels* **1987**, *1*, 138.
3. Solomon, P. R.; Serio, M. A.; Deshpande, G. V.; Kroo, E., *Energy Fuels* **1990**, *4*, 42.
4. McMillen, D.F.; Chang, S.-J.; Nigenda, S. E.; Malhotra, R. *Am. Chem. Soc. Div Fuel Chem. Preprints* **1985**, *30(4)*, 414.
5. Manion, J. A.; McMillen, D. F.; Malhotra, R. *Energy & Fuels*, **1996**, *10*, 776.
6. Eskay, T. P.; Britt, P. F.; Buchanan, A. C., III *Am. Chem. Soc. Div Fuel Chem. Preprints* **1996**, *41(2)*, 739.
7. C. Engler and Ed. Low, *Ber.*, **1893**, *26*, 1436.
8. Back, M. H.; Sehon, A.H., Can. J. Chem., **1960**, 38, 1261.
9. Katritzky; Luxem, F. J.; Siskin, M. *Energy & Fuels*, **1990**, *4*, 514.
10. Benson, S.W.; O'Neil, H.E., Kinetic Data on Gas Phase Unimolecular Reactions, National Bureau of Standards, NSRDS-NBS 21, Washington, 1970.
11. Bamford, C.H.; Dewar, M.J. S. *J. Chem. Soc.* **1949**, 2877.
12. Murawski, J.; Szwarc, M. *Trans. Faraday Soc.* **1951**, 47, 269.
13. Berkowitz, J.; Ellison, G. B.; Gutman, D. *J. Phys. Chem.* **1994**, *98*, 2744.
14. Benson, S. W., *Therochemical Kinetics*, 2nd ed; John Wiley and Sons: New York, **1976**.
15. Allen, A.D.; Kresge, J.A.; Schepp, N.P.; Tidwell, T.T. *Can. J. Chem.* **1987**, 65, 1719.
16. Miller, R. E.; Stein, S. E. *J. Phys. Chem.* **1981**, *85*, 580.
17. Serio, M. A., Kroo, E.; Charpenay, S.; Solomon, P. R.*Am. Chem. Soc. Div Fuel Chem. Preprints* **1993**, *38(3)*, 1021.
18. Song., C.; Saini, A. K.; Schobert, H. H. *Energy & Fuels*, **1994**, *8*, 301.

Table 1
MAJOR REACTION PRODUCTS OF PHENYLACETIC ACID IN NAPHTHALENE/TETRALIN MIXTURES[a]

REACTANTS[b]	J40	J75	J39	J67	J71	J70	J72	J25
% Tetralin	0.0	0.0	0.0	12.38	47.90	66.38	77.23	100.00
Ph-Acetic Acid	9.83	6.59	10.92m	11.07	10.04	9.97	9.90	10.29m
Naphthalene	79.01	59.12	89.08m	77.92	46.87	30.27	20.52	–
Tetralin	–	–	–	11.01	43.09	59.76	69.58	89.71
Pyridine	11.16	–	–	–	–	–	–	–
H_2O	–	34.17	–	–	–	–	–	–
PRODUCTS[b]								
Pyridine	77.4	–	–	–	–	–	–	–
Ph-Acetic Acid	61.3	57.5	57.1	64.8	65.9	70.4	71.9	67.2
Naphthalene	99.2	102.8	99.2	87.7	52.6	34.7	24.2	2.7
Tetralin	–	–	–	11.9	46.3	64.6	75.1	94.1
Benzene[c]								
Toluene	31.6	32.9	27.2	27.4	25.4	22.2	22.4	19.7
Bibenzyl	0.36	0.028	0.24	0.071	0.056	0.067	0.069	0.026
t-Stilbene	0.46	0.026	0.071	0.11	0.086	0.060	0.061	0.037
Benzylphenyl ketone	< 0.01	< 0.01	< 0.01	< 0.01	< 0.01	< 0.01	< 0.01	< 0.01
Dibenzyl ketone	5.10	0.75	5.57	5.75	3.87	2.71	2.92	1.40
Benzyltetralyl ketone	< 0.01	< 0.01	< 0.01	0.68	1.76	1.33	1.60	1.32
Bz-Naph$(H)_2$[d]	< 0.01	< 0.01	< 0.01	0.11	0.13	0.15	0.16	0.14
1234H-5-BzNaph[e]	< 0.01	< 0.01	< 0.01	0.049	0.098	0.23	0.21	0.26
Unk. 20.20	< 0.01	< 0.01	< 0.01	< 0.01	0.21		0.053	0.0
Bz-Naph$(H)_2$[d]	< 0.01	< 0.01	< 0.01	0.043	0.078	0.14	0.17	0.23
Bz-Naph$(H)_2$[d]	< 0.01	< 0.01	< 0.01	0.011	0.024	0.047	0.053	0.081
1-Ph-Naphthalene	0.053	< 0.05	< 0.05	< 0.05	< 0.05	< 0.05	< 0.05	< 0.05
2-Ph-Naphthalene	0.067	< 0.05	< 0.05	< 0.05	< 0.05	< 0.05	< 0.05	< 0.05
1-Bz-Naphthalene	0.025	0.0084	0.023	0.21	0.37	0.42	0.49	0.48
2-Bz-Naphthalene	0.028	0.0054	0.024	0.016	0.020	0.014	0.015	0.012
Sum Bz-Naph$(H)_x$[f]	0.053	0.014	0.047	0.43	0.72	1.01	1.10	1.19
Sum coupling	7.93	0.82	6.09	7.04	6.73	5.24	5.86	4.53
coupling/Rxn[g]	0.21	0.024	0.14	0.200	0.23	0.18	0.20	0.14
Sum PAA products[h]	98.9	91.2	90.8	99.3	97.8	97.9	100.0	93.6
Sum Bz-Naph$(H)_2$	< 0.01	< 0.01	< 0.01	0.15	0.22	0.34	0.38	0.45
1/2 Bz-Naph[i]	0.90	1.56	0.95	13.0	18.5	29.4	32.6	38.3
Sum Ketones	5.10	0.75	5.57	6.43	5.63	4.05	4.52	2.72

a. Reaction time 1 hr @ 400°C.

b. Reactants are shown in mole % of reaction mixture; products of phenylacetic acid are shown as a mole % of the starting acid, naphthalene and tetralin are shown as mole % of the sum of starting naphthalene and tetralin, and coupling products are shown as a mole % of the starting acid that they contain.

c. Benzene not determined because of interference by GC solvent.

d. An unspecified dihydro-benzylnaphthalene isomer.

e. 1,2,3,4-tetrahydro-5-benzylnaphthalene.

f. The sum of various partially hydrogenated benzylnaphthalenes.

g The ratio of phenylacetic acid incorporated in coupling products to the sum of that which has undergone reaction of any kind.

h. The sum of phenylacetic acid and all identified phenylacetic acid products, as a mole % of the starting acid.

i. The ratio of 1-benzylnaphthalene to 2-benzylnaphthalene.

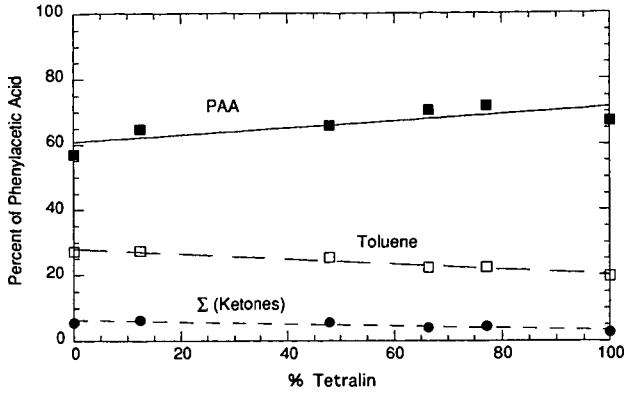

Figure 1. Formation of major products as a function of the H-donor content of the solvent.

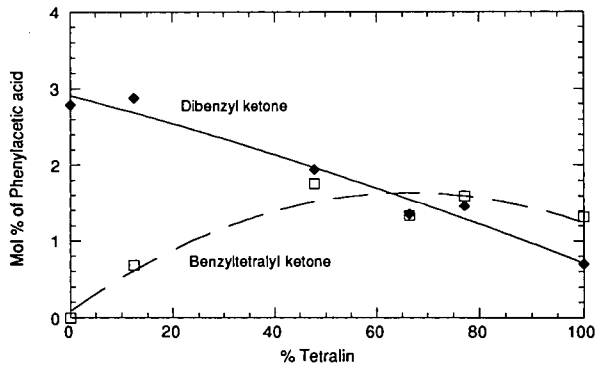

Figure 2. Ketone formation as a function of the H-donor content of the solvent.

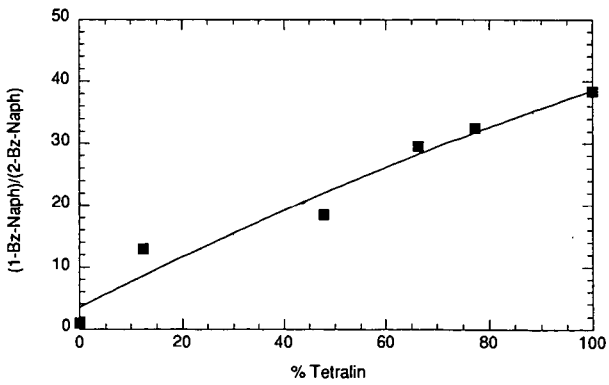

Figure 3. Ratio of 1-benzylnaphthalene/2-benzylnaphthalene as a function of the donor content of the solvent.

COPROCESSING OF POLYMERIC WASTE WITH COAL: REACTION OF POLYETHYLENE AND COAL MODEL COMPOUNDS

Matthew J. De Witt and Linda J. Broadbelt
Department of Chemical Engineering
Northwestern University
Evanston, Illinois 60208

Keywords: Coprocessing, Coal, Polymeric Waste

ABSTRACT

Environmental and economical concerns over diminishing landfill space and the growing abundance of mixed plastic waste mandate development of viable strategies for recovering high-valued resources from waste polymers. Co-processing of waste polymer mixtures with coal allows for the simultaneous conversion of coal and plastics into high-valued fuels. However, there is limited information about the underlying reaction pathways, kinetics, and mechanisms controlling coal liquefaction in the presence of polymeric materials.

A series of model compound experiments has been conducted, providing a starting point for unraveling the complex, underlying chemistry. Neat pyrolysis studies of model compounds of polyethylene and coal were conducted in batch reactors. Tetradecane ($C_{14}H_{30}$) was used as a polyethylene mimic, and 4-(naphthylmethyl)bibenzyl was used as a coal model compound. Reaction temperatures were 420 and 500°C, and batch reaction times ranged from 5-150 minutes. Detailed product analysis using gas chromatography and mass spectrometry enabled the reactant conversion and product selectivities to be determined. Reaction of single components and binary mixtures allowed the kinetic coupling between feedstocks to be examined.

INTRODUCTION

Recently, concerns over the inadequacy of current treatment and disposal methods for mixed plastic wastes have driven the exploration of new strategies for viable plastics resource recovery. The emphasis of the recovery is to obtain high-valued, useful products from the waste polymers. Post-consumer waste plastics are a major contributor to the municipal solid waste (MSW) stream, constituting approximately 11% by weight and 21% by volume of waste in landfills[1]. Over 40% of the landfills in the United States were closed in the past decade, and it is estimated that over half of the remaining ones will be full by the end of the century[2]. This poses a significant dilemma since there appears to be no immediate decrease in the usage of plastic products; in fact, due to their versatility, the usage will most likely increase.

The current motivation for the recovery of plastics is due to government mandates, rather than to industrial initiatives. Some states, such as California, Oregon, and Wisconsin, have passed laws which specify that plastic bottles must be manufactured from a minimum of 25% recycled plastics. Germany has dictated that over 80% of all plastic packaging must be recycled by methods other than combustion by 1996[3-5]. Conventional plastics recycling technologies encounter a number of difficulties which range from costly separation to removal of impurities and contaminants. A consequence of these problems is that products manufactured from recycled polymers are of lower quality and higher cost (approximately 10% higher for high-density polyethylene (HDPE)) than those from the corresponding virgin polymer[4]. As a result, in the United States, only about 4% of 30 million tons of total plastics produced each year is recycled[6].

Coprocessing of polymeric waste with other materials may provide potential solutions to the deficiencies of current resource recovery processes, including unfavorable process economics. By incorporating polymeric waste as a minor feed into an existing process, variations in plastic supply and composition could be mediated and as a result, allow for continuous operation. One option for coprocessing is to react polymeric waste with coal under direct liquefaction conditions[2,7,8]. Coprocessing of polymeric waste with coal provides for simultaneous conversion of both feedstocks into high-valued fuels and chemicals.

EXPERIMENTAL

In order to obtain information about underlying reaction pathways, kinetics, and mechanisms without the complicating effects of the macrostructure, experiments were performed using model compounds for both coal and polyethylene, a voluminous component of mixed plastic waste. To mimic the structure of coal, 4-(naphthylmethyl)bibenzyl (NBBM) was used. NBBM contains both condensed and isolated aromatic species connected by short alkyl chains. An added feature is that it contains five different aromatic-aliphatic or aliphatic-aliphatic carbon-carbon bonds. Successful predictions of the relevant primary products for real systems using NBBM confirmed the adequacy of this model compound, and thus, it will be employed in this study[9-12]. The structure of NBBM is depicted in Figure 1. Although numerous hydrocarbons may serve as appropriate model compounds for high density and low density polyethylene, tetradecane, $C_{14}H_{30}$, was chosen as an appropriate compromise in reactant size.

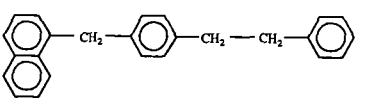

Figure 1: Structure of coal model compound 4-(naphthylmethyl)bibenzyl.

Batch pyrolyses were carried out in an isothermal (±1°C) fluidized sand bath. The experiments were conducted in 2 ml glass cryules charged with ca. 20 mg of reactant for the neat reactions. Equimolar ratios of tetradecane/NBBM were used for the binary experiments, with loadings based on ca. 10 mg of NBBM. After filling, the ampoules were purged with argon, and then sealed using an oxygen/propane flame. Pyrolysis was conducted at both 420 and 500°C, and reaction times ranged from 5-150 minutes. Upon completion of the reaction period, the ampoules were removed from the sand bath and permitted to cool at room temperature. The experiments were replicated a minimum of two times, and conversions and selectivities were reproducible with an error of less than 1%.

Soluble reaction products were extracted from the ampoules using 5 ml of methylene chloride, and an external standard (biphenyl) was added. Product identification and quantification, which enabled reactant conversions and product selectivities to be determined, was achieved using an HP 6890 GC/MS and HP 5890 GC equipped with a flame ionization detector, respectively, each employing a Hewlett Packard 30 m crosslinked 5% Ph Me Silicone capillary column .

RESULTS AND DISCUSSION

The reactant conversions for pyrolysis of tetradecane and NBBM at 500°C were very high, as almost complete conversion was achieved at a reaction time of 10 minutes for all the systems studied. As evidenced by the product spectra and the temporal variations of the major products, secondary and tertiary reactions occurred, making it difficult to deconvolute reaction pathways. Therefore, the reaction temperature was lowered to 420°C, a value still within the range of relevant liquefaction conditions, to achieve lower conversions and isolate primary decomposition pathways. It was noted from the data at 500°C, however, that the conversion of tetradecane was enhanced slightly in the presence of NBBM as compared to the neat reaction.

Reactions carried out at 420°C facilitated identification of the underlying reaction pathways and kinetics. As illustrated in Figure 2, the conversion was significantly lower at a given reaction time as compared to that observed at 500°C. For example, only 37 % of the tetradecane was converted after 150 minutes of reaction time.

The major products observed from the pyrolysis of tetradecane were α-olefins, with minor selectivity to n-alkanes. The highest selectivity, 0.13, was obtained for 1-heptene, and α-olefins with carbon numbers of 6 to 11 were also observed in significantly quantities. As reaction time increased, the selectivity to α-olefins decreased, while that of n-alkanes slightly increased, as observed in Figure 3. This behavior can be explained by noting that hydrogenation of olefins and continued thermal cracking can occur as reaction time increases.

The product distribution was rationalized in terms of the typical free radical Rice-Herzfeld and Rice-Kossiakoff mechanisms[13-16]. The mechanism is initiated by carbon-carbon bond fission along the main chain to form two primary radicals. These primary radicals form secondary radicals through hydrogen abstraction from a secondary carbon or an intramolecular hydrogen rearrangement. These secondary radicals then undergo β-scission to form α-olefins and primary radicals. Termination occurs by recombination of radicals.

Two of the major products from pyrolysis of NBBM, which are formed by carbon-carbon bond fission and subsequent hydrogen abstraction, were toluene and 1-methyl-4-(naphthylmethyl) benzene, each observed with a selectivity of greater than 0.28 at all reaction times studied. The other major product was 1-(2-phenylethenyl)-4-(naphthylmethyl) benzene, with an initial selectivity of approximately 0.35 which decreased linearly with reaction time to 0.11 at 150 minutes. Minor selectivities were observed for a number of products from NBBM pyrolysis. Methyl bibenzyl and 1-(4-(4-methyl)phenylmethyl)benzyl) naphthalene were observed with initial selectivities of 0.055 and 0.070, respectively. Other minor products included 1,4-(binaphthylmethyl) benzene, phenyl methyl naphthalene, naphthalene, methyl naphthalene, 1-(phenylmethyl)-4-(naphthylmethyl) benzene, 1-methyl-4-(2-phenylethenyl) benzene and p-xylene.

Mechanistic interpretation using the ideas put forth by Walter et al. (1994) successfully accounted for the observed product spectra. The products anticipated from scission of the five main bonds of NBBM, labeled A-E, and subsequent hydrogen abstraction and β-scission, are depicted in Figure 4. The formation of high yields of toluene and 1-methyl-4-(naphthylmethyl) benzene is consistent with the proposed mechanism involving bond D fission. This is the weakest bond in the molecule, since the radicals which are formed can be stabilized by the adjacent benzyl substituents. Similarly, the C_2 linkage in NBBM possesses the most easily abstractable hydrogens. Once a secondary radical is formed, it can undergo β-scission to form 1-(2-phenylethenyl)-4-(naphthylmethyl) benzene. This compound could then undergo degradation reactions similar to those observed for NBBM, leading to a reduction in selectivity as reaction time increases.

A comparison of the selectivities of products associated with cleavage of bond A as a function of conversion is shown in Figure 5. If these products were solely formed by bond A scission, it would be expected that the selectivities would be equal for naphthalene and the sum of methyl bibenzyl and its corresponding derivatives. This is clearly not the case. Therefore, another reaction pathway for the formation of these products must exist. Upon examination of other bond scission pairs, a discrepancy between bond C products, phenyl methyl naphthalene, which was observed, and ethylbenzene, which was not, was noted. Also, as stated, other products which can not be explained by one of the five bond scissions were observed, which leads to investigation of secondary pathways. These observations are consistent with a free radical ipso-substitution scheme for the formation of the various products as proposed by Walter et al. (1994). For example, attack by a benzyl radical of the NBBM molecule at the 1-naphthyl position would afford phenyl methyl naphthalene. This scheme would involve the formation of a mole of naphthalene and phenyl methyl naphthalene for every mole formed of methyl bibenzyl and its derivatives. This

comparison is presented in the plot of Figure 6. Likewise, various radical attack at bond C can explain the appearance of 1-(4-(4-methyl)phenylmethyl)benzyl) naphthalene, 1,4-(binaphthylmethyl) benzene, and 1-(phenylmethyl)-4-(naphthylmethyl) benzene. Overall, the main reaction families for NBBM pyrolysis are therefore bond thermolysis, hydrogen abstraction, radical ipso-substitution, β-scission, and radical recombination[12].

Reactions of binary mixtures of tetradecane and NBBM revealed interactions between the reactants and synergistic effects. As observed in Figure 2, tetradecane conversion was increased in the presence of NBBM, which can be rationalized in terms of kinetic coupling[17]. The internal carbon-carbon bonds of tetradecane have a higher bond dissociation energy (90 kcal mol^{-1}) than that of bond D in NBBM (60 kcal mol^{-1})[18]. This has the potential to increase the quantity of radicals in the system with respect to the neat tetradecane experiments at a particular reaction time. The NBBM-derived radicals can easily abstract hydrogen from the secondary carbons of tetradecane, forming a tetradecane-derived radical and converting a tetradecane molecule, enhancing its conversion. Once formed, these tetradecane-derived radicals undergo their own decomposition reactions as observed for neat pyrolysis, and similar product yields are observed.

The interactions between NBBM and tetradecane can be further supported by examining the products derived from NBBM. Since abstraction of hydrogen from tetradecane is facile and has a high reaction path degeneracy of 24, NBBM radicals are capped and stabilized through this abstraction step before undergoing secondary reactions. This effect on the overall product yields can be discerned from Figure 7. The radicals formed from bond D thermolysis abstract hydrogen with higher selectivity and afford higher yields of toluene. Correspondingly, the selectivity to the radical ipso-substitution pathway and formation of phenyl methyl naphthalene is diminished. Therefore, it can be seen that during low pressure pyrolysis, favorable interactions between the two reactants exist. The effective tetradecane conversion is increased, and primary product selectivities are enhanced.

CONCLUSIONS

Recent investigations have demonstrated the feasibility coprocessing of coal with polymers. In this study, feedstock interactions were observed using model compound mimics of both coal and polyethylene. In binary mixtures, the conversion of tetradecane increased while the selectivity to primary products of NBBM pyrolysis was enhanced. These observations were attributed to the stabilization of NBBM-derived radicals through hydrogen abstraction from tetradecane which in turn, increases the rate of tetradecane conversion In order to optimize the interaction between reactants, further experimental and theoretical studies will be conducted at high pressures and in the presence of catalysts in order to delineate the underlying kinetics, pathways, and mechanism controlling coal/polymer coprocessing.

ACKNOWLEDGMENTS

This work was supported by the United States Department of Energy Grant DE-FG22-96-PC96204.

REFERENCES

[1]-Rowatt, R.J., *Chemtech*, 1993, **23**, 56-60.

[2]-Taghei, M., Feng, Z., Huggins, F., and Huffman, G.R., *Energy & Fuels*, 1994, **8**, 1228-1232.

[3]-Menges, G., Emminger, H., and Lackner, G., *International Journal of Materials and Product Technology*, 1991, **6**, 307-330.

[4]-Graff, G., *Modern Plastics*, 1992, **69**, 45.

[5]-Fouhy, K., Kim, I., Moore, S., and Culp, E., *Chemical Engineering*, 1993, **100**, 30-33.

[6]-EPA, *U.S. Environmental Protection Agency*, 1992.

[7]-Anderson, L.L. and Tuntawiroon, W., *American Chemical Society, Division of Fuel Chemistry--Preprints*, 1993, **38**, 816-822.

[8]-Joo, H.K. and Curtis, C.W., *Energy & Fuels*, 1996, **10**, 603-611.

[9]-Farcasiu, M. and Smith, C., *Energy & Fuels*, 1991, **5**, 83-87.

[10]-Matson, D.W., Linehan, J.C., Darab, J. G., and Buehler, M. F., *Energy & Fuels*, 1994, **8**, 10-18.

[11]-Tang, Y. and Curtis, C.W., *Energy & Fuels*, 1994, **8**, 63.

[12]-Walter, T.D., Casey, S.M., Klein, M.T., and Foley, H.C., *Catalysis Today*, 1994, **19**, 367-380.

[13]-Rice, F.O., *Journal of the American Chemical Society*, 1933, **55**, 3035-3040.

[14]-Kossiakoff, A. and Rice, F.O., *Journal of American Chemical Society*, 1943, **65**, 590-595.

[15]-Voge, H.H. and Good, G.M., *Journal of American Chemical Society*, 1949, **71**, 593-597.

[16]-Mushrush, G. W. and Hazlett, R.N., *Industrial & Engineering Chemistry Fundamentals*, 1984, **23**, 288-294.

[17]-LaMarca, C., Libanati, C., and Klein, M.T., *Chemical Engineering Science*, 1990, **45**, 2059-2065.

[18]-Poutsma, M.L., *Energy & Fuels*, 1990, **4**, 113-131.

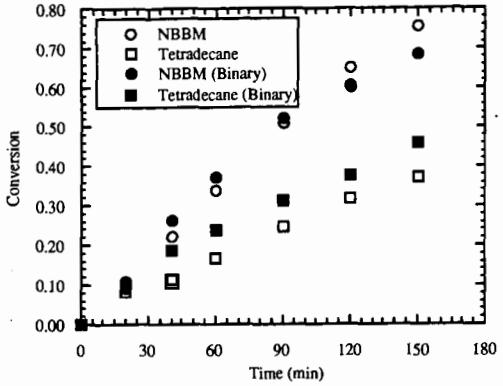

Figure 2: Conversion of tetradecane and NBBM, neat and in binary mixtures, at 420 °C.

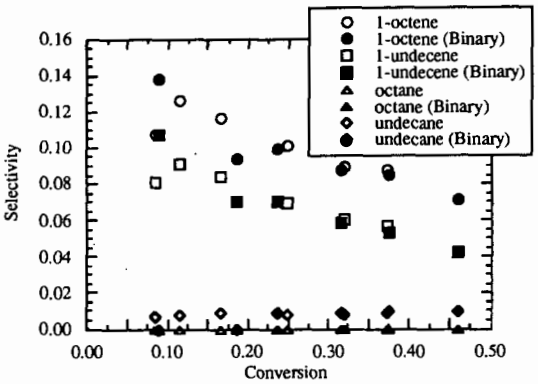

Figure 3: Comparison of alkane/alkene selectivities during neat and binary mixture reactions.

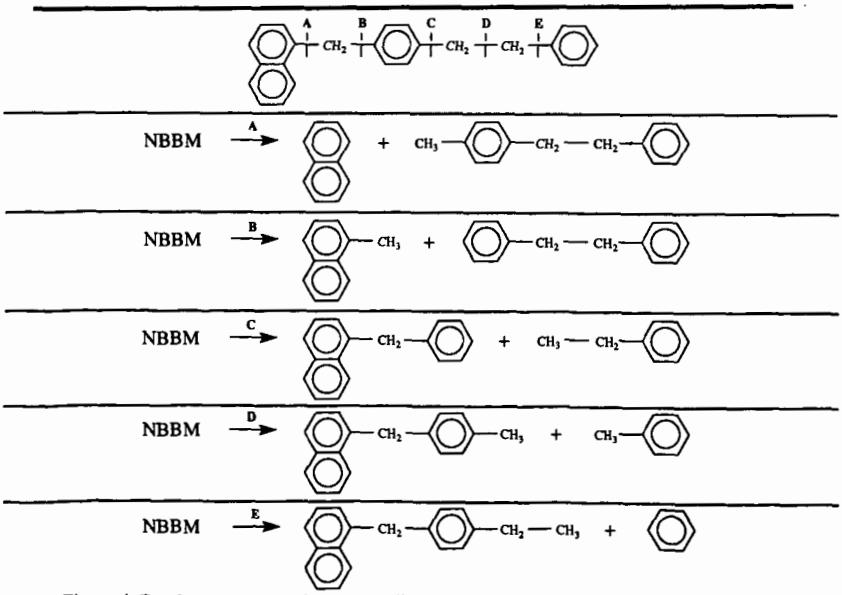

Figure 4: Bond assignment and corresponding products of NBBM pyrolysis, allowing for only bond fission, hydrogen abstraction, and β-scission.

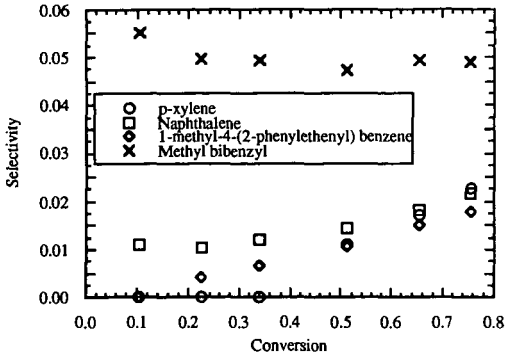

Figure 5: Comparison of selectivities of products associated with cleavage of bond A as a function of conversion.

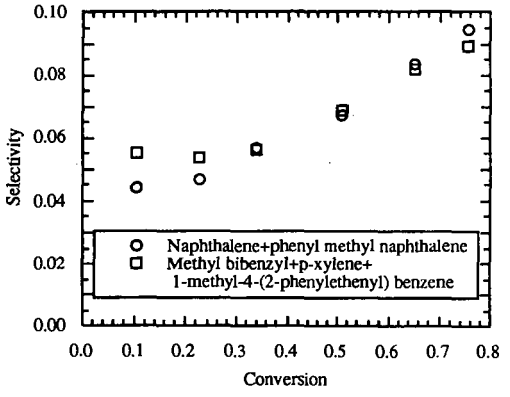

Figure 6: Comparison of products from free radical ipso-substitution reaction which accounts for cleavage of bond A.

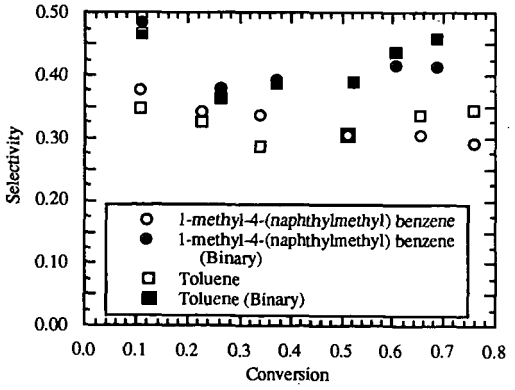

Figure 7: Comparison of products from bond D cleavage during neat NBBM and binary mixture reactions.

Catalysis of Arene Hydrogenation by Thermally Activated Silica

Todd Fields
Robert D. Guthrie
Venkatasubramanian K. Rajagopal
Department of Chemistry
University of Kentucky
Lexington, KY 40506

Burtron H. Davis
Kentucky Center for Applied Energy Research
3572 Iron Works Pike, Lexington, KY 40511

Keywords: Hydrogen, Deuterium, Tetramethyl Orthosilicate, Diphenylmethane

INTRODUCTION

Silica has been used as a support material for a variety of catalysts, usually noble metals or transition metal oxides, for many years. Recent articles attest to its continued popularity.[1] For the most part, discussions of catalytic mechanisms have focussed on the metals and ignored the support.[2] Its role in these catalytic processes has usually been considered to be passive. It is often coated with various organic compounds for use as a chromatographic stationary phase, but even when the organic ligand is attached chemically, the silica itself is regarded essentially as an anchor.[3] This has also been true for studies of thermolysis mechanisms where it was desired to immobilize organic substrates for comparison with naturally occurring nonvolatile materials such as coal.[4] Studies in which silica-immobilized substrates have been heated under pressure of H_2 and D_2 have shown no special effects that might be attributed to catalytic involvement of the support.[5]

However, recent work by Bittner, Bockrath and Solar[6] showed that fumed silica, after thermal activation above 330 °C under argon flow, will catalyze the reaction, $H_2 + D_2 \rightarrow 2\ HD$, at temperatures as low as 120 °C in a pulse-flow microreactor and will also catalyze the hydrogenation of ethene to ethane at 150 °C, producing ethane-d_6 when D_2 is used as a flow gas. This suggested that silica, by itself, could serve as a catalyst for hydrogenation reactions. Accordingly, we studied the reaction of thermally-activated, fumed silica and H_2 with selected alkenes in a static reactor and showed that it could function as a hydrogenation catalyst,[7] allowing stilbene and other alkenes to be hydrogenated at temperatures at least 100 °C below those required for a purely thermal reaction. As part of that study, we also showed that hydrogenation of diphenylacetylene gave predominantly the thermodynamically less stable *cis* isomer of stilbene, demonstrating *syn* hydrogenation in a manner reminiscent of that observed with metal catalysts.[8]

We also reported our preliminary observation that under some circumstances aromatic ring reduction was catalyzed by thermally-activated, fumed silica, but noted that this behavior varied with the source of the particular fumed silica employed. We now wish to report experiments intended to probe this phenomenon and to offer possible explanations.

EXPERIMENTAL

Materials. Hydrogenation substrates were the best available commercial grade. Fumed silica was obtained both from Cabot Corporation (Cab-O-Sil grade M-5) or from Aldrich Chemical Co. (both 0.014 and 0.007 micron size were employed.) Several different lot numbers of Cabot silica were tried some were activatable for carrying out aromatic hydrogenations, others were not. The Aldrich silicas proved inactive unless treated with HCl as described below. Tetramethyl orthosilicate was purchased from Aldrich Chemical Co. It produced an activatable silica after hydrolysis as described below.

HCl Treatment of Fumed Silica. Approximately 800 to 900 mg of commercial fumed silica was allowed to stir for approximately 15 min in 50 mL of concentrated HCl. The resulting slurry was then separated by vacuum filtration through a 50 M fritted glass filter. This produced a dull white filter cake which was allowed to dry by passing a stream of air over the cake for roughly two hours, breaking the caked silica periodically with a glass rod. The cake was allowed to dry to a point where it could be transferred conveniently, usually weighing approximately 2 g at this point. This damp silica (ca. 1 g) was then transferred into the glass reactor tube, initially open at both ends. It was activated by passing argon over the material at 430 °C for 10 to 16 h. Following the thermal activation, the non-capillary end of the reactor was sealed. Solid substrates were introduced through the wide opening in the reaction tube before sealing. Liquid substrates were introduced by syringe after sealing.

Preparation of Silica by Hydrolysis of Tetramethyl Orthosilicate. Tetramethyl orthosilicate (2 mL) was added to approximately 50 mL of deionized water. The mixture was allowed to stand at approximately 25 °C for 10 to 16 h. The resultant brittle cake was broken up with a glass stirring rod and dried in a stream of air as described for hydrolyzed fumed silica. This produced approximately 1 g of silica which was reduced to 800 mg after activation. In some experiments, the tetramethyl orthosilicate was treated with aqueous HCl prepared by passing gaseous HCl into deionized water. Treatment with aqueous HCl produced a solid gel immediately.

Hydrogenation Procedure. Reactions were carried out in glass bulbs of approximately 12 mL volume with a 16 cm section of 1 - 2 mm capillary attached to one end. The procedures for activating the catalyst, loading the reactors and carrying out the reactions have been described in earlier publications.[7]

Workup Procedures. In some cases, reaction vessels were cracked open and the silica hydrolyzed as described earlier. In others, products were removed by distillation at pressures of less than 0.1 Torr into a liquid nitrogen-cooled trap. Reaction products were combined with a measured volume of standardized biphenyl or naphthalene solution in CH_2Cl_2 then analyzed by gas chromatography (GC) and gas chromatography-mass spectrometry (GC/MS). Recoveries were generally greater than 90 % based on response factors estimated from carbon numbers or standard mixtures when available.

RESULTS AND DISCUSSION

In our previous papers[7] we reported that fumed silica which was activated by heating under argon flow at 350 °C promoted the hydrogenation of diphenylethane (**DPE**) to a mixture of cyclohexylphenylethane (**CPE**) and dicyclohexylethane (**DCE**). When the reaction was carried out using D_2 the products were highly deuterated, with the **CPE** showing ions of mass d_6 to d_{18} with maximum intensity at d_{11} and the **DCE** showing ions of mass d_{12} to d_{26} with maximum intensity at d_{19}. Using the same silica samples, naphthalene was hydrogenated to less than 2% conversion. Moreover, inclusion of naphthalene along with **DPE** prevented hydrogenation of **DPE**. During the course of these experiments, we exhausted our bottle of fumed silica and found that a new sample, obtained from the same supplier, but displaying a different lot number, used in the same procedure, failed to promote hydrogenation of **DPE**. Subsequent experiments showed that some fumed silica samples worked and some did not. Samples obtained from a second supplier in two different particle sizes also failed to promote the reaction. For reasons which may or may not explain the effect of the procedure, we tried treating the ineffective samples with concentrated HCl prior to thermal activation. This procedure had the desired effect in that the resultant samples promoted hydrogenation of **DPE**.

We then determined the effect of the various silicas on the reaction of H_2 with diphenylmethane. The products of this reaction are shown in Figure I and yields are listed in Table I. It will be noted that the variability observed for **DPE** with different silica sources is also observed with **DPM**. In an attempt to rule out trace metal contamination as a source of the differing catalytic activities, some of the silicas were subjected to ICP (inductively coupled plasm) analysis. The results are listed in Table II. We would suggest that the values determined, which generally border on the limits of experimental detection, are not sufficiently different for these samples to explain their differing effectiveness in promoting the hydrogenation of **DPM**. Data for the two ineffective silicas (C2 and A1) do not differ in any systematic way from the data for C1 and C3.

In the absence of a catalytic contaminant, we must tentatively conclude that structural differences within the silica matrix are responsible for differing catalytic effectiveness. As in the **DPE** reaction, treatment of inactivatable silica with concentrated HCl prior to the thermal activation process has the effect of producing an activatable catalyst (compare entries 5 and 6 in Table I). No chlorinated products were detected when HCl-treated silica was used for hydrogenations and it is therefore hypothesized that the effect of the HCl treatment is to disrupt the silica matrix such that subsequent thermal dehydration can produce sites which are catalytic for the hydrogenation. Thermal dehydration of fumed silica has been recently studied by NMR which showed that hydrogen bonded surface silanols are gradually reduced in number.[9] In our case, it is suspected that the disruption and dehydration is promoted by HCl during the thermal activation stage rather than during the HCl treatment itself because thorough water washing of the HCl-treated material prior to heating precludes activation as shown by entry 7 in Table I.

To provide further evidence that silica itself is responsible for promotion of arene hydrogenation, silica samples were prepared by hydrolysis of tetramethyl orthosilicate ($Si(OCH_3)_4$) using deionized water alone and with deionized water containing HCl (see Experimental). Both treatments produced thermally activatable silicas as shown by entries 8 and 9 in Table I. Having established that treatment of 0.014 micron fumed silica with aqueous HCl followed by thermal

Table I. Yields of Products from Treatment of Diphenylmethane **DPM** with H_2 (14 MPa) in the Presence of Various Thermally-Activated Fumed Silicas.

Silica Type	Products (%)				
	CPM	**DCM**	**PhMe**	**CMe**	**PhH**
C1[a]	39	12	n.d.[f]	n.d.[f]	n.d.[f]
C2[a]	3	0.3	n.d.[f]	n.d.[f]	n.d.[f]
C3[a]	31	11	0.24	<0.1	0.24
A1[b]	1.1	0.2	0.15	0.14	0.14
A2[b]	2.7	0.4	0.16	<0.1	0.16
A2 (HCl)[c]	25	54	0.2	0.2	0.4
A2 (HCl/H_2O)[d]	4.7	<0.1	0.3	<0.1	0.1
TMS (H_2O)[e]	12	62	0.25	0.6	0.7
TMS (HCl)[e]	28	60	0.3	1.0	1.0

Notes for Table I: [a] C1, C2 and C3 are Cabot Grade M5 (0.014 micron) fumed silicas having different lot numbers. [b] A1 is Aldrich 0.007 micron fumed silica; A2 is Aldrich 0.014 micron fumed silica. [c] A2 (HCl) is Aldrich 0.014 micron fumed silica treated with concentrated HCl as described in the experimental section. [d] A2 (HCl/H_2O) is the same as A2 (HCl) except for being washed with water to neutral pH before thermal activation. [e] TMS (H_2O) is silica produced by hydrolysis of tetramethyl orthosilicate with deionized water. TMS (HCl) is the same with HCl added.[f] Not determined.

Table II. Trace Metal Content of Silicas used for the Hydrogenation of **DPM** in Table I.

Silica Type[a]	Metal Content (ppm)						
	Ca	Cr	Co	Cu	Fe	Mn	Ni
C1	<30	5	<4	16	30	<2	15
C2	200	3	<4	28	68	<2	38
C3	60	<2	<4	20	67	<2	15
A1	<30	<2	6	20	40	<2	<3

[a] See notes for Table I.

activation produces an active catalyst for the hydrogenation of **DPE** and **DPM**, we reexamined the reaction of naphthalene. Results for this and other substrates are shown in Figure II. As before, only a small conversion (4%) to tetralin could be accomplished either with A2 (HCl) or withTMS (H_2O). Biphenyl was also resistant but toluene showed substantial reaction. Chloronaphthalene gave a 22% yield of naphthalene with silica A2 under the same conditions.

CONCLUSIONS

The pattern which is emerging from these studies shows that when silica possesses the proper structural characteristics, the nature of which are unknown at the present time, it can then be converted by heating at 350 °C to a form which will catalyze the hydrogenation of certain arenes. Some commercial fumed silicas work, others do not. Those that do not work benefit from treatment with aqueous HCl prior to thermal activation. One commercial sample which was ineffective in the **DPM** reaction also refused activation to promote the $H_2 + D_2 \rightarrow HD$ reaction in a pulsed microreactor. HCl treatment remedied this situation. Silica prepared from hydrolysis of $Si(OMe)_4$ with pure water proved an effective catalyst after heating. We have found that arenes which are most extensively hydrogenated are those with benzylic C-H groups, **DPE, DPM, or PhMe.** Naphthalene, which should be easier to hydrogenate in the thermodynamic sense, gave only a few percent conversion under the same conditions and seemed to poison the surface toward reactions with arenes which could be hydrogenated in its absence. As a working hypothesis, we suggest that silicas with appropriate structural features, promote isomerization of alkyl arenes to cyclic polyenes

which are then rapidly reduced. This scheme is shown in Figure I. With **DPM**, a small but significant amount of hydrocracking is also observed. We suggest that this is a high-temperature, alternate route for partially hydrogenated intermediates as shown in Figure I. Preliminary results indicate that hydrocracking is the major reaction outcome when **DPM** is treated with H_2 and silica at 450 °C.

ACKNOWLEDGMENTS

T. F. thanks Kentucky DOE EPSCoR for a traineeship as part of DE-FCO2-91ER75661. We thank Drs. B. C. Bockrath and E. W. Bittner for assistance in pulse microreactor experiments.

REFERENCES

1. (a) Kiviaho, J.; Hanaoka, T.; Kubota, Y.; Sugi, Y. *J. Mol. Catal.* **1995**, *101*, 25-31. (b) Tsubokawa, N.; Kimoto, T.; Endo, T. *ibid.* **1995**, *101*, 45-50. © Drelinkiewicz, A. *ibid.* **1995**, *101*, 61-74. (d) Startsev, A. *Cat. Rev. -Sci. Eng.* **1995**, *37*, 353-424.(g) Morys, P.; Schlieper, T. *J. Mol. Catal., A* **1995**, *95*, 27-34. (h) Voyatzis, R.; Mofat, J. B. *Energy and Fuels* **1995**, *9*, 240-247.

2. See for example, Bond, G. C. *Accts. Chem. Res.* **1993**, *26*, 490-495 and references therein.

3. (a) Vranken, K. C.; VanDerVroot, P.; Posseiers, K.; Bansant, E. F. *J. Coll. Interfac. Sci.* **1995**, *174*, 86-91. (b) Piers, A. S.; Rochester, C. H. *ibid.* **1995**, *174*, 97-103. © Kamagawa, K.; Yoshica, H. *ibid.* **1995**, *172*, 94-97.

4.(a) Buchanan, A. C., III, Dunstan, T. D. J.; Douglas, E. C.; Poutsma, M. L. *J. Am. Chem. Soc.* **1986**, 108, 7703-7715. (b) Buchanan, A. C., III; Britt, P. F.; Biggs, C. A. *Energy and Fuels* **1990**, 4, 415-417. © Buchanan, A. C., III.; Biggs, C. A. *J. Org. Chem.* **1989**, 54, 517-525. © Britt, P. F.; Buchanan, A. C., III *J. Org. Chem.* **1991**, 56, 6132-6140.

5. Guthrie, R. D.; Ramakrishnan, S.; Britt, P. F.; Buchannan, A. C. III; Davis, B. H. *Energy and Fuels* **1995**, *9*, 1097-1103.

6. Bittner, E. W.; Bockrath, B. C.; Solar, J. M. *J. Catal.* **1994**, *149*, 206

7. (a) Rajagopal, V. K.; Guthrie, R. D.; Fields, T.; Davis, B. H. *Catalysis Today* **1996**, *31*, 57-63. (b) Rajagopal, V. K.; Guthrie, R. D.; Davis, B. H. *Prep. Pap. - Am. Chem. Soc. Div. Fuel Chem.* **1995**, *40*, 945-949.

8. (a) Campbell, K. N.; Campbell, B. K. *Chem. Rev.* **1942**, *31*, 77. (b) Farkas, A.; Farkas, L. *Trans. Faraday Soc.* **1937**, *33*, 837. © Ott, E.; Behr, A.; Schroter, R. *Chem. Ber.* **1928**, *61*,2124. (d) Wessely, F. V.; Welleba, H. *Chem. Ber.* **1941**, *74*, 777.

9. Liu, C. C.; Maciel, G. E. *J. Am. Chem. Soc.* **1996**, *118*, 5103-5119.

Figure I

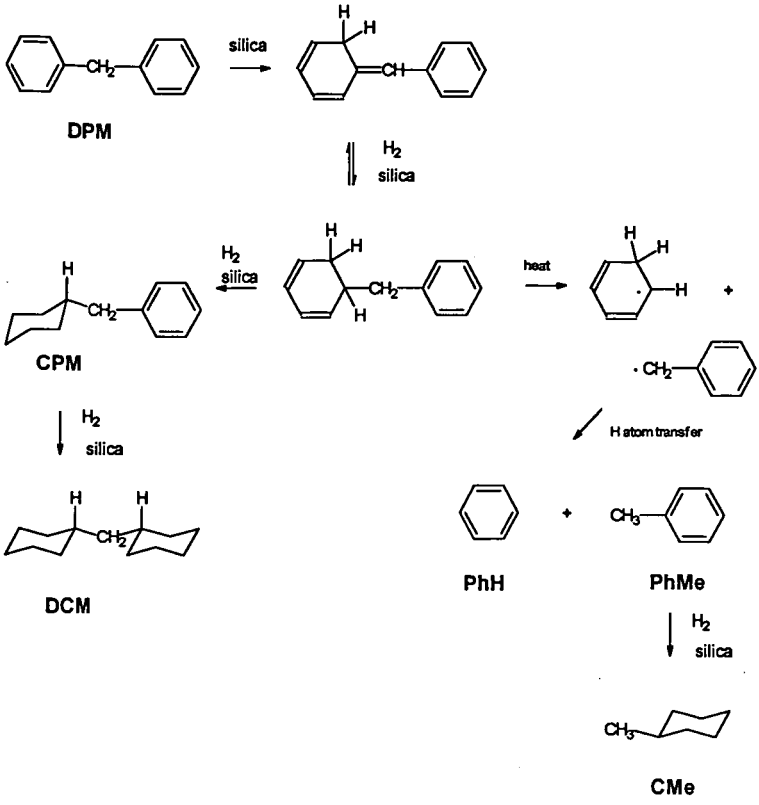

Figure II

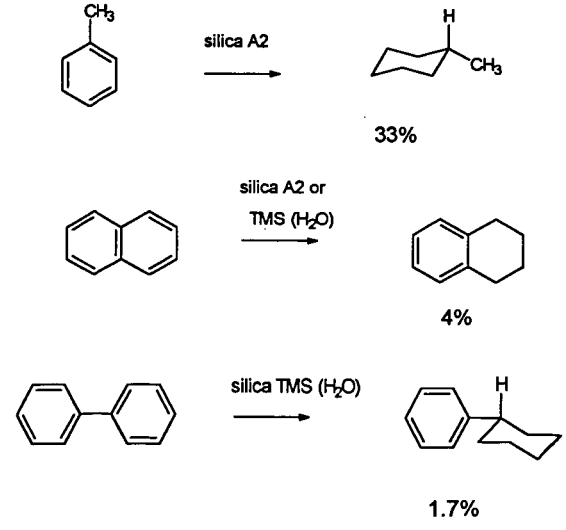

HYDRODESULFURIZATION OF THIOPHENIC COMPOUNDS ON MoS_2: A COMPUTATIONAL STUDY USING ZINDO

Xiaoliang Ma and Harold H. Schobert
Fuel Science Program, Department of Materials Science and Engineering
The Pennsylvania Stage University, 209 Academic Projects Building,
University Park, PA 16802-2303

Keywords: hydrodesulfurization, MoS_2 catalyst, computation

INTRODUCTION

To meet environmental regulations on reduction of sulfur content in fuels there has been a growing need to develop new catalysts that can carry out deep hydrodesulfurization (HDS). MoS_2 and sulfided Co (or Ni) promoted molybdenum catalysts have been used extensively in HDS, both in basic investigations and in petroleum refineries. However, the nature of the active sites, even on a single slab of MoS_2, as well as how they interact with sulfur species are still unclear. Considerable effort has been devoted to understanding the active sites of MoS_2 crystal and their HDS mechanisms. Some excellent reviews have be published in this regard (1-3). Since it is still difficult technically to characterize the chemical properties of the MoS_2 surface, some researchers have done chemical simulations or calculations in order to understand the active sites on the surface of MoS_2 catalyst and their interaction with sulfur species. Most of them used smaller clusters as a model, the classical Newtonian physics method (molecular mechanics) or the extended Hückel molecular orbital method which is an empirical approximation (4-9). The nature of the active sites and mechanisms of reaction suggested by the results were very different among these various studies.

In this study, we used a semi-empirical quantum chemical method, ZINDO (Zerner's Intermediate Neglect of Differential Overlap program), and chose a single slab of regular hexagonal $Mo_{12}S_{38}$ as a basic model to examine possible active sites or active edges by removing the sulfur atoms from the periphery of $Mo_{12}S_{38}$ cluster on the basis of their bond orders and required energy. Furthermore, the interaction of inferred active sites with the sulfur species was explored by comparison of the total energies of different adsorption states. We attempt to answer 1) which positions at MoS_2 crystal are easier to form the sulfur vacancies, or which edge in a single slab of MoS_2 is easier to form a sulfur poor edge; and 2) how such sulfur vacancies or sulfur poor edge interact with thiophenic compounds.

MODELING AND COMPUTATION

In order to make the cluster of MoS_2 be a more realistic mimic of highly dispersed MoS_2 particles, we designed a single slab of regular hexagonal $Mo_{12}S_{38}$ as a basic model cluster, which contains 12 Mo and 38 S atoms as shown in Figure 1. There are two types of edge plane, as noted by I $(10\bar{1}0)$ and II $(\bar{1}010)$ respectively. Each S atom in the edge I plane bonds with only one Mo atom, and each S atom in the edge II plane bonds with two neighboring Mo atoms. In this cluster, the S/Mo ratio is not stoichiometric. To keep the S/Mo ratio around 2 and to form the sulfur vacancies, the sulfur atoms at the periphery of the cluster should be removed. Reasonable positions of the sulfur vacancies and the sulfur-poor edge were determined by comparison of the charge distribution, bond indexes in the $Mo_{12}S_{38}$ cluster, and the total energy of the clusters with sulfur vacancies. The adsorption configuration of sulfur species on the formed sulfur vacancies was examined by locating the sulfur atom of a sulfur species at an appointed sulfur vacancy. The adsorption state was explored by comparison in the total energy of compound-cluster system.

The Mo—Mo, Mo—S and S—S bond lengths were determined according to MoS_2 crystal size from the literature (4, 6). The geometries of the sulfur species were optimized by using ZINDO before locating them at the sulfur vacancies. The calculation of charge distribution, bond order and the total energy of the clusters and compound-cluster was done without geometry optimization.

All quantum chemical calculation in this study was done by using ZINDO, which was developed by the University of Florida Quantum Theory Project. ZINDO uses the theoretically based INDO parameterization and therefore can use d orbitals, and then can be used for many transition series metals (10).

RESULTS AND DISCUSSION

1) Electronic properties of $Mo_{12}S_{36}$ cluster. According to their different positions, the sulfur atoms in $Mo_{12}S_{38}$ cluster can be classified into five types which are labeled with *a*, *b*, *c*, *d* and *e*, respectively, as shown in Figure 1. Each sulfur atom on the corner (position *b*) and in the edge plane I (position *a*) is bonded to one Mo atom, and each sulfur atom in the edge plane II (position *c*)is bonded to two Mo atoms. All sulfur atoms in the basal plane are connected with three Mo atoms. The Mo atoms sandwiched between the top and bottom basal planes in the cluster can also

be classified into three types on the basis of their positions, which are labeled with α, β and γ, respectively.

The calculated results of charge distribution and bond index of $Mo_{12}S_{38}$ cluster are listed in Table 1 and 2, respectively. The results show that the charge distribution is strongly dependent on the atomic position in the cluster. S(b), the sulfur located at the position *b*, has the least negative charge in all of S atoms, being –0.486. S(a) located in the position *a* has the second least negative charge. As connected with two Mo atoms, S(c) has larger negative charge although it is located in a edge plane. The sulfur atoms in the two basal planes, S(d) and S(e), have the largest negative charge among the five types of the sulfur atoms, due to their bonding with three Mo atoms. Such charge distribution suggests that S(b) and S(a) atoms have less interaction with the cluster whole than that of S(c) atoms.

With the bond indexes listed in Table 2, it was found that all bond indexes between neighboring S and Mo atoms are higher than 0.8, indicating that there is a strong interaction between neighboring S and Mo atoms, and the atoms in MoS_2 lattice are held together dominantly through such bonding. There is also considerable interaction between two neighboring Mo atoms, their bond indexes being in the range 0.18–0.31. Most pairs of two neighboring S atoms show weak interactions, with the exception of S(a)—S(a') and S(b)—S(b') bonds. In this study, our interest is focused on the sulfur atoms at the periphery of the cluster. The S(c)—Mo(β) bond index is 1.023, lower than those of S(a)—Mo(α) (1.248) and S(b)—Mo(β) (1.158). However, the S(c) atom is connected simultaneously with two Mo(β) atoms, and the sum of the two bond indexes is as high as 2.046. The results indicate that S(a) and S(b) atoms are the easier to be removed than an S(c) atom during the formation of the sulfur vacancies, which is in agreement with the charge distribution as stated above. The calculation of the total energy of the cluster with a sulfur vacancy at the position a, b and c, respectively, was also done, and the results show that the cluster with S(b) vacancy has the lowest energy, while the cluster with S(c) vacancy has the highest energy in three types of the sulfur atoms. These results further support the point that the sulfur vacancies formed should be on the corner and the edge plane I.

2) Adsorption of sulfur species on sulfur vacancies. In order to examine the interaction of sulfur species with the sulfur vacancies, we chose Mo(α) in the $Mo_{12}S_{36}$ cluster with six sulfur vacancies at the edge plane I as an active adsorption site, and assume that the sulfur atom of sulfur species is adsorbed at the position *a*. Considering atom limit and CPU in the calculation, a smaller cluster Mo_6S_{24} as shown in Figure 2A was designed to replace the $Mo_{12}S_{38}$ cluster used above for the compound-cluster adsorption model. The reasonableness for such replacement is based on the consideration that 1) the edge in Mo_6S_{24} cluster has the same structure as the edge plane I in $Mo_{12}S_{38}$ cluster; and 2) the calculated charge distribution in the edge plane of Mo_6S_{24} cluster shows it is similar to that in the edge plane I of $Mo_{12}S_{38}$ cluster. The structure of Mo_6S_{18} cluster, which is derived from Mo_6S_{24} cluster by removing six sulfur atoms in an edge plane, and the thiophene-Mo_6S_{18} adsorption are shown respectively in Figure 2B and 2C. The change in the total energy of the thiophene-Mo_6S_{18} with the angle included between thiophenic plane and the edge plane are listed in Table 3. It was found that the thiophene–Mo_6S_{18} has the least energy at 0° angle, meaning that a parallel adsorption as shown in Figure 3A is the most stable. The same results were also observed when replacing the adsorbate on Mo_6S_{18} cluster with dibenzothiophene. Two other adsorption configurations, as shown in Figure 3B and 3C, respectively, were also calculated, and both have higher total energy than that of the parallel adsorption. The calculated results suggest that thiophene and dibenzothiophene are adsorbed on the exposed Mo(α) atom not only through a S—Mo(α) bond but also through a bond between π electrons on the thiophenic ring and Mo(α) atom. The parallel adsorption of such sulfur compounds on the exposed Mo(α) atom is the most stable in the all adsorption cases addressed in this study.

REFERENCES

1. Startsev, A. N.*Catal. Rev. Sci. Eng.* **1995**, 37, 353-423.
2. Portela, L.; Grange, P. and Delmon, B. *Catal. Rev. Sci. Eng.* **1995**, 34, 699-731.
3. Vasudevan, P. T. and Fierro, J. L. G. *Catal. Rev. Sci. Eng.* **1996**, 38, 161-188.
4. Joffer, J.; Geneste, P. and Lerner, D. A. *J. Catal.* **1986**, 97, 543-548.
5. Pis Diez, R. and Jubert A. H. *J. Mol. Structure (Theochem)* **1990**, 210, 329-336.
6. Chen, R. and Xin, Q. *J. Mol. Catal.* **1991**, 64, 321-335.
7. Daage, M. and Murray, H. H. Preprings, Symposium on the Mechanism of HDS/HDN Reactions, 206th National Meeting, Am. Chem. Soc. Chicago, IL, August, **1993**, 660-664.
8. Smit, T. S. and Johnson, K. H. *Chem. Phys.* **1993**, 212, 525-533.
9. Diemann, E.; Weber, Th. and Müller, A. *J. Catal.* **1994**, 148, 288-303.
10. Pople, J. A. and Beveridge, D. L. Approximate Molecular Orbital Theory, McGraw-Hill, New York, 1970.

Table 1 Charge distribution in $Mo_{12}S_{38}$ cluster

Atom	Charge
Sulfur	
a	-0.550
b	-0.486
c	-0.733
d	-0.748
e	-0.808
Molybdenum	
α	+2.095
β	+2.173
γ	+1.609

Table 3 Total energy of compound-Mo_6S_{18} at different included angle θ

Included angle θ°	Total energy (a.u.*)	
	thiophene	dibenzothiophene
0	-275.53	-330.49
45	-273.65	-325.89
90	-273.00	
135	-272.90	

* atomic units

Table 2 Bond index in $Mo_{12}S_{38}$ cluster

S-Mo bond	bond index	Mo-Mo bond	bond index	S-S bond	bond index
S(a)– Mo(α)	1.248	Mo(α)– Mo(β)	0.185	S(a)– S(b)	0.153
S(b)– Mo(β)	1.158	Mo(α)– Mo(γ)	0.296	S(a)– S(d)	0.060
S(c)– Mo(β)	1.023	Mo(β)– Mo(β)	0.232	S(b)– S(c)	0.068
S(d– Mo(α)	0.815	Mo(β)– Mo(γ)	0.302	S(b)– S(d)	0.057
S(d– Mo(β)	0.844	Mo(γ)– Mo(γ)	0.308	S(a)– S(a')	0.206
S(d– Mo(γ)	0.826			S(b)– S(b')	0.738
S(e– Mo(γ)	0.836			S(c)– S(c')	0.094

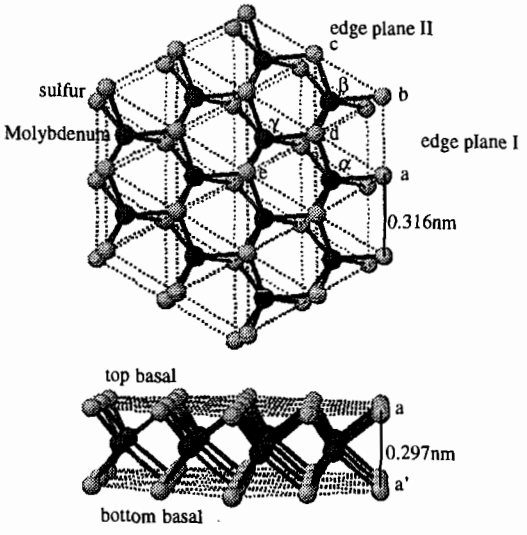

Figure 1 Schematic diagram of $Mo_{12}S_{38}$ cluster

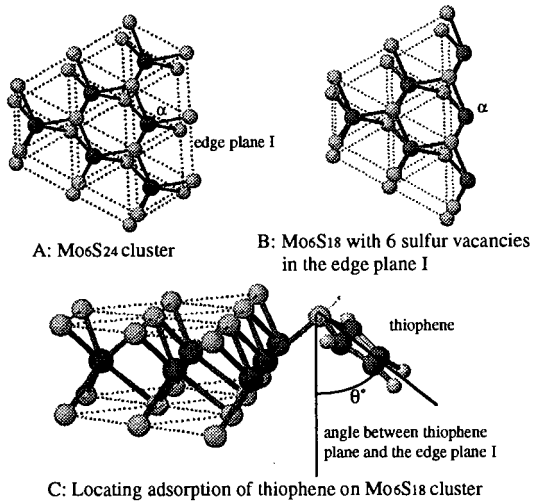

A: Mo_6S_{24} cluster

B: Mo_6S_{18} with 6 sulfur vacancies in the edge plane I

C: Locating adsorption of thiophene on Mo_6S_{18} cluster

Figure 2 Schematic diagrams of Mo_6S_{24} and thiophene-Mo_6S_{18}

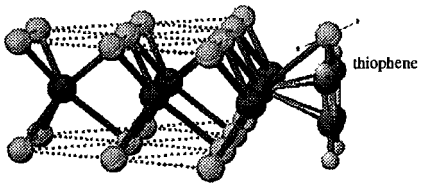

A: parallel adsorption through π electrons, total energy: -275.53 a.u.

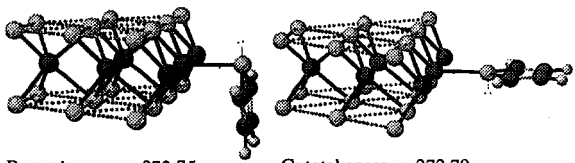

B: total energy: -273.75 a.u.

C: total energy: -272.79 a.u.

Figure 3 Different adsorption states of thiophene on sulfur poor edge of Mo_6S_{18}

PROMOTING EFFECT OF WATER ON IN-SITU GENERATED MoS_2 CATALYST FOR HYDROGENATION AND C-O BOND CLEAVAGE OF DINAPHTHYL ETHER

Yoshiharu Yoneyama and Chunshan Song*
Fuel Science Program and Laboratory for Hydrogenation Process Chemistry,
The Pennsylvania State University,
209 Academic Projects Building, University Park, PA 16802

Keywords: hydrogenation, MoS_2 dispersed catalyst, water

INTRODUCTION

In our recent work, we found a strong promoting effect of water on low-severity catalytic coal liquefaction using molybdenum sulfide catalyst in-situ generated from ammonium tetrathiomolybdate (ATTM): addition of H_2O to the run using ATTM as a catalyst precursor increased the conversion of Wyodak coal at 350 °C from 29.5 to 66.5 wt% [1]. Initially, this strong promoting effect of water was surprising to us, because it has been shown that better drying method for moisture removal results in higher coal conversion in catalytic liquefaction using molybdenum sulfide catalyst [2]. It was also observed that addition of water to catalytic coal hydroliquefaction has negative effect [3-5]. On the other hand, water addition to non-catalytic coal conversion reactions and some model reactions has been shown to have positive impacts [6-10]. More recently, it has been reported that ether compounds such as 1-phenoxynaphthalene and 9-phenoxyphenanthrene cleave in water at 315 °C, and this cleavage is enhanced at higher temperature; since water becomes a stronger acid as temperature increased, this cleavage reaction was shown to proceed through ionic process [9,10].

In the present study, in order to clarify the role of water in catalytic hydroliquefaction of coal, we carried out hydrogenation and hydrogenolysis of 2,2'-dinaphthyl ether (DNE) using ATTM as a catalyst precursor in the absence and presence of H_2O or D_2O. There are many connecting linkages in coal structures; the aromatic C-O and aromatic-aliphatic C-C bonds are believed to be important linkages between aromatic moieties of coal structures. Therefore, in order to increase the conversion of coal to liquids, it is necessary to cleave these connecting linkages. Coal structures have not been clarified at the molecular level. The use of coal-related model compounds is suitable for understanding fundamental chemistry. The products from the hydrogenation of model compounds can be easily identified by GC/MS. DNE has been shown to be thermally unreactive in the absent of catalyst, but its conversion is enhanced by some metal sulfide catalyst [11]. Here we used DNE to investigate the effect of the addition of water on cleavage of ether-linkages and on hydrogenation of aromatic rings using ATTM under the conditions of coal liquefaction.

EXPERIMENTAL

Catalyst Precursor

Ammonium tetrathiomolybdate (ATTM) was purchased from Aldrich, and 2,2'-dinaphthyl ether (DNE) from TCI America. ATTM and DNE were used without further purification. It was noted in previous work in this laboratory that long-time storage of ATTM in reagent vials in air may lead to degradation of the reagent, which results in deviations in the observed activity of in-situ generated MoS_2 catalyst from different bottles of ATTM reagent. In this work, a bottle of newly purchased ATTM was used in all the experiments on DNE runs, and the reagent bottle was stored in a refrigerator in order to minimize oxidative degradation.

Model Compound Reactions

A horizontal tubing bomb microautoclave reactor with a capacity of 25 mL was loaded with ca. 0.216 g DNE, 1 wt% catalyst precursor (1 wt % Mo based on DNE) and 1.47 g solvent (n-tridecane). When water was added, the weight ratio of H_2O to DNE was 0.56, unless otherwise mentioned. The reactor was purged four times with H_2 and then pressurized with 6.9 MPa H_2 at room temperature for all experiments. A preheated fluidized sand bath was used as the heating source, and the horizontal tubing bomb reactor was vertically agitated to provide mixing (about 240 strokes/min). After the reaction the hot tubing bomb was quenched in a cold water bath. The contents were washed out with 30-40 mL acetone, and filtered through a low speed filter paper for subsequent GC analysis of the filtrate. Two-step reaction was also carried out in a similar manner as described above, except that the active MoS_2 catalyst was prepared first using ATTM with and without H_2O in the first-step reaction, and subsequently, the reactor was opened, and DNE was then added into the reactor. DNE was treated with and without H_2O in the second-step reaction.

The products were identified by GC-MS using a Hewlett-Packard 5890 II GC coupled with a HP 5971 A mass-selective detector operating at electron impact mode (EI, 70 eV). The column used for GC-MS was a J&W DB-17 column; 30-m x 0.25-mm, coated with 50% phenyl 50% methylpolysiloxane with a coating film thickness of 0.25 μm. For quantification, a Perkin Elmer 8500 GC with flame ionization detector and the same type of column (DB-17) was used. Both GC

* Corresponding author. E-mail: csong@psu.edu; Fax: 814-865-3075; Tel: 814-863-4466

and GC-MS were programmed from 80 to 280 °C at a heating rate of 4 °C/min and a final holding time of 8 min. The response factors for 5 of the products were determined using pure compounds.

RESULTS AND DISCUSSION

One-Step Reaction

Table 1 shows the results of non-catalytic and catalytic runs of DNE with in-situ generated dispersed MoS_2 catalyst at 350, 375 and 400 °C. Without ATTM, the conversions of DNE are very low, even at 400 °C. Adding water alone seems to inhibit the conversion of DNE completely. However, in the presence of ATTM conversions are significant. An addition of water to the runs with ATTM substantially increases the conversion of DNE. Upon addition of water to the catalytic runs, the conversion of DNE increases from 46.0 % to 83.8 % at 350 °C. The principal products are tetralin, naphthalene, 2-naphthol, 5, 6, 7, 8-tetrahydro-2-naphthol, octahydroDNE, and tetrahydroDNE. Formation of these products suggests that both the ether linkage cleavage reaction and hydrogenation of aromatic rings occur simultaneously. Because the yields of tetralin are higher for the runs with added water than for those without water, the hydrogenation of aromatic ring prevails in the run with water and ATTM.

In order to clarify the role of water, DNE was hydrogenated with ATTM and D_2O. Because some aryl ethers cleave in H_2O at high temperature above 315 °C through ionic mechanism [9,10], this ionic effect of H_2O on the cleavage of C-O bond in DNE is investigated. Even though water alone has inhibition effect on conversion of DNE as described above. Table 2 represents the results of catalyst run of DNE with dispersed catalysts and H_2O or D_2O at 350, 375 and 400 °C. Comparing the results using H_2O and D_2O, the conversions of DNE are almost the same in each pair of corresponding runs. There are no apparent isotopic effect on the conversion of DNE and the yields of the products. The results of GC/MS analysis indicate that the products and recovered DNE contain a few deuterium atom, and the fragmentation of mass spectra of the products indicate that deuterium atoms are introduced into the products unselectively. These results show that the hydrogen from water has a little effect on the conversion of DNE. In other words, we have found no clear evidence that H_2O enhanced ether bond cleavage: the ionic effect of water on cleavage of ether-linkage in DNE is not significant, under the conditions employed.

Two-Step Reaction

As shown in Tables 1 and 2, the conversion of DNE increases with an addition of water. In order to further clarify the role of addition of water on the hydrogenation of DNE, two-step reaction was carried out. In the first-step, the Mo sulfide catalyst was prepared from decomposition of ATTM in the presence and the absence of water at 350, 375 and 400 °C under hydrogen pressure for 30 min. Subsequently the reactor was quenched, vented, and opened to allow the loading of DNE followed by purge and repressurization with H_2. The hydrogenation of DNE, as the second-step, was carried out with and without H_2O at 350 °C under hydrogen pressure for 30 min. Table 3 shows the results of the two-step reactions. Using the catalyst prepared from ATTM alone at 350, 375 and 400 °C, the conversions of DNE are almost the same at 64-67 %: the activities of the catalysts are very similar. However, highly active catalysts are generated from ATTM with added H_2O, the conversion of DNE is the largest at 375 °C: the catalyst prepared at 375 °C is most active. This finding corroborates with our previous results on coal liquefaction [12]. After the preparation of catalyst, the addition of water decreases the conversion of DNE. For example the conversion of DNE decreased from 64.4 % to 32.9 % at 350 °C (first-step) after the addition of water to the second-step run. In addition, after the preparation of catalyst from ATTM and water at 350 °C complete removal of water caused about 100 % conversion of DNE at 350 °C at the second-step. These results suggest that water itself does not have promoting effect on hydrogenation of DNE, but that it is effective for the preparation of active catalyst for hydrogenation and bond cleavage of DNE.

Effect of H_2O/DNE Ratio

In the test discussed above, the weight ratio of H_2O/DNE was maintained at 0.56 for the determination of role of water addition on hydrogenation of DNE. We have also attempted to determine the optimum amount of added water. This was done by examining the relationship between the conversion of DNE and amount of added D_2O. Figure 1 shows the relationship between the amount of D_2O added and the conversion of DNE from the runs at 350 °C for 30 min. The conversions of DNE gradually increase from 46 % to 100% with increasing water amount from 0 to 0.2 g corresponding to a D_2O/DNE weight ratio of about 0.93, and they decrease from 100% to 60 % with further addition of water. These results also clearly indicate that 0.026 of the ratio of ATTM to D_2O is optimum for conversion of DNE under the conditions employed. It seems that since water is used for the preparation of effective catalyst from ATTM for hydrogenation and bond cleavage of DNE, the conversion of DNE is large up to 0.235 g of D_2O. However water itself has a negative effect for the hydrogenation of DNE, further additions of D_2O over 0.235 g seem to cause the decrease of the conversion of DNE.

CONCLUSION

A proper amount of added water has a strong promoting effect on hydrogenation and hydrogenolysis of DNE using molybdenum sulfide catalyst in-situ generated from ATTM. We have found that the addition of water is not effective for DNE conversion, but is effective for the preparation of active catalyst from ATTM for hydrogenation and hydrogenolysis of DNE.

ACKNOWLEDGMENTS

We are most grateful to Prof. Harold H. Schobert for his encouragement, support, and many helpful discussion. This work was supported partially by the U. S. Department of Energy, Pittsburgh Energy Technology Center under contract No. DE-AC22-92PC92122.

REFERENCES

1 C. Song and A. K. Saini, *Energy Fuels*, **9**, 188 (1995)
2 F. J. Derbyshire, A. Davis, R. Lin, P. G. Stansberry, and M. -T. Terrer, *Fuel Process. Technol.*, **12**, 127 (1986)
3 Y. Kamiya, T. Nobusawa and S. Futamura, *Fuel Process. Technol.*, **18**, 1(1988)
4 B. C. Bockrath, D. H. Finseth and E. G. Illig, *Fuel Process. Technol.*, **12**, 175 (1986)
5 J. A. Ruether, J. A. Mima, R. M. Kornosky, and B. C. Ha, *Energy Fuels*, **1**, 198(1987)
6 R. A. Graff and S. D. Brandes, *Energy Fuels*, **1**, 84 (1987)
7 S. H. Townsend and M. T. Klein, *Fuel*, **64**, 635 (1985)
8 D. S. Ross, B. H. Loo, S. Tse, and A. S. Hirshon, *Fuel*, **70**, 289 (1991)
9 A. R. Katritzky and S. M. Allin, *Acc. Chem. Res.*, **29**, 399 (1996)
10 M. Siskin, A. R. Katritzky and M. Balasubramanian, *Fuel*, **72**, 1435 (1993)
11 L. Artok, O. Erbatur, and H. H. Schobert, *Fuel Process. Technol.*, **47**, 153 (1996)
12 C. Song, A. K. Saini, and J. McConnie, *Coal Science*, **1995**, 1391; C. Song, *Energeia*, **6**, 1 (1995)

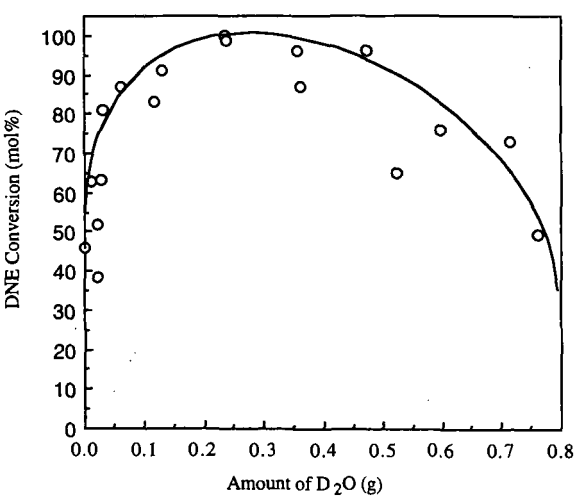

Fig. 1 Effect of addition of D_2O on conversion of 2,2'-dinaphthyl ether (DNE) at 350 °C for 30 min in 25 mL reactor. DNE: 0.216g; ATTM: 0.006g; n-C_{13}: 1.47g

Table 1 Effect of addition of H_2O on reactions of DNE at 350-400 °C under 6.9 MPa H_2.

Run No.	16	17	15	19	18	20	7	6	8	5	3	4
Catalyst Precursors	None	None	None	H_2O	H_2O	H_2O	ATTM	ATTM	ATTM	ATTM + H_2O	ATTM + H_2O	ATTM + H_2O
Temperature (°C)	350	375	400	350	375	400	350	375	400	350	375	400
DNE Conversion (mol %)	0.7	0.5	4.6	0.0	0.0	0.0	46.0	86.4	82.4	83.8	95.2	94.2
Products (mol %)												
Tetralin		0.7	5.4				31.4	70.9	66.7	72.7	106.1	109.1
Naphthalene		0.3	2.0				33.1	74.1	73.4	57.1	66.2	70.8
5,6,7,8-Tetrahydro-2-naphthol							8.0	6.2	3.6	8.1	9.5	6.0
2-Naphthol							2.2	4.7	12.6	3.4		
OctahydroDNE			0.3				1.3	2.0	1.0	2.5	2.2	
TerahydroDNE	0.6		0.6				7.4	6.5	3.2	10.6	2.1	1.2

Table 2 Catalytic reactions of DNE using ATTM and D_2O at 350-400 °C under 6.9 MPa H_2

Rnu No.	29	5	32	3	27	4
Catalyst Precursor	ATTM + D_2O	ATTM + H_2O	ATTM + D_2O	ATTM + H_2O	ATTM + D_2O	ATTM + H_2O
Temperature(°C)	350	350	375	375	400	400
DNE Conversion (mol%)	82.9	83.8	95.5	95.2	95.6	94.2
Products (mol%)						
Tetralin	68.8	72.3	106.5	106.1	106.5	109.1
Naphthalene	59.7	57.2	71.2	66.2	64.7	70.8
5,6,7,8-Tetrahydro-2-naphthol	7.9	8.0	9.0	9.5	6.6	6.0
2-naphthol	2.2	3.2			1.1	
OctahydroDNE	2.4	3.1	0.7	2.2	1.1	
TetrahydroDNE	11.2	11.3	1.5	2.1	1.2	1.2

Table 3 Two-step reactions of DNE under 6.9 MPa H_2.

Run No.	44	48	49	41	42	51	68	67	50	96*
1st-step Catalyst	ATTM	ATTM	ATTM	ATTM + H_2O	ATTM + H_2O	ATTM + H_2O	ATTM	ATTM	ATTM	ATTM + H_2O
1st-Step Temperature(°C)	350	375	400	350	375	400	350	375	400	350
2nd-step Addition	None	None	None	None	None	None	H_2O	H_2O	H_2O	None
2nd-Step Temperature(°C)	350	350	350	350	350	350	350	350	350	350
Conversion (mol %)	64.4	66.7	66.0	82.7	96.0	76.9	32.9	29.7	41.2	97.0
Products (mol%)										
Tetralin	49.1	46.9	44.7	58.6	76.5	53.1	26.8	22.9	31.9	89.6
Naphthalene	67.5	72.6	72.6	79.5	85.1	75.9	26.6	25.5	39.5	104.4
Tetrahydronaphthol	0.8	0.6	1.0	1.4	1.6	4.2	1.2	0.6	0.7	
2-naphthol	0.8	0.6	1.0	0.4	0.1	2.2	1.6	0.8	1.0	
OctahydroDNE	0.3	0.3	0.4	0.8	2.1	0.7	0.2	0.2	0.2	
TetrahydroDNE	5.1	6.1	6.0	12.0	12.2	8.5	4.6	4.6	4.4	

* After the first-step reaction, water was completely removed by hot venting at 200 °C for 35 min., prior to the addition of DNE for second-step reaction.

MECHANISM OF THE COBALT PHTHALOCYANINE-CATALYZED AUTOXIDATION OF ALIPHATIC THIOLS

E. I. Kozliak, A. Navid, Chemistry Dept., University of North Dakota, Grand Forks, ND 58202.

Keywords: cobalt phthalocyanines, autoxidation of thiols, Merox process

INTRODUCTION

Cobalt phthalocyanine (CoPc)-catalyzed autoxidation of thiols to disulfides has been used for the deodoration of oil distillates and exhaust gases in the fuel industry (1):

$$4\ RSH + O_2 \xrightarrow{CoPc} 4\ RSSR + 2\ H_2O \qquad (1)$$

The mechanism of this reaction is known to include the formation of a ternary complex of CoPc with both substrates: the thiolate-ion (RS^-) and molecular oxygen (1-5). Based on the results of our kinetic studies of cobalt tetrasulfophthalocyanine (CoTSPc)-catalyzed autoxidation of cysteine, we suggested that two thiolates and one oxygen may be bound by one molecule of CoPc to comprise the intermediate ternary complex (5). This hypothesis may be summarized by the kinetic scheme presented on Fig. 1.

In this paper we address the elucidation of the nature of the second thiolate binding to CoTSPc as well as the oxidation state of cobalt in the proposed intermediates. Association of CoTSPc occurring in the aqueous media (6) is not considered here since we have presented evidence that this phenomenon does not appear to affect the mechanism of reaction (1) (5).

EXPERIMENTAL

CoTSPc was synthesized as described by Weber and Busch (7), with minor modifications in purification. Initial reaction rates were measured by the oxygen consumption, which was monitored by one of two methods: amperometrically at a fixed potential of -0.6 V using a self-made Clark oxygen electrode, and also using an Intech oxygen monitoring system connected to a Gateway computer. The catalytic reaction rate was calculated as a difference between the rates of oxygen consumption with and without CoTSPc. All experiments were carried out at 25°C in 0.1 M sodium borate (for pH 9.0-12.2) or phosphate buffer (for pH 7.8-9.5); the reaction rates in different buffers for overlapping values of pH were similar within the margin of the experimental error. 0.5 M sodium perchlorate was added to all solutions to assure the constancy of the ionic strength. Spectral studies were conducted using a self-made evacuated cuvet on two spectrophotometers: Beckman-3600 and Shimatsu-260; the two devices gave comparable results. Before mixing, solutions of reagents (CoTSPc and a thiol) were frozen a few times by liquid nitrogen followed by the removal of the air and thawing the samples. Reactive grade reagents were used without purification.

RESULTS AND DISCUSSION

Binding of thiolate-ions by CoTSPc. Reaction of CoTSPc with low concentrations of cysteine (10^{-4}-10^{-2} M) in anaerobic conditions results in the appearance of new bands at 450 and 643 nm. Previously this spectrum was believed to be that of the plain reduced Co(I)TSPc (8). Now we report that this is not quite true. Whereas the band at 450 nm is, indeed, characteristic for any reduced complex of Co(I)TSPc, regardless of the reducing agent used, the bond at 640-650 nm turned out to be specific only for thiols (cysteine, mercaptoethanol, sodium hydrosulfide, and ethyl mercaptan have been tested). The spectra of CoTSPc with different concentrations of cysteine are provided on Fig. 2, curves 1-5). CoTSPc reduced by other reducing agents [hydrazine at pH 13, $NaBH_4$, or Cr(II)] adsorbs light at 680 nm (Fig. 2, curve 8). Upon increasing the cysteine concentration to $5 \cdot 10^{-1}$ M at pH 9.5, the difference in spectra for different reduced forms of CoTSPc disappears (Fig. 2, curves 6-8). This points to a successive binding of two thiolate molecules to CoTSPc. The stability constants found from the data of Fig. 2 are $1.7 \cdot 10^4$ M^{-1} and 52 M^{-1}; they correspond, respectively, to K_I and K_S from the suggested kinetic scheme [Fig. 1, equations (1') and (3')].

Analysis of the adsorption at 450 nm shows that binding of the first thiolate is accompanied only by a partial reduction of Co(II)TSPc, whereas the second thiolate binding

results in its quantitative reduction to Co(I)TSPc (see Fig. 2). Perhaps, this is related to an increase of the electron density on the cobalt ion upon the binding of the second basic thiolate ligand. It is logical to suggest that even more basic hydroxyl anion would cause the same effect. Indeed, at pH 12.2 the absorbance at 450 nm, reflecting the reduction of Co(II) to Co(I), is much higher than at pH 9-11.5 (Fig. 3) for any non-saturating concentration of cysteine. Actually, at pH 12.2 even as low as 10^{-2} M cysteine reduces Co(II) as efficiently as 10^{-1} M cysteine at lower pH, and at $5 \cdot 10^{-2}$M cysteine at pH 12.2 the reduction is complete (not shown). This phenomenon cannot be ascribed to the deprotonation of the amino group of cysteine since the threshold pH value 12.2 is much higher than the pK_a of the amino group [10.36 (2)]. We assumed that pH 12 appears to be the pK_a of deprotonation of the water molecule coordinated to cobalt in the monothiolate complex, (RS^-) Co(II)TSPc (H_2O).

There are other indications that pH 12 is a threshold value for the reduction of Co(II)TSPc. It is known that hydrazine and hydroxylamine reduce Co(II)TSPc only at pH>11.7, and their autoxidation occurs only at those high values of pH (9,10). In the absence of reducers in aerobic conditions, the binuclear adducts of CoTSPc with hydroxyl anion and oxygen are formed only at pH>12 (6). It was also shown that in the water-DMF system the coordination of hydroxyl anion to CoTSPc in anaerobic conditions results in the reduction of Co(II) to Co(I); in aerobic conditions the labile oxygen adduct is formed (11). In aqueous solutions, hydroxyl anion itself does not reduce Co(II)TSPc. Perhaps, the association of CoTSPc in aqueous solutions (6) interferes with the reduction of Co(II). However, despite this association, hydroxyl anion appears to reduce the monothiolate complex of Co(II)TSPc or other CoTSPc complexes with basic reducing ligands (hydrazine, hydroxylamine).

Kinetics of reaction (1) at different pH. The kinetic constants of CoTSPc-catalyzed autoxidation of cysteine at different pH are shown in Table 1. Comparison of binding constants of cysteine to CoTSPc obtained by kinetic and spectroscopic methods appears to confirm our hypothesis suggested in (5) that binding the first substrate molecule (K_1) does not show up in the kinetics because the concentration of thiolate is too high for any free CoTSPc to exist in the solution. Therefore, only the binding of the second thiol molecule shows up kinetically as K_S, see Table 1 and Fig. 1.

Kinetic data also appear to confirm the presence of a critical point at pH>12 for reaction (1) (Table 1). The value of K_S is virtually not changed at pH 9-10 when the deprotonation of the amino group of cysteine occurs, but it drops at pH 12.2 along with the reaction rate. Leung and Hoffmann (4) and Shirai *et al.* (13) observed the drop of the rate of reaction (1) for other aliphatic mercaptans, such as mercaptoethanol, aminoethanol, and ethane thiol. Therefore, this drop seems to be an inherent feature of reaction (1) and does not depend on the presence of other functional groups in cysteine. This occurs at the same value of pH 12 as the reduction of the monothiolate Co(II)TSPc complex discussed above (see Fig. 3). Hydroxyl anion, therefore, may be considered a competitive inhibitor of this reaction. The word "competitive", however, does not necessarily mean the literal competition of the hydroxyl ion and thiol for the same binding site; it merely reflects the fact that binding of the hydroxyl anion results in a decrease of the second thiolate binding constant, K_S. Apparently, the observed reduction of the monocysteinate CoTSPc complex by OH^- makes binding of the second electronodonor ligand, such as a thiol or thiolate, unfavorable.

In turn, the drop of K_S would result in the first kinetic order with respect to a thiol in alkaline solutions (pH>12) even for higher concentrations of the substrate (see kinetic equation (7') on Fig. 1). This indeed has been observed by Fomin *et al.* (14). In contrast, at lower pH, the order of reaction (1) with respect to the mercaptan should be 1 and 0 at low and high concentrations of the thiol, respectively, which has been observed in (4,5,15).

As mentioned above, the rate of reaction (1) drops at higher pH (Table 1). It may be explained in two ways: either the k_{cat} or binding constants of thiols drop above that pH, see kinetic equation (7') on Fig. 1. Both effects have been observed for the CoTSPc-catalyzed autoxidation of cysteine (Table 1). However, there are indications that the drop of k_{cat} at pH>9.5 is specific for cysteine, whereas the decrease of the thiolate binding to CoTSPc at pH>12 is a more general feature of the CoTSPc-catalyzed autoxidation of all aliphatic thiols. The drop of k_{cat} takes place at pH about 10, which is way below 12, and thus appears to be caused by the deprotonation of the amino group of cysteine [pK_a=10.36 (2)]. This deprotonation may result in a non-productive binding of some cysteine (by the amino group), thus causing the observed drop of k_{cat}. Indeed, Skorobogaty and Smith (15) did not observe any drop of the rate of reaction (1) for mercaptoethanol (no amino group) while increasing pH up to 11.5 at saturation by the thiol (zero kinetic order), when the value of k_{cat} determines the rate of the reaction.

It is interesting that the values of the constant of cysteine binding to CoTSPc, K_S, obtained from kinetic data, slightly increase while pH is decreased in the interval of pH 7.8-10.0, see Table 1. It apparently means that the complex (RS^-)CoTSPc(RSH) may be a little more stable than (RS^-)$_2$CoTSPc. That makes sense, because thiolates are much stronger electron donors than thiols, and the second thiolate binding to the electron-rich partially reduced monothiolate complex of CoTSPc may be slightly hindered even if this binding, as suggested below, takes place on the ligand.

Besides changes of K_S, there is one more kinetic parameter which is greatly affected by pH: parameter α. This parameter is actually the ratio of the oxygen binding constants of bis- and monocysteinate complexes (see equations 2' and 4' on Fig. 1). The question is: why the biscysteinate complex of CoTSPc is able to efficiently bind oxygen, especially at pH>12? It should have very low affinity to oxygen if the latter competes with the second cysteine for the second axial position of cobalt.

The most plausible explanation is the second thiolate binding is at least in part not coordinative and involves some weak interactions with the phthalocyanine ligand rather than with cobalt. Since the binding of the second thiolate results in the complete reduction of Co(II), one may assume that the RS radical formed may be shifted from cobalt into the ligand. A similar migration of the alkyl and acyl radicals was observed for alkyl- or acylcobalt(III) porphyrins by Dolphin *et al.* (12). The suggested non-axial binding of the second thiolate molecule may explain why the value of parameter α is not much less than 1 at all studied values of pH (Table 1); in other words, the second thiolate does not appear to be much in the way of the oxygen.

Let us consider the pH-dependence of α. Binding of the thiol should not contribute in the oxygen binding as much as that of the thiolate; perhaps, this is why α gets slightly lower when pH decreases within the range 7.8-10. One question remains to be answered: why the value of α sharply increases at pH 12.2? It appears to be related to the above suggested deprotonation of the water molecule coordinated to cobalt. Unfortunately, in contrast to the binding of cysteine, we have no spectral data to discuss the binding of oxygen to CoTSPc; ternary thiolate-oxygen complexes of CoTSPc are unstable in aqueous media. We may only speculate that at pH>12 the monocysteinate complex appears to have hydroxyl anion as the second axial ligand, and it may result in a poorer oxygen binding by this complex than at lower pH. So, perhaps, the axially bound hydroxyl ion slightly hinders the oxygen binding by the monothiolate CoTSPc complex (although it is not a big obstacle, the value of K_O at pH 12.2 is only slightly lower, see Table 1). However, the binding of the second thiolate increases the electron density on cobalt, thus forcing the OH^- out and facilitating the binding of the electron-acceptor oxygen molecule. The combination of those effects may result in the observed increase of α at pH 12.2, although this effect needs to be further studied.

Evidence of the hydrophobic binding of thiols to CoPc. Thus far we have considered the binding of the thiolates or thiols to CoTSPc only through coordination by their sulfur atoms. However, it is possible that hydrophobic interactions of the phthalocyanine ligand with the R group of a thiol may play some role in the substrate binding. Fomin *et al.* (14) studied the cobalt disulfophthalocyanine (CoDSPc)-catalyzed autoxidation of aliphatic thiols in very alkaline solutions (0.1 M sodium hydroxide). They found that longer-chain mercaptans are oxidized much faster, and tried to explain it by the electronic and steric effects. However, both of these effects appear to be insufficient to account for the significant increase of reaction (1) rates observed with the elongation of the carbon chain. The switch of the methyl group in the RSH to the ethyl group would result in the biggest inductive effect, and the subsequent addition of each methylene group would result in much less prominent changes. However, the observed effect is just the opposite (Table 2). This phenomenon may alternatively be explained by the binding of the R groups of thiols (RSH) or thiolates (RS^-) to the hydrophobic region of the phthalocyanine ligand. In contrast with electron effects, the hydrophobic binding would become more tenacious with addition of each methylene group, as it was observed in (14), see Table 2. We obtained a good correlation between the values of the observed first-order reaction rate constants for RSH from (14) and the distribution coefficients of the corresponding alcohols (ROH) in the system octanol-water [(16), Table 2]. Since at pH above 12 the first-order kinetics with respect to the thiol have been observed (14), the effective first-order kinetic constant should include K_S and be proportional to any factor affecting binding of the thiol, including its hydrophobicity. This is one more indication that the binding of one of the thiol molecules to CoTSPc appears to be non-coordinative.

PRACTICAL CONCLUSION

The Merox process of the removal of mercaptans from oil fractions consists of the extraction of mercaptans by alkaline solutions followed by the CoPc-catalyzed autoxidation of the mercaptides in the aqueous phase (1). For both processes the high concentrations of NaOH were considered optimal (1,17). However, we assumed that the increase of the rate of reaction (1) upon the addition of the extra sodium hydroxide observed in (17) may be irrelevant to the change of pH and may be accounted for by an unusually high salt effect in reaction (1) (5). Since the increase of pH above 12 appears to result in a decrease of the reaction rate, it would make sense to actually decrease the pH after extraction, at the same time adding some salt, such as NaCl, instead of NaOH, in order to increase the efficiency of catalysis. Obviously, this assumption takes into account only the rate of reaction (1) and disregards possible negative consequences of lowering the pH, such as an increase of thiol volatility and a decrease of its solubility in water.

ACKNOWLEDGEMENTS

The authors thank Dr. A. K. Yatsimirsky (UNAM, Mexico) for valuable suggestions. The work was supported by NSF-EPSCoR through NSF grant # OSR-9452892.

REFERENCES

1. Basu, B.; Satapathy, S.; Bhatnagar A. K. *Catalysis Reviews*, **1993,** *35*, 571-609.
2. Dolinsky, J; Wagnerova, D. M.; Veprek-Siska, J. *Coll. Czechoslovak. Chem. Commun.*, **1976,** *41*, 2326-2334.
3. Brouwer, W. M.; Piet, P.; German, A. L. *Journal of Molecular Catalysis*, **1984,** *22*, 297-308.
4. Leung, P.-S. K.; Hoffmann, M. R. *J. Phys. Chem.*, **1989**, *93*, 434-441.
5. Kozliak, E. I. *Preprints of ACS Division of Petroleum Chemistry*, **1996**, *41*, 628-631.
6. Gruen, L. C.; Blagrove, J. *Austral. J. Chem.*, **1973**, *26*, 319-325.
7. Weber, J. H.; Busch, D. H. *Inorganic Chemistry*, **1965**, *4*, 469-471.
8. Simonov, A. D.; Keyer, N. P.; Kundo, N. N.; Mamaeva, E. K.; Glazneva, E. V. *Kinetics and Catalysis (USSR)*, **1973**, *14*, 864-868.
9. Wagnerova, D. M.; Schwertnerova, E.; Veprek-Siska, J. *Coll. Czechoslovak. Chem. Commun.*, **1974**, *39*, 1980-1988.
10. Hong, A. P.; Chen, T.-C. *Environ. Sci. Technol.*, **1993**, *27*, 2404-2411.
11. Dubrovina, A. S.; Malkova, A. I.; Tupikov, V. I. *Coordination Chemistry (USSR)*, **1984**, *10*, 1207-1210.
12. Dolphin, D.; Halko, D. J.; Johnson, E. *Inorganic Chemistry*, **1981**, *20*, 4348-4351.
13. Shirai, H.; Tsiuki, H.; Masuda, E.; Koyama, T.; Hanabusa, K.; Kobayashi, N. *J. Phys. Chem.*, **1991**, *95*, 417-423.
14. Fomin, V. A.; Mazgarov, A. M.; Lebedev, N. N. *Petroleum Chemistry (USSR)*, **1979**, *18*, 298-306.
15. Skorobogaty, A.; Smith, T. D. *J. Mol. Catal.*, **1982**, *16*, 131-146.
16. Leo, A.; Hunch, C.; Elkins, D. *Chem. Rev.*, **1971**, *71*, 525-548.
17. Fomin, V. A.; Mazgarov, A. M. *Petroleum Chemistry (USSR)*, **1981**, *21*, 265-273.

Fig. 1. Suggested kinetic scheme of reaction (1).

$$CoTSPc + RS^- \xrightarrow{K_1} (RS^-)\,CoTSPc \quad (1')$$

$$CoTSPc\,(Cys) + O_2 \xrightarrow{K_O} (RS^-)\,CoTSPc\,(O_2) \quad (2')$$

$$(RS^-)\,CoTSPc + RS^- \xrightarrow{K_{RS^-}} (RS^-)_2\,CoTSPc \quad (3')$$

$$(RS^-)_2\,CoTSPc + O_2 \xrightarrow{\alpha K_O} (RS^-)_2\,CoTSPc\,(O_2) \quad (4')$$

$$(RS^-)\,CoTSPc\,(O_2) + RS^- \xrightarrow{\alpha K_{RS^-}} (RS^-)_2\,CoTSPc\,(O_2) \quad (5')$$

$$(RS^-)_2\,CoTSPc\,(O_2) \xrightarrow{k_{cat}} CoTSPc + \text{products} \quad (6')$$

Observed kinetic equation [obtained in (5)]:

$$v_0 = \frac{d[O_2]}{dt} = \frac{\alpha k_{cat} K_O K_{Cys} [CoTSPc]\,[Cys]\,[O_2]}{1 + K_O[O_2] + K_{Cys}\,[Cys] + \alpha K_O K_{Cys}[Cys]\,[O_2]} \quad (7')$$

Table 1. Kinetic parameters of reaction (1) at different pH

pH	K_O, M^{-1}	K_S, M^{-1}	α	k_{cat}, s^{-1}
7.8	$5.2 \cdot 10^4$	120	0.15	4.8
9.0	$2.7 \cdot 10^4$	90	0.33	9.4
9.5	$2.0 \cdot 10^4$	60	0.5	10.5
10.0	$3.5 \cdot 10^4$	80	0.6	4.6
12.2	$1.3 \cdot 10^4$	9	5.3	3.0

Table 2. Observed rate constants of CoDSPc-catalyzed autoxidation of alkyl mercaptides in 0.1 M aqueous solution at saturation with oxygen [k_{obs} (14)] vs. the distribution coefficient of the corresponding alcohol, ROH, between n-octanol and water, P_{ROH} (16).

Mercaptan	$k_{obs} \cdot 10^{-4}$, s^{-1}	P_{ROH}
Methyl thiol	0.9	0.2
Ethyl thiol	1.0	0.5
1-Propyl thiol	2.3	2.2
1-Butyl thiol	4.5	7.6
1-Pentyl thiol	11.7	29

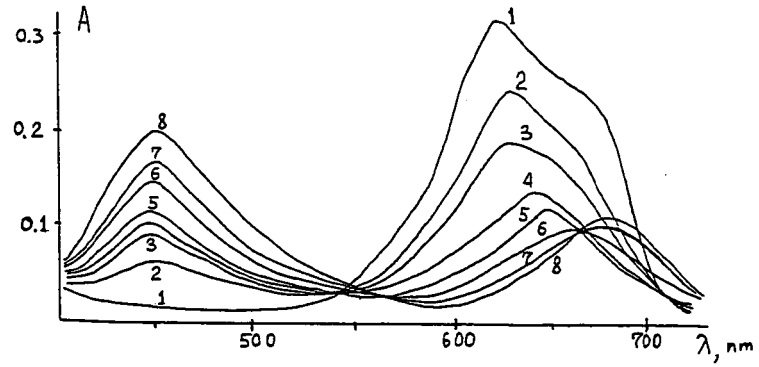

Fig. 2. Spectral changes occurring upon addition of the increased amounts of cysteine to the aqueous $8 \cdot 10^{-6}$ M solution of Co(II)TSPc in anaerobic conditions (pH 9.5, 0.1 M borate buffer, 0.5 M $NaClO_4$). 1. CoTSPc, no cysteine added; 2-7. Same solution with 10^{-4}, $2 \cdot 10^{-4}$, $5 \cdot 10^{-4}$, $5 \cdot 10^{-3}$, $5 \cdot 10^{-2}$, $5 \cdot 10^{-1}$ M cysteine, respectively; 8. Solution 1 with 10^{-2} M hydrazine, pH 13.

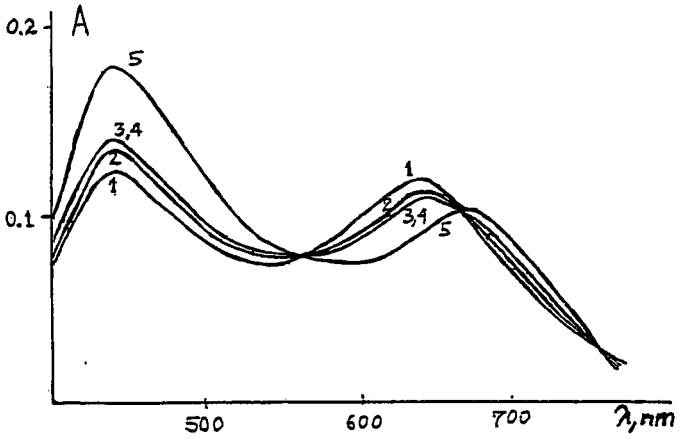

Fig. 3. Spectra of the complex of CoTSPc ($8 \cdot 10^{-6}$ M) with cysteine (10^{-2} M) at different pH: 1. 9.0; 2. 9.5; 3. 10.0; 4. 11.0; 5. 12.0, respectively.

A MECHANISTIC STUDY OF THE CHAIN PROPAGATION STEP IN THE FISCHER-TROPSCH SYNTHESIS

Ruhksana Quyoum, Helen C. Long, Michael L. Turner, Peter M. Maitlis

Department of Chemistry, The University of Sheffield, Sheffield S3 7HF, U.K.

KEY WORDS: Fischer-Tropsch synthesis, methylene, labelling studies

INTRODUCTION

The reductive polymerization of carbon monoxide to hydrocarbon mixtures (the Fischer-Tropsch synthesis) is a reaction that has attracted considerable interest ever since it was first discovered.[1,2] Typically, syn gas (CO/H_2) is passed over a heated, supported metal catalyst at atmospheric pressure or above which leads to the formation of a complex product mixture composed mainly of linear alkenes and alkanes.

The mechanism of the polymerization has long been the subject of debate. Early proposals by Fischer and Tropsch were that surface methylene, formed by the hydrogenation of dissociated CO, polymerized on the surface. Experiments by Brady and Pettit[3] confirmed the importance of methylene in hydrocarbon formation. They, and others[4] proposed that chain growth was initiated by surface alkyl/hydride groups thus giving surface alkyls as the chain carriers. This mechanism, however, is not without limitations; for example, low levels of C_2 hydrocarbons are formed which are not accounted for by this mechanism. Consequently, there has been renewed interest in the mechanism of C-C bond formation in the Fischer-Tropsch synthesis. One approach, used by us and others[5] involved studies of the reactions of well-defined metal complexes as model systems.

Early studies in this field were initiated by the decomposition reactions of organometallic complexes such as $[\{(\eta^5\text{-}C_5Me_5)Rh(CH_2)\}_2(Me)(MeCN)]^+$ which modelled a portion of a rhodium catalyst during carbon monoxide hydrogenation.[6] ^{13}C and D labelling studies indicated that C-C coupling proceeded by an unexpected route where vinyl ($-CH{=}CH_2$), rather than alkyl, was implicated as the key intermediate which coupled further with surface methylene to give the products.[7] Such alkenyl + methylene couplings may well represent lower energy processes than the couplings of the corresponding of alkyl + methylene groups.[8] These findings prompted further interest in the mechanism of C-C bond formation, and the nature of the intermediate species in the heterogeneously metal catalyzed hydrogenation of CO.

Our studies have further investigated the mechanism of the Fischer-Tropsch reaction, and in particular, evaluated the roles played by vinyl and methylene groups in hydrocarbon formation. This approach utilizes probe reactions which other workers,[9] have been found to be successful in providing mechanistic information during CO hydrogenation and extends earlier work involving the co-reaction of model reactants, including vinyl and methylene precursors, with CO and H_2 under Fischer-Tropsch reaction conditions.[10] For this study, ^{13}C probe molecules were used since unambiguous mechanistic information could be gained if they were incorporated into the products. Furthermore, other reactions of the probes could be investigated.

EXPERIMENTAL

Equipment

Quantitative analysis of the reaction products was carried out by gas chromatography on a Supelco SPB-1 (60 m x 0.53 mm x 5 mm) capillary column. The level of ^{13}C incorporation was analysed by GC-MS (HP 5890 - 5171 A).

Catalyst preparation

The catalysts were prepared by impregnation of the support (Davisil grade 645 silica gel) to incipient wetness to give metal loadings of 4%. $Rh(NO_3)_3$, $RuCl_3.xH_2O$ and $Co(NO_3).6H_2O$ were added to the support and slowly heated to 373 K with frequent stirring at which temperature the catalysts were fully dried. A solution of $Ce(NO_3)_3$ was added to the rhodium catalyst in order to increase the activity.

Reaction conditions and catalyst activation

The catalyst was reduced under a steady stream of hydrogen (1 atm, 700 $cm^3\ h^{-1}$), with programmed heating (4 K min^{-1}) from room temperature to 673 K. The catalyst was then cooled to the reaction temperature under hydrogen and the gas flow was switched to syn gas (1 atm, flow rate 500 $cm^3\ h^{-1}$). The products of the reaction were either sampled directly from the gas stream and analyzed by gas chromatography or collected in a liquid nitrogen trap and analyzed by GC-MS. For the runs with probes, the products were analyzed by GC and GC-MS before, during and after probe additions. A background GC was initially obtained to show the distribution of the products. After a period of 1.5 h, the probe molecule was added to the syn gas feed stream. Nitromethane and ethene were directly injected into the gas mixture through a septum and diazomethane gas was introduced by diverting the syn gas flow through the vessel which contained the diazomethane gas, prepared in situ. A GC analysis was performed after the probe had been added. After a further 1.5 h period, a final GC was carried out to determine the activity of the catalyst after addition of probe. Products were identified by comparison of their mass spectra with Wiley library spectra, stored in the HP ChemStation software.

RESULTS

Vinyl and methylene probes were individually reacted with $CO\text{-}H_2$ over Co/SiO_2, Ru/SiO_2, $Rh/Ce/SiO_2$ catalysts under Fischer-Tropsch reaction conditions ($CO{:}H_2$ = 1:2, 1 atm over 1 g catalyst). Diazomethane and nitromethane were used as sources of methylene (C_1) and vinyl species (C_2) were derived from ethene. Prior to any probe addition, the products of CO hydrogenation were typical for those obtained for the polymerization, containing mainly linear alkenes and alkanes together with some oxygenates. The product distribution followed modified Anderson-Schulz-Flory kinetics, with high C_1 and low C_2 fractions and a stepwise linear decrease beyond C_3.[11]

Vinyl probe addition

The effect of adding ethene as a source of vinyl to the CO hydrogenation was to increase the formation rate of the C_2 to C_7 hydrocarbons. During addition of the probe, the probability of chain growth, α, decreased for the various catalysts studied. Selected data of $^{13}C_x$ incorporation into the C_n hydrocarbons when $^{13}C_2$-ethene was used as a probe over cobalt for example, (= 0, 1, 2,...n) are given in Table 1.

Methylene probe addition

Diazomethane and nitromethane were used as sources of methylene since it was expected that under the experimental conditions those probes would decompose to give methylene intermediates, as previously reported.[12,3] Probe addition to the syn gas feed caused significant changes to the product distributions; in particular, there was an increase in the formation rate of C_3 to higher products and an increase in the probability of chain growth. The results of $^{13}C_x$ incorporation into the hydrocarbon products when $^{13}CH_2N_2$ or $^{13}CH_3NO_2$ was added to the CO hydrogenation over cobalt are summarized in Table 2.

DISCUSSION

Effect of probe molecule addition

The addition of the methylene (C_1) and vinyl (C_2) probe molecules to each of the experiments increased the amounts of higher hydrocarbons produced. Ethene addition caused an increase in C_2 to C_7 products; the effect was largest, as might be expected, for the formation of ethane by hydrogenation/hydrogenolysis. Addition of nitromethane and diazomethane probes to the CO hydrogenation increased the formation rate of C_3 to higher products. The changes in the hydrocarbon production during probe addition are marked by changes in the chain growth probabilities for each of the experiments; addition of ethene had the effect of decreasing α while methylene probe addition caused an increase in α. The latter is consistent with an increase in the rate of propagation during methylene probe addition.

^{13}C labelling studies

Addition of $^{13}C_2$-ethene to the $^{12}CO/H_2$ stream over all the catalysts studied clearly showed incorporation of $^{13}C_2$ units into the hydrocarbon products (Table 1). The levels of $^{13}C_2$ obtained are highly significant since they are many orders of magnitude greater than natural abundance. Incorporation of $^{13}C_1$ and $^{13}C_3$ units into the products are slightly higher than expected over cobalt. Thus, it is apparent that ethene undergoes some hydrogenolysis leading to the incorporation of $^{13}C_1$ units into the reaction products. Furthermore, there is little incorporation

of ^{13}C above natural abundance into the oxygenates indicating that they are not formed from vinyl groups. Similar patterns of ^{13}C labelling in the reaction products are obtained for the various catalysts studied.

The effect of adding $^{13}CH_2N_2$ or $^{13}CH_3NO_2$ to the ^{12}CO hydrogenation over cobalt gave results consistent with the incorporation of $^{13}C_1$ units into the hydrocarbon products (see Table 2). For both probes, the levels of $^{13}C_1$ incorporation are significant since they exceed those expected on the basis of natural abundance. In fact, the extent of ^{13}C incorporation in the products of the reaction is consistent with the mixing of methylene groups derived from the syn gas reaction ($^{12}CH_2$) with those derived from the probe ($^{13}CH_2$). It is clear from Table 2 that the arrangement of $^{13}C_x$ atoms in the products is close to that expected on the basis of random mixing of the methylene groups for the ratio of ^{12}C to ^{13}C used in these experiments. Furthermore, similar ^{13}C levels are obtained irrespective of whether $^{13}CH_2N_2$ or $^{13}CH_3NO_2$ is used as the methylene source suggesting that both probes react on the surface to yield a common intermediate. By contrast, identical experiments over rhodium catalysts showed quite different behaviour giving two parallel chain growth pathways each of which forms hydrocarbons. One is the hydrogenation of CO and the other is an oligomerization of the probe derived intermediates. Thus, over rhodium, there is very little crossover between the two routes and the hydrocarbon products effectively contain either only ^{12}C atoms with ^{13}C at natural abundance only, or fully ^{13}C-labelled hydrocarbons which contain little or no ^{12}C.

The alkenyl mechanism for Fischer-Tropsch homologation

The results show that there is most incorporation of $^{13}C_2$ units when $^{13}C_2$-ethene is added to the $^{12}CO/H_2$ mixture. The degree of $^{13}C_2$ incorporation decreases with increasing number of carbons in the hydrocarbon products which is consistent with the C_2 species being involved in chain initiation. Addition of other probes such as ethyl bromide, vinyl bromide and tetravinylsilane indicate that the initiating species is the unsaturated vinyl group. The addition of methylene probes to the ^{12}CO hydrogenation result in the incorporation of $^{13}C_1$ units in the reaction products according to the alkenyl mechanism. The pattern of $^{13}C_1$ distribution in the products is determined by the nature of the metal. Thus, over cobalt, the degree of $^{13}C_1$ incorporation is consistent with a distribution based on random mixing of the methylenes derived from the probe and those from the syn gas. By contrast, similar reactions over rhodium lead to parallel chain growth pathways. One is CO hydrogenation, which forms products derived exclusively from ^{12}C, the other is a homopolymerization of methylene intermediates derived from the probe giving fully ^{13}C labelled products and there is very little crossover between the two routes. It is proposed that over rhodium, alternative methylene intermediates, possibly CH_2N, may form which lead to independent polymerization pathways.

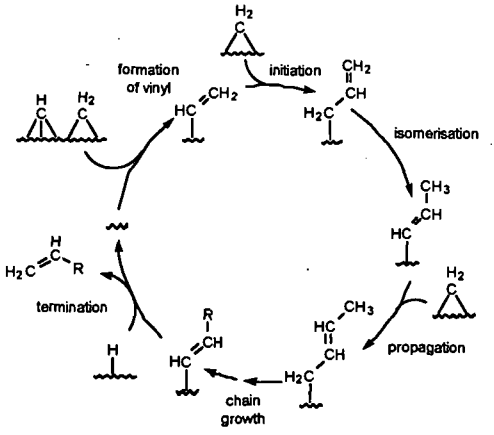

The alkenyl mechanism for Fischer-Tropsch homologation. Hydrocarbon formation is initiated by vinyl and propagated by methylene groups.

Table 1. Incorporation of $^{13}C_x$ from $^{13}C_2H_4$ over Co/SiO_2

x	0	1	2	3	4	5	6
1-butene	50	8 (2)	32	7	3		
1-pentene	55	9 (3)	27	8	2	1	
1-hexene	62	9 (4)	19	6	3	1	0

Figures in parentheses correspond to the expected % $^{13}C_1$ at natural abundance.

Table 2. Incorporation of $^{13}C_x$ from $^{13}CH_3NO_2$ and $^{13}CH_2N_2$ over Co/SiO_2

	$^{13}CH_2N_2$							$^{13}CH_3NO_2$						
x	0	1	2	3	4	5	6	0	1	2	3	4	5	6
1-butene	66	18	10	2	4			70	17	6	3	5		
1-pentene	75	15	7	2	1	0		73	15	7	2	1	0	
1-hexene	76	18	4	1	0	0	0	76	18	4	1	0	0	0

REFERENCES

1. Fischer, F.; Tropsch; H. *Brennst.-Chem.* **1926**, *7*, 97; *Chem. Ber.* **1926**, *59*, 830.
2. Anderson, R. B. *The Fischer-Tropsch Reaction*; Academic Press: London, 1984.
3. Brady, R. C.; Pettit, R. *J. Am. Chem. Soc.* **1980**, *102*, 6181; **1981**, *103*, 1297.
4. Biloen, P.; Helle, J. N.; Sachtler, W. M. H. *J. Catal.* **1979**, *58*, 95.
5. Knox, S. A. R. *J. Cluster Sci.* **1992**, *3*, 385.
6. Maitlis, P. M. *J. Organomet. Chem.* **1995**, *500*, 239.
7. Saez, I. M.; Meanwell, N. J.; Nutton, A.; Isobe, K.; Vàzquez de Miguel, A.; Bruce, D. W.; Okeya, S.; Andrews, D. G.; Ashton, P. R.; Johnstone, I. R.; Maitlis, P. M. *J. Chem. Soc., Dalton Trans.* **1986**, 1565. Martinez, J.; Gill, J. B.; Adams, H.; Bailey, N. A.; Maitlis, P. M. *J. Chem. Soc., Chem. Commun.* **1989**, 286.
8. Calhorda, M. J.; Brown, J. M.; Cooley, N. A. *Organometallics* **1991**, *10*, 1431. Evitt, E. R.; Bergman, R. G. *J. Am. Chem. Soc.* **1980**, *102*, 7003.
9. Hall, W. K.; Kokes, R. J.; Emmett, P. H. *J. Am. Chem. Soc.* **1959**, *82*, 1027. Hutchings, G. J.; Gottschalk, F. M.; Hall, M. V. M.; Hunter, R. *J. Chem. Soc., Faraday Trans. 1* **1987**, *83*, 571.
10. Turner, M. L.; Long, H. C.; Shenton, A.; Byers, P. K.; Maitlis, P. M. *Chem. Eur. J.* **1995**, *1*, 549. Maitlis, P. M.; Long, H. C.; Quyoum, R.; Turner, M. L.; Wang, Z.-Q. *J. Chem. Soc., Chem. Commun.* **1996**, 1. Quyoum, R.; Turner, M. L.; Long, H. C.; Maitlis, P. M. *J. Am. Chem. Soc.* **1996**, *118*, 10888. Quyoum, R.; Maitlis, P. M. unpublished work.
11. Biloen, P.; Sachtler, W. M. H. *Adv. Catal.* **1981**, *30*, 165.
12. Cavalcanti, F. A. P.; Oukaci, R.; Wender, I.; Blackmond, D. G. *J. Catal.* **1990**, *123*, 260.

MECHANISTIC INVESTIGATIONS OF THE IRON-SULFUR CATALYZED REDUCTION OF HYDROXYL-CONTAINING MODEL COMPOUNDS.

Tom Autrey, John C Linehan, Carrie J Stearns, Donald M Camaioni,
Lauren Kaune and James A Franz.
Pacific Northwest Laboratory, P.O. Box 999, Richland, WA 99352 USA

Key Words. Catalysis, mechanism, hydrogen transfer

INTRODUCTION.

The goal of our research has been to focus on the mechanisms of hydrogen transfer from donor solvents to coal model compounds in the presence and absence of iron/sulfur (FeS) catalysts. Previous work showed that hydrogen transfer from dihydroaromatic donor solvents occurs predominately by reverse radical disproportionation (RRD) and by free hydrogen atoms (HA) generated from the solvent derived cyclohexadienyl radicals.[1-6] Initially, our catalytic studies examined the efficiency of strong bond scission using a variety of FeS catalyst precursors.[7-9] Those studies showed that 6-line ferrihydrite (FeOOH) is an efficient precursor to highly active catalysts. A hydrogen donor solvent, 9,10-dihydrophenanthrene, promoted facile scission of strong carbon-carbon bonds (Ar-CH_2Ar) in those studies. Recent mechanistic studies have used structure reactivity arguments to show that hydrogen transfer from the FeS catalysts is consistent with selective and reversible hydrogen atom transfer from the reduced catalyst by a radical-like mechanism.[10-11]

In the present work we report our most recent results regarding the mechanistic pathways of hydrogen transfer from FeS catalysts to coal model compounds. The present study examines the effect of hydroxylic groups in the catalytic hydroliquefaction of coal. We report the results of our investigations of three different types of model compound structures, (1) *arylmethanols*; benzylalcohol, diphenylmethanol, 1-naphthalenemethanol, 1,2-diphenyl ethanol and (2) *alkyl alcohols*; 2-phenethylalcohol and octadecanol (3) *aryl alcohols*; phenol, naphthol and anisole. We show that reduction of these model compounds, by an apparent ionic pathway, competes with hydrogen transfer to the ipso-position of the substituted arenes.

EXPERIMENTAL.

Materials. All catalytic experiments used 6-line ferrihydrite, prepared by the Rapid Thermal Decomposition of Precursors (RTDS), as the catalyst precursor.[7] The 9,10-dihydrophenanthrene (DHP), 1 and 2-naphthol, phenol, 1-naphthalenemethanol, benzyl alcohol, 2-phenethyl alcohol, and octadecanol were used as purchased from Aldrich except for DHP. The DHP was distilled and recrystallized from methanol/dichloromethane. The 1,2-ditolylethanol was available from a previous study.[13]

Thermolysis Studies. Model compound (15 mg), 6-line ferrihydrite (3 mg), sulfur (3 mg), and DHP solvent (100 mg) were loaded into 5-mm o.d. borosilicate glass tubes and sealed under vacuum. Thermolysis was carried out in a fluidized sand bath regulated at the specified temperature for various times. The GC and GC/MS analyses of the products were carried out as described previously.[7]

RESULTS AND DISCUSSION.

Aryl Methanols. Thermolysis of benzyl alcohol at 270 °C in DHP containing 6-line ferrihydrite and sulfur produced toluene as the major observable product. However, the mass balance was less than 50% (Table I). Some higher molecular weight products, assigned by GC/MS analysis as benzylated phenanthrenes, were also observed, suggesting an ionic intermediate. Since benzyl alcohols readily undergo dehydration in the presence of trace amounts of acid to yield a cationic intermediate, it is reasonable to assume that the catalyst protonates the alcohol to generate a benzyl cation. Subsequent addition of the benzyl cation to the solvent, phenanthrene, is likely to provide the major pathway under the conditions used (Scheme I). This mechanistic scheme is consistent with the low mass balance observed for the catalytic reduction of benzyl alcohol.

Similarly, thermolysis of 1-naphthalenemethanol at 265°C for 60 minutes yielded 1-methylnaphthalene as the major product. Again, the mass balance for products detected by GC was low, 40-60%, based upon consumption of the starting material. Consequently it appears that the initial catalytic reduction of aryl methanols leads to retrogressive reaction products. However, at a higher temperatures of 325°C, the observed mass balance improved to 70% for the same reaction time. We believe this is a result of secondary catalytic thermolysis pathways, a reasonable assumption since we have shown that benzylated arenes are efficiently consumed in the presence of the FeS catalyst.[7]

Alkyl Alcohols. Thermolysis of 2-phenethyl alcohol led to the eventual formation of ethylbenzene (Table I). However, we observed the transient formation of phenethylthiol. The thiol concentration grew slowly during the reaction and subsequently decreased after long reaction times. This observation is consistent with dehydration of the alcohol to form styrene, an intermediate product leading to sulfur incorporation or reduction to ethylbenzene. It is reasonable to assume that the thiol is also converted to the styrene and H_2S by a similar mechanism (Scheme II).

Thermolysis of octadecanol yielded similar results. The concentration of octadecathiol was observed to grow in over a period of ca. 30 minutes and then to disappear. Analogous to the catalytic thermolysis of phenethylalcohol, aliphatic alcohols are reduced in the presence of the

catalyst.

Catalytic reduction of the methyl ester of 1,2-diphenylethanol yielded bibenzyl as the major product. This is noteworthy because if electron transfer from the arene to the catalyst were an important pathway, carbon-carbon bond scission of the 1,2-diphenylethanol radical cation is expected to yield toluene derived products.[14]

Aryl Alcohols. Thermolysis of 1- and 2-naphthol in DHP in the presence of the FeS catalyst precursor led to the formation of two major products, naphthalene and tetralin (Table I). After 60 minutes at temperatures between 320 - 330 °C, about 30% of the naphthol was consumed to yield roughly a 1 to 1.1 ratio of naphthalene to tetralin. For comparison, note that the thermolysis of phenol, even at higher temperatures (390 °C) yielded no observable chemistry. This is an interesting observation, given that in a control experiment, anisole, the methyl ether of phenol, was consumed at a comparable rate to naphthol, to yield phenol.

The observations of this study are consistent with our previously proposed mechanism involving reversible hydrogen atom transfer from the catalyst to the arene.[10] Ipso addition of a hydrogen atom is more endothermic than non-ipso addition and therefore not apt to be observed. The hydroxy group on naphthol stabilizes the radical adduct formed by transfer of a hydrogen from the catalyst. Hydrogen atoms likely transfer back and forth between the catalyst and the arene. Eventually the adduct is reduced by the transfer of a second hydrogen atom to yield dihydronaphthol. Subsequent reduction of the diene yields hydroxytetralin, followed by dehydration to dihydronaphthalene. Thermal pathways may also contribute to the observed products. (Scheme III).

As expected from our mechanistic proposal, aryl alcohols are reduced at a slower rate than either the alkyl or benzyl alcohols examined in this present work. Acid catalyzed reduction of aryl alcohols is expected to be extremely slow. Reduction of naphthol by a sequence of hydrogen atom transfer steps to yield an alkynol is the major route for the deoxygenation of 1 and 2-naphthol.

CONCLUSION.

Several pathways for the deoxygenation of the hydroxylic functional groups in model compounds are likely operating under iron/sulfur catalytic conditions. The initial step appears to be catalytic dehydration. Unfortunately, dehydration products may yield retrogressive reaction products. Catalytic dehydration of aliphatic alcohols yields intermediate olefins which incorporates sulfur under the reaction conditions. Reactions of benzylic alcohols leads to formation of benzylated solvent products. Fortunately, the formation of the thiol is reversible with the intermediate olefin being reduced to the corresponding hydrocarbon and the strong carbon-carbon bonds of benzylated arenes are efficiently cleaved in the presence of FeS catalysts in DHP. In summary: although the hydroxylic function in our model compounds are consumed at a rapid rate, they lead to products that must be 'treated' by further reactions with the catalyst to yield the desired products. The net result is a slight increase in hydrogen demand to bring about liquefaction of hydroxylated structures in coal model compounds.

ACKNOWLEDGMENT

This work was supported by the U.S. Department of Energy, Office of Basic Energy Research, Chemical Sciences Division, Process and Techniques Branch. The work was conducted at Pacific Northwest Laboratory, which is operated by Battelle Memorial Institute for the U. S. Department of Energy under Contract DE-ACO6-76RL0 1830. We thank Dean Matson for our supply of the catalyst precursors. Support for CJS and LK was provided through AWU-NW under grant DE-FG06-89ER-75522 with the U.S. Department of Energy.

REFERENCES

(1) Autrey, T.; Cleveland, E. A.; Franz, J. A.; and Camaioni, D. M. *Energy and Fuels, 1995, 9, 420-428.*

(2) Camaioni, D. M.; Autrey, T.; Salinas, T. B.; and JA Franz. *J. Am. Chem. Soc.* 1996, 118, 2013-2022.

(3) Autrey, T.; Powers, T.; Cleveland, E. A.; Franz, J. A.; and Camaioni, D. M. Proceedings, 8th International Conference on Coal Science. 1995, pp1431-1434.

(4) Camaioni, D. M.; Autrey, T.; and Franz, J. A. *J Phys. Chem.* 1993, 97, 5791.

(5) Franz, J. A.; Ferris, K. F.; Camaioni, D. M.; and Autrey S. T. *Energy and Fuels,* 1994, 8, 1016-1019.

(6) Watts, J. D.; Bartlett, R. J.; and Franz, J. A. *Chem. Phys. Letters*, 1996, 249, 496.

(7) Matson, D. W.; Linehan, J. C.; Darab, J. G.; and Buehler, M. F. *Energy and Fuels,* 1994, 8, 10.

(8) Matson, D.W.; Linehan, J. C.; Darab, J.G. ; Camaioni, D.C.; Autrey, S.T.; and E. Lui. 1995 MRS Symposium Proceedings #368, Synthesis and Properties of Advanced Catalytic Materials, E. Iglesia, P.W. Lednor, D.A. Nagaki, L.T. Thompson, eds. pp.243-248.

(9) Linehan, J. C.; Matson, D. W.; Darab, J. G. *Energy & Fuels* 1994, 56.

(11) Autrey, T.; Linehan, J. C.; Camaioni, D. M.; Kaune, L.; Wartob, H.; and Franz, J. A. *Catalysis Today* 1996, 31, 105-111.

(12) Autrey, T.; Linehan, J. C.; Camaioni, D. M.; Powers, T.; McMillan, E. F.; and Franz, J. A. *Fuel Preprints* 1995, 40(4) 973-977.

(13) Camaioni, D. M. and Franz, J. A. *J. Org Chem.* 1984, 49, 1607.

Table I
Reaction Rates and Products of Model Compounds with "Iron-Sulfide" (FeS) Catalysts in Sealed Tube Reactions with 9,10-Dihydrophenanthrene

Model Compound	Reaction Temp. (°C)	Mass Balance	Disappearance Rate (x 10^{-4} s^{-1})	Major Products
Benzyl Alcohol	270	40-50%[a]	33 ± 4	Toluene[b]
1-Naphthalene Methanol	265	40-60%[c]	80 ± 10	Naphthaldehyde 1-Methylnaphthalene
2-Phenethyl Alcohol	315	80%	4.7 ± .6	Ethyl Benzene[d]
Octadecanol	340	60-70%	5 ± 1	Octadecane[e]
Phenol	390	95%	No Reaction	None
1-Naphthol	320	90%	0.7 ± .1	Naphthalene, Tetralin[f]
2-Naphthol	330	95%	1.1 ± .1	Naphthalene, Tetralin[f]

a) Slightly higher mass balance was obtained for reactions at higher temperatures. b) Other products identified were benzaldehyde, and various isomers of benzylphenanthrene. c) Again higher mass balance was obtained for reactions at higher temperatures. d) Phenylethylthiol was identified by GC/MS. e) Octadecathiol identified by GC/MS. f) Close to a 1:1 ratio of the two major products was obtained.

Scheme I

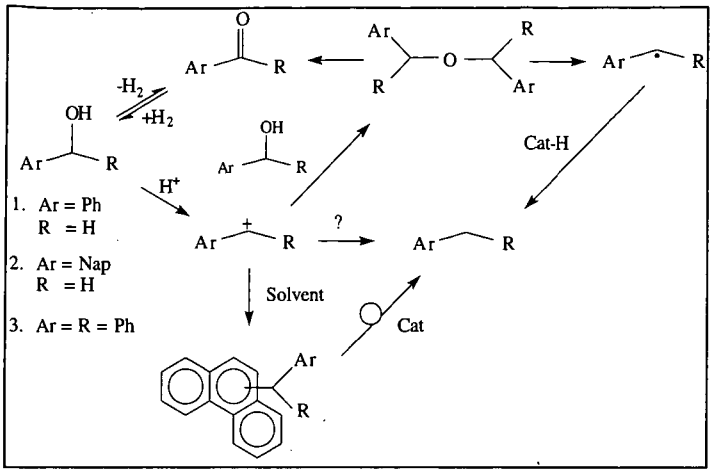

Scheme II

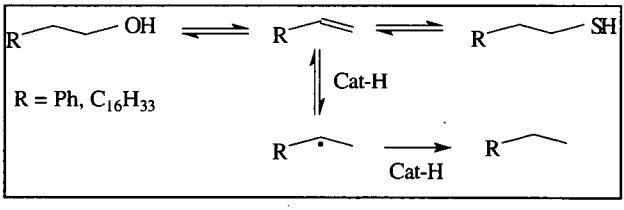

Scheme III

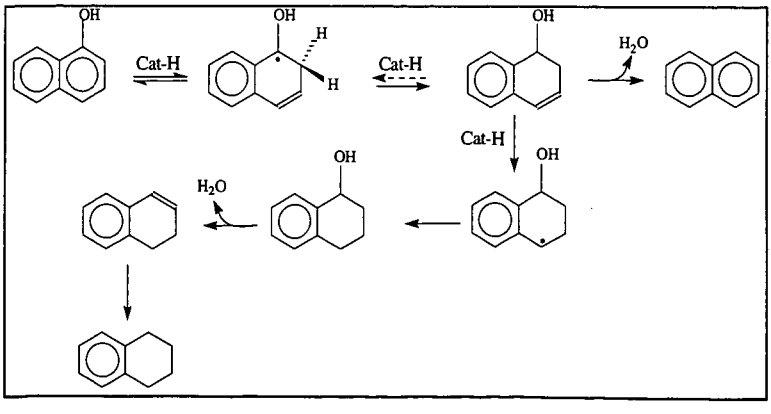

CONSIDERATION ON BOND CLEAVAGE REACTIONS OF BRIDGE STRUCTURE IN COAL MODELS AND COAL WITH TWO DIFFERENT HYDROGEN DONATING COMPOUNDS

Koh Kidena, Nobuo Bandoh, Satoru Murata, and Masakatsu Nomura
Department of Applied Chemistry, Faculty of Engineering, Osaka University
Suita, Osaka 565, JAPAN

Key words: bond cleavage, coal models, hydrogen donating compounds

INTRODUCTION

Coal organic material (COM) is believed to be an amorphous polymer consisting aromatic clusters with aliphatic side chains or bridges including naphthenic portion. Accordingly, COM should be described by certain chemical formula as other polymers are. Using various analytical methods coal chemical structure had been investigated in detail, however, COM is essentially far from the ordinal polymer. It does not contain any repeated units but many moieties and shows different behavior in its conversion reaction depending on its rank or its mining region. From these complexities, information concerning its chemical structure and reactivity is now still limited.

In coal utilization processes such as liquefaction, gasification or carbonization, decomposition of COM should be important. Judging from the accepted chemical structures for COM, the bond cleavage reaction of the bridge structure plays an important role in its decomposition. Now, we focus on this bond cleavage reaction in coal because this is one of the important reactions during heat-treatment of coal. There are many investigations which consider the coal models having the bridge structures as contained in coal and pursue the fashion of the reaction using the model compounds. Autrey et al.[1], Futamura et al.[2] and Nomura et al.[3] had mentioned the pyrolysis or hydrogenolysis of diarylmethane, while Korobkov et al.[4] reported the rate constants of thermolysis of diaryl or alkylethers in detail and discussed about their mechanisms. As to the behavior of side chains, Savage et al.[5] examined 1-alkylpyrene pyrolysis, and Nomura et al.[6] and Freund et al.[7] picked up the aromatic compounds having longer bridges or alkyl side chains. As to the mechanisms of the bond cleavage reactions occurred in coal, McMillen et al. proposed radical hydrogen transfer (RHT), which was also discussed by other researchers[1,8,9].

In a previous paper[10], we investigated the chemical structure change of coal during its carbonization process and pointed out the importance of the amount of the transferable hydrogen for development of coal plasticity. This seems to be parallel with many researcher's intentions. Here, by using DHA and DHP as the hydroaromatics, we considered two types of the bond cleavage reactions, the homolytic cleavage and the ipso position cleavage.

EXPERIMENTAL SECTION

Samples.

Coal samples employed in this work are the six kinds of bituminous coals, provided by the Iron and Steel Institute of Japan. The characteristics are summarized in Table 1. These coal samples were pulverized (-100 mesh) and dried at 100 °C for 6 h in vacuo prior to use. The substrates of model compounds 1,2-di(1-naphthyl)ethane (DNE) and 1,5-dibenzylnaphthalene (DBN), were synthesized as follows: DNE was prepared by reduction of (1-chloromethyl)naphthalene with iron powder in water and DBN was obtained by Et_3SiH/CF_3COOH reduction of 1,5-dibenzoylnaphthalene according to the method reported[3]. The other reagents or coal model compounds were commercially available and purified by recrystallization before use.

The heat-treatment of coal or its model compounds in the presence of hydrogen donating compounds.

A coal sample and 9,10-dihydroanthracene (abbreviated as DHA) or 9,10-dihydrophenanthrene (DHP) were put in a sealed tube (Pyrex, 6 mm inner diameter x 100 mm long) at the weight ratio of 1:1 (100 mg each), the tube being inserted into the electric furnace preheated at determined temperature (380 or 420 °C), and kept for 5 min. The temperature of the inside of the sealed tube was found to raise to the desired temperature within 2 min, the heating rate being about 200 K/min. After 5 min passed, the sealed tube was taken out and the products were recovered by breaking the tube and washing the inside of the tube with dichloromethane. After the addition of an appropriate internal standard, the amounts of DHA or DHP consumed were determined.

In the case of the model compounds [1,2-diphenylethane (DPE), benzylphenylether (BPE), 1,2-di(1-naphthyl)ethane (DNE) and 1,5-dibenzylnaphthalene (DBN)], 0.25 mmol of the hydrogen donating compounds and each model compound were heated under the similar conditions to those mentioned above. Qualitative and quantitative analyses of the products were undertaken by a Shimadzu QP-2000A GC/MS and a Shimadzu GC-14APSFC gas chromatograph with CBP-1 column (0.25 mm diameter x 25 m long), respectively. Duplicate runs, at least three times, were made for each set of the reaction to insure reproducibility.

RESULTS AND DISCUSSION

The reaction of coal with hydrogen donating compound.

The heat-treatment of the six sample coals with the hydrogen donating compounds, DHA or DHP was carried out at 380 or 420 °C for 5 min. The reaction gave the corresponding dehydrogenated compound, anthracene or phenanthrene, as the major product along with minor amounts of tetrahydro-derivatives (mainly 1,2,3,4-tetrahydro isomer). When either DHA or DHP was treated in a sealed tube without coal (blank runs), there observed negligible amounts of tetrahydro-derivatives. These results suggest tetrahydro-derivatives to be derived from coal-catalyzed disproportionation of DHA or DHP.

We evaluated the amounts of hydrogen transferred from DHA or DHP to coal according to the following equation:

The amount of hydrogen transferred (mg H_2/g daf coal) = [wt. of anthracene or phenanthrene (mg) x 2/178 - wt. of tetrahydro-derivatives (mg) x 2/182] x 1000/wt. of daf coal (mg)

The results of the reaction of coal with the hydrogen donating compounds are shown in Figure 1. The lower the rank of the coals was, the more amounts of hydrogen were consumed. As we had already reported, the chemistry in the reaction at around 400 °C was considered as the bond cleavage reactions of bridge structures contained in coal, this hypothesis being supported partially by the fact that lower rank coals have rich amount of easily cleavable bonds such as ether bonds due to their higher contents of oxygen.

It is interesting to note that in the reaction at 420 °C, the amounts of hydrogen transferred from DHP were larger than those from DHA, while at 380 °C, DHA tended to donate more amounts of hydrogen to coal than DHP did. It is reasonable, at first, that at 420 °C amounts of hydrogen transferred are larger than that at 380 °C because cleavage reactions took place extensively at higher temperature. As for interesting behavior of DHP and DHA, we can say that the bond cleavage reaction occurred during the heat-treatment is dependent on the type of the hydrogen donating compounds. Therefore, in order to compare the reactivity of the hydrogen donating compounds, DHA and DHP, we conducted the reaction of the coal model compounds which have the bridges between the aromatic moieties, such as 1,2-diphenylethane and so on with the hydrogen donating compounds under the similar conditions to the reaction with coal

Homolytic cleavage reaction of dimethylene and methylene-ether bonds.
Generally, coal macromolecule is considered to consist of aromatic cluster and alkyl bridges or side chains including naphthenic portion, being regarded as cross-linking polymers as a whole. In the proposed coal chemical structure models, there observed the bridge structures between two aromatic rings, such as $-CH_2-CH_2-$, $-CH_2-O-$ or $-CH_2-$ and so on, these seeming to be important in the thermochemical reaction. On the basis of this background, we employed 1,2-diphenylethane (DPE), benzylphenylether (BPE), and 1,2-di(1-naphthyl)ethane (DNE) as coal model compounds having the bridge structures.

The heat-treatment of these compounds in the presence of DHA or DHP was conducted under the similar conditions to that of coal. It was found that the conversion of BPE was rather high (> 95 %) while those of DPE and DNE were low (< 6 %). The bridge structure in coal is thought to be cleaved more easily than those in DPE or DNE were because of the relatively large size and many substituents of coal aromatic rings which can assist, in general, the cleavage reactions. On the other hand, rather high reactivity of BPE with homolytic fission of bridge bond can be easily understood because bond dissociation energy of carbon-oxygen is low. Here, in order to observe much more difference of the reactivities of DPE and DNE in either DHA or DHP, the reaction time was prolonged as 60 min. The reaction temperature of BPE was set to 380 °C for 5 min because BPE was found to be more reactive than DPE or DNE.

Figure 2 shows the results of the reactions in the presence of two different hydrogen donors. Under these conditions, considerable amounts of DHA or DHP were converted in each blank run so that the yield of anthracene or phenanthrene would not properly reflect the exact amount of DHA or DHP consumed for hydrogen transfer. Therefore, we evaluate the degree of the bond cleavage reaction on the basis of the yields of the cleaved products. The conversion of the model compounds reflects the strength of cleavable bonds (order of bond dissociation energy is $PhCH_2$-OPh << $NapCH_2$-CH_2Nap < $PhCH_2$-CH_2Ph). DPE showed less reactivity even under these conditions (420 °C, 60 min), and slightly higher yield of toluene when DHP was used as the hydrogen donor than in the case of DHA. Actually, the same trend was observed with the reaction of DNE at 420 °C for 5 min. It is thought that the less reactivity of DPE might be caused by the small size of aromatic rings and the absence of substituents like -OH or alkyl groups, however, much more reactivity would be expected with bridge bonds contained in the structure of coal. On the other hand, it should be noted that yields of the homolytic cleavage products from DNE or BPE, 1-methylnaphthalene or toluene and phenol, respectively, were higher when DHA was used than in the case of DHP. These results remind us that DHA has the higher potential to scavenge the radical generated.

Ipso position cleavage reaction of the bridge structure in model compounds.
In the reactions of DPE and DNE, there also observed the formation of the ipso position cleavage products like benzene and ethylbenzene, and naphthalene and ethylnaphthalene, respectively (eq. (1), (2)).

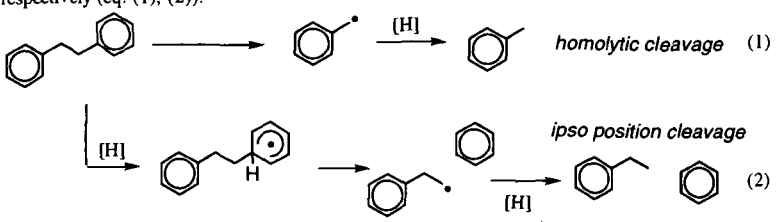

The reaction of DPE or DNE with two different hydrogen donors at 420 °C for 60 min gave the ipso position cleavage products in 0.1-6.6% yield (Figure 3). These yields from the reaction using DHP were considerably higher than the case of DHA. In the case of BPE, only homolytic

cleavage reaction occurred. However, the yields of the ipso position cleavage products were relatively low in comparison with those of the homolytic cleavage products. Here we would like to refer to the reports concerning bridge bonds contained in coal[11]. RuO_4 oxidation reaction confirmed that, in coal, dimethylene bridge connecting two aromatic moieties exists because the formation of succinic acid was observed in the oxidized products of COM. The presence of succinic acid shows the presence of dimethylene bridge. However, as for monomethylene bridge this oxidation could not confirm its presence in COM because under these oxidation conditions, the malonic acid is unstable. In generally speaking, the prevailing presence of monomethylene bridge bond in COM is supported by many coal researchers. Then, we employed 1,5-dibenzylnaphthalene (DBN) as the possible substrate of coal model compounds. It does not have homolytic cleavable linkages like $-CH_2-CH_2-$ or $-CH_2-O-$, so only the ipso position cleavage is expected to take place. Its reaction afforded benzene, toluene, benzylnaphthalene and benzylmethylnaphthalene. However, only small amount of naphthalene derivatives was obtained and the recovery of the substrate was not so high. This could be explained by assuming that some oligomerization or very complicated reaction might occur under the reaction conditions as we had pointed out in a previous paper[3]. Therefore, we judged the degree of cleavage on the basis of the sum of the yield of benzene and toluene. Also from this result, the ipso position cleavage by using DHP could proceed more efficiently than in the case of DHA. In this system, strong C_{alkyl}-C_{aryl} bond must be cleaved by solvent induced scission. It could be suggested that introduction of hydrogen atom as a result of radical hydrogen transfer or free hydrogen transfer occurred in heat-treatment of coal, and Malhotra et al. also mentioned the effectiveness of ipso position cleavage in liquefaction reaction[12].

Consideration about the bond cleavage reaction of the bridge structures in coal. In the reactions of coal with DHA or DHP, at 420 °C, DHP had been consumed at larger amounts and at 380 °C, DHA was the case as shown in Figure 1. As we had already mentioned, we thought that these consumption of hydrogen donor could correlate to the degree of bond cleavage reaction occurred in coal. Although we know that the reactions during heat-treatment would be so complex that they could not be described simply, the bond cleavage reactions of the bridge structures in coal proceeded mainly under our conditions.

If we here assume that with higher rank coal in the present study, monomethylene bridge prevails, we can easily understand the results shown in this paper. At 420 °C for 5 min, DHP shows higher extent of hydrogen transfer than that of DHA, and DHP is favorable to DHA as for ipso position cleavage and above observation is readily understood by referring to the assumption that methylene bridge is prevailing bridge bond than more longer methylene bridges. At 380 °C, carbon-oxygen related bond is cleaved so that DHA is effective hydrogen transfer reagent than DHP. Therefore, we can say that there is a possibility to use DHP or DHA as the probe to understand the reactivity and structure of coal.

ACKNOWLEDGMENT

This work was partially supported by a Grant-in-aid provided by the Iron and Steel Institute of Japan, and the authors acknowledge the support of Sumitomo Metal Industries Ltd. for useful discussion.

REFERENCES

1 Autrey, T.; Alborn, E. A.; Franz, J. A.; Camaioni, D. M. *Energy Fuels* **1995**, *9*, 420.
2 Futamura, S.; Koyanagi, S.; Kamiya, Y. *Fuel* **1988**, *67*, 436; *Fuel* **1989**, *68*, 130.
3 Murata, S.; Nakamura, M.; Miura, M.; Nomura, M. *Energy Fuels* **1995**, *9*, 849.
4 Korobkov, V. Y.; Grigorieva, E. N.; Bykov, V. I.; Senko, O. V.; Kalechitz, I. V. *Fuel* **1988**, *67*, 657; *Fuel* **1988**, *67*, 663; *Fuel* **1989**, *68*, 262; *Fuel* **1989**, *68*, 264.
5 Smith, C. M.; Savage, P. E. *Energy Fuels* **1994**, *8*, 545.
6 Murata, S.; Mori, T.; Murakami, A.; Nomura, M. *Energy Fuels* **1995**, *9*, 119.
7 Freund, H.; Matturro, M. G.; Olmstead, W. N.; Reynolds, R. P.; Upton, T. H. *Energy Fuels* **1991**, *5*, 840.
8 McMillen, D. F.; Malhotra, R.; Hum, G. P.; Chang, S.-J. *Energy Fuels* **1987**, *1*, 193.
9 Savage, P. E. *Energy Fuels* **1995**, *9*, 590.
10 Kidena, K.; Murata, S.; Nomura, M. *Energy Fuels* **1996**, *10*, 672.
11 Murata, S.; U-esaka, K.; Ino-ue, H.; Nomura, M. *Energy Fuels* **1994**, *8*, 1379.
12 Malhotra, R.; McMillen, D. F. *Energy Fuels* **1993**, *7*, 227.

Table 1. Ultimate and proximate analyses of the sample coals

Coal	Proximate analyses (wt%, db)			Ultimate analyses (wt%, daf)				
	Ash	VM	FC	C	H	N	S	O[a]
Lusca	9.5	23.5	67.0	88.3	4.6	1.5	0.3	5.3
Goonyella	9.8	23.4	66.8	88.1	5.1	1.9	0.6	4.3
Pittstone-M	7.3	34.3	58.4	85.7	5.5	1.7	1.0	6.1
Workworth	13.8	34.2	52.0	84.7	5.9	1.8	0.6	7.0
Witbank	8.0	32.9	59.1	82.7	4.5	2.2	0.6	10.0
K-Prima	3.8	43.4	52.8	81.2	5.9	1.3	0.4	11.2

[a] By difference

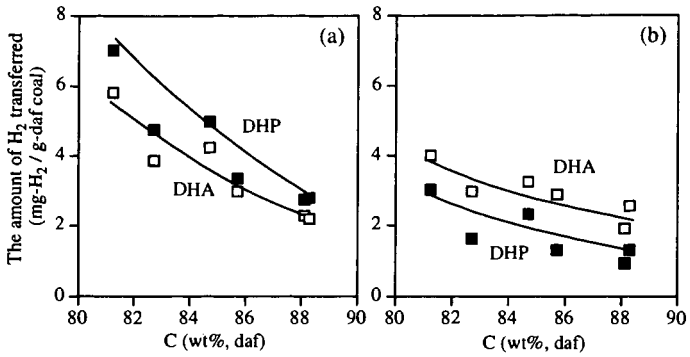

Figure 1. Evaluated amount of hydrogen trasferred from DHA (□) or DHP (■) to coal at (a) 420 °C and (b) 380 °C

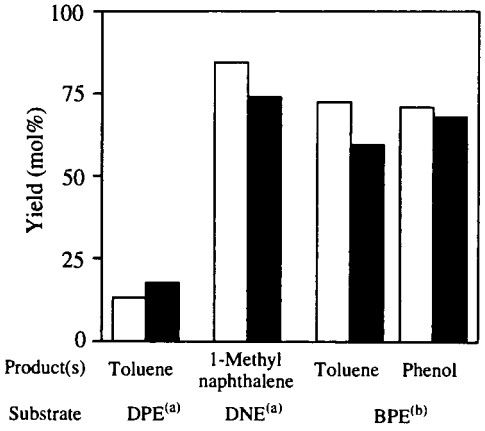

Figure 2. The yields of the homolytic cleavage products in the reaction of Ar-CH_2-X-Ar (X=CH_2, O) in the presence of hydrogen donor, DHA (□) or DHP (■); (a) 420 °C, 60 min, [Substrate]:[donor]= 0.25:0.25 (in mmol), (b) 380 °C, 5 min, [Substrate]:[donor]=0.25:0.25 (in mmol)

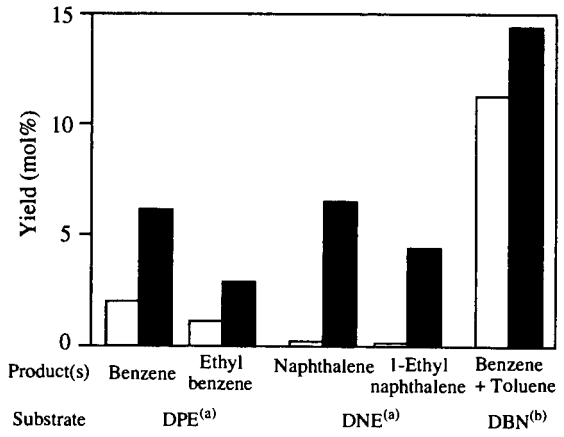

Figure 3. The yields of the ipso position cleavage products in the reaction of DPE, DNE and DBN in the presence of DHA (□) or DHP (■); (a) 420 °C, 60 min, [Substrate]:[donor]=0.25:0.25 (in mmol), (b) 430 °C, 60 min, [Substrate]:[donor]=0.25:0.25 (in mmol)

LIQUEFACTION OF MICRO ALGAE WITH IRON CATALYST

Toshimitsu Suzuki , Taka-o Matsui, Chiyo Ueda, and Na-oki Ikenaga
Department of Chemical Engineering, Kansai University
Suita, Osaka Japan 564

Keywords : Liquefaction, Micro algae, Dispersed iron catalyst

INTRODUCTION

Recently, carbon dioxide fixation by cultivating micro algae is being investigated. Since cultivated micro algae would be degraded into carbon dioxide, methane, and water by micro biological process, effective utilization of micro algae produced are highly required.

Production of liquid fuels from biomass have been extensively studied. Effects of hydrogen donor solvents[1] or alkali metal carbonate catalysts[2] on biomass conversion were reported under a hydrogen or a carbon monoxide atmosphere. Yokoyama *et al.* summarized techniques concerning the liquefaction of wood, and reported that sodium carbonate is effective catalyst for increasing the oil yield in water in the absence of reducing gas.[3] More lighter oil was obtained in a high yield by the addition of organic solvents such as propanol, butanol and ethyl acetate.[4] Dote *et al.* reported that sodium carbonate was effective catalyst for the liquefaction of Botryococcus braunii in water under nitrogen.[5]

In this work, we have investigated liquefaction of Spirulina in various organic solvents or water under a hydrogen, a nitrogen or a carbon monoxide atmosphere in the temperature range of 300-425 ℃ using Fe(CO)5-S catalyst developed for the liquefaction of coal[6] and discussed the effects of reaction conditions and catalysts on the product distribution and properties of oil.

EXPERIMENTAL SECTION

Spirulina (C 46.1; H 7.4; N 4.8; S 0.4; O 41.4 %, protein 57.5; fat 12.0; fatty acid 1.0; carbohydrate <0.5 %) was used as a micro alga. A 2.0 g of dried Spirulina, 8.0 g of tetralin, 1-methylnaphthalene, toluene or water and the prescribed amount of catalyst were put into a 50 mL magnetically stirred autoclave. The autoclave was pressurized to 5 MPa with hydrogen, nitrogen or carbon monoxide, and then the autoclave was heated up to a certain reaction temperature. After the reaction, products were separated by extraction with THF. THF soluble fraction was further separated into hexane-insoluble and hexane soluble (oil fraction). Gaseous products were analyzed by gas chromatography. As a catalyst, Fe(CO)5-S (Fe 1.0 mmol, S/Fe=2) was used. Oil fractions obtained in toluene and water were analyzed by FT-IR and gel permeation chromatography. C, H, and N elemental analyses were carried out at Osaka university.

Heating values of oil fractions were estimated by equation (1). Where C, H, N, S and O are normalized to weight fractions of respective elements in oil.[7]

$$Hg = 8400C + 27765H + 1500N + 2500S - 2650O \quad [\text{cal/g}] \qquad (1)$$

RESULTS AND DISCUSSION

Effect of reaction conditions in the liquefaction of Spirulina. Table 1 shows results of liquefaction of Spirulina at 350 ℃ for 60 min in tetralin or 1-methylnaphthalene under a hydrogen or a nitrogen atmosphere with or without a catalyst. More than 90 % of conversions and 50 % of oil yields were obtained under all the reaction conditions employed (runs 1-6). Gaseous products were mainly composed of methane (50-80 %) and carbon dioxide (10-30 %). Liquefaction of Spirulina under a nitrogen atmosphere without a catalyst gave 54.0 % of oil yield in 1-methylnaphthalene and 52.3% in tetralin. Addition of Fe(CO)5-S increased the oil yield to 63.7 and 66.9 % under a hydrogen atmosphere in 1-methylnaphthalene and tetralin, respectively. In the liquefaction under hydrogen without the catalyst (run 5), 0.28 wt% of hydrogen was absorbed from gas phase, whereas hydrogen consumption in the liquefaction increased to 1.2 wt% with the catalyst. Hydrogen activated on the dispersed catalyst might have contributed to increase the oil yield. Liquefaction of Spirulina in tetralin, a more efficient solvent for the liquefaction of woody biomass,[1] afforded similar conversion and product distribution as compare to those obtained in 1-methylnaphthalene. It is reported that tetralin is effective for the liquefaction of lignocellulose.[8] However, Spirulina is mainly composed of proteins, thus fragment from Spirulina is considered to be stabilized easily even without a hydrogen donor. This is one of the characteristic differences between the liquefaction of micro algae and coal or woody biomass. Much smaller increases in the amount of hydrogen transferred to Spirulina would be accounted for the different mechanisms in the liquefaction of these two substances.

Effects of reaction temperature and reaction time in the liquefaction of Spirulina. Effects of reaction temperature on the product distribution in the liquefaction of Spirulina in tetralin is shown in Fig. 1 with or without catalyst. More than 90 % of conversions were obtained in the temperature range of 300-425 ℃ even without catalyst. Total yield of oil and gas increased from 46.8 to 80.4 % with increasing reaction temperature from 300 to 425 ℃. Oil yield including water was 42.4 % at 300 ℃ and increased to 62.2 % at 400℃, but oil yield did not increase above 400 ℃ as compared to that at 400 ℃, due to a large increase in the gas yields from 9.8 % at 400 ℃ to 13.9 % at 425 ℃. Oil yield in the presence of catalyst showed similar tendencies, but effect of the catalyst was pronouncedly observed at 350 ℃. Again remarkable increases in gas yields were observed above 400 ℃. At a lower or a higher temperature, an addition of catalyst only slightly affected product distribution in the liquefaction of Spirulina.

Fig. 2 shows effects of reaction time on the product distribution in the liquefaction of Spirulina at 350 ℃ in tetralin without catalyst and with Fe(CO)5-S. More than 90 % of conversions were obtained irrespective of reaction time and in the presence or absence of catalyst. Oil yield without

catalyst slightly increased from 46.8 to 53.6 % with increasing reaction time from 0 to 30 min. However, product distributions were almost constant for prolonged runs in the absence of catalyst. Oil yield with $Fe(CO)_5$-S increased from 52.3 to 66.9 % with increasing reaction time 0 to 60 min, further increase in the reaction time did not change product distribution. Slower reaction producing oil was promoted with the addition of a highly dispersed catalyst under hydrogen atmosphere.

Liquefaction in water. In practical process, drying wet Spirulina required a large quantity of energy. Thus liquefaction of Spirulina in wet form is desirable.

Spirulina was liquefied in 1-methylnaphthalene under carbon monoxide atmosphere with 0.5-2.0 g of water in the presence of $Fe(CO)_5$-S catalyst. The results are shown in Table 1 (runs 8-10). Gas yields were not measured, because major gaseous products from Spirulina is carbon monoxide and carbon dioxide, and they were masked with the charged carbon monoxide and the carbon dioxide produced according to the water gas shift reaction.

Addition of 0.5 g of water in the liquefaction of Spirulina with $Fe(CO)_5$-S under carbon monoxide afforded 74.5 % of oil yield (run 8). Oil plus gas yield of 75.5 % was obtained under hydrogen (run 6) with the same catalyst. Further increases in the amount of H_2O to 2.0 g (run 10) increased the oil plus gas yield to 83.1 %. Hydrogen produced was amounted to 2.1, 4.7, and 6.3 mmol after the reaction in the presence of 0.5, 1.0, and 2.0 g of water, respectively. Oil plus gas yields obtained with H_2O exceeded those obtained under hydrogen in 1-methylnaphthalene. The result that high oil yield of 64.3 % was obtained in 1-methylnaphthalene-H_2O mixed solvent (run 7) indicates that hydrolysis of Spirulina possibly occurred. Such behavior is quite different from coal and woody biomass liquefaction.

Spirulina was liquefied in water under nitrogen without catalyst in the temperature range of 200-350 ℃ (Fig. 3). Conversion increased from 71.8 to 93.5 % with increasing the reaction temperature from 200 to 350 ℃. Gas yields were almost constant (6-8 %) in these temperature ranges. Oil yield increased from 48.4 to 78.3 % with increasing reaction temperature to 350 ℃. However, conversion was slightly smaller than that obtained in 1-methylnaphthalene-H_2O mixed system under carbon monoxide with the catalyst.

Characterization of oil fractions. In order to eliminate contamination of the solvent, for the characterization of oil fractions, a more volatile solvent toluene was used in the liquefaction of Spirulina. The results are shown in Table 1 (runs 11-13). Similar tendencies in the liquefaction behavior were observed in toluene as compared to those obtained in 1-methylnaphthalene.

Elemental compositions of feed and oil fractions are shown in Table 2. Carbon contents of oil fractions obtained in toluene are 64.2-69.0 % and these values are higher than that of feed (46.1 %). Oxygen contents (by differences) of products were lowered to 14.0-19.9 % as compared to 41.4 % of feed. Oil fractions obtained in water showed lower carbon content of 57.3 % and consequently higher oxygen content of 28.5 %. Ratio of H/C in oil was almost constant irrespective of reaction conditions and decreased to 1.50-1.55 from 1.93 in the feed and ratio of O/C decreased to 0.15-0.37 from 0.67 in feed. These findings indicate that deoxygenation through dehydration or decarboxylation proceeded in the liquefaction of Spirulina.

Heating values of oil fractions were calculated according to the formula proposed by Ringen *et al.*[7], *using elemental composition. Heating values of oil fractions were higher than that of feed.* Liquefaction of Spirulina in toluene gave oil fractions having heating values as high as 7700-7900 cal/g. Assuming water yield by the differences in the oxygen balance, 75.8 % and 71.1 % of heating values could be recovered as oil from the charged Spirulina having heating value of 4900 cal/g, in the liquefaction with or without $Fe(CO)_5$-S catalyst, respectively. Heating value of oil fraction obtained in water was 6200 cal/g and lower than that obtained in toluene, although a higher yield was obtained. Liquefaction in toluene with 1.0 g of water gave oil fraction not only in a high yield of 69.8 %, but also had a high heating value of 7300 cal/g. A presence of moderate amount of water is considered to be effective for the production of oil fraction having a high heating value in a high yield.

Fig. 4 shows FT-IR spectra of feed and oil fractions obtained in toluene and water with or without the Fe catalyst. Absorption at around 1652, 1545, and broad band 500-600 cm^{-1} ascribed to polypeptide in feed (a) are not seen in the spectrum of liquefied oil. This suggests that liquefaction of Spirulina proceeded by mainly scission of peptide linkages. Hydroxy or amine (3300 cm^{-1}), methyl and methylene (2800-3000, 1456, and 1389 cm^{-1}), and carbonyl (1705 and 1670 cm^{-1}) groups were confirmed by FT-IR spectra (b, c, and d). In the oil fraction obtained in water without the Fe catalyst (d), absorption peaks ascribed to carboxyl acid (3000-3300, 1705, and 1270 cm^{-1}) and amine (3300 and 1590 cm^{-1}) were more strongly observed as compared to the oil fraction obtained in toluene (b). This fact indicates that liquefaction of Spirulina proceeded via mainly hydrolyses of peptide linkages with water as shown in equation (2).

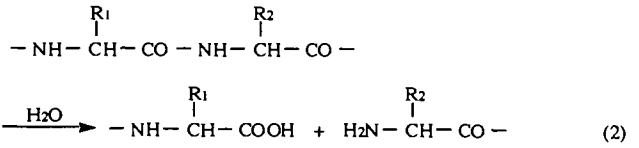

(2)

According to gel permeation chromatograms of the oil fractions prepared under different reaction conditions, molecular weights of oil fractions were distributed in broad range from 200 to 2000, showing peaks at 780 and 830. Since the evaporative light scattering detector was employed, detection of the low molecular weight component was limited to 200, possibility of the presence of lower molecular weight fraction can not be ruled out. Peaks at lower molecular weights region 400

and 490 were observed in the oil fractions obtained in toluene under hydrogen. Further increase in lower molecular weight product was observed in the liquefaction with the Fe catalyst. Thus the reactions to lower molecular weight product progressed through hydrocracking of C-C bonds with the catalyst under a hydrogen stmosphere.

These findings suggested that production of oil from Spirulina proceeded via mainly thermal decomposition or hydrolyses of peptide linkages with water fed or produced during liquefaction and hydrocracking of C-C bonds is promoted in the presence of a catalyst under hydrogen.

CONCLUSION

Liquefaction of Spirulina at 300-425 ℃ under hydrogen gave more than 90 % of conversions and 60 % of oil yields. Addition of $Fe(CO)_5$ catalyst increased oil yield from 52.3 to 66.9 % at 350 ℃ for 60 min in tetralin. Liquefaction in water gave oil yield as high as 78.3 % at 350 ℃ even under nitrogen atmosphere without the catalyst. Liquefaction in toluene gave oil fractions having high heating value of 7700-7900 cal/g, but the products containing large amount of oxygen estimated to have lower heating value of 6200 cal/g.

FT-IR and gel permeation chromatograph suggested that production of oil fractions mainly proceeded via thermal scission of polypeptide and hydrolysis with water, and further hydrocracking of C-C bond is promoted in the presence of $Fe(CO)_5$-S catalyst under hydrogen.

REFERENCES

(1) Thring, R.W., Chornet, E. Can. J. Chem. Eng. 1993, **71**, 107.
(2) Beckman, D., Boocock, D.G.B. Can. J. Chem. Eng. 1983, **61**, 80.
(3) Yokoyama, S., Ogi, T., Koguchi, K., Murakami, M., Suzuki, A. Sekiyu Gakkaishi 1986, **29**, 262.
(4) Ogi, T., Yokoyama, S., Minowa, T., Dote, Y. Sekiyu Gakkaishi 1990, **33**, 383.
(5) Dote, Y., Sawayama, S., Inoue, S., Minowa, T., Yokoyama, S. Fuel 1994, **73**, 1855.
(6) Watanabe, Y., Yamada, O., Fujita., K.,Takegami, Y., Suzuki, T. Fuel 1984, **63**, 752.
(7) Ringen, S., Llanum, J., Miknis. M.P. Fuel 1979, **58**, 69.
(8) Vasilakos, N.P., Augstgen, D.M. Ind. Eng. Chem. Process. Des. Dev. 1985, **24**, 304.

Table 1 Results of the Liquefaction of Spirulina under Various Conditions

run	Solvent	H_2O (g)	Atmosphere	Catalyst	Conv.	Oil (%)	Gas	H_2-trans[a] (mmol)
1	TL		N_2	none	91.9	52.3	5.2	0.3 [b]
2	TL		H_2	none	92.2	54.2	7.2	4.5
3	TL		H_2	$Fe(CO)_5$-S	92.0	66.9	6.2	5.6
4	1-MN		N_2	none	88.1	54.0	5.2	0.1 [b]
5	1-MN		H_2	none	91.8	54.4	8.9	2.8
6	1-MN		H_2	$Fe(CO)_5$-S	94.9	63.7	11.8	11.7
7	1-MN	1.0	N_2	none	95.4	64.3	9.7	0.6 [b]
8	1-MN	0.5	CO	$Fe(CO)_5$-S	96.1	74.5		2.1 [b]
9	1-MN	1.0	CO	$Fe(CO)_5$-S	96.6	79.0		4.7 [b]
10	1-MN	2.0	CO	$Fe(CO)_5$-S	97.8	83.1		6.3 [b]
11	TOL		H_2	none	82.6	57.0	6.9	2.7
12	TOL		H_2	$Fe(CO)_5$-S	90.1	63.3	4.1	3.6
13	TOL	1.0	N_2	none	92.5	69.8	8.9	0.8 [b]
14	H_2O		N_2	none	93.4	78.3	6.8	0.5 [b]

Reaction temperature 350 ℃, reaction time 60 min, Spirulina 2.0 g,
solvent 8.0 g, initial pressure 5 MPa, $Fe(CO)_5$ 1.0 mmol, S 2.0 mmol.
a) Amount of hydrogen transferred to products from gas phase and tetralin.
b) Amount of hydrogen produced after reaction.

Table 2 Elemental Analyses of Oil Fraction Products

run	C	H	N	O[a]	H/C	N/C	Heating Value (cal/g)
		(%)					
	46.1	7.4	4.8	41.4	1.93	0.09	4902
11	69.0	8.6	8.4	14.0	1.50	0.10	7939
12	66.7	8.6	7.5	16.2	1.55	0.10	7674
13	64.2	8.3	7.6	19.9	1.55	0.10	7284
14	57.3	7.4	6.8	28.5	1.55	0.10	6215

Reaction temperature 350 ℃, reaction time 60 min,
Spirulina 2.0 g, solvent 8.0 g, initial pressure 5 MPa,
$Fe(CO)_5$ 1.0 mmol, S 2.0 mmol.
a) by differences

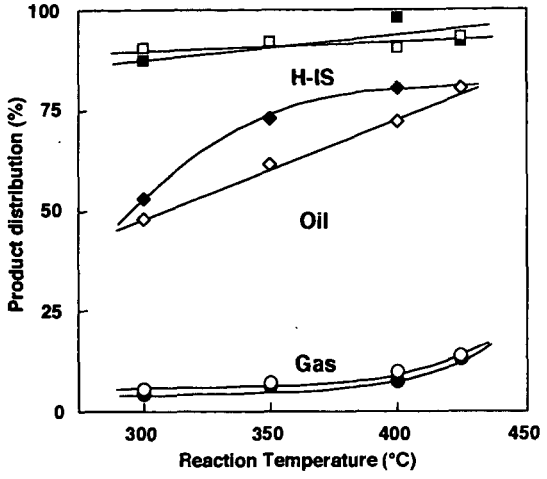

Fig.1 Effect of Reaction Temperature on the Product Distribution in the Liquefaction of Spirulina

Reaction time 60 min, Spirulina 2.0 g, TL 8.0 g,
PH_2 5.0 MPa, $Fe(CO)_5$ 1.0 mmol, S 2.0 mmol
□ ◇ ○ without catalyst, ■ ◆ ● with $Fe(CO)_5$-S

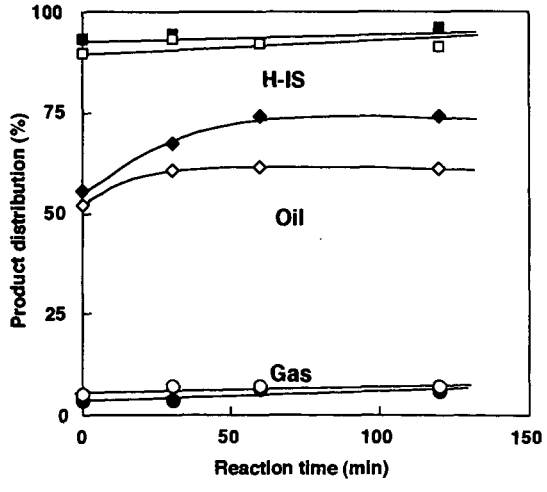

Fig.2 Effect of Reaction Time on the Product Distribution in the Liquefaction of Spirulina

Reaction temperature 350 °C, Spirulina 2.0 g, TL 8.0 g,
PH_2 5.0 MPa, $Fe(CO)_5$ 1.0 mmol, S 2.0 mmol
□ ◇ ○ without catalyst, ■ ◆ ● with $Fe(CO)_5$-S

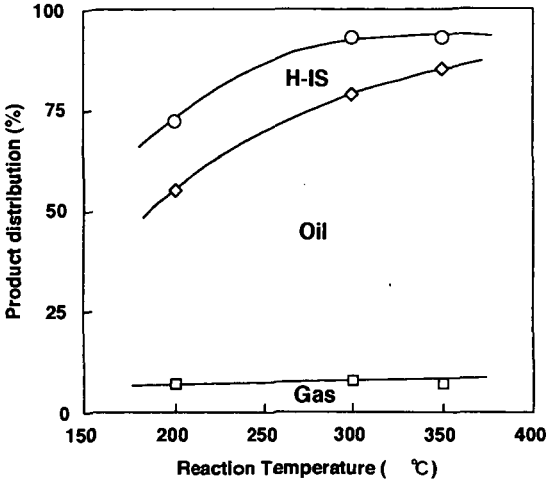

Fig.3 Effect of Reaction Temperature on the Product Distribution in the Liquefaction of Spirulina in water

Reaction time 60 min, Spirulina 2.0 g, H_2O 8.0 g, PN_2 5.0 MPa

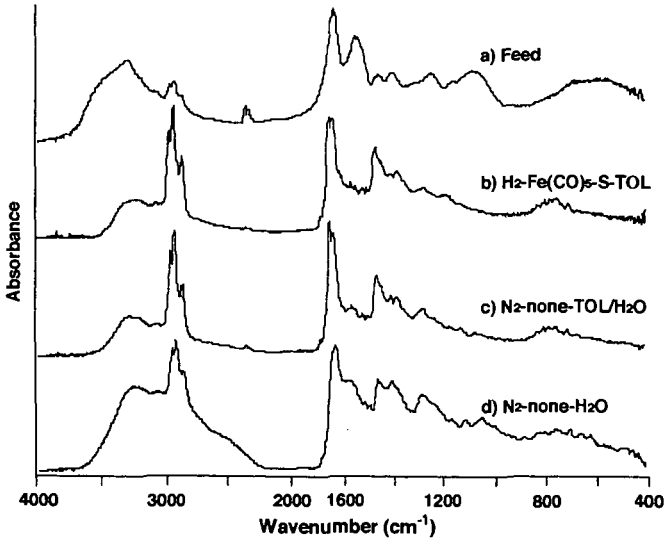

Fig.4 FT-IR Spectra of Spirulina and Liquefaction Products

Reaction temperature 350 °C, reaction time 60 min, Spirulina 2.0 g.
a) feed, b) PH_2 5.0 MPa, toluene 8.0 g, $Fe(CO)_5$ 1.0 mmol, S 1.0 mmol, c) PN_2 5.0 MPa, toluene 8.0 g, H_2O 1.0 g, d) PN_2 5.0 MPa, H_2O 1.0 g

MECHANISTIC MODELLING OF 9-METHYLANTHRACENE THERMOLYSIS

P.S. Virk and V.J. Vlastnik
Department of Chemical Engineering
M. I. T., Cambridge, MA 02139

KEYWORDS: Thermolysis, Mechanism, Kinetics, Numerical Simulation, Modelling.

INTRODUCTION

Motivation. This work on modelling thermolysis of 9-methylanthracene, abbr 9MA, continues our studies of methylated acenes, that mimic the chemical moieties found in complex fossil materials of engineering interest. Too, since 9MA is a primary product of 9,10-dimethylanthracene, abbr 910DMA, thermolyses [1, 2], it was hoped that the present work might buttress our understanding of 910DMA thermolyses at high conversions.

Previous Work. Detailed mechanistic modelling of 9MA thermolysis has not hitherto been attempted. However, the literature does contain some experimental information regarding 9MA thermolysis, which we have earlier summarized [3, 4, 5, 6].

Outline. Our modelling of 9MA thermolysis is based upon a 19-step mechanism, valid at low conversions, that was recently formulated to describe experimental observations [3]. Thermochemical parameters for all stable and radical species occurring in the mechanism were estimated from first principles. Next, enthalpies of reaction were calculated for each elementary step and used to infer Arrhenius parameters in both forward and reverse directions. Rate constants were then calculated for each reaction at a selected temperature, and these were used in conjunction with the differential conservation relations for each species to effect a full numerical solution of the model system, starting from an initial condition of pure substrate. The numerical simulation of 9MA thermolysis kinetics and product selectivities was directly compared with experimental observations at the same conditions. A sensitivity analysis was performed to discern how errors in the estimated Arrhenius parameters affected the model results. Finally, the Arrhenius parameters of certain elementary steps were adjusted, within their error limits, to provide an optimized model that best-fit the experimental observations.

REACTION PATHWAYS & MECHANISM

Pathways. Earlier experiments have identified three primary parallel pathways for thermolysis of 9MA, namely: (P1) hydrogenation to 9,10-dihydro-9-methylanthracene, abbr. DHMA, (P2) demethylation to anthracene, abbr. ANT, and (P3) methylation to 9,10-dimethylanthracene, abbr. 910DMA. The primary demethylation product ANT is associated with formation of methane gas CH4; heavy products are also formed, including both pure- and cross-termination types of dimeric species related to 9MA and DHMA, most notably a bibenzylic dimer called 9MAD.

Mechanism. A possible mechanism for 9MA thermolysis is presented in Fig. 1. This elementary step "graph" is constructed with substrate and all stable molecular products arrayed in the bottom row and unstable radical intermediates arrayed in the top row. Reaction "nodes", arrayed in the middle row, connect the individual species in the bottom and top rows with arrows indicating the initial direction of reaction (all reactions are, of course, reversible). Initiation reactions are denoted by solid interconnecting lines, propagation reactions by various kinds of dashed lines and termination reactions by dotted lines. Arrow weights qualitatively depict relative elementary reaction traffic, to be discussed in the next section.

The 9MA substrate is in the middle of the bottom row, with light (propagation) products to its right and heavy (termination) products to its left. The free-radical cycle is initiated by the bimolecular disproportionation of substrate (R1), an intermolecular hydrogen transfer reaction, to form the respectively dehydrogenated and hydrogenated radical species 9MA* and HMA10*. Of these, the latter can either abstract hydrogen from 9MA by (R2), to form DHMA product, or undergo a β-scission type of radical decomposition by (R3), forming ANT product and a methyl radical CH_3*. The CH_3* can either abstract H from 9MA by (R4), to form methane product, or add to 9MA by (R5), to form the dimethyl radical HDMA*. The latter can then abstract H from 9MA via (R6) to form the observed 910DMA product. The cycle is terminated by the species 9MA* and HMA10* engaging in both pure- and cross-combinations, (R7-R9), to form various dimeric products. HMA10* radical can also terminate by disproportionation, (R10), to form 9MA and DHMA. The foregoing portion of the full 9MA thermolysis mechanism is analogous to a 910DMA themolysis mechanism devised earlier [1, 2]. However, the 9MA substrate can also form the HMA9* radical, which can engage in all the reactions shown for HMA10* except for C-C bond scission, giving rise to steps (R11-R22) of the full mechanism. Thus substrate disproportionation by (R11) forms 9MA* and HMA9*, of which the latter can abstract hydrogen from 9MA by (R12), to form DHMA product. HMA9* can also form from H-transfer reactions (R16), between HDMA* and 9MA, and (R17), between HMA10* and 9MA, the latter causing radical isomerization. Finally, HMA9* can engage in a variety of termination reactions, including combinations (R18, R19, R21) that form dimeric products, and disproportionations (R20, R22) that form 9MA and DHMA.

The proposed mechanism accounts for the major products, ANT, DMAs, DHMA, CH4 and heavies, observed during the initial stages of 9MA thermolysis. Each of the observed triad of primary pathways, namely, P1 hydrogenation, P2 demethylation and P3 methylation, also arise naturally as limiting cases of the elementary step graph, with P1 comprising the sets [R1, R2, R7] and [R11, R12, R7], P2 the set [R1, R3, R4, R7] and P3 the set [R1, R3, R5, R6, R7]. The stoichiometry of these sets restricts the maximum selectivity of each major product to 1/3, which is of the magnitude of the highest selectivities observed experimentally. The mechanism also offers some theoretical insights. It suggests that the relative kinetics of hydrogenation to demethylation, (P1)/(P2), are controlled by the HMA9* and HMA10* radicals. The HMA10* radical propagates both hydrogenation (R2) and demethylation (R3), but HMA9* propagates

only hydrogenation (R12), leading to the pathway ratio (P1)/(P2) = [(R2)+(R12)]/(R3). Further, the methylation to demethylation ratio, (P3)/(P2), is essentially governed by competition between methyl radical reactions (R4) and (R5), in which CH_3* either abstracts H from or adds to the 9MA substrate, the latter favoured by the presence of a potent unsubstituted 10-position.

MODELLING

Thermochemistry. Enthalpies of formation, ΔH^0_f, for all chemical species participating in our 9MA thermolysis model were estimated by a "macro" group-additivity technique, using a basis set of bond strengths, D^0 kcal/mol, steric corrections, C^0 kcal/mol, and stable species enthalpies of formation, ΔH^0_f, assembled from a variety of sources cited previously [2, 7]. Fig. 2 illustrates the estimation procedures. For the stable species 9MA in (a), we started with the largest, most structurally similar basis species available, namely ANT; other basis species and steric corrections, in this case 1MN, NAP and an alkene gauche interaction, were then either added or subtracted to bridge the structural differences between the starting and the desired species. The method provided both ΔH^0_f, kcal/mol, and its rms error, kcal/mol. Calculations for a radical species, HDMA*, are shown in Fig. 2(b).

Arrhenius Parameters. Table 1 summarizes Arrhenius expressions, of the form $\log_{10} k = \log_{10} A - E^*/\Theta$, with rate constant k (l, mol, s units), pre-exponential factor A (same units as k), activation energy E^* (kcal/mol), and scaled temperature $\Theta = 0.004573*(T\,C + 273.2)$, that were generated for each step of the 9MA thermolysis mechanism. An elementary reaction was first classified (column 2) according to standard free-radical reaction notation and then kinetic data for that type of reaction were analyzed to ascertain its activation parameters. Of these, $\log_{10}A = \log_{10}A_{int} + \log_{10}(rpd)$ comprized an intrinsic portion, $\log_{10} A_{int}$ (column 3) and a reaction path degeneracy, rpd (column 4). Activation energy E^* was determined by an Evans-Polanyi expression (column 5), of form $E^* = E_0 + \alpha.\Delta H^0_r$ with $\alpha = 0$ (combinations), 0.5 (H-abstraction and transfer) or 1 (homolysis, beta-scission). Values of the enthalpy of reaction ΔH^0_r (column 6), derived from thermochemical estimates of the previous section, then led to E^* (column 7) and the final Arrhenius expression (column 8).

Numerical Solution. The model 9MA thermolysis reaction system was solved by a computer code called ACUCHEM [8]. This program numerically solves a system of differential equations that describe the temporal behavior of a spatially homogeneous, isothermal, multicomponent chemical reaction system. Integrations are performed by the method of Gear [9], appropriate for the stiff differential equations encountered in the present case. Two types of tests were performed to ensure reliable results. First, in regard to stability, it was verified that the program generated the same concentration profiles, regardless of the time step size. Second, in regard to fidelity, the concentrations of all species, both radical and stable, calculated by the numerical solution at low conversions $X < 0.1$ were found to agree with the corresponding concentrations obtained from pseudo-steady-state algebraic solutions at similar conditions.

RESULTS & DISCUSSION

Original Model. Numerical solutions of the 9MA thermolysis model were obtained at selected conditions covering the entire experimental grid, $315 < T\,C < 409$ and $0.082 < [9MA]_0$ mol/l < 2.06. The complete concentration histories of all radical and stable species obtained from each simulation are used in Figs. 1, 3 and 4.

Reaction Traffic. The arrows in Fig. 1 graphically depict the elementary reaction traffic calculated at T = 370 C, $[9MA]_0 = 0.82$ mol/l, and very low conversion $X \sim 0$, the thicker arrows denoting reactions with the greater net (forward - reverse) rates. The 910DMA substrate decomposes mainly, but not exclusively, by (R1) and (R11). The rates of hydrogenation (R2) and of demethylation (R3) are of comparable magnitudes, and the rate of methyl radical quenching by H-abstraction from substrate (R4) is appreciably less than that of its addition to the substrate (R5). Among termination reactions, 9MA* combinations, (R7) and (R18), are dominant.

Kinetics. Fig. 3 compares substrate decay half-lives t* calculated from the model (hollow points and dashed lines) with those observed experimentally, (solid points and lines). Fig. 3(a), a semi-logarithmic Arrhenius-type plot of t^* vs. $1/\Theta$, shows that, at constant $[9MA]_0 = 0.82$ mol/l, the calculated t* are about 2-fold higher than experimental and exhibit a lower apparent activation energy. Fig. 3(b), a log-log plot of t^* vs. $[9MA]_0$ at constant T = 370 C, shows that the calculated t* are 2- to 8-fold higher than experimental, the more so at the lowest $[910DMA]_0$, with the model predicting an apparent decomposition reaction order ~1.75, somewhat greater than the experimentally observed order ~1.5.

Product Selectivities. Fig. 4 compares (a) the selectivity to ANT product and (b) the ratio of 910DMA/ANT products, as calculated from the model, with those observed experimentally, using semi-logarithmic Arrhenius-type coordinates of either S(ANT) or R(910DMA/ANT) vs. $1/\Theta$ at constant $[9MA]_0 = 0.82$ mol/l. In Fig. 4(a) the model is seen to predict an ANT selectivity S(ANT) from 0.2 to 0.5 orders of magnitude below experimental, while in Fig. 4(b) model predictions of the major product ratio R(910DMA/ANT) lie within ±0.2 orders of magnitude of the experimental observations.

Sensitivity Analyses. The significance of the differences between model predictions and experimental observations was sought from sensitivity analyses at T = 370 C and $[9MA]_0 = 0.82$ mol/l, the central point of the experimental grid, by separately perturbing the kinetics of selected elementary steps. The effects of these perturbations on the predicted decay half-life t^*, ANT selectivity S(ANT), and the primary product ratio R(910DMA/ANT), are shown by the vertical dashed lines in Figs. 3 and 4. In Figs. 3(a) and (b), for example, the uncertainty in t* was estimated by perturbing the activation energies E^*_1 and E^*_{11} by ± 3.4 and ± 4.0 kcal/mol respectively (the inherent errors in ΔH^0_{r1} and ΔH^0_{r11}), since the elementary reactions R1 and R11 contribute most heavily to the destruction of 9MA substrate in our model. The upper and lower ends of the vertical dashed lines in each portion of Fig. 3 represent values of t^* obtained by joint negative and positive perturbations, respectively, of E^*_1 and E^*_{11}. This sensitivity analysis shows that the inherent uncertainties of ± 1.1 orders of magnitude in values of t^* calculated by the model considerably exceed the 0.1 to 0.5 order of magnitude differences between the model results and experimental

observations. That is, within its (large) error limits, the model yields half-lives in agreement with experiments. Similar sensitivity analyses provided the vertical dashed lines in each of Figs. 4(a) and (b), showing that, within its error limits, the model also yielded 9MA selectivities and TMA/9MA ratios in accord with experiment.

Optimized Model. The preceding comparisons between model and experimental results are noteworthy because all the kinetic parameters employed in the original model were derived from first principles and used without adjustments. However, these comparisons also revealed the empirical alterations that might permit a best-fit of experimental results for engineering purposes, termed the "optimized" model. Specifically, the best-fit of all experimental data for 9MA thermolysis at T = 370 C with $[9MA]_0 = 0.82$ mol/l arose by altering the original activation energies (E^*_1, E^*_2, E^*_{-2}, E^*_3, E^*_{11}, E^*_{12}, E^*_{-12}, E^*_{17}, E^*_{-17}) by respective amounts of (-0.4, +2.2, -2.2, -0.4, +2.2, -2.2, +2.0, -2.0) kcal/mol, all of these changes being well within the inherent uncertainties of these parameters, respectively, (±3.4, ±3.5, ±3.5, ±2.4, ±4.0, ±4.1, ±4.1, ±3.9, ±3.9) kcal/mol. Figs. 5 (a) and (b) compare substrate and product histories obtained from the optimized model (lines) to the experimental data (points) for 9MA, ANT, 910DMA, CH4, and DHDMA. Fig. 5(a) shows the optimized model to well predict the observed 9MA decay, with decay half-lives $t^* = 22000$ s from the model versus 23500 s experimental. The absolute amounts of ANT and of 910DMA formed by the model are respectively about 1.5-fold lower and higher than experimental in Fig. 5(a), and the model well predicts the relatively small amounts of DHMA, and its qualitative variation with time, in Fig. 5(b). Finally, Figs. 6(a) and (b) show that the optimized model provides the correct magnitudes of the major product ratios R[DHMA/ANT] and R[910DMA/ANT] at low conversions, $X \rightarrow 0$; at higher conversions the model qualitatively follows the variation of the former ratio but not the latter.

Modelling Perspective. In regard to both thermolysis kinetics and the selectivities of major products, the predictions of the optimized model are appreciably closer to the experimental observations than those of the original model. However, the differences between the activation parameters of the optimized and original models, of order 2 kcal/mol, are small relative to the inherent uncertainties in these parameters, of order 4 kcal/mol. Thus, although the optimized model effects an appealing cosmetic improvement over the original model, the two models remain statistically indistinguishable. Substantive scientific improvements in modelling 9MA thermolyses must await better methods, and more reliable data, for deriving the kinetics of the underlying elementary reactions.

ACKNOWLEDGEMENT: This work was supported in part by Cabot Corporation, Boston, MA.

REFERENCES

[1] Virk, P.S.; Vlastnik, V.J.: PREPRINTS, Div. of Petrol. Chem., ACS, 38(2), 422 (1993).
[2] Virk, P.S.; Vlastnik, V.J.: PREPRINTS, Div. of Fuel Chem., ACS, 39(3), 643 (1994).
[3] Virk, P.S.; Vlastnik, V.J.: PREPRINTS, Div. of Fuel Chem., ACS, 40(2), 239 (1995).
[4] Pomerantz, M.; Combs Jr., G.L.; Fink, R.: J. Org. Chem., 45, 143 (1980).
[5] Pope, J.M.: Ph.D. Thesis, Dept. of Chem. Eng., MIT, Cambridge, MA (1987).
[6] Smith, C.M.; Savage, P.E.: A.I.Ch.E. J., 39, 1355 (1993).
[7] Vlastnik, V.J.: Sc.D. Thesis, Dept. of Chem. Eng., MIT, Cambridge, MA (1993).
[8] Braun, W.; Herron, J.T. and Kahaner, D.K.: Int. J. Chem. Kinet., 20, 51 (1988).
[9] Gear, C.W.: Numerical Initial Value Problems in Ordinary Differential Equations, Prentice-Hall, N.J., 1971.

Table 1. Evans-Polanyi Relations and Arrhenius Parameters for Model Elementary Reactions.

	Type of Reaction	$\log_{10} A$ [l mol^{-1} s^{-1}]	rpd	Evans-Polanyi Relation: $E^* =$	ΔH°_{rxn} kcal/mol	E^* kcal/mol	Arrhenius Expression: $\log_{10} k =$
R1	molecular disproportionation	8.0	6	ΔH°_{rxn}	+2.7	+2.7	8.0 - 12.7/θ
R-1	radical disproportionation	8.0	1	0	+2.7	0	8.0
R2	H-abstraction	8.1	3	17.5 + ΔH°_{rxn}/3	-8.5	17.4	8.6 - 17.4/θ
R-2	H-abstraction	8.1	3	17.5 + ΔH°_{rxn}/3	8.5	17.4	8.6 - 17.4/θ
R3	methyl addition	13.5	1	8.1 + ΔH°_{rxn}	20.2	32.0	13.5 - 31.3/θ
R-3	CHD* addition	8.5	2	8.1	-20.2	8.1	8.6 - 8.1/θ
R6	H-abstraction	8.1	3	17.5 + ΔH°_{rxn}/3	-12.7	8.5	8.6 - 8.3/θ
R-6	H-abstraction	8.1	4	17.5 + ΔH°_{rxn}/3	23.7	30.9	8.7 - 31.9/θ
R8	CHD* addition	8.0	1	8.1	-20.2	8.1	8.5 - 8.1/θ
R-8	methyl addition	13.5	1	8.1 + ΔH°_{rxn}	20.5	32.6	13.5 - 32.4/θ
R9	radical H transfer	8.1	1	17.5 + ΔH°_{rxn}/3	9.3	17.65	8.1 - 17.7/θ
R-9	radical H transfer	8.1	1	17.5 + ΔH°_{rxn}/3	-9.3	17.35	8.1 - 17.4/θ
R7	radical combination	8.1	1	0	-34.7	0	8.1
R-7	homolytic dissociation	13.5	1	ΔH°_{rxn}	34.7	34.7	13.5 - 34.7/θ
R5	radical combination	9.3	1	0	-33.4	0	9.3
R-5	homolytic dissociation	13.3	1	ΔH°_{rxn}	33.4	33.4	13.3 - 33.4/θ
R4	radical combination	9.3	1	0	-32.1	0	9.3
R-4	homolytic dissociation	13.3	1	ΔH°_{rxn}	32.1	32.1	13.3 - 32.1/θ
R10	radical disproportionation	8.1	1	0	-12.9	0	8.1
R-10	molecular disproportionation	8.1	2	ΔH°_{rxn}	+2.9	+2.7	8.0 - 12.9/θ

	Type of Reaction	$\log_{10} A$ [l mol^{-1} s^{-1}]	rpd	Evans-Polanyi Relation: $E^* =$	ΔH°_{rxn} kcal/mol	E^* kcal/mol	Arrhenius Expression: $\log_{10} k =$
R11	molecular disproportionation	8.0	6	ΔH°_{rxn}	-2.5	-2.5	8.3 - 12.5/θ
R-11	radical disproportionation	8.3	1	0	-2.5	0	8.3
R12	H-abstraction	8.1	3	17.5 + ΔH°_{rxn}/3	1.0	13.0	8.6 - 13.0/θ
R-12	H-abstraction	8.1	1	17.5 + ΔH°_{rxn}/3	-1.0	17.0	8.3 - 17.0/θ
R16	radical H transfer	8.1	1	17.5 + ΔH°_{rxn}/3	-0.9	17.05	8.1 - 17.1/θ
R-16	radical H transfer	8.1	2	17.5 + ΔH°_{rxn}/3	0.9	17.05	8.4 - 15.0/θ
R17	radical H transfer	8.3	1	17.5 + ΔH°_{rxn}/3	-1.2	16.9	8.1 - 15.0/θ
R-17	radical H transfer	8.1	2	17.5 + ΔH°_{rxn}/3	1.2	18.1	8.4 - 15.1/θ
R15	radical combination	9.3	1	0	-32.0	0	9.3
R-15	homolytic dissociation	13.5	1	ΔH°_{rxn}	32.0	32.0	13.5 - 32.0/θ
R13	radical combination	9.3	1	0	-33.9	0	9.3
R-13	homolytic dissociation	13.9	1	ΔH°_{rxn}	33.9	33.9	13.9 - 33.9/θ
R20	radical disproportionation	8.0	1	0	-11.5	0	8.0
R-20	molecular disproportionation	8.0	1	ΔH°_{rxn}	+1.5	+1.3	8.1 - 12.5/θ
R21	radical combination	9.3	1	0	-11.5	0	9.3
R-21	homolytic dissociation	13.9	1	ΔH°_{rxn}	11.5	11.5	13.3 - 11.5/θ
R22	radical disproportionation	8.0	1	0	+2.7	0	8.3
R-22	molecular disproportionation	8.0	2	ΔH°_{rxn}	+2.7	+2.7	8.0 - 12.7/θ

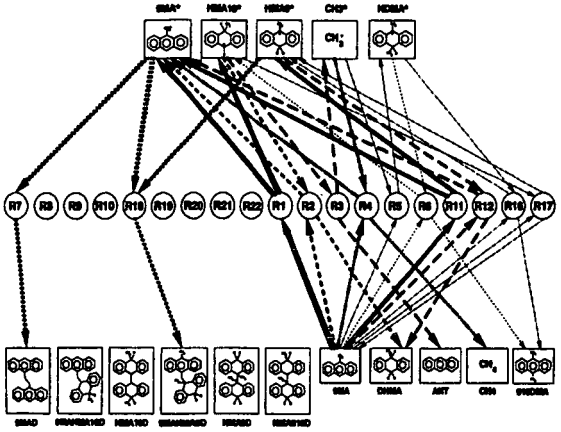

Figure 1. Elementary Step Graph of 9MA Thermolysis Mechanism. Arrow weights depict relative reaction traffic at T = 370 C, [9MA]o = 0.82 mol/l, and low conversion X ~ 0, as calculated from the original model (see text).

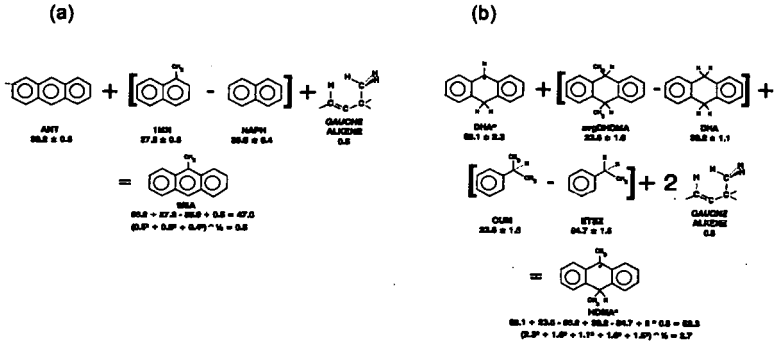

Figure 2. Illustration of Macro-Group Additivity Scheme for Estimation of Thermochemical Properties of (a) Stable and (b) Radical Species.

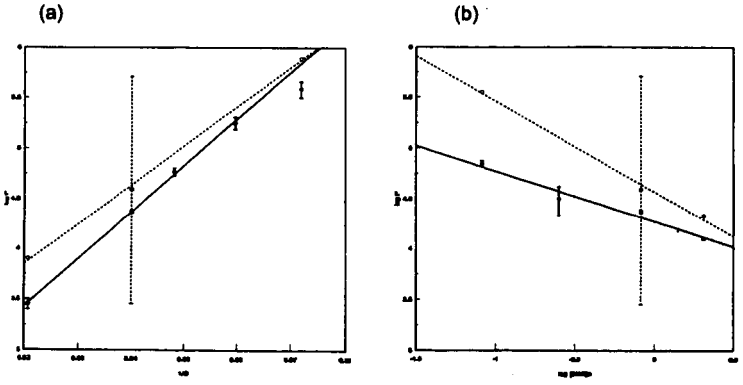

Figure 3. Decay Half-Lives t* Experimental (solid circles and lines) Versus Calculated From Original Model (hollow circles, dashed lines) at (a) constant [9MA]o = 0.82 mol/l and (b) constant T= 370 C.

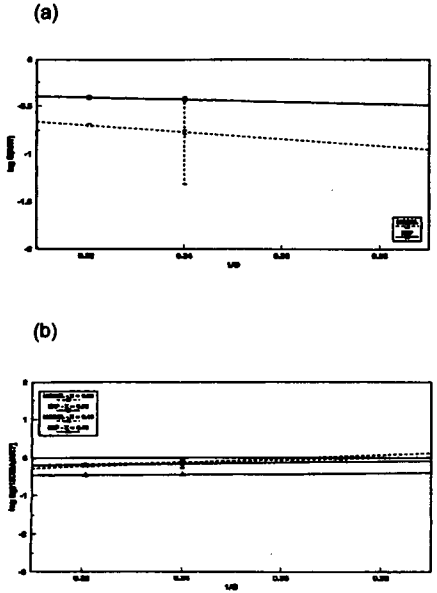

Figure 4. Original Model Results
(hollow points, dashed lines) vs.
Experiments (solid points, solid lines).
(a) Selectivity to ANT, (b) Ratio [910DMA/ANT].

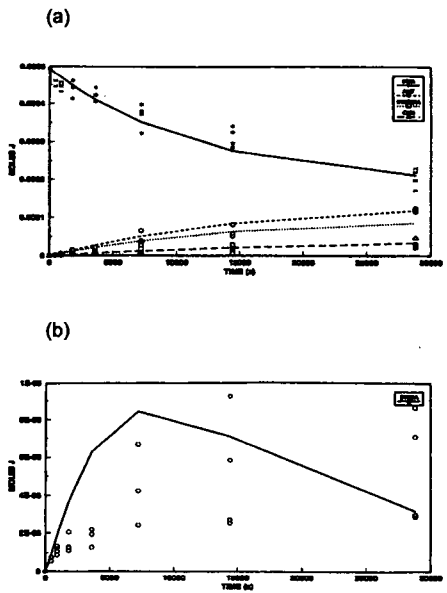

Figure 5. Optimized Model Results
(lines) vs. Experiments (points) at
T = 370 C with [9MA]o = 1.82 mol/l.
(a) 9MA, ANT, CH4, 910DMA, (b) DHMA.

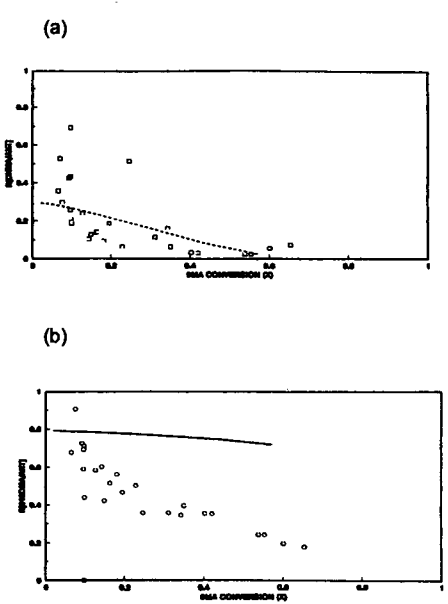

Figure 6. Optimized Model Results
(lines) vs. Experiments (points) at
T = 370 C with [9MA]o = 1.82 mol/l.
(a) Ratio DHMA/ANT, (b) Ratio 910DMA/ANT.

A Mechanistic Model for the Uncatalyzed Reaction of Stilbene with H_2

Venkatasubramanian K. Rajagopal
Robert D. Guthrie
Department of Chemistry
University of Kentucky
Lexington, KY 40506

Burtron H. Davis
Kentucky Center for Applied Energy Research
3572 Iron Works Pike, Lexington, KY 40511

Keywords: Hydrogenation, Kinetics, ACUCHEM, Glass Catalysis

INTRODUCTION

During the past few years, we have studied the thermolysis of a number of different substrates in the presence of H_2 or D_2 as models for the hydrothermolysis of coal.[1] To avoid catalysis by metal surfaces our reactions are carried out in glass reaction vessels with a length of capillary tubing separating the reaction mixture from the steel containment chamber. In our initial study of the hydrothermolysis of diphenylethane (**DPE**) we noted that the concentration of stilbene (**STB**), diphenylethene, formed in this reaction goes through a maximum value as the reaction proceeds.[1f] It was also noted that reactions carried out with lower starting concentrations of **DPE** generated less **STB** during the course of the reaction. There were few,[2] if any, examples of the uncatalyzed reactions of alkenes with H_2 in the literature, so we undertook to study the viability of such processes with selected substrates. Our initial survey used **STB**, 1-methylstyrene (2-phenylpropene), anthracene and phenanthrene.[1s] We found that the first three compounds could be hydrogenated at 410 °C and 14 MPa of D_2. In the case of **STB**, we observed an inverse concentration effect in that the yield of **DPE** was greater with lower starting **STB** concentrations under otherwise identical conditions. The reverse seemed to be true for 1-methylstyrene. Anthracene was hydrogenated with no significant concentration effect and phenanthrene refused to give hydrogenation products under conditions which were effective for the other three compounds. Of the two compounds that showed unusual concentration effects, **STB** seemed the best behaved in that it gave mainly **DPE** as a reaction product, whereas 1-methylstyrene gave higher molecular weight byproducts. For this reason and because of its relevance to our earlier study of the hydrothermolysis of **DPE**, **STB** was chosen for a more detailed investigation of its kinetic behavior.

EXPERIMENTAL

Substrate. The best grades of commercially available *trans*-stilbene (*trans*-**STB**) contained small amounts of diphenylethane (ca. 0.7 %). Some runs were carried out with **STB** synthesized by a modified Wittig procedure.[3] No significant differences were observe for reactions carried out with this pure substrate. Diphenylethane was recrystallized commercial samples and showed no gas chromatographically detectable impurities. *cis*-**STB** for preparation of GC/MS standard was a commercially available product.

Reaction Procedure. The reaction vessel and general procedure for hydrogenations has been described previously.[1s] For the experiments described in this paper, greater attention was given to control of reaction temperature. Figure I shows differences in the temperatures registered by thermocouples placed (1) in the fluidized sandbath, (2) inside the glass reaction vessel and (3) between the glass vessel and its steel container. It will be noted that both internal temperatures lag behind that of the sandbath and remain substantially below it for a period in excess of ten minutes. The temperature inside and outside of the glass reactor become equal roughly four minutes after the reactor assembly is placed in the bath. These relationships varied somewhat depending on the particular steel reaction container employed, conditions in the sandbath, the shaking rate for the reactor, the depth of immersion of the reactor assembly, etc. As a result it was very difficult to reproduce exactly the reaction temperature from run to run as evidenced by variations in yield for reactions carried out for nominally equal times and temperatures. To avoid these problems, we adopted the approach of placing a small sealed capillary ampule containing **DPE** between the glass vessel and its steel housing. The arrangement is shown in Figure II. We then used the degree of thermolysis of **DPE** within this ampule to calculate an effective reaction time based on a separately-determined rate constant for the thermolysis of **DPE** placed in similar ampules emersed directly in the sandbath at 405 °C. The plot for **DPE** conversion is shown in Figure III. In essence, if 20% of **DPE** had been converted to products in the ampule, we read the effective time at 405 °C from Figure III (corresponds to approximately 150 min at 405 °C). This calculated time was then substituted for the

actually measured reaction time for the purpose of kinetic plotting of the **STB** conversion data.

Analysis of Reaction Mixture. *trans*-**STB** was converted to an equilibrium mixture of *cis*- and *trans*-isomers at temperatures well below that required for hydrogenation. Thus the product mixture consisted of an equilibrium mixture of *cis*- and *trans*-**STB**, **DPE** and, at longer times, products of the themolysis of reduction-generated **DPE**. Unfortunately, the retention time of *cis*-stilbene was almost identical to that of **DPE** requiring that a secondary analysis of the gc peak by gas chromatography\ mass spectrometry (GC\MS) be performed. Figure IV shows a plot of composition versus ion intensity ratios for synthetic mixtures of cis-**STB** and **DPE** integrated over the entire GC peak. This standard curve was used to calculate compositions of reaction mixtures.

Calculation of Theoretical Kinetic Plots. The ACUCHEM[4] program was used to calculate theoretical curves of composition vs. time based on assumed rate constants as listed below.

RESULTS AND DISCUSSION

Although our earlier work attempted in several instances[1f, 1i, 1j] to follow the progress of hydrothermolysis reactions as a function of time, great difficulty was encountered in reproducing reaction temperatures with sufficient precision to provide data suitable for kinetic analysis. To circumnavigate this uncertainty we arranged to carry out a second, monitoring reaction inside the metal housing, but outside of the glass reactor. A small sample of **DPE** was sealed in a glass capillary tube and inserted in the reactor as shown in Figure II. The progress of this secondary reaction served as an internal clock by which we could determine an "effective" time for the reaction at 405 °C. Composition of the reaction mixture vs. effective time at 405 °C is given in Table I for a runs carried out with 50 mg starting **DPE**. It is clear from perusal of this data that we have not eliminated as much scatter as we might have wished but a reasonable relationship between effective time and conversion may be adduced. Moreover, it is clear that we are far from the sort of pseudo first-order kinetics which might be expected for any simple bimolecular reaction between **STB** and H_2.

Table I. Composition of Reaction Mixtures for *trans*-**STB** with H_2 at 14 MPa vs. Effective Time at 405 °C.

	Reaction Composition					
Effective Time at 405 °C (min)	*t*-**STB**	*c*-**STB**	**DPE**	**PhMe**	**PhEt**	**PhH**
35.4	75.9	7.2	12.1	0.5	0.4	0.3
42.4	79.4	7.5	11.1	0.1	<0.2	<0.2
42.7	80.4	7.6	9,6	0.2	<0.1	<0.1
90.4	59.9	5.7	28.7	0.9	0.2	0.1
121	61.5	5.8	30.1	0.8	<0.4	<0.4
147	57.7	5.4	33.3	0.5	0.1	<0.1
214	26.2	2.5	60.4	4.6	1.3	0.6
264	18.4	1.8	62.7	7.3	2.0	1.1
388	0.6	<0.6	63.2	14.5	8.4	5.6

A log plot for disappearance of **STB** is shown in Figure V. The solid points represent experimental data with 50 mg and with 20 mg **STB** in the reaction bulb. Runs carried out with larger starting weights gave unmanageably slow conversion under these conditions.

The mechanistic model suggested earlier for this process[1f] consists most essentially of a kinetic chain process with H atoms and 1,2-diphenylethyl radicals, **DPE**·, as chain carriers, eqs 1 and 2. The sequence generates **DPE** which can be expected to undergo its well-characterized dissociation to benzyl radicals, eq 3, followed by reaction of these both with H_2 and with **DPE**, eq 4 and eq 5, each process generating a chain carrier for the propagation cycle. The termination of the chain seems likely to be disproportionation of two **DPE**· to give **DPE** and **STB**, eq 6. There are a number of other processes known to be involved in the hydrothermolysis of **DPE** which might be considered, for example, the rearrangement of **DPE**· to give 1,1-diphenylethyl radicals. However, these would react to regenerate radicals and should not alter the kinetic pattern. Also, earlier work has shown that

the presence of H atoms can also lead to hydrocracking products, PhH and PhEt.[1f] However, Table I suggests that such processes become important only after the majority of the **STB** has been converted. This might be expected, as **STB** should be a effective trap for H atoms via eq 1.

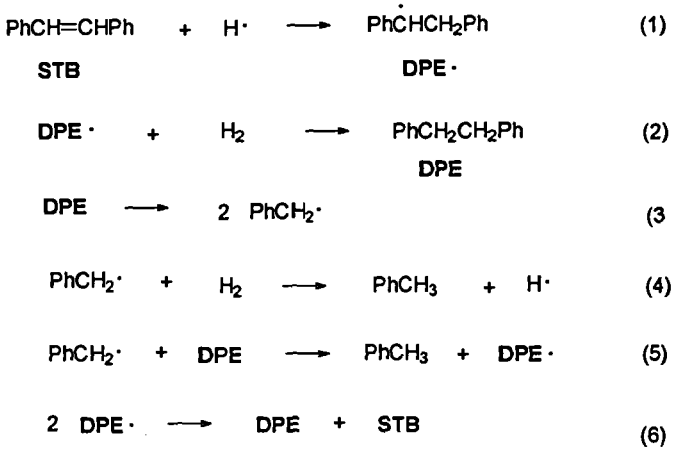

Thus, a reasonable match of the kinetic data might be expected using only the sequence of eqs 1 through 6. It will be observed, however, that unless **DPE** is present initially, there is no initiation step for the chain. We found that commercially available **STB** invariably contained small amounts of **DPE**. Therefore, we went to some effort to synthesize **DPE**-free **STB** for selected experiments. As there was no significant difference in the kinetic data for these samples, we must assume that some other initiating process is involved. Temporarily avoiding the problem by arbitrarily imposing an unspecified process to generate H atoms from H_2 (with a rate constant, $k = 1 \times 10^{-7}$ s^{-1}) leads to the calculated plot in Figure V. The other rate constants used in its generation were as follows:

$k_1 = 5.7 \times 10^9$ M^{-1} s^{-1}(Calculated from Benson's expression for the reaction of H· with ethylene.[5])

$k_4 = 50$ M^{-1} s^{-1} (This value is suggested by McMillen, Malhotra and Nigenda[6] at 400 °C.)

$k_2 = 9.3$ M^{-1} s^{-1} (There was no guidance for this number but it could reasonably be expected to be somewhat smaller than k_4.)

$k_3 = 2.4 \times 10^{-5}$ s^{-1} (This is the first order rate constant from Figure III. It is in good agreement with literature values.[7])

$k_5 = 1.7 \times 10^4$ M^{-1} s^{-1} (Calculated from the expression $\log k = 8.8 - 14.2/\phi$ (per hydrogen) estimated by Poutsma.[8])

$k_6 = 1 \times 10^8$ M^{-1} s^{-1} (Suggested by Poutsma[8] to be $\log k = 8.5$, based on studies by various groups of the rate constant for disproportionation of 1-phenylethyl radical to give styrene and ethylbenzene.[9])

Of course it is thermochemically unreasonable to assume that H_2 dissociates with a rate constant as large as 10^{-7}. It is apparent that initiation occurs via some unknown catalytic process. As recent information indicates that silica can serve as a catalyst for the hydrogenation of alkenes,[1m] it seemed worth considering that the surface of the glass container was serving as a catalyst. Based on an estimate of the concentration equivalent of catalytic sites in our glass reactor being 3.2×10^{-11}, and the following reaction sequence, eqs 7 and 8 (with $k_7 = 5 \times 10^{10}$ M^{-1} s^{-1} and $k_8 = 4 \times 10^3$ M^{-1} s^{-1}.):

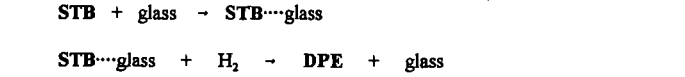

the theoretical curves in Figure VI were calculated. While the match to experimental data is not as good as that of Figure V, the pattern and concentration dependence are preserved.

CONCLUSIONS

The scheme presented explains the inverse concentration effect noted earlier. At high concentrations of **STB**, the chain-carrying **DPE**· undergo disproportionation, terminating the chain.

At lower concentrations, they stand a better chance of reacting with H_2. The rate increase with conversion is mainly due to the generation of **DPE** which serves as an initiator. We believe that this scheme is a reasonable mechanism for the hydrogenation of alkenes in the absence of metal catalysts, provided that some radical-generating initiator is present. We have also found that the hydrogen-transfer rate constants used in this scheme can be incorporated in a calculation to predict the pattern of D incorporation when **DPE** undergoes thermolysis under D_2.[1f] The proposed initiation by glass surface in the absence of a radical-generating species is, at present, purely speculative.

REFERENCES

1.(a) Guthrie, R. D.; Shi, B.; Sharipov, R.; Davis, B. *Prep. Pap.- Am. Chem. Soc. Div. Fuel Chem.* **1993**, *38*, 526-533. (b) Rajagopal, V.; Guthrie, R. D.; Shi, B.; Davis, B. H *Prep. Pap.- Am. Chem. Soc. Div. Fuel Chem.* **1993**, *38*, 1114. © Ramakrishnan, S.; Guthrie, R. D.; Shi, B.; Davis, B. H. *Prep. Pap.- Am. Chem. Soc. Div. Fuel Chem.* **1993**, *38*, 1122. (d) Sharipov, R.; Guthrie, R. D.; Shi, B.; Davis, B. H. *Prep. Pap.- Am. Chem. Soc. Div. Fuel Chem.* **1993**, *38*, 1129. (e) Shi, B.; Ji, Y.; Guthrie, R. D.; Davis, B. H. *Energy and Fuels* **1994**, *8*, 1268-1275. (f) Guthrie, R. D.; Shi, B.; Rajagopal, V.; Ramakrishnan, S.; Davis, B. H. *J. Org. Chem.* **1994**, *59*, 7426-7432. (g) Rajagopal, V.; Guthrie, R. D.; Shi, B.; Davis, B. H. *Prep. Pap.- Am. Chem. Soc. Div. Fuel Chem.* **1994**, *39*, 673. (h) Guthrie, R. D.; Ramakrishnan, S.; Britt, P. F.; Buchanan, III., A. C.; Davis, B. H. *Prep. Pap.- Am. Chem. Soc. Div. Fuel Chem.* **1994**, *39*, 668. (I) Guthrie, R. D.; Sharipov, R. V.; Ramakrishnan, S.; Shi, B.; Davis, B. H. *J. Org. Chem.*, **1995**, *60*, 4504-4509. (j) Ramakrishnan, S.; Guthrie, R. D.; Britt, P. F.; Buchanan, A. C., III. *Prep. Pap.- Am. Chem. Soc. Div. Fuel Chem.* **1995**, *40*, 555-559. (k) Rajagopal, V.; Guthrie, R. D.; Davis, B. H. *Prep. Pap.- Am. Chem. Soc. Div. Fuel Chem.* **1995**, *40*, 945-949. (l) Guthrie, R. D.; Ramakrishnan, S.; Britt, P. F.; Buchanan, A. C. III.; Davis, B. H. *Energy and Fuels*, **1995**, *9*, 1097-1103. (m) Rajagopal, V. K.; Guthrie, R. D.; Fields, T.; Davis, B. H. *Catalysis Today* **1996**, *31*, 57-63.

2. There are some indications that early hydrogenation studies by V. N. Ipatieff were carried out in the absence of catalysts. See V. N. Ipatieff "Catalytic Reactions at High Temperatures and Pressures," The Macmillan Co., New York, 1937. However, it seems likely that metal reaction vessels were used.

3. Daniel, H.; LeCorre, M. *Tetrahedron Letters* **1987**, *28*, 1165-1168.

4. Available from: Braun, W.; Herron, J. T.; Kahaner, D. K., NIST, Gaithersburg, MD 20899. See *Int J. Chem. Kinet.* **1988**, *29*, 51.

5. S. W. Benson, "Thermochemical Kinetics", 2nd Ed. Wiley, New York, N. Y. 1976, p. 168.

6. McMillen, D. F.; Malhotra, R.; Nigenda, S.E. Prepr. Pap.- Am. Chem. Soc. Div. Fuel Chem. **1987** 32(3), 180.

7. Poutsma, M. L. Energy Fuels **1990**, 4, 113.

8. Poutsma, M. L.; Dyer, C. W. J. Org. Chem. **1982**, 47, 4903 and ref. 6.

9. (a) Gibian, M. J.; Corley, R. C. J. Am. Chem. Soc. **1972**, 94, 4178. (b) Manka, M. J.; Brown, R. L.; Stein, S. E. Int. J. Chem. Kin. **1987**, 19, 943. © Manka, M. J.; Stein, S. E. J. Phys. Chem. **1984**, 88, 5919. (d) Glexner, G.; Olaj, O. F.; Breitenbach, J. W. Makromol. Chem. **1979**, 180, 258.

Figure I. Temperature Profile for Glass Reactor and Containment Vessel

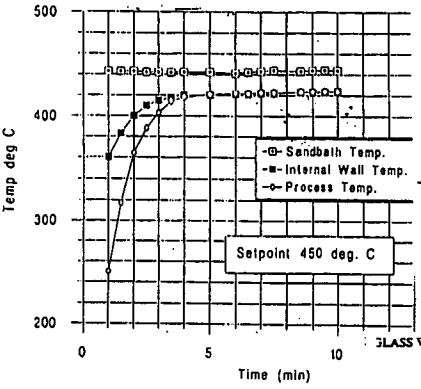

Figure II. Reactor Setup for Kinetics Experiments

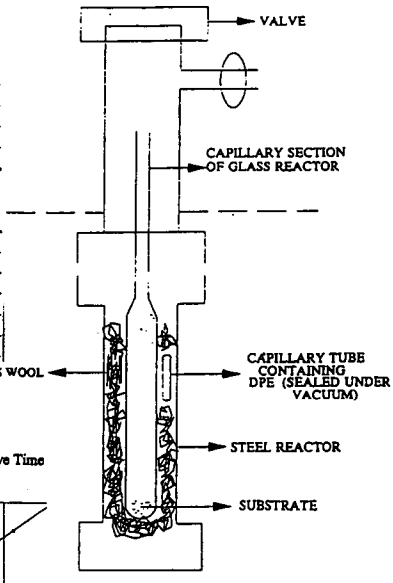

Figure III. Plot of DPE Loss Used for Calculation of Effective Time

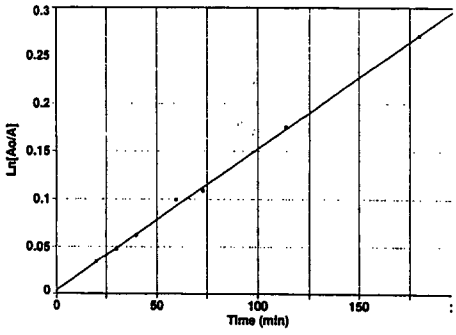

Figure IV. Calibration Curve Used to Determine DPE in the Presence of *cis*-STB

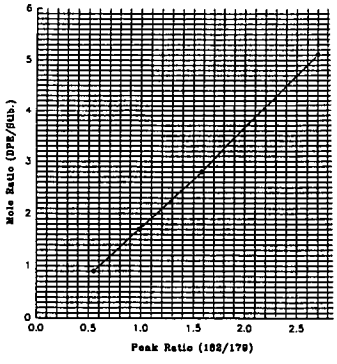

Figure V. Theoretical Matching of STB Loss (Unspecified H Atom Production)

Figure VI. Theoretical Matching of STB Loss (Catalysis by Glass Reactor)

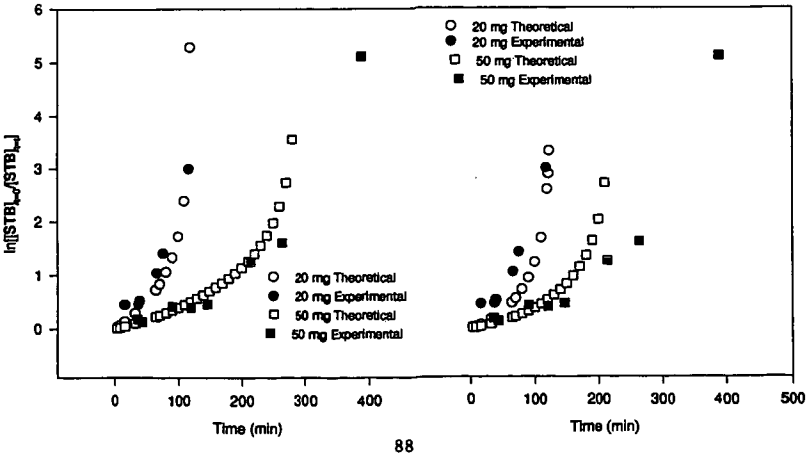

FLASH VACUUM PYROLYSIS OF LIGNIN MODEL COMPOUNDS

Mark J. Cooney, Phillip E. Britt, and A. C. Buchanan, III
Chemical and Analytical Sciences Division, Oak Ridge National Laboratory
P. O. Box 2008, Oak Ridge, Tennessee 37831-6197

Keywords: pyrolysis mechansisms, lignin pyrolysis, model compounds

ABSTRACT

Despite the extensive research into the pyrolysis of lignin, the underlying chemical reactions that lead to product formation are poorly understood. Detailed mechanistic studies on the pyrolysis of biomass and lignin under conditions relevant to current process conditions could provide insight into utilizing this renewable resource for the production of chemicals and fuel. Currently, flash or fast pyrolysis is the most promising process to maximize the yields of liquid products (up to 80 wt %) from biomass by rapidly heating the substrate to moderate temperatures, typically 500 °C, for short residence times, typically less than two seconds. To provide mechanistic insight into the primary reaction pathways under process relevant conditions, we are investigating the flash vacuum pyrolysis (FVP) of lignin model compounds that contain a β-ether linkage and α- or γ-alcohol, which are key structural elements in lignin. The dominant products from the FVP of $PhCH_2CH_2OPh$ (PPE), $PhC(OH)HCH_2OPh$, and $PhCH_2CH(CH_2OH)OPh$ at 500 °C can be attributed to homolysis of the weakest bond in the molecule (C-O bond) or 1,2-elimination. Surprisingly, the hydroxy-substituent dramatically increases the decomposition of PPE. It is proposed that internal hydrogen bonding is accelerating the reaction.

INTRODUCTION

Over the past two decades, a good deal of attention has focused on the thermochemical conversion of renewable resources into higher value products [1]. Lignin, the second-most abundant naturally occurring biopolymer and a by-product of the pulping process, has received an enormous amount of attention as a consequence of its availability and its potential to produce higher value products. However, in spite of the extensive research to expand the use of lignin, the efforts have been only moderately successful [2]. This can be attributed to the structural diversity of lignin and the dependence of the chemical structure of lignin on the method of isolation [3]. To enhance the economic production of higher value products from lignin, it is necessary to understand those factors that maximize product yields and promote product selectivity. Over the past two decades, significant advances have been made in maximizing the yields of solid (charcoal) [4], liquid and gaseous products from biomass by pyrolysis [1,5,6]. While slow pyrolysis at low temperatures and long residence times produces charcoal, fast or flash pyrolysis produces high yields of liquid products (up to 60 wt% moisture-free organic liquids on a dry feed) by rapidly heating biomass to moderate temperatures (typically 500 °C, but ranging from 400-650 °C) for short periods of time (typically less than 2 s). At temperatures above 700 °C, fast pyrolysis maximizes gas yields (up to 80 wt%). However, despite the extensive research into the pyrolysis of biomass and lignin, the fundamental chemical reactions that lead to the complex array of products remains poorly understood, and as a result, there is little insight into how to control the product selectivity [7]. Currently, the most detailed mechanistic insights on lignin pyrolysis have been obtained from model compound studies [7,8]. However, most of these studies have been done at relatively low temperature (less than 450 °C) with long residence times (greater than 5 min) or slow heating rates. This makes it difficult to extrapolate these results to the moderate temperature, short contact-time reaction condition found in fast pyrolysis. Therefore, additional model compound studies are needed under conditions relevant to current process conditions (i.e., fast pyrolysis) to provide insight into controlling the reaction chemistry and product distribution to enhance the utilization of lignin.

There are many methods to rapidly heat compounds to high temperature, each with their own set of advantages and disadvantages. This paper investigates the flash vacuum pyrolysis of lignin model compounds at 500 °C. Flash vacuum pyrolysis (FVP) or flash vacuum thermolysis (FVT) has been used for decades by organic chemists for the preparation of highly reactive intermediates, for mechanistic investigations, and for preparative organic synthesis [9]. There are many different designs of flash vacuum pyrolysis apparatus operating at pressures from 1 atmosphere to $<10^{-4}$ mm Hg depending on the specific application and method of detection of the products [9]. However, all flash pyrolysis experiments are characterized by short contact times (sample typically remains in the hot zone for 0.001 - 1 s), low steady-state concentrations of the reactants and products in the hot zone, and rapid quenching of the products to low temperatures, typically 77 K. This method has been used to study thermally labile intermediates by a variety

of spectroscopic methods (for example, NMR, UV-Vis, FTIR, Raman, and photoelectron spectroscopy). A special variation of this experiment, very low-pressure pyrolysis (VLPP), was developed to directly measure the reactive intermediates (i.e., free-radicals) from unimolecular reactions and very fast bimolecular reactions (i.e., 10^{11} L $mol^{-1}s^{-1} \geq k \geq 10^{6}$ L $mol^{-1}s^{-1}$) by mass spectrometry [10].

Flash vacuum pyrolysis seems ideally suited for the mechanistic investigation of the pyrolysis of lignin model compounds under conditions relevant to large scale fast pyrolysis reactors. Initial experiments can be run at low pressure ($<10^{-3}$ mm Hg) to characterize the primary reaction pathways and reactive intermediates that occur at moderate temperatures (500 °C) with a minimum of interference from bimolecular reactions. Next, the pyrolysis can be investigated at higher pressures (0.1 mm Hg to 1 atmosphere) under a flow of inert gas (N_2) to determine the more complex secondary reactions. A focus of this project is to characterize and quantitate the products, and to determine the origin and efficiency of their production. With the reaction pathways defined for the production of the products, we can focus on changing the experimental conditions to promote product selectivity.

Lignin is a complex, heterogeneous, three-dimensional polymer formed from the enzyme-initiated, dehydrogenative, free-radical polymerization of three *p*-hydroxycinnamyl alcohol precursors that differ by the number of methoxy groups on the aromatic ring [1a,11]. Softwood lignin is formed from *trans*-coniferyl alcohol (4-hydroxy-3-methoxycinnamyl alcohol), hardwood lignin is formed from coniferyl and *trans*-sinapyl alcohol (4-hydroxy-3,5-dimethoxycinnamyl alcohol), and grass lignin is formed from coniferyl, sinapyl and *trans-p*-courmaryl alcohol (4-hydroxycinnamyl alcohol). As opposed to other biopolymers such as cellulose, lignin has many different types of linkages between monomer units. This arises from the distribution of the π-electron density throughout the phenylpropene monomer unit and the thermodynamic principles governing radical addition reactions [1a]. The dominant interunit linkage in lignin is the arylglycerol-β-aryl ether linkage, commonly referred to as the β-O-4 linkage, and the arylglycerol-α-aryl ether linkage, referred to as the α-O-4 linkage, which accounts for approximately 48-60 % and 6-8 %, respectively, of the total interunit linkages [1a,11], exemplified by the structure below. If this structure is stripped for all its substituents, the

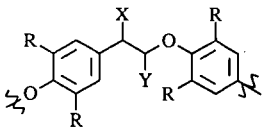

R = H or OCH_3

X = OH, OAr or =O

Y = CH_2OH or CH_2OR

skeletal remnant would be phenethyl phenyl ether, the simplest model of the β-O-4 linkage, and the starting point for this mechanistic investigation.

In this paper, the flash vacuum pyrolysis of lignin model compounds will be studied to determine the primary reaction that occurs at 500 °C and low pressures ($<10^{-3}$ Torr) and the impact of substituents on the reaction pathways. As a consequence of the complexity of the pyrolysis reactions and the thermal sensitivity of the products, a graded approach is used to solve this problem in which simple model compounds are thoroughly studied to provide a solid foundation to assist in the interpretation of more complex model compounds and lignin. This investigation will focus on FVP of the β-O-4 linkage, and the impact of hydroxy functional groups on the reaction pathways. To our knowledge, this is the first investigation of the reaction pathways of the γ-alcohol (i.e. β–CH_2OH-PPE).

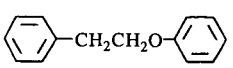

PPE

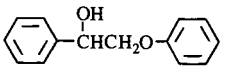

α–HO-PPE

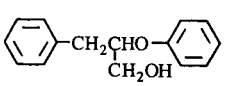

β–CH_2OH–PPE

EXPERIMENTAL

The synthesis of PPE and $PhCD_2CH_2OPh$ has been previously described [12]. The preparation of α–HO-PPE was accomplished by alkylation of α–bromoacetophenone with phenol (K_2CO_3 in DMF), reduction with lithium aluminum hydride, and recrystallization with hexanes/toluene. The preparation of β-CH_2OH-PPE was accomplished by alkylation of the enolate of ethyl

phenoxyacetate (by the reaction of lithium hexamethyldisilazide with ethyl phenoxyacetate in THF at -78 °C) with benzyl bromide, reduction with lithium aluminum hydride, and purification by reverse phase flash chromatography. All compounds were >99.5 % pure by GC analysis.

The FVP apparatus was based on the design reported by Trahanovsky [13, 14] and available from Kontes. The pyrolysis tube consisted of a quartz tube (62.5 cm x 2.5 cm) with a 34/45 male joint on one end and a 90° bend with a size 40 o-ring joint on the other end. The tube was packed with short pieces (1/4" x 6 mm OD) of quartz tubing to a length of ca. 40 cm and held in place by a small plug of quartz wool. The quartz chips prevent streaming of the substrate and increase residence time in the hot zone. The quartz tube was heated with a Carbolite three zone furnace (45 x 3.8 cm (ID)) and the temperature was maintained within ± 1 °C of the setpoint (500 °C) over a length of 30 cm (out of total heated zone of 40 cm). The sample (typically 100-200 mg) was weighed into a sublimation tube made from a 34/45 female joint and connected to the horizontal quartz pyrolysis tube. The pyrolysis tube was connected by a size 40 o-ring joint to a trap which is cooled with liquid nitrogen. To prevent products from condensing in the tube before the cold trap, the pyrolysis tube was warmed with a heating tape at the exit of the furnace. At the start of a pyrolysis experiment, the system was pumped down to $<10^{-4}$ mm Hg (measured after the cold trap), the furnace was equilibrated at 500 °C, and the sublimation chamber was enclosed in an aluminum cylinder wrapped with a heating tape. The temperature of the sublimation tube (monitored by a thermocouple in the aluminum cylinder) was increased to provide a throughput of 50 - 100 mg h^{-1}. Under these conditions, the residence time (i.e., contact time) is estimated to be ca. 10 ms and the steady state concentration of materials in the hot zone is 10^{-8}-10^{-9} mol L^{-1} such that only fast bimolecular reactions can occur in the hot zone, such as radical-radical couplings [9]. After the reaction, the trap was opened, products were washed out with a high purity acetone containing internal standards (cumene, dimethylphenol, and diphenyl ether), and the samples are analyzed by GC-MS at 70 eV and quantitated by GC with measured response factors. Products were identified by comparison of GC retention time and mass spectral fragmentation patterns with authentic samples or based on MS fragmentation patterns and comparison with the NIST spectral library. After each run, the tube was "burned out", by blowing air through the tube at 600 °C for 1 h, to remove any carbonaceous deposits (which were visible in the pyrolysis of phenethyl 2,6-dimethoxyphenyl ether). Duplicate pyrolyses were remarkably reproducible with similar mol % of products, mass balances (typically >95 %), and conversions (± 15%). Changing the injection rate by a factor of two (50 to 100 mg h^{-1}) did not change the product distributions. To check the long term reproducibility of the pyrolysis runs to ensure that the relative reactivity of the substituted phenethyl phenyl ethers could be compared over time, the pyrolysis of phenethyl *o*-methoxyphenyl ether was run after every 3-5 pyrolyses and compared to previous pyrolyses. Currently, similar pyrolysis results (% conversion, mass balances, and product yields) have been obtained over the span of a six week period (over 30 pyrolyses).

RESULTS AND DISCUSSION

FVP of PPE. The major products from the FVP of PPE at 500 °C are shown below (average mol % from three runs). As a consequence of the low % conversions (0.94 ± 0.16 %), the

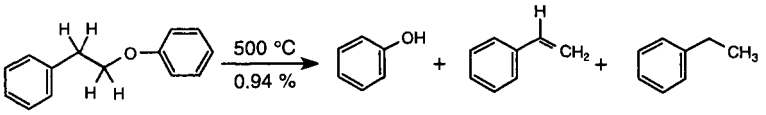

55.9 ± 2.8 % 40.5 ± 2.5 % 0.38 ± 0.07 %

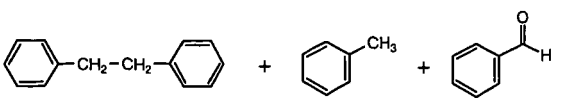

1.5 ± 0.1 % 0.25 ± 0.05 % 1.4 ± 0.3 %

reproducibility and the mass balances were not as good as that found at higher conversions. In addition to the products shown below, a small amount (typically, ≤1 % of the starting material) of rearranged PPE, *o*-(2-phenylethyl)phenol and *p*-(2-phenylethyl)phenol, was also found. At higher temperatures (550 and 600 °C), the conversion of PPE increased to form the products shown above, but the yield of the rearranged products did not increase (ca. 1 % of the starting

material). Recombination of the phenoxy and phenethyl radicals (see below) to form the rearranged products seems unlikely on the basis that no cross-coupling products, phenoxyphenol or 1,4-diphenylbutane, were observed. Trahanovsky has shown that FVP (650 °C and 0.05 mm Hg) of an unsymmetrical oxalate, benzyl *p*-chlorobenzyl oxalate, lead to statistical scrambling of the benzyl group indicating intermolecular coupling of benzyl radicals [14]. Therefore, the rearranged products were attributed to a small amount of acid catalysis from the quartz chips. In the decomposition of an analogous alkyl phenyl ether, *n*-butyl phenyl ether, it was proposed that products were formed by C-O homolysis (log k (s^{-1}) = 16.0 - 65.5 / 2.303 RT (kcal mol^{-1})) and by 1,2-elimination (log k (s^{-1}) = 13.6 - 57.4 / 2.303 RT (kcal mol^{-1})) [15]. At 500 °C, the ratio of homolysis to 1,2-elimination is 1.3. Therefore, in the pyrolysis of PPE, the major products, styrene and phenol, could be produced by two competing pathways: a) homolytic cleavage of the weakest bond in the molecule ($D°_{C\text{-}O}$ estimated as 63 kcal mol^{-1}) to give PhO• and $PhCH_2CH_2$• which can gain and lose a hydrogen atom, respectively, or b) 1,2-elimination to produce the phenol and styrene products directly. Unfortunately, it is very difficult to deconvolute these two pathways in the decomposition of PPE since both routes lead to the same products. However, if PPE were substituted with deuterium in the benzylic position ($PhCD_2CH_2OPh$, PPE-d_2), the rate of 1,2-elimination would be slower, as a consequence of the deuterium isotope effect in breaking the C-D bond, while the homolytic cleavage should not be influenced by the substitution (since β-scission of $PhCD_2CH_2$• is fast compared to C-O homolysis). At 500 °C, a maximum rate difference (in the absence of tunneling) of k_H/k_D = 2.1 is predicted. In the pyrolytic 1,2-elimination of hydrogen halide from ethyl chloride, ethyl bromide, and their deuterated analogues, the measured isotope effect was (k_H/k_D) 2.0 - 2.2 at 500 °C [16]. Comparison of the % conversion from three FVP runs of PPE-d_2 and PPE under similar conditions found that the deuterated PPE reacted approximately 20 % slower than PPE indicating that the 1,2-elimination contributes to the decomposition of PPE at low pressures. At higher pressures, radicals produced from C-O homolysis can start a chain reaction and the contribution of 1,2-elimination will most likely be small.

The small amounts of toluene, bibenzyl, and benzaldehyde that are observed can be formed from the homolysis of the C-C bond ($D°_{C\text{-}C}$ estimated as 72 kcal mol^{-1}). Under the low pressure reaction conditions, a majority of the benzyl radicals couple to form bibenzyl. The phenoxymethyl radical ($PhOCH_2$•) produces benzaldehyde by a 1,2-phenyl shift, to form the benzyloxy radical ($PhCH_2O$•), followed by loss of a hydrogen atom. In support of this mechanism, the benzaldehyde formed in the FVP of PPE-d_2 contained no deuterium.

FVP of α-HO-PPE. The major products from the FVP of α-HO-PPE at 500 °C are shown below (average mol % from three runs). The reproducibility and mass balances (98.5 ± 1.5 %) of these runs are excellent. Surprisingly, the α-hydroxy group dramatically accelerates the rate of decomposition (46.8 ± 0.4 % conversion, 23.4 ± 0.9 % without dehydration) of PPE. The major reaction is the 1,2-elimination of the α-hydroxy group to form the more refractory vinyl ether. The most studied 1,2-eliminations involve loss of hydrogen halide from alkyl halides to form alkenes, although loss of water, alcohol, ammonia, and hydrogen sulfide from alcohols, ethers, amines, and mercaptans have also been reported [15-17]. The transition state is proposed to be highly polar and electron donating species at the α-carbon dramatically accelerate the reaction

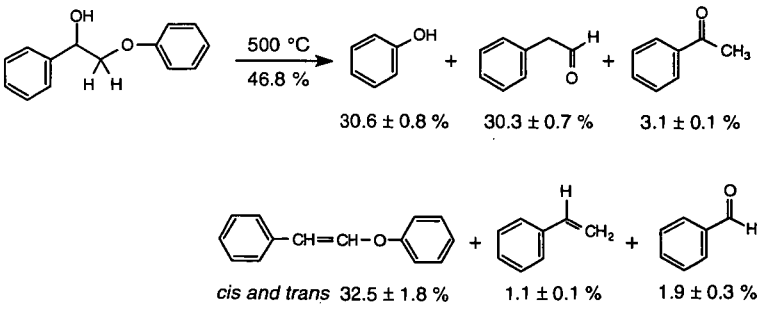

while electron donating substituents at the β–carbon have only a small effect [17]. Since the aromatic ring is typically substituted with a *p*-hydroxy or *p*-alkoxy group in lignin, it is predicted that 1,2-elimination will be an dominant reaction pathway in lignin pyrolysis. It would be

beneficial to find reaction conditions to minimize the dehydration reaction since it produces a more refractory product with the ejection of hydrogen (as water) from a carbon rich material.

On the basis of the FVP results of PPE, we would predict that the dominant products from the FVP of α-HO-PPE would be phenol and acetophenone ($PhCOCH_3$) by the C-O homolysis or 1,2-elimination pathway. Surprisingly, acetophenone is a minor product indicating that 1,2-elimination is not a significant pathway in the decomposition of α-HO-PPE. The formation of phenol and phenylacetaldehyde could arise from two different pathways as shown below: a) intramolecular attack of the hydroxyl group on the β–carbon to eliminate phenol and styrene oxide which can undergo additional decomposition by pyrolysis; or b) homolysis of C-O bond, 1,2-phenyl shift, followed by loss of a hydrogen atom and tautomerization. Alkaline cleavage of

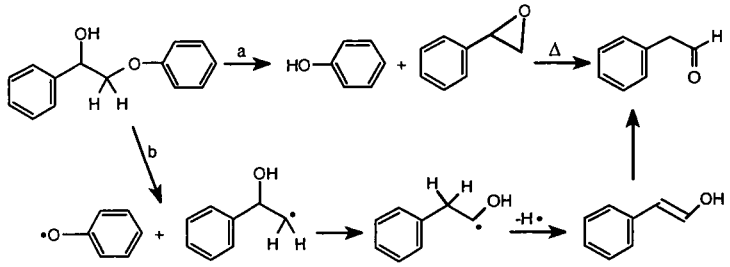

lignin model compounds at low temperatures (220-300 °C) was shown to proceed through an epoxide intermediate by an internal displacement reaction [18]. Pyrolysis of substituted styrene oxides have been shown to produce alkyl benzyl ketones (or aldehydes). For example, pyrolysis of 3,4-dimethoxyphenyloxirane at 500 °C produces 3,4-dimethoxyphenylacetaldehyde as the major product [19]. To determine the contribution between these two possible pathways, we are currently synthesizing α-hydroxy-α-deuterophenethyl phenyl ether ($PhC(OH)DCH_2OPh$). Pathway (a) will provide phenylacetaldehyde labeled with deuterium in the benzylic position ($PhCHDCHO$) while pathway (b) will produce phenylacetaldehyde labeled in the aldehydic position ($PhCH_2CDO$). The contribution from the two pathways will be deduced from the mass spectrum fragmentation pattern of the phenylacetaldehyde produced in the FVP of $PhC(OH)DCH_2OPh$.

FVP of β–CH_2OH-PPE. The major products from the FVP of β-$HOCH_2$-PPE at 500 °C are shown below (average mol % from three runs). The reproducibility of the % conversion (22.4 ± 0.7 %) and mass balances (100.4 ± 0.4 %) of these runs are excellent. As observed for α-HO-

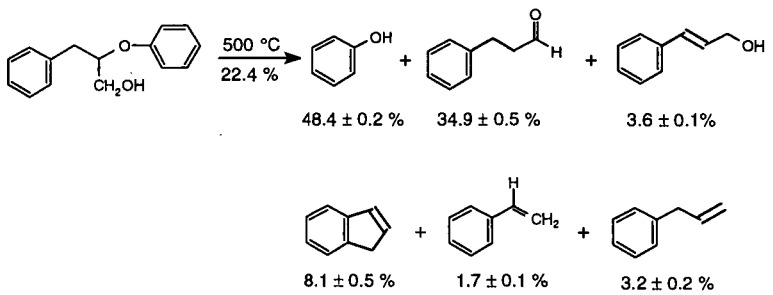

PPE, the rate is dramatically accelerated by the addition of the hydroxy group to the β-ether linkage. As predicted from the documented substituent effects on 1,2-elimination reactions, dehydration of the primary alcohol is a minor pathway for β-$HOCH_2$-PPE, since there are no electron donating substituents to stabilize the polar transition state as found in α-HO-PPE [17]. The dominant pyrolysis products can be rationalized by C-O homolysis, followed by β-scission of a hydrogen or a hydroxyl radical (see below). Thermochemical estimates predict that pathway (a) should be favored over (b) and (c) by 5-6 kcal mol^{-1} [20] and $PhCH_2CH_2CHO$ is found to be the dominant product. However, it is impossible to rule out a contribution of a 1,2-elimination in the formations of $PhCH_2CH_2CHO$ and $PhCH{=}CHCH_2OH$. The origin of the indene is unclear,

but it has been shown that $PhCH{=}CHCH_2{\bullet}$ can cyclize to indene [21]. However, under the low pressure conditions, hydrogen abstraction from $PhCH_2CH{=}CH_2$ is unlikely and thermochemical

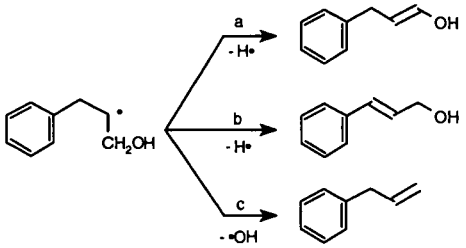

estimates indicate that the homolysis of the C-O bond in $PhCH{=}CHCH_2OH$ would be slow at 500 °C [20]. Nevertheless, the indene most likely arises from decomposition of $PhCH{=}CHCH_2OH$.

Impact of the hydroxy group on the decomposition of the β-ether linkage. One surprising outcome of this investigation was the dramatic increase in the decomposition of PPE by the addition of a hydroxy-substituent. The average % conversion without dehydration for the FVP of PPE, α-HO-PPE, and β-$HOCH_2$-PPE at 500 °C was 0.96 %, 23.4 %, and 22.4 %. Thermochemical estimates, assuming C-O homolysis is the rate determining step, predict a β-hydroxy substituent might enhance the decomposition by a factor of 1-4 [22]. However, we observe rate enhancements greater than a factor of 20. One possible explanation for the similar rate enhancement for an α- and γ-hydroxy group is that internal hydrogen bonding is accelerating the C-O homolysis. Suryan, Kafafi, and Stein have measured the C-O bond dissociation energy of a series of substituted anisoles and found that the bond weakening caused by the *o*-hydroxy group was 4.7 kcal mol^{-1} greater than that for the *p*-hydroxy group [23]. This additional stabilization was attributed to internal hydrogen bonding and not a destabilizing interaction in the guaiacol molecule. In α-HO-PPE and β-$HOCH_2$-PPE, molecular mechanics calculations indicate that the hydroxy group can interact with the ether oxygen without a significant energy penalty. The 20 fold rate enhancement in the decomposition of hydroxy-substituted PPE's at 500 °C corresponds to a difference of ca. 4.5 kcal mol^{-1} in C-O bond strengths (assuming all products arise from C-O homolysis). Additionally, King and Stock have reported that hydrogen bonding by phenols or benzoic acid enhance the rate of decomposition of benzyl phenyl ether and dibenzyl ether [24]. However, it is still remarkable for weak hydrogen bonding interactions to have such a dramatic influence on the reaction chemistry at high temperatures. Therefore, to further investigate the potential role of hydrogen bonding in the decomposition of hydroxy-substituted PPE's, the methyl ether of α-HO-PPE and β-$HOCH_2$-PPE will be synthesized and subjected to FVP. This will remove the hydrogen bonding interactions and the conversions should be more similar to that found for PPE if hydrogen bonding is important.

ACKNOWLEDGMENTS

Research sponsored by the Division of Chemical Sciences, Office of Basic Energy Sciences, U.S. Department of Energy, under contract DE-AC05-96OR22464 with Oak Ridge National Laboratory, managed by Lockheed Martin Energy Research Corp. M. J. Cooney was supported by an appointment to ORNL Postdoctoral Research Associate program administered jointly by Oak Ridge Institute for Science and Education and ORNL.

REFERENCES

1. (a) A. V. Bridgwater (Ed.),Thermochemical Processing of Biomass, Butterworths, London, 1984. (b) E. J. Soltes and T. A. Milne (Eds.), Pyrolysis Oils from Biomass-Producing, Analyzing, and Upgrading, ACS Symposium Series No 376, American Chemical Society, Washington, DC 1988. (c) I. S. Goldstein (Ed.), Organic Chemical from Biomass, CRC Press, Boca Raton, Fl 1981, Chapters 5 and 8.
2. Glasser, W. G.; Sarkanen, S. (Eds:), Lignin Properties and Materials, ACS Symposium Series No. 397, American Chemical Society, Washington, DC, 1989.
3. van der Hage, E. R. E.; Mulder, M. M.; Boon, J. J. *J. Anal. Appl. Pyrolysis* **1993**, *25*, 149.
4. Antal, Jr., M. J.; Croiset, E.; Dai, X.; DeAlmeida, C; Mok, W. S-L.; Norberg, N.; Richard, J-R.; Majthoub, M. A. *Energy Fuels* **1996**, *10*, 652.
5. Elliott, D. C.; Beckman, D.; Bridgwater, A. V.; Diebold, J. P.; Gevert, S. B.; Solantausta, Y. *Energy Fuels* **1991**, *5*, 399.

6. Bridgwater, A. V.; Cottam, M-L. *Energy Fuels* **1992**, *6*, 113.
7. a) Antal, Jr., M. J. in Boer, K. W. and Duffie, J. A. (Eds.), *Advances in Solar Energy*, Vol 2, ASES Publication, New Toyk, 1985, p.175 and references therein. (b) Evans, R. J.; Milne, T. A.; Soltys, M. N. *J. Anal. Appl. Pyrolysis* **1986**, *9*, 207.
8. Klein, M. T.; Virk, P. S. *Ind. Eng. Chem. Fundam.* **1983**, *22*, 35.
9. (a) Brown, R. F. C. Pyrolytic Methods in Organic Chenistry, Academic Press, New York, 1980. (b) Seybold, G. *Angew. Chem. Int. Ed. Engl.* **1977**, *16*, 365. (c) Schaden, G. *J. Anal. Appl. Pyrolysis* **1985**, *8*, 135. (d) Wiersum, U. E. *Rec. Trav. Chim. Pays-Bas* **1982**, *101*, 317 and 365. (e) Hedaya, E. *Acc. Chem. Res.* **1969**, *2*, 367.
10. Golden, D. M.; Spokes, G. N.; Benson, S. W. *Angew. Chem. Int. Ed. Engl.* **1973**, *12*, 534.
11. Glasser, W. G.; Glasser, H. R.; Morohoshi, N. *Macromolecules* **1981**, *14*, 253. (b) Nimz, H. *Angew Chem. Int. Ed. Engl.* **1974** , *13*, 313.
12. Britt, P. F.; Buchanan, III, A. C.; Malcolm, E. A. *J. Org. Chem.* **1995**, *60*, 6523.
13. Trahanovsky, W. S.; Ong, C. C.; Pataky, J. G.; Weitl, F. L.; Mullen, P. W.; Clardy, J. C.; Hansen, R. S. *J. Org. Chem.* **1971**, *36*, 3575.
14. Trahanovsky, W. S.; Ong, C. C.; Lawson, J. A. *J. Am. Chem. Soc.* **1968**, *90*, 2839.
15. Walker, J. A. ; Tsang, W. *J. Phys. Chem.* **1990**, *94*, 3324.
16. Maccoll, A. *Chem. Rev.* **1969**, *69*, 33.
17. Maccoll, A.; Thomas, P. J. *Progress in Rection Kinetics* **1967**, *4*, 119.
18. Nelson, D. A.; Samuels, W. D.; Hallen, R. T. *Energy Fuels* **1987**, *1*, 239.
19. Kuroda, K. *J. Anal. Appl. Pyrolysis* **1995**, *35*, 53.
20. (a) Benson, S. W. Thermochemical Kinetics, Wiley, New York, 1978. (b) Benson, S. W. *Chem. Rev.* **1993**, *93*, 2419 (c) NIST Structure and Properties Database and Estimation Program Version 2.02, S. E. Stein, J. M. Rukkers, and R. L. Brown NIST Reference Database 25 1994.
21. Trahanovsky, W. S.; Ong, C. C. *J. Am. Chem. Soc.* **1970**, *92*, 7174.
22. The $D°_{C\text{-}H}$ of $PhCH(OH)CH_2$–H is set equal to $CH_3CH(OH)CH_2$–H. Holmes, J. L.; Lossing, F. P.; Mayer, P. M. *J. Am. Chem. Soc.* **1991**, *113*, 9723.
23. Suryan, M. M.; Kafafi, S. A.; Stein, S. E. *J. Am. Chem. Soc.* **1989**, *111*, 1423.
24. King, H.-H.; Stock, L. M. *Fuel* **1984**, *63*, 810.

MODELING BIOMASS PYROLYSIS KINETICS AND MECHANISMS

Yonggang Chen, Sylvie Charpenay, Anker Jensen*, Michael A. Serio, and Marek A. Wójtowicz

Advanced Fuel Research, Inc., 87 Church Street, East Hartford, CT 06108-3742
*Department of Chemical Engineering, Technical University of Denmark, 2800 Lyngby, Denmark

Keywords: Biomass, Pyrolysis, Modeling

ABSTRACT

Over the next decade there will be a renewed emphasis on the production of chemicals and liquid fuels from biomass, the use of agricultural wastes as feedstocks, and the co-firing of coal and biomass materials. In view of the tremendous diversity of biomass feedstocks, a great need exists for a robust, comprehensive model that could be utilized to predict the composition and properties of pyrolysis products as a function of feedstock characteristics and process conditions. The objective of this work is to adapt an existing coal pyrolysis model and make it suitable for the pyrolysis of biomass. The soundness of this approach is based on numerous similarities between biomass and coal. There are important differences, however, which preclude direct application of the coal model. This work involved: 1) selection of a set of materials representing the main types of biomass; 2) development of a biomass classification scheme; 3) development of a modeling approach based on modifications of a coal pyrolysis model; 4) calibration of the model for a set of standard materials against pyrolysis data taken over a range of heating rates; 5) validation of the model against pyrolysis data taken under other (higher) heating rate conditions.

INTRODUCTION

The future outlook for biomass pyrolysis is quite promising, despite the fact that petroleum prices should remain low for at least the next decade [1]. The political and environmental benefits of using biomass will continue to provide impetus to the development of biomass pyrolysis processes (indigenous supply, low sulfur, no net CO_2, biodegradable, etc.). The current level of activity is high (about 650 activities were identified in a recent study [2]), and international in scope. Over the next several years there will be a renewed emphasis on the production of chemicals from biomass with minimal upgrading, and on the use of agricultural wastes as feedstocks. Research and development activities will also continue on the production of liquid fuels and chemicals from biomass, and on the development of crops and farming techniques optimized for fuel or chemical production.

In view of the anticipated rapid development of pyrolysis-based processes, and because of the tremendous diversity of biomass feedstocks, a great need exists for a robust, comprehensive model that could be utilized to predict yields, composition and properties of pyrolysis products. Such a model would constitute a valuable tool in process development and scale-up. No such model is currently available. The specific problem addressed in this study was related to the inability to predict *a priori* gas, liquid, and solid products on the basis of known feedstock characteristics and process conditions (temperature, pressure, heating rate, residence time, etc.). This makes it difficult, of course, to design a process where the most desirable slate of products is produced. This, in turn, leads to appreciable, and often unnecessary, costs of product upgrading.

This work involved modifying the currently available FG-DVC coal devolatilization model [3,4], and making it suitable for modeling pyrolysis of agricultural and forestry feedstocks. The soundness of this approach was based on numerous similarities between biomass and coal, such as the fact that coal was formed from biomass, and that it can actually be viewed as petrified biomass. There are important differences, however, which preclude direct application of the coal model to pyrolysis of biomass, and which make it necessary to create a separate model dedicated to biomass conversion.

The FG-DVC model for coal pyrolysis combines a functional group (FG) model for gas evolution and a statistical depolymerization, vaporization, and cross-linking (DVC) model for tar and char formation [3,4]. The FG model currently predicts gas yields from the functional group sources in the coal using rank-dependent kinetics. The DVC model simulates coal as a macromolecular network and includes the processes of depolymerization, cross-linking, and transport. The model accurately predicts volatile yields, extract yields, cross-link densities, fluidity, and tar (oil) molecular weight distributions. The variations of the variables with pressure, devolatilization temperature, rank, and heating rate are also accurately reproduced.

A version of the FG-DVC model has been developed for lignin [5], which is similar to coal in being a cross-linked aromatic structure. However, in the case of whole biomass, the lignin component is a relatively minor constituent and the modeling approach must be adjusted to account for the dominant components (cellulose and hemi-cellulose).

BACKGROUND

The pyrolysis of biomass has been the subject of numerous studies, as summarized in several reviews and collected papers [6-12]. Biomass pyrolysis is similar to coal pyrolysis with respect to pyrolysis products, which are char, tar and gases. Analogies are often drawn between pyrolysis of biomass and low-rank coals, but this should be done with caution. One of the principal differences is the fact that coal is predominantly an aromatic material, whereas the aromatic component of biomass (lignin) is a relatively minor constituent (~20%). In addition, because of the fossil nature

of coal, the mineral matter which has been incorporated into its structure influences the pyrolysis behavior in a different way than in the case of biomass. Biomass also has a much higher oxygen content as compared with coal. The oxygen is present as ether, hydroxyl, carboxyl, aldehyde, and ketone functionalities, which decompose during pyrolysis to produce oxygenated gases (CO, CO_2, H_2O). The yields of these species are similar to those produced by pyrolysis of low-rank coals (5–10 dry wt.% for CO_2 and H_2O, 5–15 dry wt.% for CO). Biomass pyrolysis, however, produces much higher tar (liquid) yields as compared with low-rank coals (40–50% versus 10–20% on a dry basis). The increased tar yield comes primarily at the expense of char, the yield of which is much lower for biomass than for low-rank coals (<10% versus 40–50%). Apparently, the depolymerization of biomass is the predominant pyrolytic reaction, whereas, in the case of coal, depolymerization reactions compete with cross-linking events, which enhances char formation. Most of the char formed from biomass is derived from the lignin component, which is closest to low-rank coal in its chemical composition. As in the case of coal, the yield and distribution of products from pyrolysis of biomass depend on other variables in addition to the final temperature and holding time. These include heating rate, total pressure, ambient gas composition, and the presence of catalysts. An overview of these is given by Shafizadeh (in reference [10]). The trends are similar to those observed in coal, i.e., higher yields of volatiles are usually observed at higher heating rates, lower pressures, and in the presence of hydrogen. However, the data are quite scattered.

Historically, the quantitative modeling of biomass pyrolysis has proceeded along similar lines as for coal [1]. One approach is based on the approximation that the three main components of biomass (cellulose, hemi-cellulose, and lignin) behave independently during pyrolysis (see, e.g. Nunn *et al.* in ref. [10]). Consequently, yields can be predicted based on a knowledge of the pure component behavior. The shortcoming of this technique is that it cannot account for possible interactions between the biomass components. A more phenomenological approach was successfully used by Serio *et al.* [5] in modeling the pyrolysis of lignin. Their model was focused on observed evolution rates of major products rather than on the many individual reactions leading to the evolution of each product. The model of Serio *et al.* [5] and that of Petrocelli and Klein (discussed in reference [10]) involve a statistical treatment of lignin pyrolysis reactions. For the reasons discussed above, the network features of the FG-DVC model and similar models (such as the one proposed by Petrocelli and Klein) will be de-emphasized in favor of the original functional group (FG) description of gas and tar evolution [13,14]. While this is a more empirical approach, there is flexibility in the model to add more details of the whole biomass pyrolysis chemistry as these become known and can be represented in a tractable mathematical expression. A detailed review of modeling chemical and physical processes occurring during whole biomass pyrolysis can be found in reference [15]. Unlike in the case of coal, no comprehensive model of whole biomass pyrolysis has yet been developed.

EXPERIMENTAL

Sample Selection - A number of biomass samples were first recommended based on the abundance and availability of agricultural and forestry feedstocks in the United States. The initial recommendations included softwood, hardwood, corn stalk, wheat straw, copy paper and newspaper. Cellulose, lignin, and hemi-cellulose were also recommended in order to individually study the three main components of biomass independently. This initial list was modified due to the limited ability to acquire standardized materials. Six samples were obtained from the Nation Institute of Standards and Technology's Standard Reference Materials Program which included microcrystalline cellulose (C), sugar cane bagasse (B), wheat straw (WS), corn stalk (CS), softwood *Pinus radiata* (PR), and hardwood *Populus deltoides* (PD). These six samples were supplemented with two samples of the pure component materials: lignin (L) and hemi-cellulose (HC). The identification and elemental composition of all nine samples is given in Table 1. To understand the chemical structure of these feedstocks, the starting materials were characterized by several methods including trace elemental analysis, ultimate analysis, proximate analysis, Field Ionization Mass Spectrometry (FIMS), solvent extraction and solvent swelling. This was complemented by a compilation of relevant literature data. FIMS and solvent extraction/swelling data will be reported in a separate publication.

Ultimate and Proximate Analysis - This work was done by Huffman Laboratories (Golden, Colorado). In addition, the samples were subjected to trace element analysis. Trace elements have often been implicated in influencing the pyrolysis behavior of whole biomass ([16]; also Shafizadeh in reference [10]).

TG-FTIR Method - Details of the TG-FTIR method can be found in references [17] and [18]. The apparatus, consists of a sample suspended from a balance in a gas stream within a furnace. As the sample is heated, the evolving volatile products are carried out of the furnace directly into a 5 cm diameter gas cell (heated to 150 °C) where the gases are analyzed by FT-IR spectroscopy. The FT-IR spectrometer obtains spectra to determine quantitatively the evolution rate and composition of several hydrocarbon compounds. Coal tars can also be quantified but biomass tars are appreciably different and for the lack of calibration data are determined from the mass balance. The system allows the sample to be heated on a pre-programmed temperature profile, at rates 3–100 °C min^{-1}, up to a temperature between 20 °C and 1100 °C. Isothermal steps with a specified hold time are also possible.

RESULTS AND DISCUSSIONS

Biomass Classification Scheme- The first step in modeling was to develop a classification scheme for whole biomass samples. Several researchers have taken the approach of modeling the pyrolysis of whole biomass using a linear superposition of the results for the three main components, i.e., cellulose, hemi-cellulose, and lignin ([19–21]; also Nunn *et al.* in reference [10]). However, a problem with this approach is that input information is not always known or easily obtained, and the amounts determined are not always consistent from one laboratory to another. In addition, Nunn *et al.* reported that modeling the evolution of individual species in high-heating-rate experiments was unsuccessful, although the modeling of the char yield produced good results [10]. The above scheme was also tested at Advanced Fuel Research (AFR) by trying to reproduce the TG-FTIR results for a whole biomass sample using a superposition of the TG-FTIR evolution profiles obtained for pure components. In general, this approach was unsuccessful for the evolution of individual species, and this is thought to be due to variations in the component compositions depending on their source, the effect of trace components on the pyrolysis behavior, and the problem in isolating unaltered pure components.

For this reason, it was decided that an alternative approach would be pursued, in which the samples are classified based on a van Krevelen diagram (plot of H/C versus O/C atomic ratios). A similar classification scheme has been successfully used for coal pyrolysis [22]. A plot of the six samples and the pure component samples are shown in Figure 1, along with literature results for other biomass samples. In general, the H/C ratio correlates with the O/C ratio, especially for the data collected at AFR. Variations in moisture content and errors in elemental analysis results are believed to be responsible for part of the scatter.

Model Calibration - The classification scheme lends itself to a linear interpolation of the total yields of pyrolysis products as well as the kinetic files based on the known elemental composition. However, since most of the whole biomass samples are closely clustered to either one of the woody (PD, PR) or herbaceous samples (CS, WS), it was decided to use a close-neighbor approximation. In this case, the input files are obtained from the nearest neighbor of the standard set of samples which were chosen to be L, CS, PD, and C. These samples were subjected to a more detailed characterization in order to calibrate the kinetic and composition files. In future work, some refinement of this scheme will be developed which allows for discrimination of small differences in composition.

The close-neighbor approximation is also confirmed by the TG-FTIR data as shown in Figures 2 and 3, where the evolution profiles for PR, PD, and B, and WS and CS are compared. The TG-FTIR data shows that PR, PD and B behave similarly, which is in agreement with the van Krevelen data from Figure 1. The same can be said about WS and CS. In addition, the following general observations conceming the TG-FTIR data can be made: (1) for each biomass sample, all gas-evolution peaks (except for methane) occur at approximately the same temperature; (2) the methane evolution peak of woody samples is bimodal, whereas only a single peak is present in the case of herbaceous biomass; (3) all the herbaceous-samples peaks occur at temperatures approximately 30 °C lower than the corresponding peaks for the woody samples; and (4) a small low-temperature peak can be seen in the evolution patterns of the herbaceous samples.

Kinetics and Yields Determination - In what follows, the determination of the kinetic parameters and total yields of individual species is described in some detail. In general, the approach is similar to that applied to coal, i.e., the evolution of each functional group is described by a first-order reaction with a distributed activation energy of width σ [4]. In the case of biomass pyrolysis, a smaller number of functional groups is required to describe the process as the evolution of each species can usually be represented by the decomposition of a single functional group. In other words, each gas species released during biomass pyrolysis evolves in the form of a single peak, which is in contrast to coal pyrolysis where several peaks can be observed for an individual species. Methane is an exception, in the sense that it requires two functional groups in the case of coals and woody biomass, but only a single peak for herbaceous biomass.

Since the TG-FTIR biomass data show that, for each sample, the tar and other gas species evolve at the same temperature (Figs. 2 and 3), the same value of the activation energy was used for all species. This activation energy was derived from the overall weight-loss curve, and a non-isothermal T_{max} method was used for this purpose [23]. T_{max} is the temperature at which the rate of volatile evolution is maximum. Typically, T_{max} is measured at several heating rates, and the activation energy E and the pre-exponential factor A can be extracted from the equation : $ln(M/T^2_{max}) = ln(AR/E) - E/(RT_{max})$ [23].

Although the value of E was kept identical for the biomass tar and all the gas species, slight adjustments in the value of σ were performed in order to match more closely the width of the evolution peak of each species. The amounts of the functional groups, and the corresponding yields of the volatiles, were obtained by fitting the model to the TG-FTIR data. The results from this analysis are given in Table 2. The values for the activation energies obtained are consistent with previous literature results [24]. The apparent discrepancy between our kinetic parameters and those reported for cellulose by Antal and Varhegyi [25] can be explained by the differences in the processing of raw experimental data. A detailed discussion of this topic will be included in a future publication.

Model Validation - Model predictions were compared with the yields and composition of pyrolysis products obtained under different conditions from those used to determine model

parameters (e.g., different heating rates). An example is shown in Fig. 4 for the high heating rate data of Nunn *et al.* (1000 K/sec) [26]. Experimental data for sweet gum hardwood are compared with model predictions generated using the kinetic input files for PD. The results are reasonable for the overall weight loss (Fig. 4) and CO_2 (not shown), but they are less good for the other gas species. In addition to the simplifications inherent in the predictive model, and the differences in the composition of the two materials, the observed discrepancies could also result from uncertainties in the time-temperature history and/or secondary reactions which alter the product distribution. Future work will involve refinement of the model to include secondary reactions, mineral effects, heating-rate effects, and an improved classification scheme to account for composition differences.

CONCLUSIONS

The FG-DVC coal pyrolysis model has been successfully applied to biomass. Preliminary data show that it may be possible to model the pyrolysis behavior of different biomass feedstocks using kinetic parameters and product yields interpolated among selected data-base materials (standards). The linear interpolation scheme is based on the feedstock elemental composition. Refinements of the proposed scheme and further validation of the model are under way.

ACKNOWLEDGMENTS

The support for this work came from the U.S. Department of Agriculture under Research Agreement No. 96-33610-2675. A research scholarship for Anker Jensen was provided by the Technical University of Denmark. The authors also acknowledge helpful discussions with Professor Eric M. Suuberg of Brown University.

REFERENCES

1 Serio, M. A., Wójtowicz, M. A. and Charpenay, S., "Pyrolysis," *Encyclopedia of Energy Technology and the Environment* (A. Bisio and S. G. Boots, Eds.), John Wiley & Sons, New York, 1995.
2 Bridgwater, A. V., *Biomass*, **22** (1-4), 279 (1990).
3 Solomon, P. R., Hamblen, D. G., Carangelo, R. M., Serio, M. A., and Deshpande, G. V., *Combustion and Flame*, 1988, **71**, 137.
4 Solomon, P. R., Hamblen, D. G., Serio, M. A., Yu, Z. Z., and Charpenay, S., "A Characterization Method & Model for Predicting Coal Conversion Behavior," *Fuel*, **72**, (4), 489 (1993).
5 Serio, M. A., Charpenay, S., Bassilakis, R., and Solomon, P. R., "Measurement and Modeling of Lignin Pyrolysis", *Journal of Biomass & Bioenergy*, Vol. 7, Nos. 1-6, 107 (1994)
6 Antal, M. J., Jr., in Adv. in *Solar Energy* (Boer, K. W., Duffie, J. W., Eds.), American Solar Energy Society, Boulder, CO, **1**, 61 (1984); **2**, 175 (1985)
7 Shafizadeh, F., in *Proc. Specialists' Workshop on Fast Pyrolysis of Biomass* (J. Diebold, Ed.), SERI/CP-622-1096, Solar Energy Research Institute, Golden, CO, 79 (1980)
8 Shafizadeh, F., in *The Chemistry of Solid Wood* (R. M. Rowell, Ed.), Advances in Chemistry Series No. 207, American Chemical Society, Washington, DC (1984).
9 Bridgwater, A. V., and Cottam, M.-L., *Energy and Fuels*, **6**, (2), 113 (1992)
10 Overend, R. P. Milne, T. A. , and Mudge, L. K., Eds., *Fundamentals of Thermochemical Biomass Conversion*, Elsevier, (1985)
11 Soltes, E. J., and Milne, T. A., Eds., *Pyrolysis Oils from Biomass: Producing, Analyzing and Upgrading*, ACS Symposium Series No. 376, American Chemical Society, Washington, DC (1988)
12 Chum, H. L., and Powers, A. J., in *Emerging Technologies for Materials and Chemicals from Biomass* (R. M. Rowell, T. P. Schultz, and R. Narayan, Eds.), ACS Symposium Series No. 476, ACS, Washington, DC, pp. 339–353 (1993).
13 Solomon, P. R. and Hamblen, D. G., Ch. 5 in *Chemistry of Coal Conversion* (R. H. Schlosberg, Ed.), Plenum, New York, 1985, , pp. 121–251.
14 Serio, M. A., Hamblen, D. G., Markham, J. R. and Solomon, P. R., *Energy & Fuels*, **1**, 138 (1987).
15 Di Blasi, C., *Prog. Energy Combust. Sci.*, **19**, 71 (1993).
16 Varhegyi, G., Antal, M. J., Jr., Szekely, T., Till, F., Jakab, E. and Szabo, P., *Energy & Fuels*, **2**, 273 (1988).
17 Carangelo, R. M., Solomon, P. R. and Gerson, D. J., *Fuel*, **66**, 960 (1987).
18 Whelan, J. K., Solomon, P. R., Deshpande, G. V., Carangelo, RM., *Energy and Fuels*, **2**, 65, (1988)
19 Koufopanos, C. A., Maschio, G. and Lucchesi, A., *Can. J. Chem. Eng.*, **67**, 75 (1989).
20 Ward, S. M. and Breslaw, J., *Comb. Flame*, **61**, 261 (1985).
21 Miller, R. S. and Bellan, J., submitted to *Combust. Sci. Tech.* (1996).
22 Zhao, Y., Serio, M. A., Bassilakis, R. and Solomon, P. R., *Twenty-Fifth Symposium (International) on Combustion*, The Combustion Institute, Pittsburgh, PA, 1994, pp. 553–560.
23 Van Heek, K. H. and Juentgen, H., *Ber. Bunsenges. Phys. Chem.*, **72**, 1223 (1968).

24 Milosavljevic, I. and Suuberg, E. M., *Ind. Eng. Chem. Res.*, **34**, 1081 (1995).
25 Antal, M. J., Jr. and Varhegyi, G., *Ind. Eng. Chem. Res.*, **34**, 703 (1995).
26 Nunn, T. R., Howard, J. B., Longwell, J. P. and Peters, W. A., *Ind. Eng. Chem. Process Des. Dev.*, **24**, 836 (1985).

Table 1. Proximate, ultimate, and trace-element analyses of the biomass samples used in this study (wt.%). Dry loss is on an as-received basis, while all other results are reported on a dried-sample basis. Legend: CS = Corn Stalk; WS = Wheat Straw; B = Sugar Cane Bagasse; PR = *Pinus radiata*; PD = *Populus deltoides*; C = Cellulose; ALC = ALC Lignin

	CS	WS	B	PR	PD	C	ALC
Dry Loss	5.0	7.9	7.1	6.6	6.6	4.8	N/A
Carbon	45.6	43.7	47.3	49.9	49.1	44.0	67.4
Hydrogen	5.9	5.6	5.8	6.1	6.0	6.4	6.2
Oxygen	44.0	40.9	42.8	43.6	43.8	49.5	26.3
Nitrogen	0.72	0.62	0.17	0.05	0.09	0.03	0.20
Sulfur	0.10	0.19	0.04	0.02	0.06	< 0.01	N/A
Ash	3.8	9.0	3.9	0.25	0.91	< 0.05	< 0.05
Vol. Matter	89.8	72.8	79.3	82.8	83.5	92.7	N/A
Fixed Carbon	6.4	18.2	16.8	17.0	15.6	7.3	N/A
Al	N/A	N/A	0.2%	L	L	N/A	N/A
Si	N/A	N/A	0.3%	L	L	N/A	N/A
Na	N/A	N/A	L	L	L	N/A	N/A
K	N/A	N/A	0.03%	0.02	0.02%	N/A	N/A
Fe	N/A	N/A	0.1%	N	N	N/A	N/A
Mg	N/A	N/A	L	N	N	N/A	N/A
Ca	N/A	N/A	0.05%	L	0.1	N/A	N/A
Ti	N/A	N/A	0.05%	N	N	N/A	N/A
Mn	N/A	N/A	50 ppm	N	N	N/A	N/A
B	N/A	N/A	L	N	N	N/A	N/A
Ba	N/A	N/A	L	N	N	N/A	N/A
Be	N/A	N/A	L	N	N	N/A	N/A
Cr	N/A	N/A	L	N	N	N/A	N/A
Ni	N/A	N/A	L	N	N	N/A	N/A
V	N/A	N/A	10 ppm	N	N	N/A	N/A

L = Detected but below detection limit, N = Not detected, N/A = Not Available

Table 2. Kinetic parameters and yields for the pyrolysis of corn stalk and *Populus deltoides*.

Sample	Species	A (s^{-1})	E/R (K)	σ/R (K)	Yield (wt.% daf)
Corn Stalk	CO_2	8.3×10^{13}	22500	700	5.1
	CO	8.3×10^{13}	22500	700	2.2
	H_2O	8.3×10^{13}	22500	700	7.4
	CH_4 Tight	N/A	N/A	N/A	N/A
	CH_4 Loose	5.2×10^{12}	27500	2000	0.8
	Tar	8.3×10^{13}	22500	100	63.5
Populus Deltoides	CO_2	2.8×10^{9}	17000	700	5.2
	CO	2.8×10^{9}	17000	700	3.4
	H_2O	2.8×10^{9}	17000	700	10.4
	CH_4 Tight	6.0×10^{13}	31000	2500	0.54
	CH_4 Loose	3.0×10^{13}	25000	1500	0.36
	Tar	2.8×10^{9}	17000	100	55.2

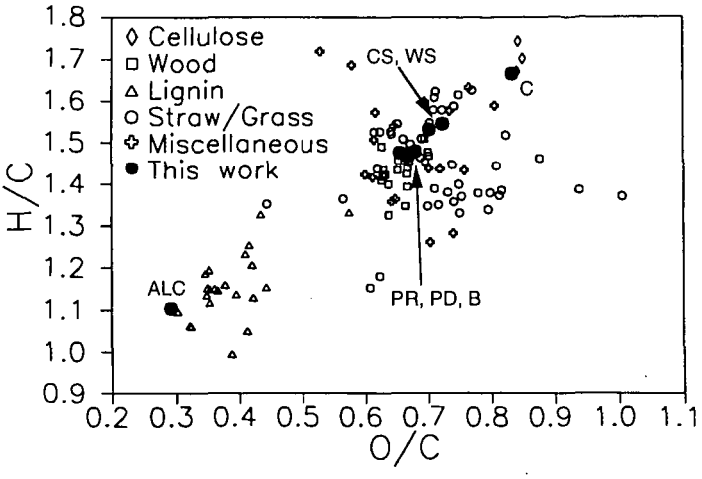

Figure 1. The van Krevelen diagram for biomass samples. H/C and O/C are atomic hydrogen-to-carbon and oxygen-to-carbon ratios.

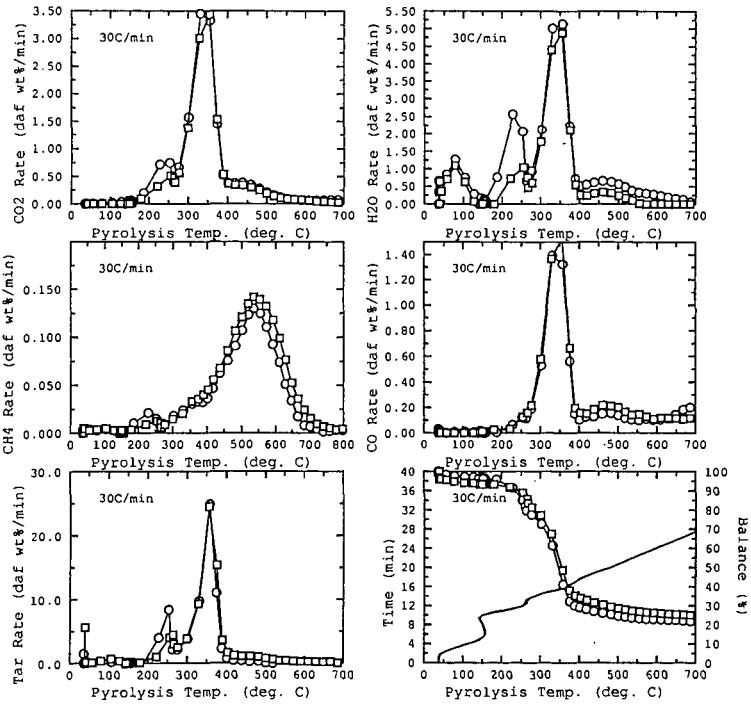

Figure 2. The TG-FTIR data for two herbaceous samples: corn stalk (circles) and wheat straw (squares).

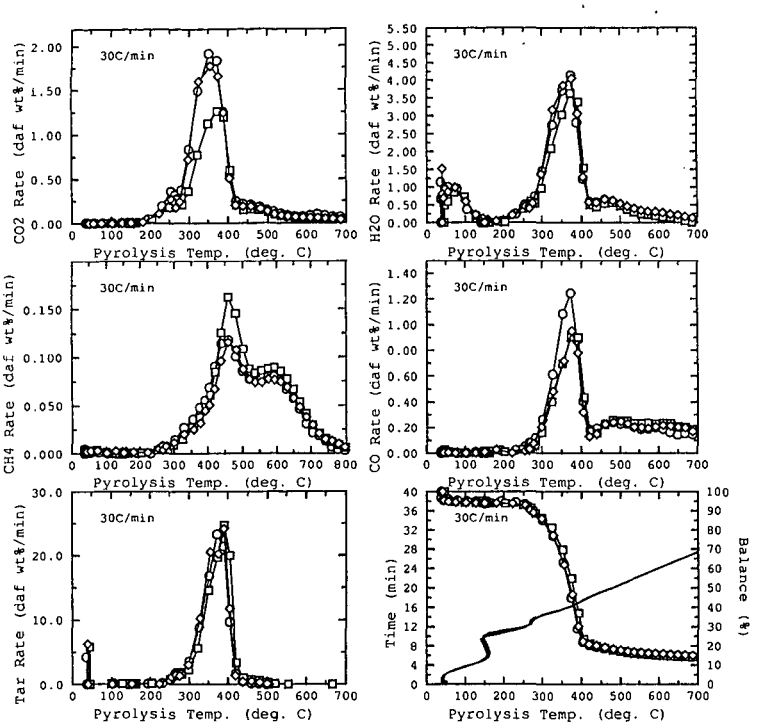

Figure 3. The TG-FTIR data for two woody samples: *Populus deltoides* (circles) and *Pinus radiata* (squares). The position of sugar cane bagasse on the van Krevelen diagram is in close proximity to the above two samples, and the TG-FTIR data for bagasse (diamonds) exhibit gas-evolution patterns similar to those of *Populus deltoides* and *Pinus radiata*.

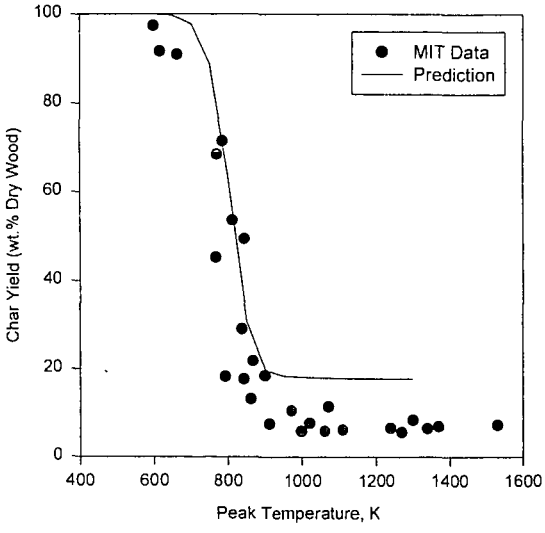

Figure 4. The comparison of char-yield experimental data (Nunn *et al.* [26]) and model predictions using the kinetic input files and product yields for *Populus deltoides*. The heating rate is 1000 K/s.

MECHANISM OF SILICA-IMMOBILIZED THIOANISOLE CONVERSION DURING AN AP-TPR-EXPERIMENT

H. Van den Rul, J. Yperman, A. C. Buchanan III [a], P. F. Britt [a], I. I. Maes, D. V. Franco, J. Mullens and L. C. Van Poucke, Laboratory of Inorganic and Physical Chemistry, Limburgs Universitair Centrum, B-3590 Diepenbeek, Belgium, [a] Chemical and Analytical Sciences Division, Oak Ridge National Laboratory, P. O. Box 2008, Oak Ridge, TN 37831-6197, USA

Keywords: Non-Isothermal Kinetics, AP-TPR, Model Compounds

ABSTRACT

A kinetic study of the AP-TPR-profile of silica-immobilized thioanisole was carried out, resulting in a better understanding of the mechanistic behaviour of this model compound under the specified conditions. AP-TPR (Atmospheric Pressure - Temperature-Programmed Reduction) with potentiometric sulfur detection is a thermoanalytical method used to differentiate between sulfur forms in solids like coals. In this respect, silica-immobilized thioanisole was recorded as a nonmelting calibrant. Several kinetic methods exist to analyze a heterogeneous process involving a solid that is heated by a linear temperature programme. The isoconversional method can be considered as one of the most accurate. It was applied to the AP-TPR-profile of thioanisole, showing the reduction of this compound very quickly becomes a diffusion-controlled reaction. Kinetic parameters are reported for this process under the AP-TPR-conditions.

INTRODUCTION

Temperature-Programmed Reduction (TPR) of sulfur-containing solid samples under atmospheric pressure (AP), is a method to study different sulfur functionalities in the sample [1]. Knowledge of the distribution of sulfur functional groups in materials is of practical importance. For example, the ease with which sulfur is released from coal is determined by the functional form of the sulfur present. Thiols and sulfides are labile sulfur compounds and undesirable because of environmental consequences. Thiophenes on the other hand are more stable.
Recording of model compounds for sulfur functionality (in coal for example) is a key step in AP-TPR to evaluate characteristic temperature intervals where reduction of the specific sulfur group occurs.
A study of the AP-TPR-profiles of model compounds can also provide information about the mechanistic pathway of the occurring reactions that involve sulfur. In combination with other techniques a more detailed description can be given [2].
Also, a non-isothermal kinetic analysis of the AP-TPR-curves can be performed to get a better insight into the mechanism. A kinetic investigation of an AP-TPR-profile is different from conventional kinetics: the reaction studied is heterogeneous, a solid is involved and the temperature is raised during the experiment. Kinetic laws for homogeneous processes under isothermal conditions have been accurately determined. They can be considered as component parts of more complex kinetic models applied to heterogeneous processes [3].
For AP-TPR experiments, calibrants must neither melt nor evaporate before they are reduced in order that they remain in the reaction zone of the reactor. In this respect, nonmelting silica-immobilized (SI) substrates can be employed. It has been demonstrated the Si-O-C_{aryl} linkage is stable up to 500°C, even in reducing atmospheres [4].
In this work, AP-TPR-profiles of silica-immobilized thioanisole (≈Ph-S-CH_3) are analyzed by non-isothermal kinetics, and more specifically by the isoconversional method [7].

EXPERIMENTAL

The AP-TPR-set-up is shown in figure 1. During an AP-TPR-experiment, the sample is located at the bottom of a quartz reactor, while H_2 gas is constantly flowing through it (fluidized bed system) at a rate of 50 ml/min. The oven is heated by a constant linear temperature programme, and the different sulfur functional groups are reduced in a characteristic temperature interval. The released H_2S is detected potentiometrically, resulting in a spectrum of H_2S evolution.
Silica-immobilized thioanisole was prepared from the sulfur-containing phenol (4-hydroxy-thioanisole, Aldrich Chemical Co.) and Cabosil fumed silica on a gram scale, as described previously for the synthesis of silica-immobilized diphenylalkanes [5].
For the AP-TPR-experiments, 20.0 mg SI thioanisole was used.

RESULTS AND DISCUSSION

Kinetic methods

Generally a simplified rate equation is used to describe reactions in solids [3]:

$$\frac{d\alpha}{dt} = k(T).f(\alpha) \qquad (1)$$

where $\alpha = \frac{X_b - X}{X_b - X_e}$ is the degree of conversion (X is the measured quantity, e.g. mass sulphur in AP-TPR), normalised from 0 to 1, k(T) is the Arrhenius rate constant, T is the temperature, t is the time and f(α) is a mathematical description of the reaction model. The form of f(α) is related to physico-geometric assumptions on the development of the reaction boundary between the initial solid substance and the product.

For non-isothermal conditions, when a constant heating rate $\beta = \frac{dT}{dt}$ is applied, eq. (1) is transformed:

$$\frac{d\alpha}{dT} = \frac{A}{\beta}\exp(-\frac{E}{RT})f(\alpha) \qquad (2)$$

where E is the Arrhenius activation energy, A the pre-exponential factor and R the gas constant. In integral form:

$$\int_0^{\alpha}\frac{d\alpha}{f(\alpha)} \equiv g(\alpha) = \frac{A}{\beta}\int_0^{T}\exp(-\frac{E}{RT})dT \equiv \frac{A}{\beta}I(E,T) \qquad (3)$$

Equation (2) as well as numerous approximations of its integral form (3) underlie most of the methods of kinetic processing [3].

Most frequently, those methods are utilized that employ data obtained at one heating rate. Different reaction models are fitted to the dataset, the best f(α) is discriminated using some criterion, and the Arrhenius parameters are evaluated based on this choice. The problem [6] is that usually quite different reaction models fit the data equally well (from a statistical point of view), whereas the values of the corresponding Arrhenius parameters markedly differ. The ambiguity of the kinetic parameters obtained by these "discriminating" methods implies that their physical meaning is doubtful. Moreover [6] this type of analysis yields a single kinetic triplet (A, E and f(α)) for the overall process of thermal transformation and doesn't allow the detection of a possible change of rate-limiting step (and associated Arrhenius parameters).

Overcoming these problems can be done by using methods that employ data at different heating rates, like isoconversional methods [7]. Without having to discriminate a reaction model, values of E are obtained at each given conversion α. The isoconversional method used in this work can be described as follows [7]:

assuming the reaction model is independent of the heating rate, eq. (3) can be written for a given conversion and a set of data obtained at different heating rates β_i (i=1, ..., n) as:

$$\frac{A_\alpha}{\beta_1}I(E_\alpha,T_{\alpha,1}) = \frac{A_\alpha}{\beta_2}I(E_\alpha,T_{\alpha,2}) = \ldots = \frac{A_\alpha}{\beta_n}I(E_\alpha,T_{\alpha,n}) \qquad (4)$$

Strict fulfilment of eq. (4) results in:

$$\sum_{i\neq}^{n}\sum_{j}^{n}\frac{I(E_\alpha,T_{\alpha,i})\beta_j}{I(E_\alpha,T_{\alpha,j})\beta_i} = n(n-1) \qquad (5)$$

where j = 1, ..., n. Because the T_α values are measured with some experimental error, eq. (4) can only be satisfied as an approximate equality, in other words: eq. (5) can be met as a condition of minimum value:

$$n(n-1) - \sum_{i\neq}^{n}\sum_{j}^{n}\frac{I(E_\alpha,T_{\alpha,i})\beta_j}{I(E_\alpha,T_{\alpha,j})\beta_i} = \min \qquad (6)$$

Substituting experimental values of T_α and β into eq. (6) and varying E_α to reach the minimum gives the value of the activation energy at a given conversion. The values of I(E,T) are approximated.

Applying the isoconversional method to a multi-step process shows the dependence of E_α on α. This dependence can be used as a criterion for a multi-step process [8]. Moreover, the shape of the dependence can help to elucidate the mechanism of the occurring reactions [8].

Kinetic analysis of the AP-TPR profiles of silica-immobilized thioanisole

Several AP-TPR experiments for silica-immobilized thioanisole were performed at four different heating rates (3.5, 5, 8 and 12 °C/min). All profiles were normalised and converted to (α, T) dependences: see figure 2. Before 400 °C no reaction was detected. When the heating rate is increased, a shift of the profile is observed to higher temperatures [3].

Several combinations of curves at different heating rates were selected, and analyzed by the isoconversional method, resulting in a typical E-α dependence: see figure 3. At the very beginning of the process, values of E higher than 100 kJ/mol are observed, but immediately the activation energy reduces to values lower than 45 kJ/mol. These low values are typical for the diffusion of a gas in a solid [6, 9].

This E-α dependence can be interpreted as follows. The values of E (>100 kJ/mol) in the beginning refer to a chemical reaction that controls the rate. To determine what reaction is occurring, a comparison could be made with bond dissociation energies for the thioanisole compound. However, at very low values of α, the calculation of E is less accurate and an exact value of E can not be given. It can only be proven E-values typical for chemical reaction are seen here. Moreover, even at the beginning diffusion could influence the reaction rate, thus lowering the calculated E-values. Subsequently, the dependence shows a decrease of E to values lower than 45 kJ/mol. This means there is a transition from a reaction-controlled process to a regime that is completely controlled by diffusion of a gas in a solid. A possible explanation for this transition can be as follows. The sulfur-containing particles that can easily be reached by the H_2 gas react quickly to release H_2S with an activation energy E > 100 kJ/mol. The rate of the process is controlled by this hydrogenation. The rest of the particles that are not in direct contact with the H_2 gas, react next. But at this point, diffusion of H_2 or H_2S gas through the bulk of firstly reacted particles becomes the rate-limiting step. Another explanation for the transition to a diffusion regime involves reaction of the evolved H_2S with the siloxanes of the silica support to generate OSi-SH species that are then released slowly out of the solid.

A comment can be made here on the use of this model compound (SI thioansiole) for AP-TPR calibration. Since the hydrogenation is only rate-determining at the beginning of the process under AP-TPR-conditions, only the rate at the beginning is reproducible. The rest of the AP-TPR-rate-profile (differential form) is diffusion controlled, and can vary according to the specific conditions inside the AP-TPR-reactor. Because the sample amount used is very small (20 mg), and the experimental AP-TPR conditions are almost invariant, the differential profiles of thioanisole are very similar. Still, the diffusion-control has to be taken into account. This means that only the onset temperature can be used as a calibrant temperature for this thioanisole model compound. Additional studies have to be done to see if this conclusion also holds for other model compounds.

CONCLUSIONS

Application of the AP-TPR-technique in combination with non-isothermal kinetic analysis, is an efficient tool to study mechanistic pathways of reduction of sulfur in model compounds. The term "mechanism" indicates a kinetic scheme in this context, and not a sequence of elementary steps, because only those reactions can be seen in AP-TPR that induce the change in the measured quantity.

The results for silica-immobilized thioanisole show a transition from a (chemical) reaction-controlled process to a regime that is completely controlled by diffusion of a gas in a solid. Kinetic analyses of other model compounds like cysteine and silica-immobilized phenylbenzyl-sulphide will be discussed later.

ACKNOWLEDGEMENTS

This work is financed with a specialization grant of the 'Vlaams Instituut voor de bevordering van het wetenschappelijk-technologisch onderzoek in de industrie (IWT)'.

REFERENCES

1. Maes, I. I.; Yperman, J.; Van den Rul, H.; Franco, D. V.; Mullens, J.; Van Poucke, L. C.; Gryglewicz, G.; Wilk, P. *Energy & Fuels* **1995**, 9, 950
2. Ismail, K.; Mitchell, S. C.; Brown, S. D.; Snape, C. E.; Buchanan III, A. C.; Britt, P. F.; Franco, D. V.; Maes, I. I.; Yperman, J. *Energy & Fuels* **1995**, 9(4), 707
3. Sestak, J.; Thermal Analysis. Part D. Thermophysical Properties of Solids, Elsevier, New York, 1984
4. Lafferty, C. J.; Mitchell, S. C.; Garcia, R.; Snape, C. E.; Buchanan III, A. C.; Britt, P. F.; Klavetter, E. *Energy & Fuels* **1993**, 7, 331
5. Britt, P. F.; Buchanan III, A. C. *J. Org. Chem.* **1991**, 56, 6132
6. Vyazovkin, S. *Int. J. Chem. Kin.* **1996**, 28, 95
7. Vyazovkin, S.; Dollimore, D. *J. Chem. Inf. Comp. Sci.* **1996**, 36, 42
8. Vyazovkin, S. V.; Lesnikovich, A. I. *Thermochim. Acta* **1990**, 165, 273
9. Attar, A.; Dupuis, F. *Ind. Eng. Chem. Process Des. Dev.* **1979**, 18(4), 607

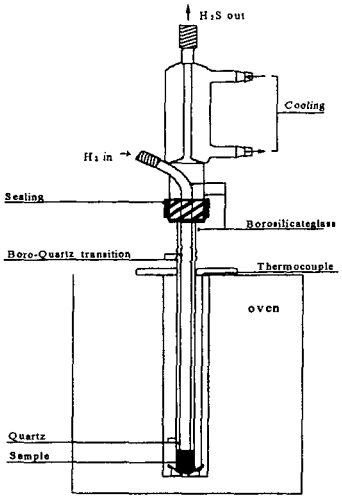

Figure 1: AP-TPR set-up

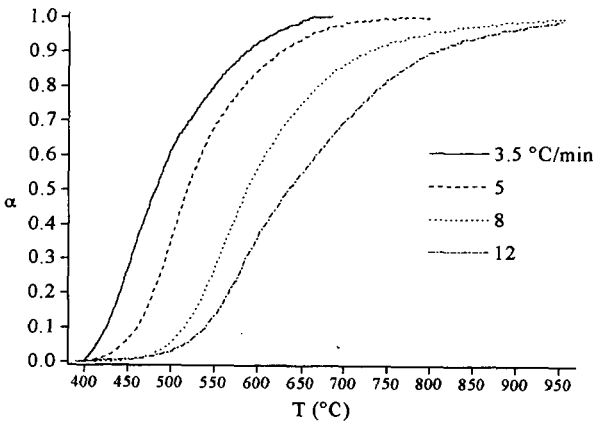

Figure 2: AP-TPR profiles of SI thioanisole shown as α, T dependences for 4 heating rates

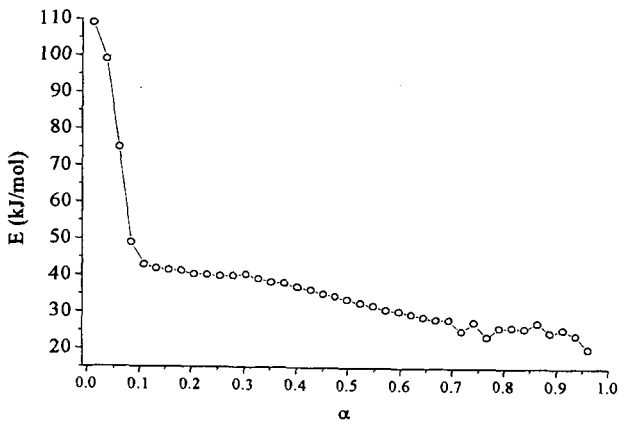

Figure 3: Typical E, α dependence for AP-TPR profiles of SI thioanisole

THE USE OF PHENOLIC RESINS CONTAINING POLYNUCLEAR AROMATIC MOIETIES TO MODEL ASPECTS OF COAL PYROLYSIS

C. McRae, O. Sirkecioglu and C. E. Snape

Department of Pure & Applied Chemistry, University of Strathclyde, Thomas Graham Building, 295 Cathedral St., Glasgow G1 1XL, Scotland, UK

Keywords : *Phenolic resins, polycyclic aromatic hydrocarbons, carbonisation*

INTRODUCTION

Coals and oil shales have highly complex, macromolecular organic structures[1-3] and, in order to obtain insights into the multitude of reactions which occur during their thermal breakdown, detailed compositional information on the aromatic, aliphatic and heteroatomic groups present and an understanding of how these different functionalities behave under processing conditions are required. To achieve the latter goal, model compound studies performed in both vapour and liquid phases have been used extensively[4]. However, a major drawback with such studies is that radical species generated by bond homolysis are mobile and free to diffuse independently prior to further reaction. In contrast, for highly cross-linked macromolecular solids such as coals and oil shales, many of the reactive intermediates remain covalently attached to the matrix of the solid and thus their reactivity is subject to diffusional constraints. Further, for thermal studies in open systems the use of non-softening substrates that neither melt nor vaporise and hence remain in the reactor is essential.

In order to probe the effects of restricted mobility in free radical reaction pathways during coal liquefaction, Buchanan and co-workers studied the thermal decomposition of model compounds immobilised on silica[5,6]. It was recognised that these substrates also have considerable potential for modelling many aspects of solid fuel behaviour, including the release of sulphur and nitrogen species during coal conversion processes and the cleavage of diphenylalkane bridging groups during pyrolysis. Preliminary work establish that the SiO-C bond linking the substrate to the surface is reasonably stable and does not cleave below 500°C[7]. Immobilised sulphur moieties, typical of those found in solid fuels were subsequently prepared and used as calibrants in temperature programmed reduction (TPR)[8], a thermal technique used to specify organic sulphur forms from their characteristic reduction temperatures [9,10].

Cured phenol-formaldehyde (PF) resins were identified as another flexible class of materials that could be used for investigating thermochemical phenomena in the solid state since a wide spectrum of hydrocarbon and heteroatomic moieties can readily be introduced into their macromolecular framework. A series of sulphur and nitrogen containing co-resoles and resites have been prepared and their characterisation has been reported previously[11]. These resites have been used to study the release of sulphur dioxide during coal combustion[12] and as an alternative calibrant to the silica immobilised substrates for TPR[13,14]

Polycyclic aromatic hydrocarbons (PAH) are a series of ubiquitous environmental pollutants containing two or more fused benzene rings that are widely produced by the incomplete combustion of fossil fuels and other organic materials[15-17]. Due to the lack of mechanistic information concerning their formation during solid fuel conversion processes, there is a need for suitable model substrates and, in this investigation, a suite of PAH-containing resites have been prepared, with, as the second component, diphenylmethane, benzylnaphthalene, benzylanthracene, benzylphenanthrene and 2-naphthol. To illustrate the potential of the resites to study the formation of PAH in the utilisation of solid fuels, the carbonisation of the 9-(4-hydroxybenzyl) anthracene-containing resite has been investigated in a fluidised-bed reactor.

EXPERIMENTAL

Synthesis of precursors

The mono- or dihydroxydiphenylalkane and monohydroxy-phenyl PAHs used to prepare the resins were 4-hydroxy-diphenylmethane, 4,4'-dihydroxydiphenylethane, 2-naphthol, 4-naphthobenzylphenol , 9-(4-hydroxybenzyl)anthracene and 9-(4-hydroxybenzyl)phenanthrene. Of these, only 4-hydroxydiphenylmethane and 2-naphthol were commercially available.

To prepare 4,4'-dihydroxydiphenylethane, a Wolff-Kishner reduction was conducted on 4'-methoxy-2-(p-methoxyphenyl)acetophenone (deoxyanisoin) to yield 4,4'-

dimethoxydiphenylethane. This compound was then subjected to demethylation by refluxing for 20 minutes in 20 g of redistilled pyridine hydrochloride. This yielded the crude product which was recrystallised from hexane-ethylacetate to yield white shiny prismatic crystallites (M.Pt. 198-199°C).

To prepare 1-(4-hydroxybenzyl)naphthalene, naphthalene was first acylated with p-anisoylchloride to yield 1-(4-methoxybenzoyl)naphthalene. A Wolff-Kishner reduction was conducted on this compound to produce 1-(4-methoxybenzyl)naphthalene. This compound was then demethylated as described above. After cooling, the reaction product was extracted in diethylether and purified by vacuum distillation (180-182°C, 3-4 mmHg). The product was recrystallised from benzene-acetone (3:1v/v) to yield yellow shiny needle crystallites (M.Pt.166-167°C).

9-(4-hydroxybenzyl)anthracene was prepared by first reacting 9-anthracenecarboxylic acid with oxaylchloride to yield 9-anthracene carbonyl chloride. This was then acylated with anisole to produce 9-(4-methoxybenzoyl)anthracene which was then subjected to a Wolff-Kishner reduction. The resultant 9-(4-methoxybenzyl)anthracene was then demethylated as described above and the crude product was recrystallised from toluene to yield yellow shiny needle crystallites (M.Pt.187-188°C).

To prepare 9-(4-hydroxybenzyl)phenanthrene, phenanthrene was first acylated with p-anisoylchloride to yield 9-(4-methoxyben-zoyl)phenanthrene. A Wolff-Kishner reduction was conducted on this compound to yield 9-(4-methoxybenzyl) phenanthrene which was then demethylated as described earlier. The crude product was purified by vacuum distillation (200-201°C, 3-4 mmHg) and recrystallisation from hexane which yielded yellow shiny needle crystallites (M.Pt.85-86°C).

Synthesis of resins

The co-resoles were prepared using a total phenol to formaldehyde mole ratio of 1:2.5 following established procedures[18,19]. The mole ratio of phenol to the monohydroxydiphenylalkanes or monohydroxybenzyl PAHs was 3:1 to ensure that a reasonably high degree of crosslinking was achieved in the initial resoles. Sodium hydroxide was used as catalyst in the condensation reaction with mole ratio of 0.1 with respect to phenol. Phenol ,the monohydroxydiphenylalkane or mono-hydroxybenzyl PAHs and formaldehyde (37% formaldehyde) were mixed in 250 cm^3 3-neck round bottom flask and stirred until all the phenol was in solution. The mixture was then cooled in an ice-bath for about 10 minutes before sodium hydroxide (0.006mol,20 M) was added dropwise to the reaction mixture. This was then refluxed at 70°C for 30 min., acidified with 85% lactic acid to a pH of 4-5 (indicated by universal indicator paper) before excess water was removed by vacuum distillation. The thick resinous material was poured into a capped container for curing in an oven purged with nitrogen gas that was initially set at 70°C for 4 days. The oven temperature was then raised to 130 and 200°C for additional 24 hour periods. For purposes of comparison, a normal PF resite and resole were prepared by the same procedure.

Pyrolysis

An all-silica fluidised-bed reactor system (5 cm dia.), based on the design used by Tyler and coworkers[20], was used to pyrolyse a normal PF resite and the 9-(4-hydroxybenzyl)anthracene - containing resite at a temperature of 900°C in a bed containing *ca.* 100g of acid-washed sand (200-300 μ). This was fluidised using a flow of 2-3 $dm^3\ min^{-1}$ of nitrogen. Approximately 4 g of resite (75-212 μ) was fed at a constant rate from a hopper, which was also fluidised with a flow of nitrogen (1 $dm^3\ min^{-1}$), over 20-30 minute period into the fluidised-bed at 900°C. Two 500 cm^3 Dreschel bottles in series cooled with dry ice were used to trap the tars with virtually no carry over into the gas.

After the tests, the tars were recovered in toluene for analysis. The char and tar yield were calculated from the weight gains of the bed and the traps during each run with the weight gains of the traps being corrected for any water present determined via the Dean-Stark method. After the water had been removed from the toluene solutions of the tars, these were concentrated to facilitate fractionation of the tars by preparative-scale open-column alumina chromatography to provide aromatic fractions for high performance liquid chromatography (HPLC) analysis. The alkanes, aromatics and polars were eluted successively from the column containing activated alumina (500°C for 16 hr.) with n-hexane, toluene and methanol.
For HPLC separation of the aromatic fractions by ring size, an electron-deficient, nitroaromatic-bonded silica column manufactured by Shandon (Hypersil CTA) was used in conjuction with an

Applied Chromatography Systems gradient elution pump, a Waters UV detector at 254 nm and a PC-based software package for peak integration. The volumetric flowrate was set at 0.6 cm^3 min^{-1} and a standard mixture of 16 PAHs (supplied by Supelco) was used to optimise the separation achieved with n-hexane and dichloromethane (DCM) mixtures, the most satisfactory gradient elution scheme being 10 % v/v DCM in hexane for 20 min., followed by 10 to 100 % v/v DCM in 60 min. and, finally, 100 % v/v DCM.

RESULTS AND DISCUSSION

The total yields of tar and aromatics and the yield of anthracene obtained from the fluidised-bed pyrolysis experiments on the normal PF and the 9-(4-hydroxybenzyl) anthracene-containing resite are listed in Table 1, together with the HPLC-determined distribution of ring size in the aromatics. Figure 1 compares the HPLC traces for the aromatics obtained from the two resites. The high pyrolysis temperature of 900°C ensures that parent PAH dominate over the alkyl-substituted counterparts (most alkyl and parent PAH co-elute in the HPLC seperation). As expected from the volatile matter contents also shown in Table 1, a much higher tar yield has been obtained from the 9-(4-hydroxybenzyl)anthracene-containing resite. Indeed, the higher tar yield is accounted for completely by the additional aromatic material obtained (*ca.* 10% w/w resite).

As anticipated, anthracene dominates the HPLC trace of the aromatics for the 9-(4-hydroxybenzyl)anthracene-containing resite (Figure 1, phenanthrene being the major peak in the trace for the normal resite). However, the increase in anthracene yield of *ca.* 5% w/w resite only accounts for about half that in the total tar yield. Further, when this fact is taken with the estimated anthracene content of *ca.* 30% in the initial resite, strong evidence emerges for the anthracene becoming involved in many other reaction pathways other than simple homolytic cleavage of the anthracylbenzyl methane linkage. Since the total tar yield is only 34%, it can be inferred that a substantial portion of the anthracene is incorporated into the char. Further, the following HPLC results provide evidence that some of the anthracene present rearranges to form other low molecular mass PAH, particularly phenanthrene and acenaphthene, during pyrolysis.

Table 2 compares the mass ratios of phenanthrene (the major constituent in the aromatics from the normal resite, Figure 1) to a number of other PAH present. With the exception of acenaphthene, the ratios increase considerably indicating that the yields of phenanthrene and acenaphthene are both considerably greater for the 9-(4-hydroxybenzyl)anthracene-containing resite with the implication that they have been formed by rearrangement of the anthracene present. Indeed, it is estimated from the data in Table 2 that the phenanthrene yield increases from 2.2% (w/w) for the normal resite to 5.5% for the 9-(4-hydroxybenzyl)anthracene-containing resite.

The fact that the yield of aromatic material is significant from the normal PF resites provides direct evidence that phenolic moieties can transform directly into PAH during devolatilisation. The first step in this complex reaction pathway probably involves dehydration to form diphenyl ether and furan moieties, which then undergo subsequent ring growth with further dehydration. Since phenolic moieties are the major building blocks of both low-rank and high volatile bituminous coals[1], these are likely to be the prime source of PAH rather than the much smaller concentrations of large aromatic ring systems in these coals.

CONCLUSIONS

Although van Krevelen was the first to use PF resins in coal science to account for the plasticity behaviour of different coals[1], the approach adopted here for PAH represents a new direction in fuel science for investigating, in a macromolecular environment, the behaviour of the individual functional groups present during conversion processes. Non-softening PF co-resites are ideal substrates for probing the reaction pathways leading to PAH formation during devolatilisation since they facilitate the incorporation of individual PAHs into a highly cross-linked matrix. The volatile matter contents of the PAH-containing resites were higher than the corresponding normal PF resins due to the lability of the single diarylmethane linkage anchoring the PAHs into the macromolecular structure. The carbonisation of the normal PF and 9-(4-hydroxybenzyl)anthracene-containing resite in a fluidised-bed reactor served to illustrate the complexity of the reaction pathways undergone by the anthracene moiety, with evidence of rearrangement of the anthracene structure to form other PAH, primarily phenanthrene and acenaphthene.

REFERENCES

1. W. Van Krevelen, *Coal: Typology-Physics-Chemistry-Constitution,* 3rd ed., Elsevier (1993).
2. J. G. Speight, Ed., *Fuel Science & Technology Handbook,* M. Dekker, New York (1992).
3. C. E. Snape, Ed., *Geochemistry, Characterisation and Conversion of Oil Shales,* NATO ASI series Vol. C455, Kluwer (1995).
4. M. L. Poutsma, *Energy & Fuels,* **4(2)**, 113, (1990) and references therein.
5. A. C. Buchanan III and C. A. Biggs, *J. Org. Chem.* **54**, 517, (1989).
6. P. F. Britt and A. C. Buchanan III, *J. Org. Chem.* **56**, 6132, (1991).
7. S. C. Mitchell, C. J. Lafferty, R. Garcia, K. Ismail, C. E. Snape, A. C. Buchanan III, P. F. Britt and E. Klavetter, *Energy & Fuels,* **7**, 331, (1993).
8. K. Ismail, S. C. Mitchell, S. D. Brown, C. E. Snape, A. C. Buchanan III, P. F. Britt D. Franco and J. Yperman, *Energy & Fuels,* **9**, 707, (1995).
9. S. C. Mitchell, C. E. Snape and K. D. Bartle, *Fuel,* **73**,1159, (1994).
10. C. E. Snape, S. C. Mitchell, K. Ismail and R. Garcia, *Euroanalysis V111: Rewiews on Analytical Chemistry*, Royal Society Chemistry, (1994), p. 103.
11. K. Ismail, O. Sirkecioglu, J. M. Andersen, S. D. Brown, P. J. Hall, C. E. Snape and W. Steedman, *Polymer,* accepted for publication.
12. S. D. Brown, K. Ismail, C. E. Snape, A. Harding and K. M. Thomas, *Energy & Fuels,* **9**, 1104, (1995).
13. K. Ismail, G. D. Love, S. C. Mitchell, S. D. Brown and C. E. Snape, *Prepr. Am. Chem. Soc. Div. Fuel Chem.*, **39(2)**, 551, (1994).
14. K. Ismail, S. D. Brown, O. Sirkecioglu, C. E. Snape, D. V. Franco, I. I. Maes and J. Yperman, *Proc. 8th Int. Conf. Coal Science,* Vol. 1, (1995). p.351, Elsevier Science Amsterdam.
15. I. M. Smith, PAH from coal utilisation - emissions and effects, *IEA Coal Research Report No. ICTIS/TR29*, London, UK, 1984.
16. C.V. Knight, M. S. Graham and B. S. Neal, in *Polynuclear Aromatic Hydrocarbons : formation, metabolism and measurement, Seventh International Symposium on Polynuclear Aromatic Hydrocarbons,* Columbus, OH, USA, Batelle, 1983, pp 689-710.
17. A. R. Collier, M. M. Rhead, C. J. Trier, and M. A. Bell, *Fuel*, **74**, 362 (1995)
18. Y. Zaks, J. Lo, D. Raucher and E. M. Pearce, *J. Appl. Polymer Sci.*,**27**, 913, (1982).
19. H. Bar and Z. Aizenshtat, *J. Anal. Appl. Pyrolysis,* 265, (1991).
20. P. F. Nelson, I. W. Smith, R. J. Tyler and J. C. Mackie, *Energy & Fuels*, **2**, 391 (1988)
21. P.J. Hall, M.M. Antxustegi and J.M.Calo, *Proc.Carbon'94,* p.442, Granada, Spain.
22. G.E. Maciel, I.S.Chuang, and L.Gollob, *Macromolecules,***17**,1081,(1984).
23. K.Hultzsch, *Chem.Ber.*,**74**,1539,(1941).
24. A.B. Turner,*Quart.Rev.*,**18**,347, (1964).
25. A.J. Mackinnon, P.J. Hall and M.M. Antxustegi, *Fuel,***73**,113,(1994).
26. A.J. Mackinnon, P.J. Hall, C.E. Snape and P. Burchill, *Fuel,***74**,136,(1995).
27. O. Sirkecioglu, P. McQueen, W. Steedman and C. E. Snape, *Fuel*, submitted.

	Normal PF	Anthracene-containing resite
Volatile Matter (% w/w)	40	58
Tar (% w/w resin)	25	34
Aromatics (% w/w resin)	10	20
Anthracene (% w/w resin)	1.8	7.0
Anthracene (% aromatics)	18	34
2-ring (% aromatics)	25	9
3-ring (% aromatics)	64	85
4-ring (% aromatics)	9	5
5-ring (% aromatics)	2	1

Table 1 : Yields from fluidised-bed pyrolysis of resites

	Normal PF	Anthracene-containing resite
Naphthalene	6	9
Acenaphthene	4	3
Acenaphthylene	10	27
Fluorene	6	16
Anthracene	1.2	0.8
Fluoranthene	16	40
Pyrene	12	34
Benzanthracene	9	28
Chrysene	8	15

Table 2 : Mass ratios of phenanthrene to other PAH in fluidised-bed pyrolysis tars

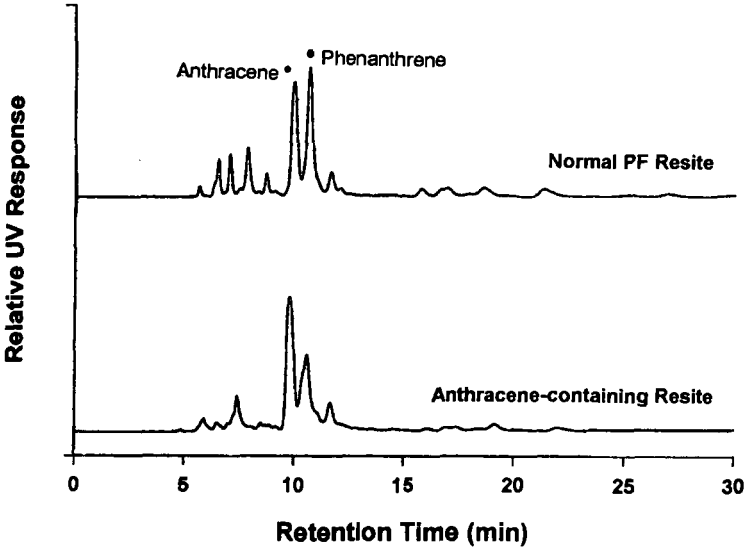

Figure 1 : HPLC traces of the aromatic fractions obtained from fluidised-bed pyrolysis of normal PF resite (top) and 9-(4-hydroxybenzyl)anthracene-containing resite (bottom)

LOCATION OF THE HYDROCARBON POTENTIAL DURING COAL PYROLYSIS: IMPLICATIONS ON THE CHEMICAL MODELLING

E. Langlois, R. Michels, M. Elie, L. Mansuy, O. Ruau and P. Landais

CNRS-CREGU, BP 23, 54501 Vandoeuvre Cedex, France.

Key words: artificial maturation, asphaltenes, resins, hydrocarbon generation.

INTRODUCTION

The modelling of hydrocarbon generation and the understanding of the compounds distributions (i.e. correlations on the basis of geochemical fingerprints) necessitate to establish genetic relationships between the kerogen and the corresponding rock extracts and oils (containing free hydrocarbons, but also the polars). These genetic relationships imply that the fate of the hydrocarbons in the organic system during maturation is known qualitatively (hydrocarbons distribution) and quantitatively (hydrocarbons potential). Hydrocarbons distributions and potential must therefore be defined for each organic fraction: the kerogen, the asphaltenes and resins as well as the free hydrocarbons. This implies a carrefull study of the composition of each fraction in regards to the degree of maturation and their respective behavior in the chemical maturation processes involved.

A precise study on the geochemical fingerprint and hydrocarbon potential of each organic fraction has been performed on an artificially matured coal. The combination of GC-MS and Py-GC-MS accompanied by semi-quantitation calculations allowed to identify the hydrocarbons distribution in each phase, to relate it to the respective hydrocarbon potential, and this for each maturation level.

EXPERIMENTAL

Sample. The sample used in this study is an immature homogeneous vitrinite-rich coal from the Mahakam delta (Indonesia) of low ash content (H/C=0.97; O/C=0.21; HI=335 mg/g) This sample has been widely studied and numerous data on both natural and artificial maturation are available[1,2].

Artificial maturation. 1 gram aliquots of the coal were loaded in gold cells (L=5cm; I.D.=1cm) under inert atmosphere. Isothermal confined pyrolysis runs were conducted at temperatures ranging from 250°C to 400°C by 10°C steps during 72h at 700bars pressure. The procedure and the pyrolysis apparatus are described elsewhere[3]. Detailed geochemical data on this series of maturation are available[2].

Collection of the different fractions. After pyrolysis, bitumen were extracted with chloroform at 60°C during 45 minutes. Asphaltenes were precipitated with 40 volumes of n-heptane at 40°C during 15 minutes. The maltene fraction, soluble in the n-heptane was fractionated into saturates, aromatics and resins using microcolumn liquid chromatography. Mass balance allowed quantitation of each fraction.

Gas Chromatography-Mass specrometry (GC-MS). Saturates and aromatics were analyzed by gas chromatography-mass spectroscopy (HP 5890 Serie II GC coupled to a HP 5971 mass spectrometer), using an on-column injector, a 60 m DB-5 J&W, 0.25 mm i.d, 0.1mn film fused silica column. The temperature program was 40 to 300°C at 3°C/min followed by an isothermal stage at 300°C for 15 min (constant helium flow of 25 cm/s)

Flash pyrolysis-Gas Chromatography-Mass Spactroscopy(Py-GC-MS). Py-GCMS of asphaltenes, resins and extracted residual kerogen were performed with a CDS 2000 pyroprobe. Samples were loaded in quartz tubes and heated at 620°C for 15s. The GCMS caracteristics and temperature program were the same as described above. Flash pyrolysis yields were estimated by mass balance.

Semi-quantitation of the Pyrograms:. The comparison of the absolute hydrocarbon potential of the asphaltenes, resins and residual kerogen in relation to the free hydrocarbons is very difficult because any quantitation technique has its limits and the actual quantitation of the source in the initial sample is impossible (it would require the quantitation of each functionnal group suspected to be the source of free hydrocarbons). However, the combinaison of the different techniques used in this work allows a relative mass balance to be calculated. The saturates potential has been assessed using a semi-quantitative approach combining Py-GC-MS yields, chromatogram integration, confined pyrolysis yields, the final value being expressed in m/g of coal before pyrolysis. This method allows a relative comparison of the saturates potential of each fraction standardized to the initial coal potential.

RESULTS AND DISCUSSION

Table 1 gives the yields of hydrocarbons, asphaltenes, resins obtained after confined pyrolysis of Mahakam coal. The maximum of resins generation is reached at 320°C, while that of the asphaltenes occurs at 330°C. The maximum of $C15^+$ saturates is reached at far higher temperature (360°C) while the $C15^+$ aromatics are released over a large range of temperatures.

As far as the $C15^+$ saturates are abundant in this sample and have a very characteristic pattern, the n-alkanes distribution will be used as tracer of hydrocarbons release in this study. Figure 1 gives an example of the m/z=57 chromatograms obtained for the free $C15^+$ saturates (GC-MS), the resins, asphaltenes and residual kerogen (Py-GC-MS) obtained after confined pyrolysis at 260 and 350°C.

At a given maturation temperature, the aliphatic chain distribution in the resins pyrograms is quite similar to the free saturates chromatograms. The same odd-alkanes predominance is characteristic. On the contrary, the aliphatic distribution is different in the asphaltenes as well as in the residual solid: the odd alkanes predominance is less pronounced, and the maximum of the distribution is shifted towards the lower molecular weigh hydrocarbons for the residual kerogen. An increased apparent maturity is therefore observed in the following order: the free saturates and resins look less mature than the asphaltenes which look less mature than the residual kerogen. These results show that although the coal has experienced the same thermal history, the compounds distribution in each organic phase does not reflect the degree of maturation in the same manner.

The flash pyrolysis yields of the Mahakam extracted residual kerogen, asphaltenes and resins have very different values and evolutions with maturation. Solid yields decrease from 40% (initial sample) to about 10% at 390°C, the main cause being the decrease of the oil potential. For asphaltenes and resins the pyrolyzate yields are

more important (about 60 and 80% respectively), and increase of about 10 to 15% with maturity, a behavior quite different from that of the resid.

Figure 2 shows the evolution of the saturates potential of each fraetion (as defined in the experimental section) as a function of maturation. At the beginning of the maturation process the kerogen, of course, contains the most important amount of aliphatic hydrocarbons. In the mean time, the generation of polars is dominant. Consequently, the saturates potential of the kerogen decreases, while that of the polars increases. The decrease of the saturates content in the kerogen cannot be totally explained by the fairly low increase of the amount of free saturates (neither by the generation of the aromatic fraction that does not contain high amounts of long-chain alkyl-aromatics). A great part of the saturates potential is therefore transfered to the polars.

After the maximum of polars generation has been reached (330°C), the saturates potential calculated for the polars and the residual kerogen is fairly similar, and both contribute to the generation of the increasing amounts of free saturates. However, a look at the n-alkanes distribution within each of these fractions shows major differences between the polars and free saturates on one side and the residual kerogen on the other. This latter is highly dominated by lighter molecular weight n-alkanes, while the others still display a strong contribution of n-paraffins with a marked CPI. This feature suggests that the polars are mainly a source of C15$^+$ n-alkanes at T>330°C, while the residual kerogen rather contributes to the generation of the C7-C14 n-alkanes. This picture is still valid at temperatures up to 360°C. From 360°C and higher, secondary cracking of the generated alkanes occurs, and the n-alkanes distribution in the various fractions is tending to homogenize (i.e. getting lighter), thus increasing the difficulty to properly identify the various sources of n-alkanes.

It has been shown earlier that the asphaltenes, resins and residual kerogen do not bear the same geochemical signature (i.e. alkanes and biomarkers distributions) at a given maturation step, the signature being the "most mature " for the solid and the "less mature" for the resins. Correlatively, their respective contribution to the generation of the free saturates, in terms of quality (hydrocarbon distribution) and timing (dominant hydrocarbon source) are different.

Thus, at the beginning of maturation (stages 250-330°C), a part of the kerogen (and its corresponding alkanes potential) is converted into the polar fraction in relation to the removal of low energy bonds (such as oxygen bonds). In a following maturation stage (330-360°C), the residual kerogen and the polars are thermally degraded and do not generate the same hydrocarbons.

CONCLUSIONS

The use of artificial maturation allows to compare the yields and composition of the free hydrocarbons, asphaltenes, resins and residual kerogen obtained from the pyrolysis of an immature coal. An integrated study of the various fractions gives interesting information concerning the evolution of the hydrocarbon potential of each phase and of the compounds distribution. The sample being characterized by a high n-paraffin content with a very typical distribution, the alkanes were used to discuss this aspect. It could be shown that:

- a great part of the hydrocarbon potential initially present in the kerogen, is progressivelly transfered into the polars (bitumen generation phase). At the mean time, low amounts of saturates are generated. Once the thermal degradation of asphaltenes and resins has been reached, both phases together with the residual kerogen contribute to the generation of free hydrocarbons.
- however, the distribution of the hydrocarbons released are different between the residual kerogen, asphaltenes, resins and free hydrocarbons. As a consequence, the relative maturity indicated by geochemical markers (biomarkers, compounds distribution) are different in each fraction.

It has been shown elsewhere[4,5,6] that the polars have a different reactivity from the residual kerogen. Especially their interaction capabilities with the surrounding medium and their interaction with water imply that they play a specific role in the maturation process. This study shows that polars have also specific structural characteristics compared to the residual kerogen. As a consequence, the hydrocarbon release depends on a great part from the chemical recativity of the polars, both quantitatively and qualitatively (the free hydrocarbons distribution mainly derives from the resins). This work suggests that the modellisation of hydrocarbons generation needs to take into account the specific behavior of the polars.

REFERENCES.

(1)Monthioux M., Landais P., Monin J. *C. Org. Geochem.*, **1985**, *8*, 275-292.
(2)Landais P. and Gérard L. *Coal geology*, **1996**, *30*, 285-301.
(3)Landais P., Michels R. and Poty B. *Journal of Anal. and Appl. Pyrolysis*, **1989**, *16*, 103-115.
(4)Mansuy L., Landais P. and Ruau O. *Energy Fuels*,**1995**, *9*, 691-703.
(5)Mansuy L. and Landais P. *Energy Fuels*, **1995**, *9*, 809-821.
(6)Michels R., Langlois E., Ruau O., Mansuy L., Elie M., and Landais P. *Energy Fuels*, **1996**, *10*, 39-48.

FIGURES AND TABLES

T(°C)	Asphaltenes	Resins	Saturates
250	1.7	3.2	0.3
260	1.9	3.1	0.4
270	2.1	4.1	0.5
280	2.0	4.1	0.4
290	2.1	5.6	0.8
300	2.7	6.4	1.0
310	3.1	8.6	1.5
320	3.8	9.0	1.8
330	4.8	8.7	2.5
340	2.2	7.3	3.1
350	1.6	6.2	4.6
360	1.0	6.2	5.8
370	1.0	3.2	3.3
380	0.6	1.9	2.5
390	0.5	1.1	1.8
400	0.3	0.8	1.0

Table 1: Asphaltenes, resins and saturates yields (in mass percent of initial coal) obtained after confined pyrolysis of Mahakam coal.

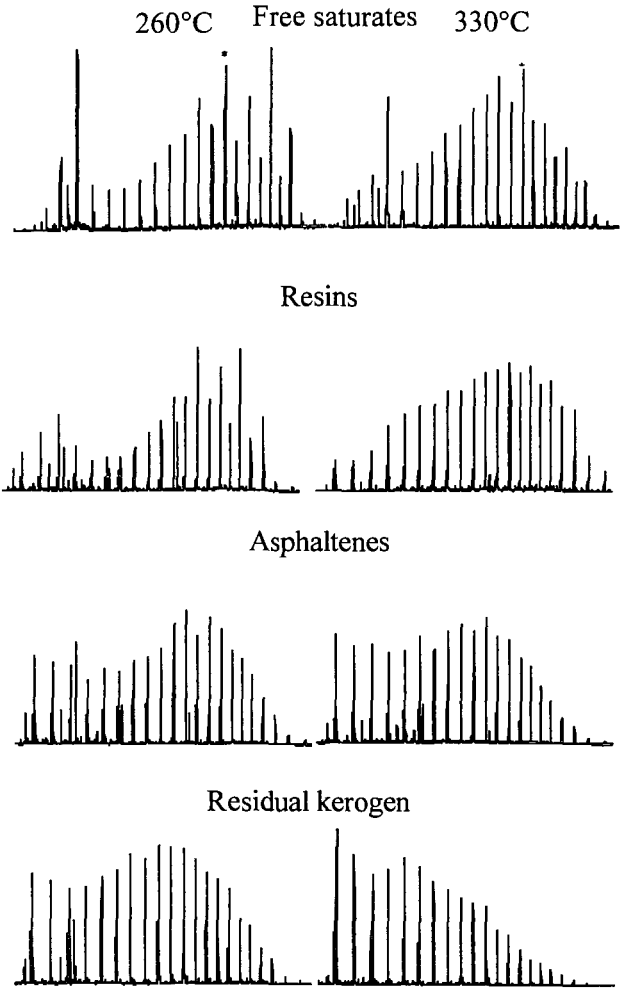

Figure 1: Comparison of the n-alkanes distributions (m/z=57; C17-C35 range, the star indicating nC27) observed in the free hydrocarbons (GC-MS) the resins, asphaltenes and residual kerogen (Py-GC-MS) generated from the Mahakam coal during confined pyrolysis at 260 and 330°C.

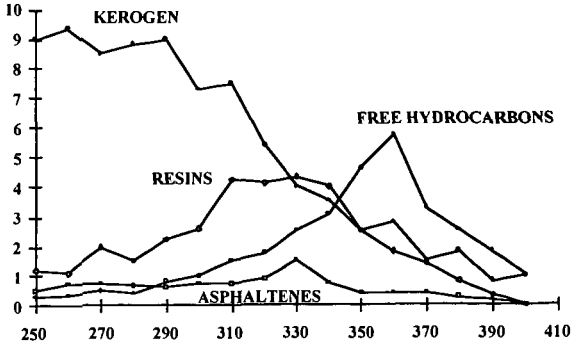

Figure 2: Evolution of n-alkanes yields (in weight percent of immature coal) obtained after semi-quatitative calculations based on Py-GC-MS yields, chromatogram integrations as well as confined pyrolysis yields of asphaltenes, resins and residual kerogen. These values represent the relative hydrocarbon potential for each phase.Are also plotted the free saturates yields obtained after confined pyrolysis (values also normalized to immature coal mass).

REACTIONS OF SOME ORGANIC CHLORINE AND SULFUR COMPOUNDS IN SUPERCRITICAL WATER

Thomas J. Houser and Xu Liu

Department of Chemistry
Western Michigan University
Kalamazoo, MI 49008-3842

Keywords: supercritical water, organic chloride and sulfur removal, reactor corrosion

INTRODUCTION

Because of the possible use of supercritical water (SW) for fuels processing and coal extraction to obtain cleaner, less polluting products, and its potential use as a medium for the efficient oxidation and destruction of environmentally hazardous materials there has been an increase in the number of reports on the basic chemistry that may be taking place in the presence of SW [1-24]. The results that are being reported are primarily concerned with the reactions of organic model compounds thought to contain functional groups representative of hazardous materials, and/or coal structures. Because of the difficulty of removing heterocyclic nitrogen, our previous experiments were initiated by extensively examining the reactivities of quinoline and isoquinoline, as well as brief examinations of the reactivities of other compounds [1]. The selection of water as the fluid was based on its physical and chemical properties [25]. Zinc chloride was chosen as a catalyst in the previous studies because of its reported catalytic activity for hydrocracking aromatic structures [26]. The current study examines the reactions of SW with 1-chloro-3-phenylpropane (CPP), 2-chlorotoluene (CT),and 4-chlorophenol (4CP). A problem that we observed in our results with SW - chlorocarbon reactions which had not been adequately addressed in previous studies [11,13] was the fate of HCl assumed to be formed. In our studies HCl was not found but significant amounts of soluble metal salts were observed. This led to the conclusions that significant corrosion of the reactor walls takes place which may also occur in the entrance lines of flow systems if reaction is initiated there, and the chemistry of the chloride - SW reaction may be affected by this wall reaction. These conclusions are consistent with the observations of previous investigators [10,24]. In addition, the HCl formed may erode oxide supported metal catalysts. Thus, experiments were conducted with Vycor ampoule inserts, the results of which are compared to those obtained from the metal reactors.

In addition, a few experiments were conducted to determine the influence of SW on the destruction of benzyl sulfide and thianaphthene.

EXPERIMENTAL

The experiments were carried out in small, cylindrical, Inconel 600, batch reactors, (10.2 cm long x 1.9 cm dia.), which were not equipped for the collection of gaseous products for analysis. The reactor was loaded with about 0.3 to 0.6g of an organic compound. The liquid reactants were introduced using about 0.5 ml. from a 1.0 ml. syringe; however since 4CP is a solid and the necks of the Vycor ampoules were too narrow for efficient solid loading, a solution of 54 wt% in toluene was used. The ampoules were constructed of standard 15mm. Vycor tubing, closed at one end and drawn to a thin capillary at the other for easy sealing once they were loaded. Their internal volumes were about 9ml. which were determined by filling with water and weighing; their external volumes were about 13ml. which were determined by water displacement. After the reactants were introduced the deionized, conductivity water was added for the SW experiments to produce the desired density or pressure at reaction temperature (the 0.255 M $NiCl_2$ and 0.050M $FeCl_2$ solutions or CaO were added as needed), then the reactor was bolted closed using a copper gasket as a seal. The reactant concentrations ranged between 1.5 and 7 mole %. For the ampoule experiments the water was added in amounts such that the internal and external densities were equal. The reactor was placed in a fluidized sand bath furnace for the required reaction time, about 5-10 minutes were required for a thermocouple embedded in the flange of the reactor to reach a temperature of 375°C. It was reasonable to assume that for those experiments with inserts the temperature rise of the reaction mixture would be more gradual due to slow heat transfer across the Vycor barrier. However, it was not possible to measure the temperatures of these mixtures. Thus, several insert experiments were run for longer reaction times than those without inserts at the same temperature setting to insure that the observed lower extents of reaction when inserts were used were not due to shorter times at the reaction temperature.

Following the reaction, the vessel was air cooled, opened, the reaction mixture or

ampoule removed, the ampoule broken open when applicable, and the water and organic layers separated. Portions of solvent, methylene chloride, were used to rinse the reactor or ampoule and extract the water layer; however some solids could not be removed from the walls of the ampoules. These portions were combined with the organic layer and additional solvent plus a known amount of an internal standard were added to a fixed volume for quantitative determinations made gas chromatographically using peak area calibrations from known solutions. The GC system consisted of a Varian model 3700 which used a 50cm x 1/8" column packed with 5% OV - 101 (liquid methyl silicone) on chromosorb G-HP (100/120) and an HP 3396 A integrator. The peak areas were normalized using a ratio of compound area to area of standard/mole. The product yields and extents of reaction were determined from calibration factors (normalized area/mole compound) obtained from known solutions. Because of the pressure buildup in the ampoules when there was significant reaction some solids and gases were lost when they were opened, liquid losses appeared negligible. The components of these solutions were identified using a Hewlett Packard Model 5890 GC with a 1.2m x 0.2mm x 0.33μm capillary column packed with HP-1 (crosslinked methyl silicone gum), and an HP Model 5970 Mass Selective Detector. There were certain limitations on the GC-MS determinations: some products are reported as an isomer of a probable structure as deduced from the molecular weight and MS fragmentation pattern. In addition, many of the higher molecular weight minor products could be measured only with a low degree of precision by GC and calibration factors were estimated.

RESULTS AND DISCUSSION

The volatile product yields are presented as moles formed/mole of reactant consumed. The terms char and tar refer to insoluble solids and non volatile liquids respectively and are reported as mass formed/mass reactant consumed. Many experiments did not produce significant amounts of char or tar.

1-Chloro-3-phenylpropane. CPP was used to represent alkyl chlorides; Table I presents the data for its reactions. The CPP was completely consumed at all conditions and the products and their yields were very similar from the SW reactions in metal and Vycor. However, some small differences were observed, the most significant of which was that the yields of the 118 molecular wt species (isomers of dihydroindene, methylstyrene, etc.) were below detection limits from the reaction in Vycor but were easily measured from the reaction in metal. The odor of HCl was not detected in the evolved gases from any of the SW- chloride experiments without inserts, but was readily noted on breaking open the ampoules. In addition, the water layer color from experiments without inserts indicated significant concentrations of metal ions. The metal ion concentrations in the water layer were determined by Inductively-Coupled Plasma (ICP) analysis, and show an amount about equivalent to the CPP loading. Thus, the reactant, or any HCl formed, reacted with the metal walls to form metal chlorides which dissolved in the water layer on cooling. An ICP analysis of the water layer from a 1-chlorohexane - SW reaction discussed previously, [16], also showed metal ion amounts equivalent to the reactant loading. The addition of CaO did reduce the HCl attack on the metal walls but did not eliminate it. ICP analysis showed only trace amounts of metal ions in the water layers from reactions when chlorine was absent.

2-Chlorotoluene. The most interesting results were obtained with CT. Table II shows that SW had a very significant effect on the rate of consumption of CT, increasing extents of reaction at 450°C from only about 10% up to 80 to 100% at the same reaction times; similar increases were observed at 500°C. Thus, the presence of SW does facilitate the removal of aromatic chlorine at a lower temperature (450°C) where less char and tar are formed and produces good yields of toluene. At 500°C more C-C bond rupture took place increasing char/tar and benzene yields at the expense of toluene. However, the results of the experiments with Vycor inserts show that these increases in extents of reaction in the SW experiments are promoted, both directly and indirectly, by the metal walls, Table III. The extents of reaction with added $NiCl_2$ and $FeCl_2$ clearly show that these have a catalytic effect on CT consumption; however, these extents are still less than those obtained directly in the metal reactor, at 450°C and shorter times, indicating that both metal salts and metal walls are catalysts. The 0.255 and 0.050 molar concentrations for the $NiCl_2$ and $FeCl_2$ respectively were chosen since they were about the values calculated from the ICP analysis of the water layer from the CPP experiment. This catalytic effect appears to be considerably reduced in the absence of SW, however it is still present in the dry reactor, as indicated by extents of reaction at 500°C without water and at 495°C with SW in Vycor. For example, if first order kinetics are assumed and that the extents of reaction with inserts represent the uncatalized reaction, a very rough calculation of the activation energy leads to a predicted value for the uncatalized extent of reaction at 500°C and 60 min of about 17%, well below that observed in the dry metal reactor.

4-Chlorophenol. A brief examination of 4 CP indicated a similar behavior to that of CT although somewhat more reactive. Again the catalytic effect of metal walls and/or salts was evident, Table IV. The extents of reaction may have been influenced by toluene used as a solvent to aid in loading the ampoules. However, if it had reacted with radicals formed from 4 CP some bibenzyl should have been formed, but none was observed. The ampoules will be modified in future experiments to allow loading of solid reactants.

Sulfur Compounds. Table V shows benzyl sulfide reacts completely at our mildest conditions with and without SW. However, the SW reaction yielded cleaner products, in the organic layer only hydrocarbon compounds were detected. Since pyrolysis formed significant amounts of thiophenes, yields of which were estimated, the complete removal of sulfur without SW would be much more difficult, as shown by the lack of reactivity of thianaphthene discussed next. The formation of these thiophenes appears to come at the expense of the benzene yield. There were several very minor products that were detected by GC-MS but could not be measured by our GC, as well as small amounts of tar were formed. Finally, there was a strong odor of H_2S from the SW reaction which was absent from the pyrolysis.

Table VI shows that SW may promote the reaction of thianaphthene somewhat and the addition of NH_3 further increases the extents of reaction. However, these reactions were still not very rapid and a more effective catalyst, $ZnCl_2$, was used again producing some improvement. The NH_3 was tried as a catalyst because it was previously found to promote the reaction between SW and benzaldehyde [14]. It should be noted that in some experiments small amounts of styrene and a C_3 benzene were detected, however, no odor of H_2S was evident. From these data it is clear that extreme conditions are needed for heterocylic sulfur to be removed.

ACKNOWLEDGEMENTS

Supported by, or in-part by, the U.S. Army Research Office.

REFERENCES

1. Houser, T.J.; Tiffany, D.M.; Li, Z.; McCarville, M.E.; Houghton, M.E., *Fuel*, vol. 65, 1986, p 827.
2. Houser, T.J.; Tsao, C.C.; Dyla, J.E.; VanAtten, M.K.; McCarville, M.E., *Fuel*, vol. 68, 1989, p 323.
3. Abraham, M.A.; Klein, M.T., *Ind. Eng. Chem. Prod.-Res. Dev.*, vol. 24, 1985, p 300.
4. Townsend, S.H.; Klein, M.T., *Fuel*, vol. 64, 1985, p 635.
5. Lawson, J.R.; Klein, M.T., *Ind. Eng. Chem. Fund.*, vol. 24, 1985, p 203.
6. Helling, R.K.; Tester, J.W., *J. Energy & Fuels*, vol. 1, 1987, p 417.
7. Helling, R.K.; Tester, J.W., *Environ. Sci. Technol.*, vol. 22, 1988, p 1319.
8. Webley, P.A.; Tester, J.W., *Fundamental Kinetics and Mechanistic Pathways for Oxidation Reactions in Supercritical Water*, SAE Technical Paper Series #881039; 18th Intersociety Conference on Environmental Systems: San Francisco, CA, 1988.
9. Webley, P.A.; Holgate, H.R.; Stevenson, D.M.; Tester, J.W., *Oxidation Kinetics of Model Compounds of Metabolic Waste in Supercritical Water*, SAE Technical Paper Series #901333; 20th Intersociety Conference on Environmental Systems: Williamsburg, VA, 1990.
10. Yang, H.H.; Eckert, C.A., *Ind. Eng. Chem. Res.*, vol. 27, 1988, p 2009.
11. Jin, L.; Shah, Y.T.; Abraham, M.A., *J. Supercritical Fluids*, vol. 3, 1990, p 233.
12. Thornton, T.D.; Savage, P.E., *J. Supercritical Fluids*, vol. 3, 1990, p 240.
13. Lee, D.S.; Gloyna, E.F.; Li, L., *J. Supercritical Fluids*, vol. 3, 1990, p 249.
14. Tsao, C-C.; Zhou, Y.; Liu, X.; Houser, T.J., *J. Supercritical Fluids*, vol. 5, 1992, p107.
15. Li, Z; Houser, T.J., *Ind. Eng. Chem. Res.*, vol. 31, 1992, p 2456.
16. Houser, T.J.; Ying, Z.; Tsao, C-C,; Liu, X.; ACS Synposium Sevies No. 514, *Supercritical Fluid Engineering Science Fundamentals and Applications*, Eds. E. Kiran and J.F. Brennecke, 1993, pp 327-337.
17. Aki, S.N.V.K.; Abraham, M.A., *J. Supercritical Fluids*, vol. 7, 1994, p 259.
18. Savage, P.E.; Li, R.; Santini Jr., J.T., *J Supercritical Fluids*, vol. 7, 1994, p 135.
19. Katritzky, A.R.; Barcock, R.A.; Balasubramanian, M.; Greenhill, J.V.; Siskin, M.; Olmstead, W.N., *J.Energy & Fuels*, vol. 8, 1994, p 487.
20. Katritzky, A.R.; Barcock, R.A.; Balasubramanian, M.; Greenhill, J.V.; Siskin, M.; Olmstead, W.N., *J.Energy & Fuels*, vol. 8, 1994, p 498.
21. Katritzky, A.R.; Shipkova, P.A.; Allin, S.M.; Barcock, R.A., *J.Energy & Fuels*, vol. 9, 1995, p 580.
22. Katritz ky, A.R.; Barcock, R.A.; Siskin, M.; Olmstead, W.N., *J.Energy & Fuels*, vol. 8, 1994, p 990.

23. Li, R.; Savage, P.E.; Szmukler, D., AIChE J., vol. 39, 1993, p 178.
24. Marrone, P.A.; Lachance, R.P.; DiNaro, J.L.; Phenix, B.D.; Meyer, J.C.; Tester, J.W.; Peters, W.A.; Swallow, K.C., ACS Synposium Series No. 608, *Innovations in Supercritical Fluids: Science and Technology*, Eds. K.W. Hutchenson and N.R. Foster, 1995, pp 197-216.
25. Frank, E.U., *Endeavor*, vol.27, 1968, p 55.
26. Salim, S.S.; Bell, A.T., *Fuel*, vol. 63, 1984, p 469.

Table I: 1-Chloro-3-phenylpropane Pyrolysis and SW Reaction Data at 400 °C [a]

Vycor Insert	No	Yes	Yes	Yes
Time (min)	60	60	120	50
Water Pressure (bar)	270	270	270	270
CaO added (g)	0	0	0	0
Volatile Product Yields (mols/mol reactant-all 100% consumed)				
Benzene	<0.01	0.026	0.017	0.021
Toluene	<0.01	0.014	0.021	<0.01
Ethyl Benzene	0.010	<0.01	<0.01	<0.01
Ethyl Toluene	0.036	0.06	0.06	0.06
Propyl Benzene	0.28	0.17	0.18	0.17
C_9H_{10}[b]	0.05	-	-	-
M.W. 196-236[c]	0.13	0.11	0.04	0.03
Tar (g/g reacted)	0.23	0.33	0.29	0.22

[a] Dashes indicate these products were not detected.
[b] Estimated yield. Several isomers of 118 M.W. were present, they could be cyclopropyl benzene, dihydroindene, methyl styrene and propenyl benzene.
[c] Estimated yields. These are principally isomers of diphenyl cyclohexane, with very small amounts of several compounds with molecular weights between diphenyl propane (196) and diphenyl cyclohexane (236).

Table II: 2-Chlorotoluene Pyrolysis and SW Reaction Data, without Vycor Inserts.

Temperature (°C)	400	400	450	450	450	450	500	500	500	500
Time (min)	60	60	30	60	30	60	30	60	30	60
Water Pres. (bar)	0	270	0	0	364	364	0	0	454	454
% Reaction	0	0	11	10	82	99	36	87	100	100
Volatile Product Yields (mols/mol reacted)[a]										
Benzene	-	-	0	<.01	<.01	<.01	0.02	0.04	0.18	0.15
Toluene	-	-	0.29	0.45	0.67	0.68	0.41	0.46	0.27	0.43
Char/Tar Yields (g/g reacted)	-	-	0.08	0.11	0.11	0.12	0.37	0.29	0.34	0.32

[a] Very small amounts of phenol, cresol and an isomer of $C_{14}H_{13}Cl$ were detected in some experiments.

Table IV: 4 -Chlorophenol - SW Reaction at 450 °C and 310 bar Water Pressure

Vycor Insert	No	Yes	Yes
Time (min)	60	75	120
% Reaction	100	30	41
Detectable Products			
Phenol (mol/mol reacted)	0.65	0.15	0.31
Tar (grams/gram reacted)	-	-	0.15

Table III: 2-Chlorotoluene - SW Reaction Data with Vycor Inserts

Temperature (°C)	425	450	450	495	450	450	450
Time (min)	60	120	365	260	95	95	155
Water Pressure: (bar)	280	320	320	280	320	320	320
% Reaction	0	0	8	46	54	28	83
Catalyst[a]	0	0	0	0	$NiCl_2$	$FeCl_2$	$NiCl_2$
Volatile Produ Yields (mols/mol reacted)							
Benzene	-	-	-	0.014	0.015	0.032	0.030
Toluene	-	-	-	0.049	0.45	0.35	0.47
$C_{14}H_{13}Cl$[b]	-	-	-	0.07	0.04	-	-
Tar[c] (g/g reacted)	-	-	-	0.14	0.27	-	0.19

[a] The concentrations of $NiCl_2$ and $FeCl_2$ were 0.255 and 0.050 molar respectively.
[b] Estimated yields; this product appears to be 2-Chlorodiphenyl methane.
[c] Chars could not be removed quantitatively from inserts, thus were not measurable.

Table V: Benzyl Sulfide Pyrolysis and SW Reactions

Temperature (°C)	400	400	400	450
Time (min)	30	30	30	60
Water Pressure (bar)	0	260	260	340
Volatile Product Yields (mols/mol reactant - all 100% reacted)				
Benzene	0.011	0.359	0.413	0.408
Toluene	0.816	0.849	0.811	0.832
$C_{13}H_{12}$ Isomer	-	0.011	-	0.006
$C_{14}H_{14}$ Isomer	-	-	-	0.011
Bibenzyl	0.154	0.031	0.041	0.052
Stilbene	0.033	0.063	0.099	0.023
Phenyl Benzothiophene	0.055	-	-	-
Tetraphenyl Thiophene	0.125	-	-	-

Table VI: Thianaphthene Pyrolysis and SW Reaction Data

Temperature (°C)	450	450	475	475	475	505	500	500	500
Time (min)	120	300	300	300	300	300	360	300	360
% Reaction	1	44	28	51	62	17	39	45	55
H_2O Pres. (bar)	370	283	365	365	269	0	335	335	335
NH_3 added	0	0	2M	6M	0	0	0	6M	6M
$ZnCl_2$ (g)	0	0.677	0	0	0.513	0	0	0	0
Volatile Product Yields (mols/mol reacted)									
Benzene	-	0.06	0.08	0.05	0.05	0.08	0.09	0.05	0.05
Toluene	-	0.18	0.20	0.21	0.12	0.02	0.20	0.19	0.22
Ethyl Benzene	-	0.18	0.19	0.38	0.23	<.01	0.09	0.20	0.26
$C_6H_4C_2HSCH_3$	-	0.03	-	-	0.01	0.03	0.02	0	0.01
$C_8H_4C_2H_4S$	-	0.05	-	-	0.03	-	-	-	-

CO-PROCESSING OF COAL AND RESID UNDER DELAYED COKING CONDITIONS

Shona C. Martin, Jasna Tomiç and Harold H. Schobert

Fuel Science Program, Department of Materials Science and Engineering
The Pennsylvania State University, University Park, PA 16802 USA

Keywords: Coal/resid co-coking, retrogressive reactions, coal characteristics

Introduction

Delayed coking is a universal conversion process which utilizes long reaction times to produce gases, distillates and coke from relatively low value feedstocks such as vacuum resid [1,2]. It does not suffer from many of the inherent disadvantages associated with direct liquefaction, i.e. high pressure operation in hydrogen atmospheres, and hence is an attractive alternative to conventional coprocessing methods. In practice [1-3], the feed is rapidly heated to *ca* 500 °C in the coke drum. The vapor products (gases, naphtha and gas oil) are stripped off and sent to a fractionator tower whilst the coke remains in the drum, reacting to produce a high quality coke. The distillates can be subsequently catalytically upgraded to produce synthetic fuels. One further advantage is that the associated condensation reactions produce a highly aromatic coke enriched in S, N and metals relative to the feed. Typical product distributions from industrial coking operations are: 10-15% gas; 50-60% liquids; 30-35% coke [1-3].

Optimum coal/resid coprocessing conditions are governed by many factors including feed characteristics and reaction conditions [4-6]. Wallace and co-workers reported an improved interaction between coal and petroleum residua with resid Car values >40% [7]. Curtis and Hwang observed a decreased oil yield and increased asphaltene, preasphaltene and residue concentrations commensurate with addition of 30 wt% coal to residuum [8].

The work presented here represents a continuation of previous studies, primarily concerned with evaluation of retrogressive studies during coal/oil coprocessing [9,10]. Rather than focussing on the relative yields of soluble and insoluble product, this present work will incoporate qualitative analysis of the liquid products.

Experimental

Samples Three petroleum vacuum residua were used in the duration of this work. Elemental and NMR analyses are presented in Table 1. The residua were used as received. Six coal samples were utilized in this study from the Penn State Coal Sample Bank and Data Base. Analyses of the relevant samples are summarized in Table 2. Samples were ground to -60 mesh and dried under vacuum at 110 °C for 2 hours prior to use.

Coprocessing The reactions were carried out in vertical 25 ml microautoclave reactors with *ca* 8g feed (resid:coal ratio of 2:1 w/w) at 450 °C for 60 and 120 min. Tests were conducted under 3.5 MPa and atmospheric N_2 environments, respectively. The gaseous products vented and the liquid and solid products recovered and separated by sequential Soxhlet extraction into *n*-hexane solubles (oils), toluene solubles (asphaltenes) and THF solubles (preasphaltenes). The THF-insoluble residue was washed with acetone followed by *n*-pentane to remove any residual THF. All recovered products were finally dried under vacuum at 110 °C for *ca* 10 hours. The conversion of coal into soluble products and gases was calculated on the basis of recovered THF-insoluble residue and reported on a dry, ash free (daf) basis. The concentration and composition of the liquid component was determined by GC/GC-MS to evaluate the contribution of the coal and resid to the overall reaction mechanism.

GC/GC-MS n-Hexane soluble products were analyzed by GC and GC-MS using a Hewlett Packard 5890 II GC coupled with an HP 5971 A mass spectrometer operating at electron impact mode (EI, 70 eV). The column was a DB-17 column; 30m x 0.25mm, coated with 50% phenyl 50% methylpolysiloxane with a film thickness of 0.25µm. A temperature program of 40 to 280 °C at heating rate of 4 °C/min and a final holding time of 15 min were used.

Results and Discussion

Figures 1 and 2 summarize the reaction conversions for the experiments conducted at 60 and 120 min, respectively, comparing the amount of THF-insolubles from coprocessing resid independently and in the presence of coal. Although the two sets of data were compiled under slightly different reaction conditions, they serve to illustrate that concentrations of THF-insoluble material are comparable for the two sets of feed.

At 450 °C, coking the coals and resid together for 60 min under 3.5 MPa N_2 was found to produce more solids than the sum expected from the independent reactions. Obviously, coal retrogressive reactions dominate at this higher temperature. However, it may also be that these resids coke more readily in the presence of coal, as suggested by the lower THFI concentrations from similar reactions with a more aromatic resid [10].

There are many possible reaction mechanisms in coprocessing, as each of the feedstocks can lead to a variety of products. Therefore, it must be stressed that the separation of coprocessing products into insoluble and soluble material does not discriminate between the amount of insoluble matter originating from the independent reactions of the coal or residuum or, indeed, any resultant interactions. The overall negative conversions measured at 450 °C (Table 3) may be a result of the coking reactions of each feedstock independently or the product of interactions between the two components.

From Table 3, it can be seen that the presence of coal in the coking medium presents no significant deterioration in product distribution, with the bituminous coals displaying similar conversion data, especially asphaltene and preasphaltene concentrations. However, as anticipated there appears to be a rank effect on the enhancement of coke formation. This is in agreement with the preliminary results presented here. An important criterion in behavior in coprocessing systems is that the interactions leading to retrogressive reactions are influenced by the thermoplastic properties of the feedstock. Indeed, retrogressive reactions only arise when both the coal and the residuum are undergoing active thermal decomposition. The bituminous coal were therefore chosen, in part, due to their fluidity profiles. The existence of a fluid-like state enhances mixing with the resid and enables hydrogen transfer reactions. This is illustrated by the improved liquid product distribution in reactions of Pittsburgh #8, Upper Banner and Illinois #6 with VR1; all have maximum fluidity in the temperature range of 410-447 °C. Conversely, Wyodak coal, a low-rank subbituminous sample, demonstrates no plastic behavior, as reflected by the smaller THF-insoluble residue concentration; subbituminous coals offer restricted mobility and contact in comparison to their higher rank counterparts, resulting in limited surface interactions with the residuum components.

As cited earlier, product quality is a factor in determining the "success" of any experiment. Preliminary analysis of the n-hexane soluble fraction (oils) has shown significant differences in composition between samples from the latter reactions. A selected chromatogram is shown in Figure 3. VR1 oils are characterized by mainly small chain paraffins and 1-2 ring hydroaromatic structures. However, upon reaction in the presence of coal (irrespective of rank) heavier hydroaromatics were identified; in each case, selected 4 ring structures such as benzo(a)pyrene were observed.

Conclusions

Microautoclave reactions conducted with a range of coals and commercial residua demonstrated that at 450 °C and reaction times of 60 and 120 min, vacuum residua coke more readily in the presence of coals. Continued characterization of both the soluble and insoluble products by standard analyses such as HPLC, NMR, FTIR, optical microscopy, will determine the contribution of the coal and resid to the overall reaction mechanism. Finally, the solvating capacity of petroleum feedstocks has been reported to be enhanced by addition of an aromatic species, such as anthracene oil [11]. Further work will therefore include reactions with ternary systems, e.g. addition of decant oil to resid/coal mixtures.

References

1. Speight, J.G. 'The Chemistry and Technology of Petroleum: Second Edition', Marcel Dekker, Inc. New York 1991
2. Gray, M.R. 'Upgrading of Petroleum residues and Heavy Oils' Marcel Dekker, Inc. New York (1994)
3. Rodriguez, J., Tierney, J.W., Wender, I. Fuel **73**, 1863 (1994)
4. Fouda, S.A., Kelly, J.F., Rahimi, P.M. Energy and Fuels **3**, 154 (1989)
5. Ceylan, K., Stock, L.M. Energy and Fuels **5**, 482 (1991)
6. Moschopedis, S.E., Hawkins, R.W., Speight, J.G. Fuel Proc. Tech. **30**, 205 (1982)
7. Wallace, S., Bartle, K.D., Burke, M.P., Egia, B., Lu, S., Taylor, N., Flynn, T., Kemp, W., Steedman, W. Fuel **68**, 961 (1989)
8. Curtis, C.W., Hwang, J. Fuel Proc. Tech. **32**, 47 (1992)
9. Tomic, J. PhD Thesis Dissertation, The Pennsylvania State University, 1993
10. Tomic, J., Schobert, H.H. Energy and Fuels 1997, in press
11. Rincorn, J.M., Ramirez, J., Cruz, S. Fuel **69**, 1052 (1990)

Table 1. Properties of Petroleum Residua.

Resid	Hydrogen Distribution				Elemental Composition (%w/w)				
	Har	Hα	Hβ	Hγ	C	H	N	S	H/C
VR1	6.44	12.58	62.88	18.11	85.9	10.82	0.43	1.53	1.51
Hondo	10.7	7.9	52.7	26.5	79.1	10.50	0.80	5.45	1.58
Blend	10.5	12.7	60.7	16.2	84.8	9.9	0.61	4.74	1.39

Table 2. Analysis of Project Coals.

		Coal					
		Upper Sunnyside	Dietz	Pittsburgh #8	Upper Banner	Illinois #6	Wyodak
	Rank	hvAb	subB	hvAb	hvAb	hvCb	subC
Proximate Analysis (wt%, as received)	Moisture	3.38	23.66	2.40	2.44	13.20	28.42
	Ash	7.54	5.35	10.0	6.2	11.62	9.90
	Volatile Matter	n/a	n/a	35.16	33.46	35.44	32.38
	Fixed Carbon	n/a	n/a	52.44	57.89	39.74	29.30
Ultimate Analysis (wt%,daf)	C	82.0	76.0	83.3	86.6	76.3	74.4
	H	5.8	5.2	5.7	5.5	5.3	5.2
	N	1.8	0.9	1.4	1.6	1.3	1.0
	S	0.8	0.5	1.3	0.6	6.4	0.9
	O	9.7	17.3	8.4	5.7	10.7	18.5

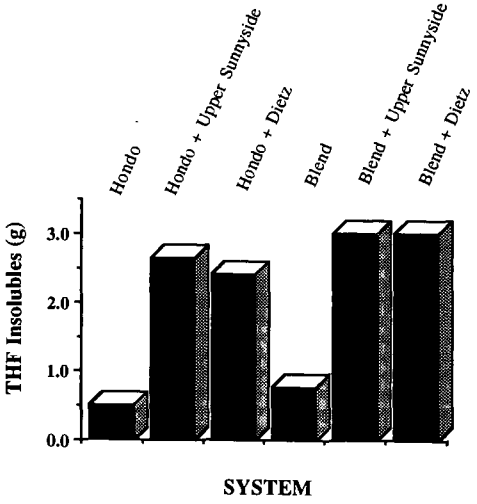

Figure 1. Comparison of THF-insoluble residue concentration from reaction conducted at 450 °C, under 3.5 Mpa N_2, 60 min.

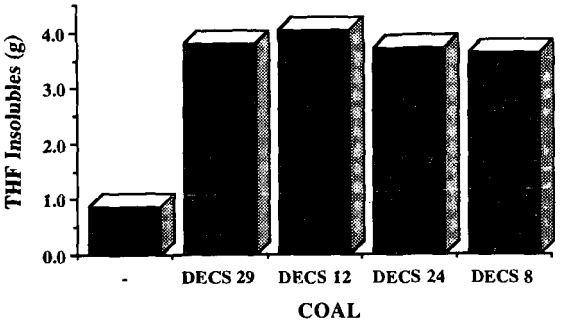

Figure 2. Comparison of THF-insoluble residue concentration from reaction conducted at 450 °C, under atmospheric N_2 environment, 120 min.

Table 3. Results of Simulated Delayed Coking of Vacuum Resid and Selected Coals at 450 °C for 2 hours, under atmospheric N_2.

Feed		Conversion	Liquid Product Distribution (wt%, daf)		
Resid	Coal	(wt%, daf)	Oils	Asph	Preasph
VR1	-	80.6	4.8	2.1	0.7
VR1	Upper Banner	-37.5	10.4	5.4	2.9
VR1	Pittsburgh #8	-39.0	6.6	5.3	2.8
VR1	Illinois #6	-36.6	11.6	4.9	2.5
VR1	Wyodak	-27.4	8.0	7.2	2.8

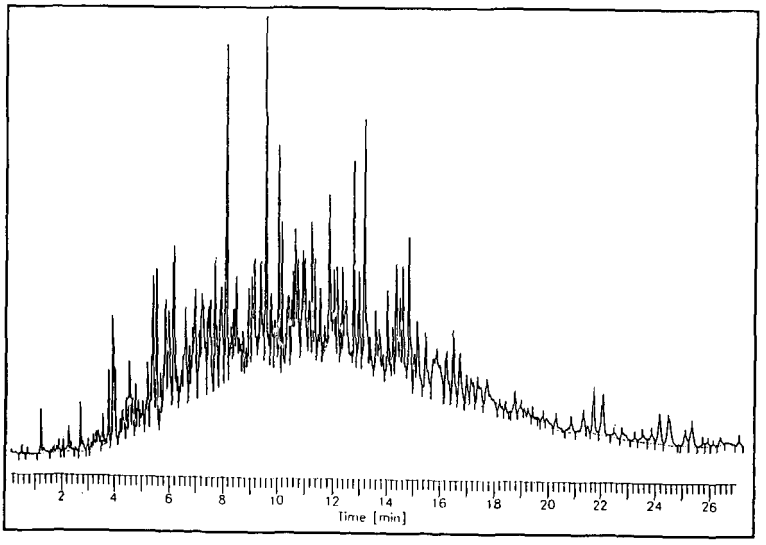

Figure 3. Chromatogram of n-Hexane Solubles from Co-coking Upper Banner with VR1, 120 min, atmospheric N_2 environment.

KINETICS OF HYDROPROCESSING OF COAL-DERIVED VACUUM RESIDS

Shaojie Wang, He Huang, Keyu Wang, M.T. Klein and W.H. Calkins*
Department of Chemical Engineering
University of Delaware
Newark, DE 19716

Key words: coal-derived resid, hydroprocessing, kinetics

Introduction

The direct liquefaction of coal produces a substantial amount of high boiling, non-distillable residuum, whose amount depends upon a number of factors such as the coal type, the hydrogen donor strength of the solvent, activity of the catalyst, and the conditions under which the direct liquefaction was run. Because of its high boiling point and potential thermal instability, this material is not suitable for processing in a conventional petroleum refinery. In a commercial liquefaction process as visualized today, therefore, this material would be recycled to the process to recover its energy value and to provide some of the solvent needed for the coal liquefaction process itself. Furthermore, this recycle oil has been shown to have a beneficial effect (i.e. increased oil yield) in the liquefaction process (1,2). Thus, it became important to determine the rates of conversion of these residual materials to products boiling in the fuel range (e.g. $< 850°F$) and to know whether these high boilers will build up or be rapidly broken down in the recycling process. It was to follow the rates of resid breakdown (resid reactivity) under conditions approximating the conditions in the liquefaction process that this program was undertaken. Knowing the rates of resid condensation as well as breakdown are also important as retrograde processes reduce product yields and foul catalysts and equipment. This required the use of a reactor system capable of measuring hydroprocessing rates at very short contact times and the development of analytical methods for measuring the conversion and boiling ranges of the products. Resid conversion rates (both condensation and breakdown) would be correlated with composition data obtained by other analytical methods (e.g. TGA, NMR, elemental analysis etc.)

Experimental Section

Apparatus. The design and operation of the Short Contact Time Batch Reactor (SCTBR) system have been described in detail elsewhere (3). In operation, both the empty 30 cm^3 reactor and the preheater and precooler are immersed in a fluidized sand bath and brought up to reaction temperature. High pressure hydrogen gas provided the driving force to deliver the reaction mixture of solvent, coal and catalyst from a blow case into the reactor at reaction temperature in of the order of 0.3 seconds, eliminating the heat up limitations in kinetic measurements. Discharging and quenching of the reaction mixture was carried out in the similar time frame. Hydrogen bubbled through the reactor from the bottom provided the necessary agitation. Temperature control was within $\pm$ 2°C. Reaction times as short as 5 seconds could be measured with considerable precision.

Materials Studied. Thirteen resid samples (boiling above 850°F) from coal liquefaction runs made at the Wilsonville pilot plant and two resid samples from Hydrocarbon Research Institute bench scale unit were prepared and supplied by CONSOL Inc. The feed coals for the resids produced at the Wilsonville pilot plant were Wyodak-Anderson, Illinois #6 and Pittsburgh coals. Selected properties, such as elemental analysis and the ^{13}C NMR patterns obtained by CONSOL Inc., of each resid are shown in Table 1.

Resid Conversion Reactions. All reactions were run as mixtures of tetralin T (the donor solvent) and resid R over a range of T/R ratios, temperatures and catalyst. For each reactor run, 5 - 10 grams of resid were used together with added tetralin to make up the desired T/R ratio. Holdup of material prevented complete recovery of the reaction products. Recoveries varied from 75 to 85 wt%, depending upon the T/R ratio used. The determination of conversion and subsequent analytical results were therefore based on representative aliquots. Molybdenum naphthenate was used as the catalyst and was sulfided *in-situ* using methyldisulfide.

Reaction Product Workup Procedure. The reaction products were worked up by separating the solids from the liquids by filtration (Figure 1). The solid filter cake was washed with methylene chloride which went into the filtrate with the product liquids. The filtrate was then distilled at low temperatures (45°C) to remove the methylene chloride. The resulting solid cake and the filtrate were analyzed separately.

Analytical Methods - Conversion. The conversion to liquid was determined using thermogravimetric analysis (TGA) on the solid cake by an ash balance calculation.

The tetralin content of the methylene chloride-free filtrate was determined by gas chromatography using an added 1-methylnaphthalene internal standard.

To determine the amount of liquid product boiling above and below 850°F (454 °C), a

boiling range method, SimDis TG, was developed based on TGA (4).

The conversion of resid to the material boiling below 850 °F was estimated by Equation 1:

$$Conversion\ (< 850\ °F) = TSF \times \left(1 - \frac{850\ °F^{+}}{RSF}\right) \qquad (1)$$

where TSF is the Tetralin Soluble Fraction of the resid (daf basis) determined by ash content in the solid resid after resid hydroprocessing; RSF is the Resid Soluble Fraction in tetralin and 850 °F^{+} is the fraction boiling above 850 °F.

Analytical Methods - Resid Characterization. The resids studied were characterized by thermogravimetric analysis at 10°C/min in nitrogen from room temperature to 600 °C. This was followed by combustion of the remaining organic material at 100 °C/min to 850 °C in air. The derivative DTG curves, Volatile Matter (VM), Fixed Carbon (FC), and ash were determined. These TGA parameters as well as the peak temperatures and peak heights from the DTG curves are also included in Table 1.

Results and Discussion

As discussed in a previous section of this paper, conversion has been determined in part by an ash balance. Efforts to carry out hydroprocessing of resids using the Ni/Mo on alumina catalyst used in Wilsonville, however, resulted in unreliable conversions data because of the large amount of ash in the catalyst. In addition, it was found that the supported catalyst changed as the hydroprocessing progressed, making the calculations of conversion unreliable. Sulfided molybdenum catalyst, on the other hand, contributed little ash (which can be corrected for) to the system and gave very reproducible results. Preliminary experiments using a range of sulfided molybdenum naphthenate catalyst concentrations from 0.9 wt% to 5.0 wt% showed that 0.9 wt% catalyst resulted in only a barely detectable increase in conversion over uncatalyzed runs. However, 3 to 5 wt% (based on the resid) gave significant conversion to lower boiling products.

After considerable experimentation to determine appropriate reaction conditions, all 15 resids were hydroprocessed for 30 minutes at 420°C in 3 to 1 tetralin to resid weight ratio and 1500 psig hydrogen with and without sulfided molybdenum naphthenate catalyst (as 3 wt% molybdenum based on the resid charged). Each resid was also run at ambient temperature for comparative purposes.

Tables 2 and 3 show the conversions to material boiling below 850°F for the thermal and catalyzed hydroprocessed resids, respectively. It is to be noted that significant conversion to lower boiling material occurs even in the absence of catalyst. However, in the presence of the molybdenum catalyst, conversion to the lower boiling material was at least doubled. To attain as much as 30 to 40% conversion requires a significant amount of catalyst.

As Tables 2 and 3 show, there is considerable variation among the resids in terms of their reactivity and convertability to lower boiling products. Plots of the thermal and catalyzed conversions of the resids vs the feed coal types are shown in Figure 2. In the thermal hydroprocessing, there appears to be a correlation with the coal type used in the liquefaction, i.e., the lower rank coal produced resid which gave higher conversion on hydroprocessing in the absence of catalyst. On the other hand, if a catalyst is used, the resids from the three coals studied showed little or no difference in conversion under the conditions used. It will be noted in Figure 3 and Tables 1, 2 and 3 that those resids having high DTG peaks and high aromatic carbon content (by ^{13}C NMR) generally show low conversions under the thermal hydroprocessing conditions while lower aromatic carbon containing resids show higher conversions in thermal hydroprocessing. Use of a strong catalyst apparently compensates in part for the high aromaticity.

SimDis TGA on the solid filter cake showed that, whereas there is considerable solubility of the resid in tetralin, up to 80 wt%, the solids themselves are not degraded to lower boiling material. Therefore, the resid must be solubilized in the recycle solvent for the resid breakdown to occur.

Summary and Conclusions

With the appropriate catalyst and conditions approximating coal liquefaction, high boiling coal-derived resids do break down to lower boiling products as they are recycled to the coal liquefaction process.

Coal-derived resids vary widely in their reactivity toward breakdown to lower boiling products under both thermal and catalytic conditions.

High catalyst activity appears to be necessary to convert these refractory materials to lower boiling materials.

Solubilization of the resid in the processing solvent is necessary for the molecular breakdown.

Acknowledgements

The support of various portions of this work by the Department of Energy and CONSOL Inc. under subcontract DE-AC22-94PC93054 is acknowledged. The guidance and assistance of Drs F.P. Burke, R.A. Winschel and S.D. Brandes in providing samples, analytical data and other assistance were also major factors in the progress of this project.

References

1. Whitehurst, D.D.; Mitchell, T.O.; Farcasiu, M. *Coal Liquefaction the Chemistry and Technology of Thermal Processes* Academic Press: New York, 1980.
2. Grint, A.; Jackson, W.R.; Larkins, F.P.; Louey, M.B.; Marshall, M.; Trewhalla, M.J.; Watkins, I.D. *Fuel* 1994, **73**, 381.
3. Huang, H.; Calkins, W.H.; and Klein, M.T. *Energy & Fuels* 1994, **8**, 1304.
4. Huang, H.; Wang, K.; Wang, S.; Klein, M.T.; and Calkins, W.H. *ACS Fuel Chem. Div. Prep.* **40**, (3) 485, 1995.

Table 1 Selected properties of the resids

Resid	Feed Coal	Number	Stream*	f_a	VM wt%	FC wt%	Ash wt%	Tpeak C	Peak Height wt%/min (daf)
Resid L	Wyodak-Anderson	4	V 1067	34.0	51.3	48.7	19.1	470.7	4.59
Resid K	Black Thunder	5	R 1235	24.6	53.6	46.4	17.2	464.8	4.60
Resid H		6	V 131B	33.3	57.1	42.9	15.2	475.3	4.67
Resid F		10	V 1067	24.3	55.2	44.8	17.5	461.5	4.36
Resid E		11	R 1235	26.0	53.4	46.6	15.6	454.4	4.24
Resid G		12	V 131B	25.9	55.7	44.3	15.9	462.2	5.02
Resid I	Illinois No. 6	7	V 1067	30.4	61.5	38.5	15.9	480.1	6.44
Resid M	Burning Star No. 2	8	R 1235	29.4	59.7	40.3	13.7	481.8	6.16
Resid D		9	V 131B	29.2	70.9	29.1	9.9	490.5	6.83
Resid J	Pittsburgh	1	V 1067	31.6	57.6	42.4	10.2	490.1	7.20
Resid B	Ireland	2	R 1235	33.3	61.1	38.9	8.7	493.6	7.43
Resid C		3	V 131B	31.5	61.0	39.0	8.5	490.2	6.23
Resid A				38.9	51.8	48.2	17.0	472.1	4.75
Resid N				20.6			0.4		
Resid O				18.8			4.1		

*
V 1067 = interstage stream
R 1235 = 2nd stage product stream
V 131B = recycle stream

Table 2 Conversion of thermal hydroprocessing of resid

Resid			Solid Residue		Liquid Residue			Conversion to 850 F-
Sample	Name	Ash	Ash	TSF	Tetralin	SRF	850 F+	
Resid A	W258V-131B	17.0	50.1	79.7	88.2	11.8	9.6	15.0
Resid B	W259R-1235	8.7	33.5	81.0	88.0	12.0	9.6	15.9
Resid C	W259V-131B	8.5	35.0	82.7	86.2	13.8	10.8	17.7
Resid D	W261V-131B	9.9	45.8	87.1	87.9	12.1	9.7	17.1
Resid E	W262R-1235	15.6	43.5	76.0	88.4	11.6	8.6	19.6
Resid F	W262V-1067	17.5	47.8	76.9	87.4	12.6	9.7	17.7
Resid G	W262V-131B	15.9	46.5	78.3	88.7	11.3	8.7	18.2
Resid H	W260V-131B	15.2	46.6	79.5	87.7	12.3	9.0	21.3
Resid I	W261V-1067	15.9	50.8	81.8	88.9	11.1	8.5	19.4
Resid J	W259V-1067	10.2	38.7	82.0	86.4	13.6	11.5	12.9
Resid K	W260R-1235	17.2	49.0	78.4	86.9	13.1	9.8	19.7
Resid L	W260V-1067	19.1	51.3	77.6	89.2	10.8	8.3	17.8
Resid M	W261R-1235	13.7	45.6	81.1	90.1	9.9	7.9	16.0
Resid N	HTI POC-01, O-43	0.4	33.0	99.2	80.6	19.4	14.1	27.0
Resid O	HTI POC-02, O-43	4.1	38.0	93.1	70.6	29.4	22.4	22.1
Thermal: 420 C; 30 min; 1500 psig H2								
Catalytic: 420 C; 30 min; 1500 psig H2; 3 wt% Mo								
Control: 25 C; 10 min; 1500 psig H2								
TSF: Tetralin Soluble Fraction of resid, wt% (daf basis)								
RSF: Resid Soluble Fraction in tetralin, wt%								
850 F+: fraction of boiling above 850 F								

Table 3 Conversion of catalytic hydroprocessing of resid

Resid			Solid Residue		Liquid Residue			Conversion
Sample	Name	Ash	Ash	SF	Tetralin	SR in Tetralin	850 F+	
Resid A	W258V-131B	17.0	51.5	80.7	82.5	17.5	9.9	35.0
Resid B	W259R-1235	8.7	40.0	85.6	79.8	20.2	11.2	38.1
Resid C	W259V-131B	8.5	41.4	86.8	81.4	18.6	11.5	33.1
Resid D	W261V-131B	9.9	54.9	91.0	77.9	22.1	14.1	32.9
Resid E	W262R-1235	15.6	44.2	76.6	80.6	19.4	11.3	32.1
Resid F	W262V-1067	17.5	49.4	78.3	79.6	20.4	10.7	37.4
Resid G	W262V-131B	15.9	48.3	79.8	79.2	20.8	11.5	35.8
Resid H	W260V-131B	15.2	50.9	82.7	75.6	24.4	11.3	44.6
Resid I	W261V-1067	15.9	56.6	85.5	76.2	23.8	11.9	42.7
Resid J	W259V-1067	10.2	43.8	85.4	76.5	23.5	11.9	42.1
Resid K	W260R-1235	17.2	52.1	80.8	78.1	21.9	12.4	35.2
Resid L	W260V-1067	19.1	53.5	79.5	79.1	20.9	11.7	35.0
Resid M	W261R-1235	13.7	53.7	86.3	80.2	19.8	11.7	35.3
Resid N	HTI POC-01, O-43	0.4	36.4	99.3	67.9	32.1	16.7	47.6
Resid O	HTI POC-02, O-43	4.1	48.3	95.4	70.2	29.8	19.1	34.3
Thermal: 420 C; 30 min; 1500 psig H2								
Catalytic: 420 C; 30 min; 1500 psig H2; 3 wt% Mo								
Control: 25 C; 10 min; 1500 psig H2								
TSF: Tetralin Soluble Fraction, wt% (daf basis)								
RSF: Resid Soluble Fraction in tetralin, wt%								
850 F+: fraction of boiling above 850 F								

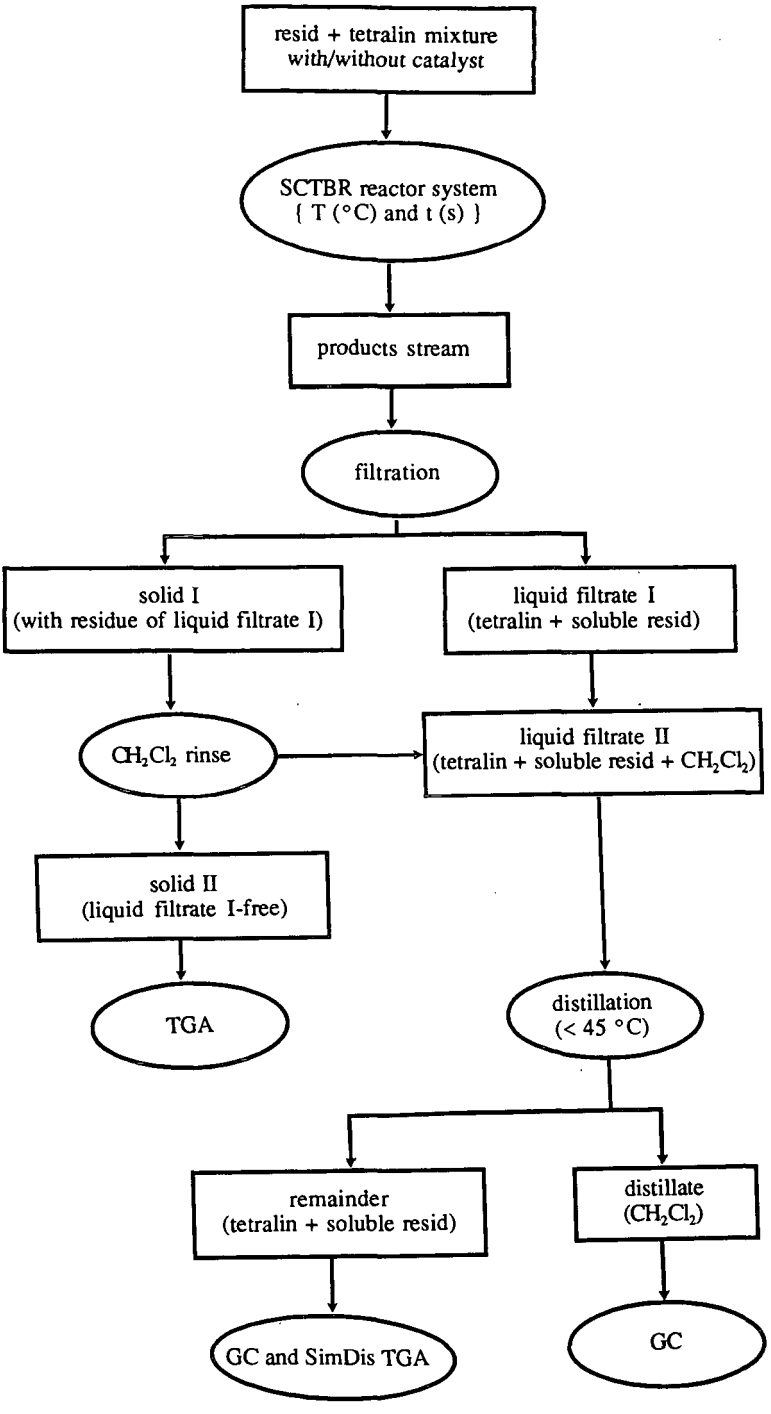

Figure 1 Scheme of the reaction product workup procedure

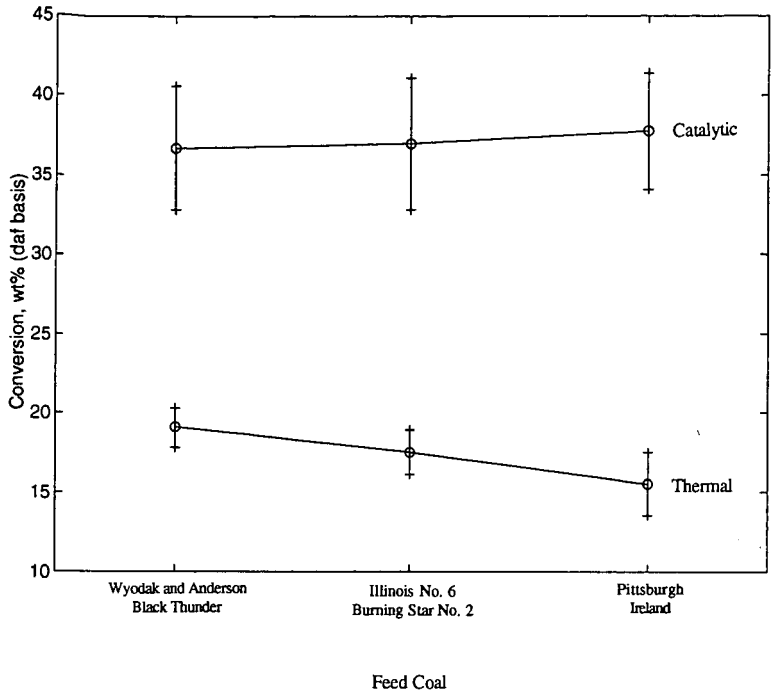

Figure 2 Thermal and catalyzed hydroprocessing conversions of the resids vs feed coal type

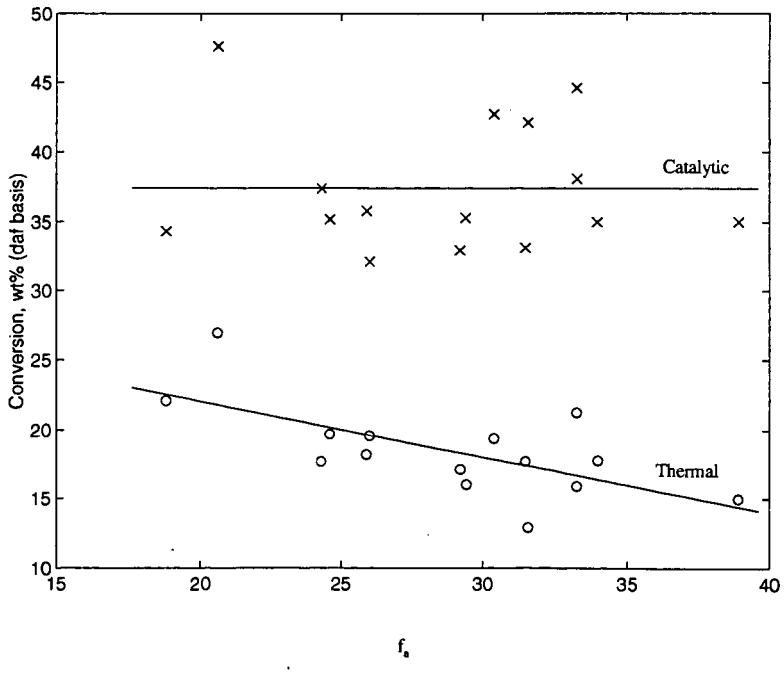

Figure 3 Thermal and catalyzed hydroprocessing conversions vs f_a of the resids

EVALUATION OF Mo CATALYST PRECURSORS FOR HYDROTREATING COAL DERIVED LIQUIDS

Richard K. Anderson, Deana R. Gibb, Geoff M. Kimber and Frank J. Derbyshire
Center for Applied Energy Research, University of Kentucky, 3572 Iron Works Pike
Lexington, KY 40511-8433

Keywords: Coal liquefaction, molybdenum catalyst, activation

INTRODUCTION

Numerous studies have examined the use of dispersed catalysts for promoting the dissolution of coal and upgrading high-boiling and residual liquids.[1] Catalysts have been added in various forms, including oil soluble organometallics and carbonyls,[2,3,4] with industrial interest for application to a spectrum of residual feedstocks,[5] and demonstration in coal liquefaction at the pilot plant scale.[6] Dispersed catalysts offer certain advantages over supported catalysts for hydroprocessing such feedstocks. Because of their large molecular size, many of the feed constituents cannot access the internal pore structure of supported catalysts, and hence upgrading must proceed by an indirect process, probably involving H-transfer via lower molecular weight species. Another major deficiency of supported catalysts is their susceptibility to deactivation by reactions which cause the deposition of carbon and metals.

Dispersed catalysts can overcome the first of these obstacles and may be less susceptible to deactivation. At the same time, there are also difficulties in the utilization of dispersed catalysts. These include: attaining and maintaining adequate dispersion; and converting the precursor to the active phase. Moreover, the effective catalyst metals, such as Mo, are expensive and their application is only economically viable if they can be used at very low concentrations or efficiently recycled. In direct coal liquefaction, the presence of mineral matter and undissolved coal in the products of coal solubilization mean that a solids separation step is necessary and, inevitably, catalyst will be removed with the reject stream. However, in upgrading solids-free coal liquids and petroleum residua, there exists the potential to recycle nearly all of the catalyst with the unconverted residue. Hence, the catalyst inventory in the reactor can be maintained at a high concentration with only a low level of fresh catalyst addition. The success of such a process depends upon the ability to maintain catalyst activity during repeated recycles, and to avoid the substantial generation of solids or refractory liquid products that have to be removed in a drag stream, together with the catalyst.

With this concept in view, we have initiated a study of the effectiveness of dispersed Mo catalysts for hydroprocessing solids-free residual coal liquids that were obtained from the former Wilsonville Advanced Coal Liquefaction Research and Development Facility, while operating with Black Thunder subbituminous coal. In this work, comparisons are made between three different Mo-containing catalysts: a ground commercial NiMo supported catalyst, and two organometallics which, being oil-soluble, are expected to facilitate dispersion in the reactor feed. A series of experiments was made to examine the influence of presulfiding conditions on catalyst activity which was assessed by the extent of resid conversion and hydrogen consumption under a standard set of reaction conditions.

EXPERIMENTAL

Materials- The following reagents were used: high purity tetrahydrofuran (THF), Burdick & Jackson Brand from Baxter S/P; ultra high purity grade H_2 and a 7.93% H_2S/H_2 gas mixture, Air Products and Chemicals, Inc. A deashed resid (DAR) derived from Black Thunder mine coal processed at Wilsonville in Run 258A[7] was provided by CONSOL, Inc. This material was used as the hydrotreating feedstock. It contained 0.13% ash, and 76% 566°C+ (1050°F+) resid (af). Three hydrotreating catalyst precursors were evaluated: Molyvan L containing 8.1% Mo, RT Vanderbilt Co.; Mo naphthenate containing 6.1% Mo, ICN Biomedicals, Inc.; and AKZO AO-60, an alumina supported Ni/Mo catalyst, Hydrocarbon Technologies, Inc. In-house determinations of the Mo and Ni content of the AO-60 were 11.3 and 2.7 wt% respectively (dried sample), compared to 12.3 and 2.6% reported by the manufacturer. Because of the small quantities of catalyst used, an equal weight of 99% anhydrous hexadecane (Aldrich) was used to dilute the organometallic precursors to improve the precision of addition to the reactor.

Liquefaction Experiments- Catalytic hydrotreating experiments were conducted in microautoclaves; the methods and microautoclaves used have been described in detail elsewhere.[8] In a typical experiment, 3 grams of DAR and the appropriate amount of catalyst precursor (to give either 1000 ppmw Mo or Mo+Ni, total DAR feed basis) are added to the reactor. The reactor is sealed, purged with hydrogen, pressurized to 10.1 MPa total pressure (2% hydrogen sulfide, balance hydrogen) and leak tested. The reactor is heated by immersing it into a hot, fluidized sandbath. Real-time measurements of both the reaction temperature and pressure are recorded with a computer. For some experiments, a pretreating period was used where the reactor was heated at a lower

temperature before going to the final reaction temperature. At the end of the reaction period, the cooled reactor is vented into a 10-liter gas collection cylinder at atmospheric pressure. The gas mixture is analyzed with a Carle Series AGC 400 Refinery Gas Chromatograph (Application 397-B). Vacuum distillations are performed on the remaining products using a modified ASTM D-1160 procedure to give a cutpoint of 566°C. Material balances are based upon a forced catalyst balance with any loss and error being assigned to the yield of distillate product.

In order to more fully characterize the reaction products, a high-temperature simulated distillation method has been developed. The SIMDIS apparatus (a Hewlett-Packard model 6890 gas chromatograph) and application software were developed by AC Analytical Controls, Inc. The method is designed to analyze hydrocarbons up to a boiling point of 750°C.

To select one of the catalysts for detailed parametric studies, a series of hydrotreating experiments was conducted at 440°C for 60 minutes. Each precursor was evaluated in a single run, in which it was used directly or was presulfided *in situ* at 375 °C for 30 minutes. A sample of the AO-60 was also sulfided *ex situ*. The presulfided AO-60, which had been delivered in its oxidic form, was prepared[8] *ex situ* by grinding the 1/16" extruded pellets, sizing to -100 mesh, air drying, and sulfiding in the microautoclave in the H_2S/H_2 gas mixture at 400°C. The dry, black powder was stored under dry N_2. Analysis of the sulfided material showed 1.9 mol S_{added} /mol of Mo, compared with the stoichiometric (including Ni) requirement of 2.3 mol S_{added}/ mol Mo. Sulfur addition rates reported in the literature typically range from 1.6 to 2.0 S/Mo, depending on pre- and post-treatment conditions.

From the test results, Molyvan L was selected for further activation studies. A parametric study was conducted in which a mixture of DAR and 1000 ppmw Mo as Molyvan L was presulfided for selected times and temperatures, followed by a hydrotreating reaction. Using 2% H_2S in hydrogen to sulfide the Mo, the influences of time (0, 5 and 30 minutes), temperature (300, 340, 375 and 440°C) and hydrotreat time (30 and 60 minutes) were examined. Estimates were also made of the activity of the dispersed catalyst after reaction, to assess its utility for recycle. Two different approaches were used to simulate recycled catalyst and resid combinations. In the first, an experiment was conducted using the DAR in reactions at 440°C for 60 minutes as the single-pass condition. Molyvan L, sufficient to give 1000 ppmw Mo, was added to only 10% of the DAR, and this mixture was reacted to simulate the first pass at an equivalent Mo concentration of 10,000 ppmw. The gases were collected, the reactor opened and the remaining 90% of the DAR was added and the second pass effected (labeled Method RM1). In a parallel study, the DAR was again reacted with Molyvan L at the 1000 ppmw Mo level in a first pass, only this time feeding 100% of the feedstock. The products were distilled to 566°C, and the residual fraction recovered. Fresh DAR and heavy distillate were then added to restore the reactor feed to 3 g for a second pass with the same 566°C+ composition as in the first pass (Method RM2). Because of losses in recovering the resid, the concentration of Mo in the second pass was 200 ppmw lower than the first pass, but the effect of conversion changes due to this lower concentration is less than can be estimated from the available data.

RESULTS AND DISCUSSION

As shown in Table 1, each of the Mo precursors improved resid conversion over that found (19%) without added catalyst, increasing conversion to 34-38%, either with or without the presulfiding procedure used. The one exception was the *in situ* presulfided AO-60 catalyst, which increased resid conversion to an average of 45%. Both organometallic precursors exhibited reasonably good activity, with resid conversion somewhat less than that found for the presulfided AO-60 catalyst, and with little apparent effect from the presulfiding step.

Based on a comparison of resid conversion and hydrogen consumption data, Molyvan L was selected for the parametric study, to evaluate the benefits of presulfiding in some detail. These results are presented in Figure 1 (30 and 60 minute conversion reactions). At lower presulfiding temperatures, it appears there is little effect of this pretreatment on catalyst activity, and it may even be adverse. The data, therefore, suggest that Molyvan L attains an active form within the first few minutes of the reaction under hydrotreating conditions. This finding is consistent with other research[9] using a dispersed Mo precursor at short reaction times. Based on these results, it was determined that presulfiding over the times and temperatures tested was not necessary to produce an active catalyst, and this step was omitted in subsequent work.

A plot of reaction time vs log (wt percent resid remaining) for three pairs of duplicate experiments is shown in Figure 2, where it is seen that the early portion of the reaction may be fairly well represented by first order kinetics with respect to the disappearance of resid. The reaction clearly slows in the 60 to 90 min period when presumably only the more refractory resid remains. The progressive reduction in rate is of interest from a presulfiding viewpoint since there is no suggestion that a more active Mo catalyst form was generated, either in combination with carbon, sulfur or other species, as the reaction steadily progressed, but lends further support to the suggestion that the active species was present fairly soon into the experiment.

Table 2 reports the results of the simulated recycle experiments with Molyvan L. Using data

from an earlier experiment with 10,000 ppmw Mo loading to calculate the total resid feed to the second pass, a second pass resid conversion of 33.7% was calculated for Method RM1. This is the same as the single pass resid conversion (33.6%) determined earlier using all fresh feedstock (ie, no recycle). However, lower conversion (24.7% vs 33.7% in RM1) was found in Method RM2, that could have reflected reduced reactivity of the recycled residual fraction, which in this experiment comprises most of the second pass reactor feed and contains the recycled catalyst. Figure 3 is a plot of the total reactor pressure for the two passes of RM2, and their nearly equal pressure histories suggest that the Mo is similarly active in both passes. A pressure profile for the same reaction without added Mo is shown for reference, where the immediate pressure reduction evident in the previous experiment is absent.

To determine the effect of fresh catalyst addition to the recycled catalyst in between the first and second pass (similar to catalyst make-up in an operating plant) 100 ppmw fresh Mo was introduced between the two reaction steps (Method RM2'). This increased the total Mo concentration from 800 to 893 ppmw. Other procedures remained the same as with the previously described experiment. Resid conversion in the second pass for this experiment was almost restored to that obtained in a single pass. Previous work has shown that resid conversion is relatively insensitive to fresh Mo concentrations above about 500 ppmw. Consequently, it may also be supposed that the freshly added catalyst is more active than the recycled Mo. The apparent reduction in recycle activity may be due to the conditions used for catalyst and resid recovery. Thus there appears to be two reasons for the reduced second pass conversion in the RM2 experiment, namely reduced resid reactivity and reduced catalyst activity. Note that for each of the recycle experiments, hydrogen consumption is reduced below that of the single pass experiment, as is hydrocarbon gas make. Relatedly, SEM/EDS studies of the hydrotreating residues at high catalyst loading showed the Mo species were well distributed across the recovered residual fractions.

CONCLUSIONS

Similar hydrotreating activity was found for the two dispersed organometallic catalyst precursors studied, and presulfiding over the times and temperatures tested was not required for high catalytic activity. Simulated recycle experiments have shown that conversion is reduced, the causes of which are attributed to reduced activity of the recycled resid and lower catalytic activity of the recycled Mo. Both of these factors could be affected by the process steps required to recover the catalyst and resid, and are the subject of continuing investigation.

ACKNOWLEDGMENTS

The authors gratefully acknowledge the support of the Department of Energy (no. DE-AC22-95PC95050), funded through a CONSOL, Inc subcontract, and the Commonwealth of Kentucky. We also thank Hydrocarbon Technologies, Inc. for providing the AKZO AO-60; the RT Vanderbilt Co. for supplying a sample of Molyvan L; Dr. Scott Carter of the CAER for his development work with the AC SIMDIS equipment; and Rebecca Cash of the CAER for her work in the laboratory.

REFERENCES

1. Derbyshire, F. J. *Catalysis in Coal Liquefaction*, IEACR/08, IEA Coal Research: London, UK, 1988, 69 pp.
2. Hawk, C. O.; Hiteshue, R. W. "Hydrogenation of Coal in the Batch Autoclave" *Bulletin 6322* US Department of the Interior, Bureau of Mines: Washington, DC, USA, 1965, 42 pp.
3. Watanabe, Y.; Yamada, O.; Fujita, K.; Takegami, Y.; Suzuki T. *Fuel* 1984, *63*, 752-755.
4. Suzuki, T.; Yamada, O.; Then, J. H.; Ando, T.; Watanabe, Y. *Proceedings 1985 International Conference on Coal Science;* Pergamon Press: New York, 1985, pp 205-8.
5. Aldridge, C.L.; Bearden, R.Jr. *Energy Progress* 1981, *1 (no.1-4)*, 44-48.
6. Southern Electric International, Inc., Technical Progress Report, "Run 262 with Black Thunder Mine Subbituminous Coal" *Document No. DOE/PC/90033-22*, September, 1992.
7. Southern Electric International, Inc., Technical Progress Report for Run 258 with Subbituminous coal, *Document No. DOE/PC/50041-130*, May, 1991, Advanced Coal Liquefaction Research and Development Facility, Wilsonville, AL.
8. CONSOL, Inc, Exploratory Research on Novel Coal Liquefaction Concept, Topical Report, *Document No. DOE/PC 95050-22,* December, 1996.
9. Huang, H.; Wang, K.; Shaojie,W.; Klein, M.T.; and Calkins, W.H. "Kinetics of Coal Liquefaction at Very Short Reaction Times" *Prepr. Pap.- Am. Chem. Soc., Div. Fuel Chem.* 1995, 40(3), pp 550-554.

Table 1. Results of hydrotreating tests of catalyst precursors in deashed resid.

Catalyst precursor	Feed	none	Molyvan L	Molyvan L	Mo naph-thenate	Mo naph-thenate	AO-60	AO-60	AO-60 sulfided ex situ
Pretreat time @ °C	-	none	none	30 @ 375	none	30 @ 375	none	30 @ 375	none
Reaction time @ °C	-	60 @ 440	60 @ 440	60 @ 440	60 @ 440	60 @ 440	60 @ 440	60 @ 440	60 @ 440
Ni, ppmw feed	-	-	-	-	-	-	173	171	175
Mo, ppmw feed	-	-	1013	988	997	1010	817	803	825
Products, wt% maf feed									
Hydrocarbon gas, C_1-C_6+	-	6.2	6.0	6.2	9.4	6.0	9.4	7.2	5.7
$CO + CO_2$	-	0.3	0.1	0.4	0.9	0.2	1.1	0.3	0.1
566°C-	24.3	32.3	43.6	45.2	42.2	45.7	41.0	51.0	47.5
566°C+	75.7	61.2	50.3	48.2	47.5	48.1	48.5	41.5	46.7
Total	100	100	100	100	100	100	100	100	100
Resid conversion, wt % 566°C+	-	19.2	33.6	36.3	37.3	36.5	36.0	45.2	38.4
H_2 consumed, mg/ g maf feed	-	7	22	18	17	16	19	18	16

Note: 10.1MPa total pressure (cold, 2% H_2S in H_2 mixture) used for all hydrotreating tests.

Table 2. Evaluation of Molyvan L activity in simulated recycle.

Method	RM1	RM2	RM2'
Rxn temp., First pass Second pass	440 440	440 440	440 440
Run time, First pass Second pass	60 60	60 60	60 60
Fresh Mo, ppm feed	-	-	100
Recycle Mo, ppm feed	1006	800	793
Products, wt% maf feed			
Hydrocarbon gas, C_1-C_6+	4.4	4.6	5.0
$CO + CO_2$	0.1	0.1	0.1
566 °C-	47.0	38.3	43.9
566 °C+	48.5	57.0	51.0
Total	100	100	100
Second-pass resid conversion, wt % 566 °C+	33.7	24.7	32.7
H_2 consumed, mg/ g maf feed	15	12	14

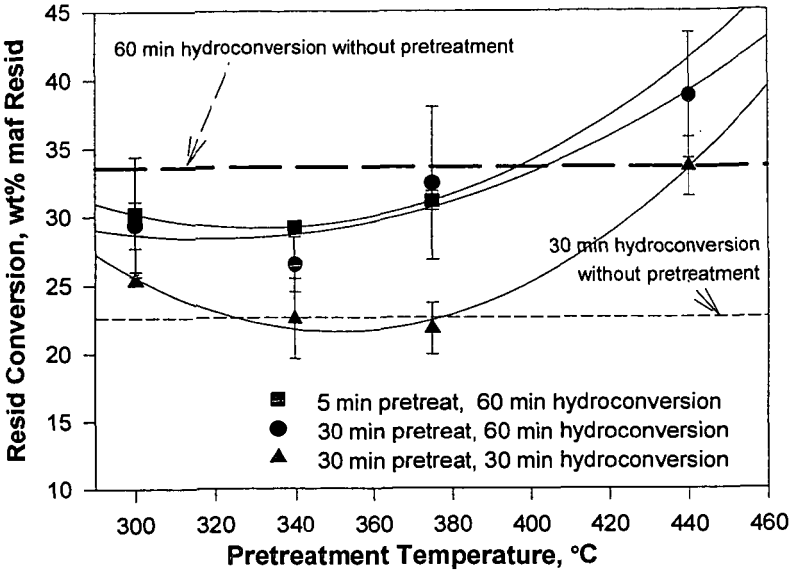

Figure 1. Effect of pretreatment time and temperature on 566°C+ resid conversion in 30 and 60 minute reactions of a deashed resid with 1000 ppmw Mo in Molyvan L, at 440°C.

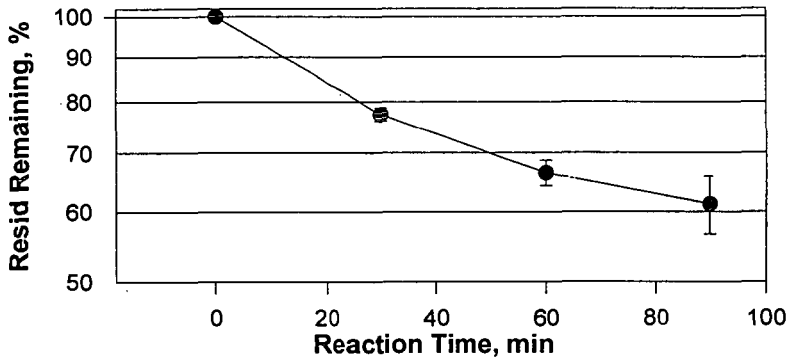

Figure 2. Disappearance of 566°C+ resid vs reaction time, hydrotreating deashed resid with 1000 ppmw Mo in Molyvan L at 440°C, without pretreatment.

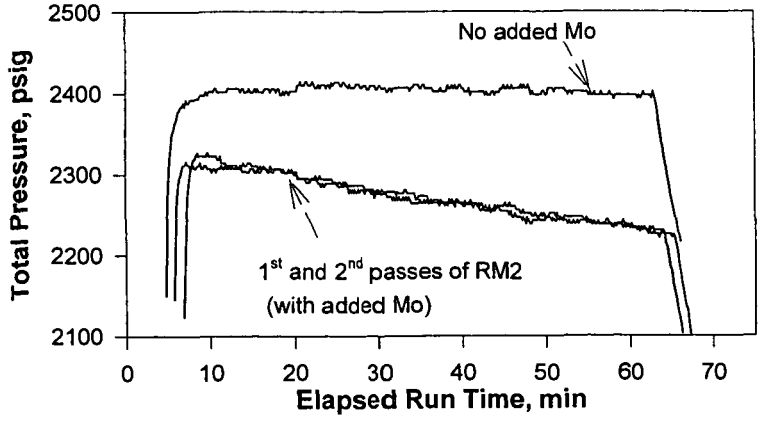

Figure 3. Impact of fresh and recycled Mo on total pressure in 60 min reactions at 440°C.

FREE RADICAL CHAIN REACTIONS OF BITUMEN RESIDUE

Carolyn M Blanchard and Murray R Gray
Department of Chemical and Materials Engineering
University of Alberta
Edmonton, AB T6G 2G6

ABSTRACT

The mechanism of residue cracking was probed by diluting Athabasca bitumen with a solvent capable of accepting free radicals: 1-methyl naphthalene. The dilute solution was cracked at 400° C and 13.8 MPa hydrogen pressure. In the presence of a free radical chain reaction, this solvent would reduce the rate of cracking and give characteristic bi-naphthyl products due to recombination of radicals. Both of these trends were verified by comparing conversion of residue and liquid phase composition to data from control experiments. We conclude that the residue fraction of bitumen cracks by the same type of mechanism as lighter hydrocarbons, i.e. chain reactions involving free radical intermediates. Similar experiments under coking conditions suggest that free radical chain reactions are also important for coke formation.

INTRODUCTION

Free radicals are formed during pyrolysis reactions due to the breakage of covalent bonds, and essentially all mechanisms for thermal cracking involve the formation and reaction of radical species. The unpaired electron in these radicals makes these highly reactive, unless the unpaired electron is stabilized, as in high viscosity pitches or in coke residues. Rice and Hertzfeld (1934) recognized that free radicals were the active intermediates in thermal cracking of n-alkanes. The main steps of the chain reaction are as follows:

Initiation:	$M \longrightarrow R_i^{\bullet} + R_j^{\bullet}$	(1)
Hydrogen Transfer:	$R_1^{\bullet} + M \longrightarrow R_1H + M^{\bullet}$	(2)
β-scission:	$M^{\bullet} \longrightarrow n\text{-}R_2^{\bullet} + \text{Olefin}$	(3)
	$R_i^{\bullet} \longrightarrow n\text{-}R_{i-2}^{\bullet} + CH_2{=}CH_2 \ (i \geq 4)$	(4)
Isomerization:	$R_p^{\bullet} \Leftrightarrow R_s^{\bullet}$	(5)
Termination:	$R_i^{\bullet} + R_j^{\bullet} \longrightarrow \text{Products}$	(6)

where M and $M^{\bullet}$ are the parent alkane and the parent radical, $R_1^{\bullet}$ and R_1H are the methyl or ethyl radical and the corresponding alkane, $R_2^{\bullet}$ is the methyl, ethyl or higher primary alkyl radical, $R_i^{\bullet}$ is the butyl or higher radical and $R_p^{\bullet}$ and $R_s^{\bullet}$ are the primary and secondary pentyl or higher radicals. The simple model of Hertzfeld and Rice (1934) has been continuously expanded to allow detailed molecular modeling of ethylene cracking furnaces (Hillewaert et al., 1988). Free radical chain reactions are also observed in a variety of alkyl-aromatic and alkyl-cycloaromatic compounds. Of the thermal reaction mechanisms reviewed by Poutsma (1990), for example, all compounds with aliphatic side chains or rings with a least two carbons followed a free radical chain reaction. The predominant mechanism for thermal cracking reactions of alkanes, alkylaromatics, cycloalkanes, ethers and thioethers is free radical chain reactions.

Application of a free radical chain mechanism to a complex hydrocarbon mixture, such as coal or bitumen, is much more difficult. The reactants and products are poorly defined, and direct observation of radical species *in situ* can be obscured by highly stabilized radicals. Mechanisms proposed for thermal cracking of these complex mixtures have normally invoked free radicals as intermediates, but the crucial role of chain reactions has often been ignored. The most common type of reaction that is amenable to manipulation is hydrogen transfer, either from a hydrogen donor species such as tetralin or from molecular hydrogen. One the earliest mechanisms suggested for the role of donor solvents in coal liquefaction was proposed by Curran et al. (1967):

Initiation:	$M \longrightarrow 2\,R^{\bullet}$	(7)
Hydrogen Transfer:	$R^{\bullet} + \text{Tetralin} \longrightarrow RH + \text{Tetralin}^{\bullet}$	(8)
Disproportionation:	$\text{Tet}^{\bullet} \longrightarrow \text{Dihydronaphthalene} + H^{\bullet}$	(9)
Hydrogen Transfer:	$H^{\bullet} + \text{Tetralin} \longrightarrow \text{Tetralin}^{\bullet} + H_2$	(10)
Termination:	$R^{\bullet} + \text{Tet}^{\bullet} \longrightarrow RH + \text{Dihydronaphthalene}$	(11)

where M is the coal extract and $R^{\bullet}$ is a general radical species. This mechanism spawned the idea of *capping of free radicals*. The role of hydrogen sources (donor solvents and molecular hydrogen) is to stabilize the reactive radical species, thereby giving stabilized molecular products.

The only cracking reaction in the sequence of reactions (7) through (11) is the initiation step. In fact, this reaction scheme lacks a propagation step that involves cracking. Each breakage of a carbon-carbon bond requires an initiation reaction.

Thermodynamics are clearly against this view of thermal reaction chemistry. Homolytic cleavage of a stable carbon-carbon bond requires an activation energy larger than the bond dissociation energy, or approximately 345.6 kJ/mole at 25°C. Actual activation energies for initiation reactions of alkanes consistent with this value, with reported values in the range 213 - 398 kJ/mol. In contrast, the propagation steps of a chain reaction face a much lower energy barrier. The β-scission reaction (equation 3) has an activation energy of 125 - 146 kJ/mol, while hydrogen abstraction has an energy of 46 - 71 kJ/mol. The chain reaction proceeds because the initial radical species turn over hundred or thousands of times to give many moles of cracked products per mole of initiation reactions. In contrast, the radical capping model has a chain length of unity. Observed rates of conversion by thermal cracking in the liquid phase are much higher than would be expected on the basis of scission of carbon-carbon bonds, i.e. initiation reactions only.

The concept of capping of radicals appears widely in the fuel science literature, to explain the reactions of coal liquids and other materials such as bitumens (for example, Sanford, 1994). The literature presents a paradox: model compounds follow free radical chain reactions as long as 2-carbon or longer aliphatic groups are present, while complex mixtures are presumed to generate radicals which are capped by donated hydrogen. Radical species are used to explain both processes, but one has a chain reaction and the other doesn't. A limited number of crossover studies have used insights into chain reaction mechanisms to explain observations of cracking kinetics (Thomas et al., 1989), or proposed new propagation steps for heavy hydrocarbons such as radical hydrogen transfer (McMillen et al., 1987).

Two barriers have likely prevented wider acceptance of the importance of chain reaction in thermal cracking of mixtures of heavy hydrocarbons. First, the chain reaction mechanisms are more complex, and lack the attractive simplicity of the radical capping mechanism. Second, the existence of chain reactions is difficult to prove in complex reaction mixtures. Compounds which are capable of trapping free radicals are routinely used in organic chemistry, however, such compounds are unstable at the temperatures of over 400°C typical of thermal cracking. The toluene carrier technique, developed by Swarcz (1949) to measure bond dissociation energies, offers one method of determining the significance of chain reactions. Homolytic scission of an alkyl-benzene is a slow step due to the high energy requirement: decomposes

$$C_6H_5CH_2R \longrightarrow R^{\bullet} + C_6H_5CH_2^{\bullet} \qquad (12)$$

In the presence of a large excess of toluene, the radicals will react with the toluene rather than abstracting hydrogen form the parent alkyl benzene. Abstraction of hydrogen from toluene generates a stabilized benzyl radical, therefore, the reaction is fast in comparison to initiation:

$$R^{\bullet} + C_6H_5CH_3 \longrightarrow RH + C_6H_5CH_2^{\bullet} \qquad (13)$$

The formation of benzyl radicals diverts the chain reaction away from the parent compound, so that β-scission is suppressed. In the very dilute case, cracking of the parent compound proceeds at the rate of the initiation reaction, thereby giving an estimate of the bond dissociation energy.

Khorasheh and Gray (1993) reacted n-hexadecane in a variety of aromatic solvents in dilute solution in the liquid phase. Formation of solvent radicals was indicated by two observations; first the rate of cracking of n-hexadecane was reduced by the addition of solvent, and second the solvent radicals reacted with each other to give dimerized products. Cracking in benzene formed biphenyl, while cracking in toluene and ethylbenzene gave alky-diphenyl methanes and diphenyl ethanes. In general, therefore, we would expect dilution in a solvent capable of forming radicals to slow the rate of cracking by diverting the chain reaction, and to form solvent dimers.

Another important free radical reaction in vacuum residues is coking, Usually attributed to some combination of condensation reactions and phase behavior, coke formation may begin with dimerization or polymerization of residue molecules. Although cracking is favored at temperatures over 400°C, addition reactions have been observed in the liquid phase at these temperatures. For example, Khorasheh and Gray (1993) observed significant formation of addition products in the cracking of n-hexadecane in the liquid phase. The toluene carrier technique would prevent the interaction of residue radicals with other species, and thereby block any dimerization reactions.

The purpose of this study was to apply the toluene carrier technique to liquid-phase thermal cracking of vacuum residues, to verify the role of free radical chain reactions in both cracking and coking reactions.

EXPERIMENTAL

The solvent 1-methylnaphthalene (1-MN) was selected as a less volatile analog to toluene to serve as a radical acceptor in the liquid phase. Like toluene, 1-MN would form relatively stable benzyl radicals upon loss of a hydrogen to a radical. Athabasca vacuum residue (424°C+) was blended with 1-MN to give a 17 weight% solution, for an approximate molar concentration of 1.2%. The solution of residue was reacted in a 500 mL batch reactor (Parr) under hydrogen at 400°C and 13.8 MPa. The solution was degassed by pressurizing with nitrogen, purging the gas, then pressurizing twice with hydrogen and purging each time. The reactor was then pressurized for a final time at a hydrogen pressure just below the amount required to achieve 13.7 MPa at reaction temperature. As the reaction temperature was approached additional hydrogen was added to the reactor to bring it to the final pressure. The reaction time was 1hr, measured from the time that the final temperature was achieved. Two control experiments were also conducted: reaction of solvent only to determine the background yield of dimer products in the absence of residue, and reaction of residue only to determine conversion in the absence of solvent. Reaction conditions were similar for coking, except that the reaction time was only 30 min, and the atmosphere was nitrogen at an initial cold pressure of 101 kPa.

The reactor products were separated first by spinning band distillation, to remove components boiling below 343°C, particularly the solvent. Several batches of material from the spinning band distillation were then combined to give enough sample for determination of the vacuum residue by ASTM D-1160 distillation. The liquid products were also analyzed by gas chromatography using a 30 m HP-1 capillary column in a Hewlett Packard 5890 GC equipped with a flame ionization detector. Individual peaks were identified by GC-MS.

RESULTS AND DISCUSSION

The conversion of the residue fraction with an without dilution in 1-MN is shown in Table 1. The mean conversion without solvent was 48.6%, but the conversion in dilute solution was much more variable, ranging from 1.5% to 41.6%. The distillation data from one batch of residue reacted in 1-MN (data not shown) were anomalous in giving half the amount of gas oil compared to the other experiments, therefore, the results were excluded. The remaining experiments with 1-MN diluent were more variable than without 1-MN, giving a mean conversion of 35.7%. In replicate experiments, therefore, the addition of 1-MN as a radical acceptor reduced the conversion of the residue fraction, consistent with a chain reaction mechanism.

Each set of five experiments with 1-MN diluent was pooled, then distilled. Spinning band distillation to remove of the large volume of solvent was followed by a single vacuum distillation to determine the amount of unconverted residue. This sample handling was the most likely source of variability. Other possible causes, such as variations in solvent purity, batch to batch variation in time-temperature history, sensitization by trace oxygen in the reactor or the catalytic effects of the reactor walls would all tend to average out from run to run due to the pooling of products from five reactor experiments.

Reaction of 1-MN without residue gave a series of dimers, illustrated in Figure 1. Structures of two of the compounds were identified by GC-MS, as compounds I and II shown below. All of the GC peaks in Figure 1 had the same molecular weight of 282.

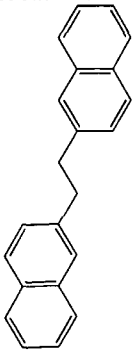

I 2,2'-(1,2-ethanediyl)bis-naphthalene

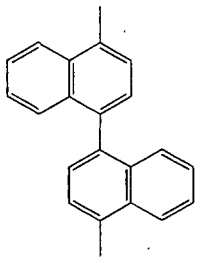

II 4,4'-dimethyl-1,1'-binaphthyl

The formation of a series of termination products, including I and II, was consistent with reaction of the various resonance forms of the methyl naphthyl radicals that would form from 1-MN.

When the solvent was reacted in the presence of residue, the total concentration of termination products increased by a factor of 5.88, taking into account the interfering signals from the cracked products of the residue (Table 2). The concentration of compound I was the largest in most samples, and its concentration was increased by a factor of 3.64 when the solvent was reacted in the presence of residue (Table 3). This increase in the concentration of products from

the solvent clearly shows that radicals were transferred from the bitumen to the solvent by hydrogen abstraction, and that the cracking of the residue sensitized the solvent for free radical reactions.

The experimental data were, therefore, consistent with both predictions of the effect of adding a free radical acceptor to the residue; reduced cracking of the residue due to the transfer of radical species to the solvent, and a concomitant increase in dimers formed from the solvent. These data can only be interpreted in light of a chain reaction mechanism for the cracking of the residue. As a non-donor compound, 1-MN should have had no effect on the rate of cracking had the radical capping mechanism been in effect.

When 1-MN was added to residue under coking conditions (i.e. a nitrogen atmosphere) the yield of coke decreased from 0.011 g coke/g feed residue to 0.022 g/g. The coke product was separated by diluting the product in methylene chloride and filtering through a 0.22 μm filter, therefore, the solids recovered would include clays and mineral solids from the feed oil. The determination was in triplicate. The concentration of termination products from the solvent in the presence of residue increased by a factor of 2.05 relative to solvent alone reacted under nitrogen. These results suggest that coking is also suppressed by addition of a radical acceptor, but further work is required at higher coke yields to verify the trend.

The main gap in the radical capping model is the lack of propagation steps that result in breakage of carbon-carbon bonds. The β-scission reaction is the most reasonable candidate in petroleum and bitumen residue materials, which contain an abundance of aliphatic carbon-carbon bonds in side chains and in bridges between aromatic clusters. A radical such as the following hypothetical structure:

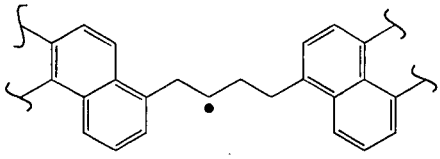

can undergo β-scission to form an olefin and benzyl-type radical. The benzyl radical would then either abstract a hydrogen from another residue molecule (eqn 2) or isomerize (eqn 5) or terminate (eqn 6). Strong aryl-alkyl C-C bonds may crack by mechanisms such as the radical hydrogen transfer (RHT) mechanism (McMillen et al., 1987), an alternate propagation step:

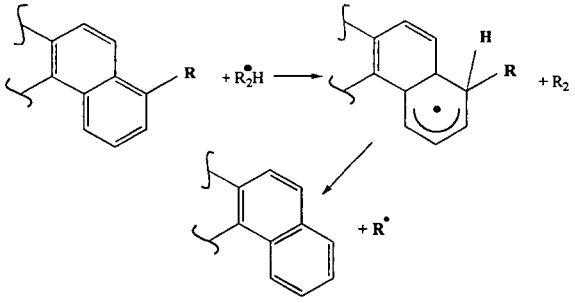

(14)

Although the RHT mechanism remains controversial, it is consistent with some important experimental observations (Savage, 1995) and it provides for continuation of a chain reaction once a radical is formed by homolytic bond cleavage.

CONCLUSIONS

1. Residue conversion was more variable when diluted with 1-MN, but always lower than without dilution.
2. Residue cracking increased the concentration of termination products from 1-MN, consistent with and increase in radical concentration.
3. Experimental data were consistent with a free radical chain mechanism

ACKNOWLEDGMENTS

The authors gratefully acknowledge financial support and technical assistance from Syncrude Canada Ltd, particularly the encouragement from Maya Veljkovic to study mechanisms.

REFERENCES

Curran, George P.; Struck, R.T.; Gorin, E. *Ind. Eng. Chem. Process Des. Dev.* **1967**, *6*, 166-173.

Khorasheh, F.; Gray, M.R. *Ind. Eng. Chem. Res.* **1993**, *32*, 1864-1876.

McMillen, D.F.; Malhotra, R.; Chang, S-J.; Ogier, W.C.; Nigenda, S.E.; Fleming, R.H. *Fuel* **1987**, *66*, 1610-1619.

Poutsma, M.L. *Energy Fuels* **1990**, *4*, 113-131.
Rice, F.O.; Herzfeld, K.F. *J. Am. Chem. Soc.* **1934**, 56(1), 284 - 289.
Sanford, E.C. *Ind. Eng. Chem. Res.* **1994**, *33*, 109-117.
Savage, P.E. *Energy Fuels* **1995**, *9*, 590-598.
Szwarc, M. *J. Chem. Phys.* **1949**, *17*, 421-435.
Thomas, M.; Fixari, B.; Le Perchec, P.; Princic, Y.; Lena, L. *Fuel* **1989**, *68*, 318-322.

Table 1. Conversion of the Residue Fraction with Hydrogen Atmosphere

Experiment Type and #	# of Reactor Expts Mixed	Conversion of Residue, %	Average
Undiluted Residue Series A	2	50.3 %	
Undiluted Residue Series B	2	48.6 %	
Undiluted Residue Series C	2	46.9 %	**48.6%**
Residue in 1-MN Series D	5	26.8 %	
Residue in 1-MN Series E	5	38.9 %	
Residue in 1-MN Series F	5	41.6 %	**35.7%**

Table 2. Ratio of Termination Products From Residue in 1-Methyl Naphthalene Experiments to Pure 1-Methyl Naphthalene Experiments

Rxn Description and Series	# of Reactor Expts Mixed	Termination Products, g/g (n=2)	Mean Concentration	Correction for Residue Contribution	Ratio of Residue in 1-MN to Pure 1-MN
Pure 1-MN (Series G)	1	0.320 E-3	0.224 E-3		
Pure 1-MN (Series H)	1	0.128 E-3	g/g 1-MN		
Residue in 1-MN (D)	5	1.23 E-3	1.63 E-3		
Residue in 1-MN (F)	5	2.03 E-3	g/g Mixture		5.88
Correction for Background signal for Residue					
Undiluted Residue (A)	2	0.461 E-3		1.32 E-3	
Undiluted Residue (C)	2	0.597 E-3	0.535 E-3	g/g 1-MN	
Undiluted Residue (5)	2	0.548 E-3	g/g Mixture		

Table 3. Ratio of Diphenyl Ethane Found in Residue in 1-Methyl Naphthalene Experiments to Pure 1-Methyl Naphthalene Experiments

Reaction Description	Series Number	# of Reactor Expts Mixed	Termination Products in Sample g/g (n=2)	Termination Products in Sample Mean	Ratio of Residue in 1-MN to Pure 1-MN
Pure 1-MN	1	1	1.33 E-4	0.902 E-4	
Pure 1-MN	4	1	0.473 E-4	g/g 1-MN	3.64
Residue in 1-MN	1	5	1.93 E-4	3.29 E-4	
Residue in 1-MN	4	5	3.52 E-4	g/g 1-MN	

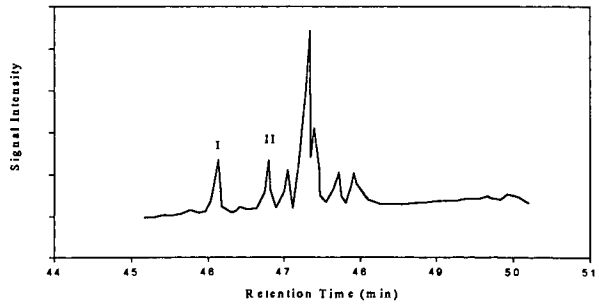

Figure 1. Chromatogram of Termination Products

HYDROGEN TRANSFER REACTIONS IN COAL/TYRE LIQUEFACTION : QUANTIFICATION OF H-DONOR CONTENTS.

Graham Harrison and Andrew B. Ross,
School of Sciences (Chemistry Division),
Staffordshire University,
College Road,
Stoke-on-Trent, ST4 2DE
England.

Keywords: coal liquefaction, H-donor, tyre pyrolysis oils

Introduction

The traditional view of the mechanism of coal liquefaction of thermal cleavage followed by radical stabilisation by hydrogen transfer explained why solvents with a good hydrogen donor potential were the best solvents for coal liquefaction. The excellent work by McMillen et al [1] effectively challenged this traditional view and showed that the solvent could be even more reactive and could initiate bond cleavage. The actual situation is probably a combination of the two, with the weaker linkages between polyaromatic centres undergoing thermal cleavage followed by radical stabilisation and the stronger linkages undergoing solvent initiated cleavage followed by radical stabilisation. For the weaker bonds, the rate determining step would be radical stabilisation whereas solvent initiated cleavage would be rate determining for stronger bonds.

As shown by the research of McMillen et al, certain hydroaromatic molecules are more effective than others at intiating cleavage. Bate and Harrison [2] emphasised this point by showing that symmetrical octahydrophenanthrene was much more effective than its antisymmetric isomer at inducing bond cleavage. Thus ideally it would be useful to have not only a measure of the total H-donor content, but also an indication of the relative amounts of individual donors. Unfortunately, the complex composition of a liquefaction process solvent (LPS) makes identification and hence quantification of individual donors difficult if not impossible even by gc-ms so that only measurements of total H-donor contents are usually carried out.

Various methods have been developed to quantify H-donor contents. Our research has made extensive use of sulphur as a H-acceptor, following an approach developed originally by Aiura et a [3] and modified later by Bate and Harrison [4]. This method has produced results which agree well with other methods, both for model compounds and LPS's. When other materials are introduced into the liquefaction mixture, measurement of H-donor contents becomes more difficult, especially when an highly aromatic material such as tyre pyrolysis oil (TPO) is introduced. This paper examines the sulphur test approach using various substituted aromatic compounds and relates the results to measurements of H-donor contents of TPO and TPO/LPS mixtures.

Experimental

Materials
A bulk sample of TPO was provided by Bevan Recycling and a sample of hydrogenated anthracene oil (HAO) was provided by British Coal Corporation, who also supplied a sample of Point of Ayr (POA) coal and the sulphided NiMo catalyst used for hydrogenation experiments. POA coal had the following analysis : moisture 3.8, ash 14.6, volatile matter 30.9 wt% as received basis; C 68.4, H 4.7, O 8.4, N 1.34 wt% dmmf; S 2.59 wt% dry basis

Coal dissolution
Coal, TPO (or hydrogenated TPO, HTPO) and HAO were reacted in spinning/falling basket autoclaves at 400°C for 1 h. After the autoclave had cooled, the contents were removed and filtered under vacuum through glass fibre filter paper. The dichloromethane -insoluble residue was Soxhlet extracted with THF. The solid residue was dried to constant weight and its ash content was determined to calculate percentage dissolution by ash balance.

Solvent hydrogenation
Samples (150g) of TPO were hydrogenated at 420°C for various lengths of time at an initial H_2 overpressure at temperature of 170 bar, using sulphided NiMo catalyst (5g) in the spinning/falling basket autoclave. The catalyst basket was retained above the liquid charge until the temperature reached 370°C when it was released to stir in the charge at 500 rpm. After the autoclave had cooled, the liquid contents were removed by suction and stored in sealed glass jars.

H-donor tests
Weighed amounts of sulphur and test material (approximately 0.5g each giving an excess of sulphur) were introduced into a bomb type autoclave. The bomb was connected to a pressure transducer and placed in its electrical heater. The bomb was heated to its set temperature and its pressure reading noted. For the model compound test materials, the contents of the bomb were dissolved in dichloromethane and most of the excess sulphur was removed by evaporating the

dichloromethane and extracting with diethylether. The diethylether extract was analysed by gc-ms using a VG-TRIO-1 bench top quadruple mass spectrometer with a direct capillary interface (DB17 column) from a Carlo Erba HRGC 5160 chromatograph.

Results and Discussion

Figure 1 shows a plot of relative dissolution of POA coal in various HTPO samples against the relative H-donor content of the HTPO sample. The base line represents the situation if dissolution was not being enhanced by using HTPO rather than HAO. As expected the percentage dissolution increased with increasing H-donor content, but unexpectedly dissolution was enhanced. Figure 2 shows the influence of adding various amounts of TPO or HTPO to HAO in solvent augmented coal dissolution. The H-donor content of the HTPO sample was 85% of that of HAO and the TPO sample, 23% of HAO. On addition of TPO, dissolution was reduced but not as much as might be expected by the reduction in the H-donor content alone. This point was emphasised by the increase in dissolution when HTPO was added. This apparent improvement in coal dissolution ability can be either related to compounds in the HTPO/TPO samples having a better potential to initiate bond cleavage in POA coal than the compounds in HAO, or to the sulphur procedure underestimating the H-donor content.

Analysis of TPO samples has shown that they contain a considerable content of alkyl-subtituted aromatic compounds (much more than is present in HAO), and only a very low content of hydroaromatic compounds. [5] Consequently the sulphur test procedure was carried out with a series of alkyl-substituted aromatic compounds to assess their influence. Table 1 shows the results relative to a base sample of hydrogenated phenanthrene (HP) at three temperatures. The TPO sample tested had been pre-distilled to remove material boiling below 275°C. Obviously a pressure increase would result from the vapour pressure of the model compound, all of which would boil below 275°C at atmospheric pressure. As an approximation, the values for toluene could be subtracted from the other values (not TPO or HP) to indicate potential of reaction with sulphur. Certain trends can be derived from the results :- (i) the number of aromatic rings - the free radicals generated by hydrogen abstraction by sulphenyl radicals will be stabilised more effectively as the number of aromatic rings increases (a fact that is important in the relative effectiveness of H-donors to initiate bond cleavage); (ii) the degree of substitution - this dependency is not as great as the previous one and probably relates to the likelihood of occurrence of cylclisation reactions; and (iii) the position of substitution - certainly 2-methylnaphthalene reacted more than 1-methylnaphthalene and para xylene did not show the same reactivity as ortho and meta xylene, probably again as a result of the likelihood of cyclisation reactions. In addition, the high reactivity of TPO should be noted.

The reactions of a wide range of hydroaromatic compounds have been reviewed.[6] The reactions were initiated by abstraction of hydrogen from a benzylic position to produce a hydroarene radical. Combination of a sulphenyl radical with the hydroarene radical produced sulphur adducts which may react to relase H_2S and form the dehydrogenated hydroaromatic. The review also suggested that toluene could dimerise to stilbene and 1, 1'-dimethy biphenyl could cyclise to phenanthrene, each resulting in the production of H_2S. Analysis of the reaction products confirmed these earlier observation, e.g. small amounts of stilbene together with bibenzyl were identified in the toluene reaction. The ge-ms also confirmed that cyclisation reactions had occured, producing benzothiophenes, benzodithiopheres, dithiols and phyenyl thiophenes. The production of such sulphur heterocycles may have a bearing on the direct inclusion of tyre pieces into coal liquefaction. Sulphur is included in tyre formulations and breakdown of the tyre radicals could produce sulphenyl radicals which could abstract hydrogen causing retrograde reactions and depletion of valuable H-donors.

The outcome of these results is that the sulphur test would over rather than underestimate the H-donor contents. Therefore, the presence of alkyl substitution in LPS's could be advantageous. Hydropyrenes are more effective than hydrophenanthrenes at initiating bond cleavage for model compounds, reducing the activation energy for the cleavage of the ether bond in diarylethers by about 50 kJ mol^{-1} and the alkyl link in diarylmethanes by at least 50kJ mol^{-1}.[7] However large amounts of hydropyrenes were not found in HTPO's which tended to contain more hydroderivatives of alkyl-substituted phenanthrene. Thus addition of HTPO to liquefaction, either by addition after the coal dissolution stage as TPO or by separate hydrogenation and addition at the dissolution stage could be beneficial; but the addition of tyre pieces could have both negative (production of sulphur heterocycles) and positive (improved solvent properties) effects.

Acknowledgements

The authors acknowledge the European Coal and Steel Community for the financial support under contract 7220-EC866. Gratitude is also expressed to British Coal Corporation and Bevan Recying for the supply of materials

References

1. McMillen, D.F., Malhotra, R., Chang, S.J., Ogier, W.C., Nigenda, S.E. and Flemming, R.H. Fuel, **66**, 1613 (1987)
2. Bate, K and Harrison, G. Fuel, **71**, 289 (1992)
3. Aiura, M., Masunaga, T., Moriya, K. and Kageyama, Y. Fuel **63**, 1138 (1984)
4. Bate, K. and Harrison, G. Am. Chem.Soc, Div, Fuel Prepr. **34**, 839 (1989)
5. Harrison, G. and Ross, A.B. Fuel **75**, 1009 (1996)
6. Fu, P.P. and Harvey, R.G. Chemical Reviews, **78**, 317 (1978)
7. Sage, A.B. PhD Thesis, Staffordshire University, July 1996.

Table 1. Pressure readings per unit mass relative to hydrogenated phenanthrene (HP) for H-donor test using sulphur. n/v - no value.

Sample	Relative reading at temperature		
	230°C	275°C	300°C
toluene	0.24	0.24	0.28
ethyl benzene	0.28	0.78	0.79
o-xylene	0.26	0.32	0.46
m-xylene	0.26	0.32	0.44
p-xylene	0.26	0.29	0.29
l-methylnaphthalene	0.16	0.46	0.79
2-methylnaphthalene	0.18	0.74	0.90
dimethylnaphthalene	n/v	0.87	0.95
TPO	0.69	0.74	0.71
HP	1.0	1.0	1.0

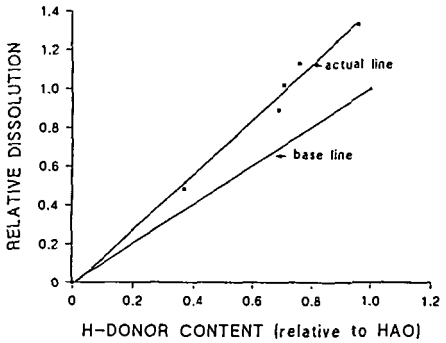

Figure 1 Graph of dissolution vs. H-donor content relative to HAO - base line shows situation for no enhancement

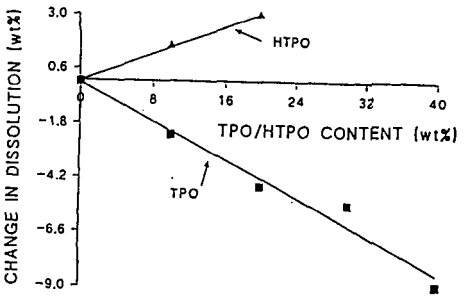

Figure 2 Graph of change in dissolution relative to HAO vs. amount of augmenting solvent

CORRELATION OF CHEMICAL COMPOSITION OF EXTRA HEAVY OILS WITH INCIPIENT COKE FORMATION USING HOT-STAGE MICROSCOPY

P.M. Rahimi[1], T. Gentzis[2], K. Chung[3], V. Nowlan[3] and A. DelBianco[4]

[1] National Centre for Upgrading Technology, One Oil Patch Drive, Devon, Alberta, Canada T0C 1E0
[2] Alberta Research Council, P.O. Box 8330, Edmonton, Alberta, Canada T6H 5X2
[3] Syncrude Research, 9421 17th Ave, Edmonton, Alberta, Canada T6N 1H4
[4] Enitricerche SpA, San Donato Milanese, Italy

Keywords: Chemical composition, hot-stage, mesophase

INTRODUCTION

Upgrading bitumen to more valuable products involves a host of chemical reactions. The conversion of relatively low-value bitumen to high-value transportation fuels is usually limited due to coke formation. Bannayan et al. (1) discussed possible mechanisms for deposit formation in the reactor recycle cup and vacuum tower of a commercial unit. These authors proposed asphaltenes to be the cause of vacuum tower fouling in the H-oil unit.

In this study we investigated the coking propensities of extra heavy oil fractions from Athabasca bitumen vacuum bottoms. Athabasca bitumen vacuum bottoms (+524°C) was fractionated into10 sub-fractions using pentane as super-critical solvent. The super-critical fluid extraction technique allowed the pitch (+524°C) to be extracted into narrow boiling point cuts with different chemical compositions. The development of mesophase was followed using hot-stage microscopy. The coking tendencies (the onset of mesophase formation) of these extra heavy oil fractions are correlated with their chemical compositions. The data from the hot-stage microscopy are also compared with the results obtained from autoclave studies of these fractions. The advantages and limitations of hot-stage microscopy for studying the hydrocracking behavior of heavy oils are discussed.

EXPERIMENTAL

Super-critical fluid extraction (SCFE) of Athabasca bitumen vacuum bottoms (+524°C) into 10 fractions was performed at the State Key Laboratory of Heavy Oil Processing (SKLHOP) of the Petroleum University at Beijing, China. The details regarding the preparation of narrow fractions of petroleum residue using SCFE have been described elsewhere (2). Hot-stage microscopy was carried out on all 10 fractions. In this paper, we report hot-stage and autoclave experiments on selected fractions whose properties are shown in Table 1. The details regarding development of the technique have been described elsewhere (3). The system was pressurized with H_2 (750 psi) and the flow of the gas was maintained at 35 mL/min during the experiments. The most critical factors in mesophase formation are temperature, residence time, heating rate, gas flow rate, and stirring rate (4). In this study, the feedstocks were heated from room temperature to 440°C at 11°C/min. The amount of material used varied between 5 and 12 mg depending on the nature of the fractions (liquid or powder form). Once at 440°C, the experiment was continued for about 3 h. Due to limitations of the experimental setup the samples were not subjected to stirring. The cooling effect of the flowing gas made it necessary to adjust the furnace temperature upward by approximately 50°C to maintain the appropriate sample temperature. This was confirmed by determining the melting points of K_2CrO_7 and Zn. The process was recorded by a video cassette recorder (VCR) for further observations. Mesophase diameter and growth with time were measured periodically using a micro scaler device. Photomicrographs were taken in polarized light under cross polars to show the optical texture of mesospheres and isochromatic regions. Combined magnification was 200X.

In order to compare the coking propensity of the heavy oil fractions obtained from hot-stage microscopy to those obtained from the autoclave, a series of experiments were carried out using fractions 1, 2B, 4, 7, and 9. Hydrocracking experiments were performed at 440°C, 2000 psi H_2 (13.9 MPa) for 30 min using a microautoclave. Hydrogen flow rate was constant at 3 L/min for all the experiments. Autoclave results are shown in Table 2.

Hydrocarbon-type analyses of maltene fractions from the selected samples were carried out before and after autoclave experiments to determine the reaction chemistry at the hydrocracking conditions. These results are shown in Table 3. The detailed experimental setup and hydrocarbon-type analyses were reported earlier (5).

RESULTS AND DISCUSSION

Autoclave results

The results are shown in Table 2. Fractions 1, 2B, 4, and 7 contain no asphaltenes. However, the amount of polar materials in these fractions increased from 9.25 wt % in fraction 1 to 22.61 wt % in fraction 7 (Table 3). Although only a negligible amount of coke (methylene chloride insolubles) was formed from fraction 1 (0.03 wt %), coke formation from fraction 7 was significantly higher (1.4 wt %). Asphaltenes were also produced in all fractions ranging from 2.67 wt % in fraction 1 to 28.38 wt % in fraction 7. Thermal reaction of fraction 9 produced a relatively large amount of coke as well as 45.94 wt % pentane-soluble maltenes. The data indicate that fractions having higher molecular weight, MCR, and aromaticity are more prone to coke formation. These results also confirm the proposed reaction mechanism for coke formation as:

Maltenes --------▷ Asphaltenes ----------▷ Coke

In order to investigate the reaction chemistry in more detail, the maltene fractions in the feedstocks and the products were separated into saturates (M1), mono/diaromatics (M2), polyaromatics (M3), and polars (M4). Significant amounts of saturates were produced, in part, at the expense of polyaromatics and polars (Table 3). The results may indicate that dealkylation reactions are major reaction paths leading to products under the thermal conditions employed. Possible mechanisms for dealkylation are ipso attack by hydrogen radicals (6) and electron transfer from aromatic rings to metal porphyrins present in the tar sand fractions (7). Analysis of the reaction products under way indicates that dehydrogenation of cycloparaffins is also a major reaction leading to products having significantly higher aromaticity than the feedstocks.

Hot-stage microscopy results

When an organic material such as pitch is heated to temperatures between 350°C and 500°C, decomposition and polymerization reactions result in the formation of polycondensed aromatic hydrocarbons which eventually leads to mesophase. Upon further heating, mesophase spheres coalesce to form bulk mesophase and coke having different textures (4). Although hot-stage microscopy was carried out on all 10 SCFE fractions, in this paper we will discuss only the results obtained from fractions 1, 2B, 4, 7, and 9. Observations of hot-stage microscopy experiments are described below. The stated times are referenced to the beginning of the experiments which is taken as time zero (room temperature).

Fraction 1: Due to the high volatility of this fraction no mesophase was observed.

Fraction 2B: Tiny mesophase appeared approximately after 65 min. Mesophase diameter grew from 4 to 30 microns after 84 min (Figure 1a). The growth continued forming particles of more than 50 microns diameter after 94 min. Coalescence of mesophase accelerated and large isochromatic areas (>100 microns) showing domain anisotropy formed after 105 min (Figure 1b). Even at this time smaller mesospheres (< 10 microns) were forming in the isotropic matrix (Figure 1b). By 116 min, the entire field of view was covered by coke with domain anisotropy. Upon termination of experiment, the temperature of the cell decreased rapidly (from 440°C to 410°C in one minute). At the lower temperature it was observed that the previously isotropic areas had become anisotropic due to the reappearance of mesophase. When the residue in the cell was reheated to 440°C the anisotropic texture was converted to isotropic. This confirms the presence of a soluble and fusible mesophase in this fraction and shows that the phase change is reversible with temperature. This phenomenon was reported on hydrogenated coal tar pitch by Honda (4). Due to the high volatility of fraction 2B, the reproducibility of mesophase formation time was poor. Less volatile fractions (fractions 7 and 9) showed better reproducibility.

Fraction 4: Mesophase first appeared after 105 min. The growth of the spheres was as follows: 4 microns after 106 min, 9 microns after 116 min, and 33 microns after 127 min. Growth and coalescence of mesophase resulted in the formation of larger mesophase (>50 microns) after 136 min (Figure 1c). After 166 min the mesophase particles had formed a "donut-shaped" structure surrounded by mesospheres of various sizes and shapes (Figure 1d). When the residue was cooled and reheated to 440°C the same behavior as fraction 2B was observed.

Fraction 7: The time of mesophase formation was 70 min. Mesophase spheres grew from 3 microns in diameter after 74 min to 21 microns after 98 min (Figure 1e) and finally formed large coke areas with flow domain anisotropy after 153 min (Figure 1f). The flow domain was observed only in this fraction. The flow domain texture enclosed smaller patches of isotropic matrix, which, in itself, contained numerous tiny mesospheres (1-2 microns in size). The disc-like inclusions of isotropic pitch

surrounded by anisotropic pitch are similar to the results reported by Hüttinger et al. (8). Complete conversion of this isotropic phase to coke could take place only after a long time at 440°C. The behavior of this fraction in forming flow domain warrants further investigation.

Fraction 9: The first mesophase spheres were noticed after 57 min which is faster than any of the other fractions examined. After 95 min the sample had developed large isochromatic areas with domain anisotropy and rounded margins (Figure 1g). After 104 min some small mesophase spheres could still be seen floating in an isotropic matrix. The resulting coke was angular with serrated edges (Figure 1h). Upon cooling, these isotropic areas became anisotropic with a mosaic texture, which is consistent with observations in previous samples. When the residue was cooled and reheated to 440°C the same behavior as fractions 2B and 4 was observed.

The above data indicate that the incipient mesophase formation is dependent on the chemical composition of the fractions. For instance, the chemical analysis of fraction 9 (Table 1) indicates that this fraction contains 88.0 wt % asphaltenes and has the highest molecular weight, aromatic carbon, and MCR. Compared to the more aliphatic fractions 2B and 4, the molecules in fraction 9 require shorter heating time to become the lamellar molecules which eventually are involved in mesophase formation. Thermal hydrocracking of this fraction in the autoclave also produced the highest coke yield (Table 2). Overall, the results of hot-stage microscopy are consistent with the autoclave experiments for fractions 4, 7, and 9. Fraction 2B produced the least amount of coke in the autoclave runs. However, the time of mesophase formation for this fraction in the hot-stage run was earlier than expected. This was attributed to the fact that this fraction is relatively volatile and, under hot-stage conditions, evaporated significantly leaving the most refractory components behind.

The second important observation that can be related to the chemical composition of the fractions is the relative rate of mesophase formation at 440°C. Mesophase growth rate as a function of time was recorded for fractions 4 and 7. It was observed that in fraction 4 the growth rate was slower in the first 60-75 min at isothermal temperature (440°C) followed by much faster growth. In contrast, fraction 7 showed a continuous linear growth rate. These observations indicate possible differences in the reaction kinetics of the two fractions which, in turn, relates to the differences in their chemical compositions (Table 1). Fraction 9, being the most refractory according to the chemical characteristics, showed the highest rate of growth compared to the other three fractions examined. Accordingly, it was observed that mesophase growth was faster in the first 40-45 min of formation at isothermal temperature. These results are in agreement with data reported by Hüttinger et al. (8).

References

1- Bannayan, M.A., Lemke, H.K. and Stephenson, W.K., "Fouling mechanisms and effect of process conditions on deposit formation in H-Oil equipment", Catalysis in petroleum refining and petrochemical industries 1995. M. Absi-Halabi et al. Editor, 1996 Elsevier Science B.V.

2- Jiang, T., Wang, R.A. and Yang, G., "Simulated Distillation of Residue by Fractional Destraction (I)", Proceedings of the International Symposium on Heavy Oil and residue Upgrading and utilization, Fushun, China, 53 (May 1992).

3- Sears, P.L., "Hot-Stage Microscopy", Division Report ERL 93-03 (CF), CANMET, Energy, Mines and Resources Canada, 1993.

4- Honda, H. "Carbonaceous mesophase: History and prospects", Carbon, 26, (2), 139, (1988).

5- Rahimi, P.M., de Bruijn, T.J.W., Dawson, W.H., Charland, J.P., Heitz, M., and Chornet, S. "Thermal hydrocracking of heavy oils and their components", Division Report ERL 93-67 (CF), CANMET, Energy, Mines and Resources Canada, 1993.

6- McMillen, D.F., Manion, J.A., Tse, D. S., and Malhotra, R. ACS Div Petroleum Chem Preprints 39:2:422, 1994.

7- Franz, J.A., Camaioni, D.M., Alnaijar, M.S., Autrey, T. And Linehan, J.C., "Fundamental hydrogen transfer studies in coal liquefaction: understanding the answers and questions."ACS Div Petroleum Chem Preprints 40:2:203, 1995.

8- Hüttinger, K.J., Bernhauer, M., Christ, K., and Gschwindt, A., "Kinetics of mesophase formation in a stirred tank reactor and properties of the products, IV: Carbon dioxide atmosphere", Carbon, 30, (6), 931 (1992).

Figure 1

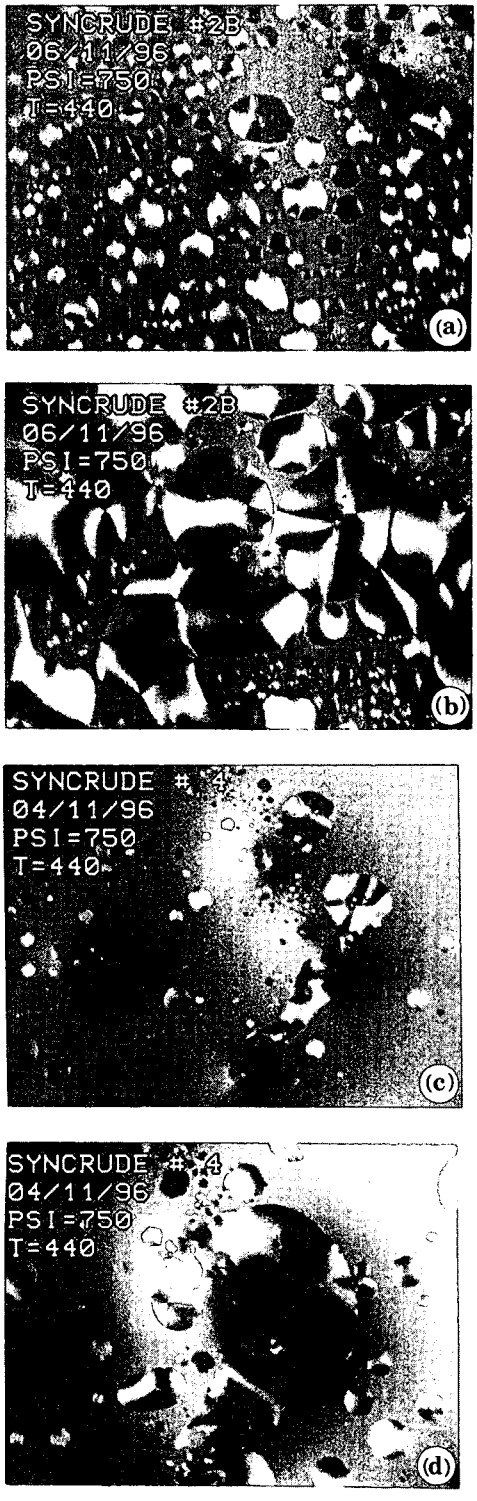
SYNCRUDE #2B
06/11/96
PSI=750
T=440
(a)
SYNCRUDE #2B
06/11/96
PSI=750
T=440
(b)
SYNCRUDE #4
04/11/96
PSI=750
T=440
(c)
SYNCRUDE #4
04/11/96
PSI=750
T=440
(d)

Figure 1

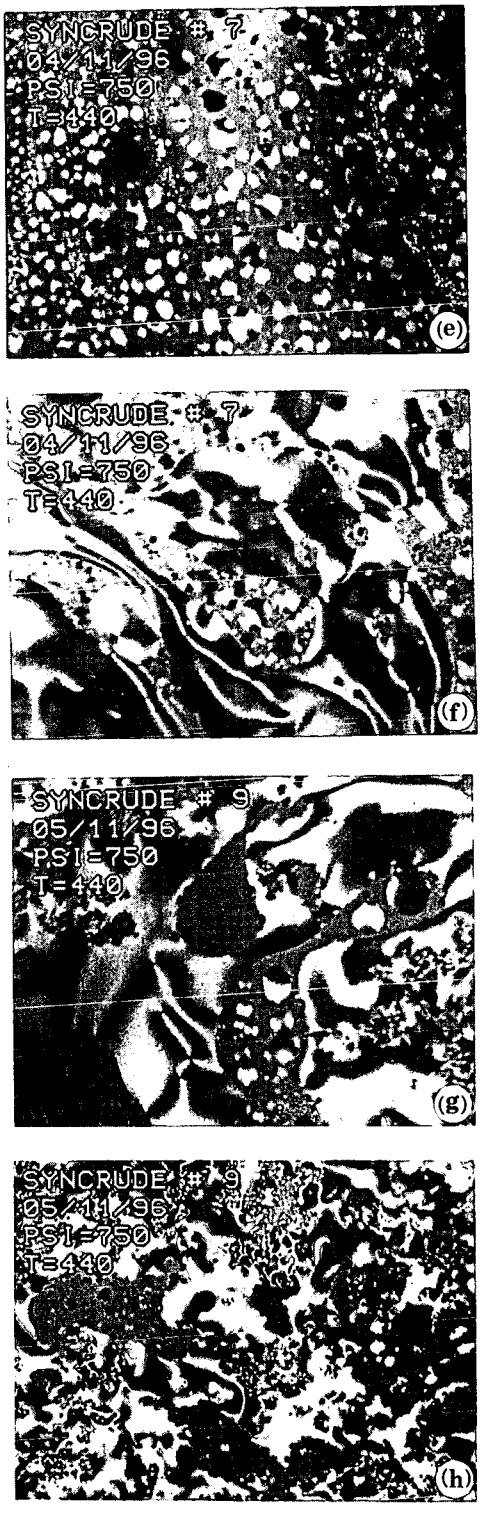
SYNCRUDE # 7
04/11/96
PSI=750
T=440
(e)
SYNCRUDE # 7
04/11/96
PSI=750
T=440
(f)
SYNCRUDE # 9
05/11/96
PSI=750
T=440
(g)
SYNCRUDE # 9
05/11/96
PSI=750
T=440
(h)

Description of photomicrographs

(a) Fraction 2B- Growth of mesophase spheres from isotropic matrix after 84 min.
(b) Fraction 2B - Coalescence of mesophase spheres after 105 min.
(c) Fraction 4- Growth of mesophase spheres from isotropic matrix after 136 min.
(d) Fraction 4- Coalescence of mesophase to 'donut' shape structure after 166 min.
(e) Fraction 7 - Formation of mesophase from isotropic matrix after 98 min.
(f) Fraction 7 - Development of flow domain and domain anisotropy after 153 min.
(g) Fraction 9 - Formation of mesophase and coke with domain anisotropy after 95min.
(h) Fraction 9 - Coke with angular and serrated texture after 104 min.

Table 1 - Characteristics of Athabasca bitumen vacuum bottoms fractions obtained by SPCE technique

Fraction #	1	2B	4	7	9
Pressure, MPa	4-5	5.5-6	7-8	10-11	>12
Wt% of pitch	12.7	7.6	6.5	2.6	40.4
Density, g/ml @20°C	0.9745	1.0061	1.0427	1.0678	N/a
Molecular weight, g/mol	506	711	825	1209	4185
Sulphur, wt %	4	5	6	6.8	7.6
Nitrogen, ppm	3080	4330	6160	7530	10500
Carbon, wt %	84.5	83.5	83	83	78.5
Hydrogen, wt %	11.5	10.95	10.25	9.7	8
C/H (atomic)	0.612	0.635	0.675	0.713	0.818
Aromatic carbon*, %	26	25	36	43	49
Nickel, ppm	12.8	30.1	71.1	138	339
Vanadium, ppm	30.7	69.8	166	355	877
MCR, wt %	5.64	10.83	18.16	26.46	48.94
Saturates, wt %	26.86	9.68	1.36	0.28	0
Aromatics, wt %	57.23	65.7	63.86	45.91	2.19
Resins, wt %	15.91	24.62	34.78	53.81	9.38
Asphaltenes, wt %	0	0	0	0	88.03

*^{13}C NMR
Pitch = +524°C fraction

Table 2- Thermal hydrocracking products (wt %) of selected fractions

Fractions	Gases	Coke	Asphaltenes	Maltenes
1	14.61	0.03	2.67	82.69
2B	14.15	0.09	10.54	75.22
4	12.34	0.12	22.08	65.08
7	13.47	1.40	28.38	56.75
9	12.98	8.68	32.40	45.94

Maltenes = pentane solubles
Asphaltenes = pentane insolubles
Coke = methylene chloride insolubles

Table 3- Hydrocarbon-type distribution (wt % of feed) of selected fractions before and after thermal hydrocracking

	feed				product			
fraction	M1	M2	M3	M4	M1	M2	M3	M4
1	15.08	9.63	66.04	9.25	30.39	10.65	36.05	5.60
2B	5.29	5.29	75.02	14.40	23.64	9.80	36.81	4.97
4	2.34	1.08	73.97	22.61	18.24	8.62	33.83	4.39
7	0.06	0.08	72.66	27.20	18.90	6.61	27.67	3.58
9	Approximately 88 wt% asphaltenes				17.16	4.80	20.61	3.37

M1 = saturates
M2 = mono/diaromatics
M3 = polyaromatics
M4 = polars

ASSESSMENT OF COAL REACTIVITY DURING PREHEATING BY THE RELATIONSHIPS BETWEEN STRUCTURAL AND PLASTIC PROPERTIES. CHEMOMETRIC ANALYSES.

N. Pieri,. L. Quoniam, J. Kister, Laboratoire GOAE, Aix-Marseille III University, Case 561, 13397 Marseille Cedex 20, France,
M. A. Diez, R. Alvarez, J.J. Pis, Instituto Nacional del Carbón (INCAR), CSIC, Apartado 73, 33080 Oviedo, España.

Key-Words: Coking coals, chemical characterization, chemometrics

ABSTRACT

Relatively little attention has been given to determine the coal structural changes induced by industrial preheating process. In this work, a series of ten coking coals was characterized, before and after industrial preheating, by FTIR and Synchronous UV Fluorescence (SF) spectroscopies and by petrography and plastic properties (e.g. mean Reflectance and Gieseler maximum fluidity, Fm). Specific structural indices derived from FTIR and SF data were defined and used in Principal Component Analysis to determine the effects of coal preheating on structural changes and to classify coals on the basis of plastic and petrography characteristics. Predicted models of plastic and petrography properties were established from FTIR and SF indices using Multivariate Linear Regression. For example, Gieseler Fm and volatile matter content, two main parameters for coal blending, can be estimated from the FTIR and SF indices for wet and preheated coals. Thus a better insight into reactivity of coking coals and a valuable estimation of their properties can be accounted.

INTRODUCTION

Recently, reserves of good coking coals have become less available and comparatively more expensive. Resources are extended by using coal blends with different coking properties and/or selective additives. Coal preheating technology has emerged as a technique to overcome some of these problems. This technolology, preheating of coal at about 200°C in an inert atmosphere, in combination with the dry cooling of the resulting coke, is now incorporated into the operation of the Jumbo Coking Reactor (JRC, European Eureka Research Project)[1].

Most studies of preheating have focused on advantages in terms of technological improvements to coke quality and productivity, together with widening the range of coals suitable for coking compared to conventional wet gravity charging[2]. Industrial preheating produces a decrease in the volatile content of the preheated coal compared to the original coal due to a devolatilization of the coal particles, accompanied by coal particle pore formation[3]. However, relatively little attention has been given to determining the structural changes induced in coals by industrial preheating process. These chemical transformations can be accurately evidenced by routine or more sophisticated analytical techniques.

The small molecules, trapped in the pores of coal macromolecular structure, have been defined as the mobile components in coals, and they are extractable using organic solvents[4-5]. Brown and Waters[6] have shown that the mobile component extracted with $CHCl_3$ plays an important role in the development of coking ability. Previous studies have shown that UV Synchronous Fluorescence (SF) spectroscopy is interesting for qualitative and quantitative analysis of aromatic compounds present in the extractable organic matter[7-8]. Furthermore, a new ranking parameter for coals which present a large range of petrographic and chemical characteristics has been established from SF data[9]. Despite of the non applicability of this ranking parameter for coals comprised in a similar range, this technique can be used to determine the structural changes related to aromatics in the extractable phase[10-12]. Moreover, structural information of coal residue can be assessed by Fourier transformed infrared (FTIR) spectroscopy[13-15].

It may be assumed that the nature and the extent of the chemical transformations associated with the preheating process depend on the initial composition of coal i.e. its origin and its rank. In order to evidence the effects of initial composition on the rank and the coking properties of coals, a coal series was preheated and analyzed by FTIR and SF spectroscopies before and after preheating. This paper presents the results of the analysis of the different coals and emphasizes the effect of origin-preheating pair on the plastic behavior of coals, using chemometric analyses.

EXPERIMENTAL

A series of international coking coals (H) was selected for the industrial coal preheating process (Table 1). Coal preheating was carried out in the 2t/h INCAR pilot plant -Precarbon process- at 210 ± 10 °C under an inert atmosphere[16]. A coal sampling was performed : the wet coal before

being charged into the preheating pilot plant (H) and the preheated coal in the closed conveyor before entering to the coke-oven (P).

The particle fractions of wet and preheated coals (< 150μm) were ultrasonically extracted with $CHCl_3$ (100 mg coal / 30 ml solvent) for 45 min. Extract yields were about 2 wt%. After removing solvent, extracts were dissolved in THF (10 mg/l) for SF measurements. SF spectra were obtained at a fixed excitation and emission wavelength interval of 23 nm, excitation and emission beams being kept at a width of 5 nm and a scanning rate of 200 nm/s, in the 200-600 nm range. Selected indices derived from SF data using the integrated area (A) of different spectral bands are described in Table 2.

The extraction residues were analyzed by FTIR spectroscopy using KBr standard pellets (1:150 coal residue to KBr ratio). Each spectrum resulted from the accumulation of 128 scans, recorded with a spectral resolution of 4 cm^{-1} in the 4000-400 cm^{-1} spectral domain, was normalized to 1 mg of sample. Mineral matter interferences were eliminated by substracting the corresponding spectrum of the low-temperature ash (LTA). The detailed band assigments of coal spectra and the integration method of these FTIR bands were widely described elsewhere[14,17]. Selected indices derived from FTIR data using the integrated area (A) or the maximum intensity (H) of different spectral bands are described in Table 2.

Statistical analyses.

The factor analysis used is based on the Principal Component Analysis or PCA (STATISTICA softwear, Statsoft Inc.). The principle of this multivariate statistical method[18] is to create new independant variables (*i. e.*, factors) that are the linear combination of original variables (i. e., FTIR and SF indices) which are correlated to each other. The primary objective of the statistical analysis is to reduce the dimensionality of the data to a few important components or factors that best explain the variation in the data. From the data matrix, its standardized version Z and correlation matrix R were calculated. The correlation matrix R was used as a starting matrix in PCA. Principal components (PC) were determined by considering eigenvalues and associated eigenvectors. For plotting purpose only two or three PC scores were used. These must explain over 80% of the total variance. In R-mode factor analysis, the initial variables are scalled, thus the links between variables can be easily visualized. In Q-mode, the observations are scalled on the same set of factor axes. Coking coals with similar FTIR and SF index values are gathered in factor space and specific variables, which are important in distinguishing the different groups of coals, are determined.

RESULTS AND DISCUSSIONS

The chemical characteristics of coals, before and after preheating, have been studied using FTIR and SF spectroscopies in order to determine (i) the structural modification occuring during preheating, (ii) the relationships between Reflectance and Volatile Matter (VM) amount, standing for thermal maturity reference parameters, and structural parameters, (iii) the chemical structures acting on plastic properties (Gieseler maximum fluidity, GI ; Arnu dilatation)[10, 19].

As a matter of fact, the fluid properties (i.e. plastic properties) is an important step of coking because of the quality dependence of the semi-coke. However, fluidity leads to gas production increasing pressure inside the coke oven[1]. The optimization of the fluidity and the gas pressure becomes necessary. Moreover, preheating produces a decrease in the volatile matter content of the preheated coal compared to the original coal[11]. All those parameters could be maturity-/ origin-dependent. To get coking performance related to structural parameters, Gieseler Index (maximum fluidity), Arnu (dilatation), Reflectance and Volatile Matter (maturity) were included in the statistical analysis.

The first step of this work was to characterize wet coking coals. Along this line, a first Principal Component Analysis was performed to relate chemical features to plastic properties as well as to visualize the main characteristics of the total sampling. The first PCA explains 87% of the total variance with 3 factors (Table 3). The factor 1 is related to the coking coal maturity with, in its positive way, a high reflectance value (i.e. REFLECT) and a low volatile matter amount (i.e. VM) (Figure 1a). This corresponds to a high aromatic structure amount in the residue (i.e. Aromatic H Index: H ARO and Aromatic/Aliphatic ratio : AH) and a high amount of highly polycondensed aromatics in the extract (predominance of 4-5 polycondensed aromatic rings compared to 2-3 rings, i.e. A3/A1). The factor 2 is characteristic, in its positive way, of an important dilatation of coal during coke making corresponding to a low branched aliphatic content in the residue (BA index). This PCA allows to classify three groups of coking coals. We can notice that the intermediate group shows the lowest expansion (Figure 1b). The third factor, representative of aliphatic structures within coking coal residues, underlines that the volatile matter amount (VM on factor 1) is independent of these structures (Figure 2).

A second PCA has been performed from spectroscopic data and plastic properties measured before and after preheating in order to know the chemical structures involved in coking property changes during preheating. This second PCA which explains 83% of the total variance with 3 factors (Table 4), underlines the main chemical changes during this step. The aromaticity of all the coals increases with a loss of aliphatic structures, in the residues (increase in Aromatic Index: AI and decrease in Factor of Aliphaticity: FA and in νCH_2 asym/νCH_2 sym: W) in spite of their maturity rank except for one coal which underwent a low evolution (i.e. T3595H). The fluidity and the volatile matter of coals, related to factor 1, slightly decrease during preheating except for T3614H (Figure 3). In its negative sense, the third factor concurrently underlines the loss of alkane side-chains on aromatic structures (i.e. SS1) in the residues and an increase in aromatic hydrogen content (i.e. H ARO) (Figure 4). Some coals act during preheating as described above (e.g. T3637H, T3614H, T3595H, T3591H). No changes are noted for aromatic structure substitutions of the other coals. This PCA underlines that the preheating mainly consists in an aromatization and thermodesorption, the chemical structures within the more mature coals changing less than the less mature ones. Consequently, coals have a slight difference in their properties after preheating.

Then, from those spectral data, multivariate linear regressions were performed to determine the relationships between structural characteristics, petrography parameters and plastic properties.

The first model was established to estimate the Reflectance from only three independent and standardized spectroscopic variables calculated from wet coals. The following equation was obtained :

$$Y_{REFLECT} = -0.59\ X_{H/C} + 0.37\ X_{ACI} + 0.68\ X_{A3/A1} \qquad (1)$$

The first model explains 96% of the total adjusted variance (adjusted $r^2 = 0.96$), the standard error of the predicted value being 0.3. This model underlines an increase in maturity with the decrease in H/C ratio. The higher the maturity of coking coals, the higher their aromaticity in their residue and the higher their highly condensed aromatic content in their extract (Figure 5a).

Gas emission during coke making can also be evaluated by the volatile matter content in wet and preheated coals. Consequently, a second predictive model of the volatile matter amount was performed from structural indices measured before and after preheating (equation 2):

$$Y_{V.M.} = -0.63\ X_{BA} - 0.34\ X_{H\ ARO} - 0.22\ X_{ACI} - 0.48\ X_{A3/A1} \qquad (2)$$

This model explains 85% of the total variance and the standard error of the predicted value is 2 (Figure 5b). Few changes in volatile matter amount is noted during preheating. This parameter inversely depends on the maturity (aromaticity of coking coals). The less aromatic the structures and/or the more substituted the aromatic structures within coal residues, the less polycondensed the aromatic structures within extracts, the more the volatile matter amount within coals. The V.M. also depends on the aliphatic nature in the residue because the volatile matter content inversely relates to the branched aliphatic index (i.e. BA).

Those two predictive models underline the relationships within coals between chemical structures, their reflectance and their volatile matter amount.

At last, one of the most important factors occuring on coke making has been predicted : the Gieseler Index, representing the maximum fluidity for coking coals. The optimal values of this index are between 500 and 1500 ddpm[1]. To simplify, GI values have been expressed in log ddpm. Two models were established, one for wet coals and one for preheated coals (equations 3 and 4) because the predictive model of GI, after preheating, requires one more parameter which is the H/C ratio.

For wet coals : $$Y_{GI} = -0.84\ X_{BA} + 0.61\ X_{SS1} - 0.61\ X_{AH} - 0.27\ X_{A3/A1} \qquad (3)$$

For preheated coals : $$Y_{GI} = 0.25\ X_{BA} - 0.40\ X_{SS1} - 0.74\ X_{AH} - 0.34\ X_{A2/A1} + 0.63\ X_{H/C} \qquad (4)$$

Those models respectively explain 95% and 97% of the total variance. In both cases, standard error of estimate is 0.2. Those models depend, in the coal residue, on the branched aliphatic ratio, the percentage of the highly substituted aromatic structures and the aromaticity (Figure 6). GI is inversely linked to the polycondensation of aromatic structures, in the coal extracts. However, even if trends are the same in coal extracts towards GI, before or after preheating, that is not the case in coal residues. Before preheating, the higher the maximum fluidity for coals, the more substituted the aromatic structures and the less branched the aliphatic structures. After preheating, one can observe the opposite relationships between the maximum fluidity, the aromatic substitution level and the branched aliphatic ratio. Furthermore, GI parameter decreases during preheating. Those results would underline the irreversible changes which occur in the organic matrix and pore structure of coal during preheating process and would explain the

different behaviors of the preheated coals during carbonization[11, 20]. As a matter of fact, preheated coals cannot be compared with wet coals because of the differences noted in the relationships between chemical structures and plastic properties.

CONCLUSION

FTIR data on coal residues and SF data on coal extracts give complementary information. Coking coal chemical composition can be quantified from few spectroscopic indices. A ranking of coking coals from those data would be possible.

The main changes occuring during preheating are an aromatization with loss of alkane side-chains, in the solid residue for some coals, and a thermodesorption of the volatile compounds.

Principal Component Analysis showed the correlation between some structural indices and coal rank parameters, and the combined effects of some composition parameters on the plastic properties.

Some physical and plastic properties were predicted from few FTIR and SF indices of coking coals: Reflectance, the Volatile Matter amount and the Gieseler maximum fluidity.

Such investigations provide global as well as structural parameters that facilitate the understanding of the mechanisms involved during the different natural and industrial transformations of coals.

REFERENCES

(1) Diez, M. A.; Alvarez, R.; Sirgado, M.; Marsh, H.; *ISIJ International* **1991**, *31*(5), 449-457.

(2) Alvarez, R.; Alvarez, E.; Canga, C.S.; Diez, M. A.; Gonzales, A. I.; Marsh, H. *Fuel Proc. Technol.* **1993**, *33*, 117-135.

(3) Menendez, J. A.; Alvarez, R.; Alvarez, E.; Canga, C.S.; Diez, M. A.; Gonzales, A. I. *Fuel* **1992**, *71*, 1265-1270.

(4) Marzec, A.; Jurkiewicz, A.; Pislewski, N. *Fuel* **1983**, *62*, 996-998.

(5) Given, P. H.; Marzec, A.; Barton, W. A.; Lynch L. T.; Gerstein, B. C. *Fuel* **1986**, *65*, 155-163.

(6) Brown, H. R.; Waters, P.L. *Fuel* **1966**, *45*, 17-39, 41-59.

(7) Kister, J.; Guiliano, M.; Mille, G.; Dou, H. *Fuel* **1988**, *67*, 1076-7081.

(8) Mille, G.; Guiliano, M.; Kister, J. *Org. Geochem.* **1988**, *13*(4-6), 947-952.

(9) Kister, J.; Doumenq, P.; Mille, G.; Landais, P.; Pis, J. J. In *Synthesis, properties, analytical measurements, occurrence and biological effects*, Polycyclic Aroamtic Compounds; Garrigues, P and Lamotte, M., Eds.; Gordon and Breach Science Publishers: Switzerland, 1993, pp 639-646.

(10) Kister, J.; Pieri, N.; Diez, M. A.; Alvarez, R.; Pis, J. J. In *Coal Science*; Coal Science and Technology 24; Pajares, J. A. and Tascon, J. M. D., Ed.; Elsevier: Amsterdam, **1995**, pp 381-384.

(11) Kister, J.; Pieri, N.; Alvarez, R.; Diez, M. A.; Pis, J. J. *Energ. Fuel* **1996**, *10*(4), 948-957.

(12) Benkhedda, Z.; Landais, P.; Kister, J.; Dereppe, J. M.; Monthioux, M. *Energ. Fuel* **1992**, *6*(2), 166-172.

(13) O. Ruau, Thèse en Sciences de l'Institut National Polytechnique de Lorraine, **1996**, pp 300.

(14) Kister, J.; Ruau, O.; Landais, P.; Alvarez, R., Diez, M. A.; Pis, J. J. *Fuel Proc. Tech.* **1993**, *36*, 313-318.

(15) Pieri, N.; Planche J. P.; Martin, D.; Germanaud, L.; Kister, J. *Proc., Eurasphalt & Eurobitume Congress* **1996**, *5.120*, 1-13.

(16) Alvarez, R.; Diez, M. A.; Menendez, J. A.; Pis, J. J.; Suarez, C.; Sirgado, M. *Cokemaking Int.* **1993**, *5*(2), 36-40.

(17) Guiliano, M.; Mille, G.; Doumenq, P.; Kister, J.; Muller, J. F. In *Advanced Methodologies in Coal Characterization*, Coal Science and Technology 19; Charcosset, H., Ed.; Elsevier: Amsterdam, **1990**, pp 399-417

(18) Escofier, B.; Pages, J. *Analyses factorielles simples et multiples- Objectifs, méthodes et interprétation*. Dunod, Ed.; Bordas: Paris, **1988**

(19) Lloyd, W. G.; Reasoner, J. W.; Hower, J. C.; Yates, L. P. *Fuel* **1990**, *69*, 1257-1270.

(20) Landais, P.; Langlois, E.; Pis, J. J.; Diez, M. A.; Alvarez, R.; Kister, J. In *Coal Science*; Coal Science and Technology 24; Pajares, J. A. and Tascon, J. M. D., Eds.; Elsevier: Amsterdam, **1995**, pp 453-456.

Table 1 : Petrography and plastic porperties of a series of ten coking coals, before and after preheating. These data have been given by INCAR-CSIC, Oviedo, Spain.

Origin	Coking coals: Wet (H) Preheated (P)	H atom/ C atom : H/C	Reflectance: REFLECT	Volatile Matter VM	Dilatation: ARNU	Maximum fluidity, Gieseler Index : GI
Australia	T3631H	0.720	1.41	19.5	70	1.68
Germany	T3637H	0.695	1.18	22.4	52	1.64
Australia	T3622H	0.751	1.09	23.2	75	3.17
USA	T3639H	0.683	1.15	24.2	123	2.50
Spain	T3595H	0.726	1.25	25.6	171	3.99
Poland	T3625H	0.728	1.00	28.5	147	2.59
USA	T3658H	0.760	1.00	30.8	279	4.25
Spain	T3590H	0.720	0.96	31.4	218	4.00
USA	T3614H	0.750	0.90	33.8	143	4.01
Spain	T3591H	0.760	0.84	35.9	135	4.03
Australia	T3631P	0.669		20.4	33	0.78
Germany	T3637P	0.694		22.3	42	0.90
Australia	T3622P	0.732		23.4	66	2.57
USA	T3639P	0.713		24.1	109	2.02
Spain	T3595P	0.756		24.0	134	3.16
Poland	T3625P	0.753		28.1	88	2.60
USA	T3658P	0.763		30.6	273	3.90
Spain	T3590P	0.692		32.1	177	3.37
USA	T3614P	0.746		33.6	137	3.67
Spain	T3591P	0.724		35.8	101	3.43

Table 2 : FTIR and SF indices calculated from spectral data measured for each coking coal. A: Area, H : Height. For FTIR data, the subcribed number of Area (e.g. A_{3050}) represents the wavenumber (cm^{-1}) at the top of the spectral band, integrated from valley to valley. The subscript number of Height (e.g. H_{1600}) represents the wavenumber (cm^{-1}) at the top of the band at which the height is measured. For SF data, the two subscript numbers represent the area band limits (nm), used to measure the absolute value of the fluorescence emission. These indices and their significance have been well described by Kister *et al.*[14]

	From FTIR spectra							From SF spectra	
Indices calculated from :	H ARO A_{3050}/A_{2920}	W H_{2920}/H_{2855}	BA H_{1380}/H_{1440}	ACI $H_{1600}/(H_{1440}+H_{1440})$	FA $(H_{2920}+H_{2850})/(H_{1600}+H_{2920}+H_{2850})$	SSI $A_{864}/A_{864-743}$	AH $A_{864-743}/A_{2920}$	A2/A1 $A_{460-370}/A_{370-300}$	A3/A1 $A_{580-460}/A_{370-300}$
T3631H	0.142	1.675	0.807	0.586	0.472	0.186	0.941	3.46	0.936
T3637H	0.108	1.695	0.850	0.511	0.504	0.201	0.811	2.85	0.667
T3622H	0.113	1.646	0.826	0.577	0.481	0.204	0.809	2.44	0.600
T3639H	0.176	1.733	0.799	0.533	0.504	0.185	0.919	2.62	0.568
T3595H	0.163	1.684	0.771	0.573	0.475	0.214	0.917	2.98	0.832
T3625H	0.113	1.692	0.807	0.519	0.491	0.182	0.863	2.55	0.604
T3658H	0.102	1.800	0.791	0.596	0.491	0.170	0.697	2.49	0.528
T3590H	0.115	1.708	0.767	0.523	0.517	0.170	0.734	2.73	0.767
T3614H	0.107	1.681	0.796	0.568	0.474	0.194	0.772	2.19	0.444
T3591H	0.091	1.667	0.779	0.566	0.457	0.154	0.713	1.82	0.308
T3631P	0.149	1.565	0.796	0.623	0.444	0.226	1.033	3.61	0.819
T3637P	0.177	1.671	0.852	0.572	0.430	0.178	1.174	2.41	0.394
T3622P	0.114	1.613	0.839	0.582	0.429	0.180	1.051	2.29	0.408
T3639P	0.190	1.657	0.806	0.550	0.474	0.173	1.044	2.92	0.571
T3595P	0.164	1.597	0.788	0.586	0.480	0.207	0.930	3.13	0.727
T3625P	0.122	1.619	0.816	0.501	0.447	0.208	0.958	2.48	0.482
T3658P	0.118	1.706	0.801	0.585	0.462	0.201	0.778	2.32	0.374
T3590P	0.126	1.626	0.804	0.543	0.465	0.166	0.809	3.20	0.706
T3614P	0.097	1.627	0.771	0.577	0.457	0.171	0.848	2.70	0.472
T3591P	0.101	1.623	0.773	0.576	0.425	0.136	0.788	1.87	0.318

Table 3 : Results of the first PCA performed from wet coal data. 9 variables (V.M., ARNU, REFLECT, H ARO, AH, BA, W, FA and A3/A1) were selected for 10 coking coals. 3 factors were extracted and explain 87 % of the total variance.

Factor	Eigenvalues	% total variance	Cumul. Eigenval.	Cumul. % total variance
1	4.4	49	4.4	49
2	2.1	23	6.5	72
3	1.3	15	7.8	87

Table 4 : Results of the second PCA performed from wet and preheated coal data. 9 variables (V.M., GI, H ARO, ACI, AH, BA, W, FA and SSI) were selected for 20 coking coals. 3 factors were extracted and explain 83 % of the total variance.

Factor	Eigenvalues	% total variance	Cumul. Eigenval.	Cumul. % total variance
1	4.0	44	4.0	44
2	2.3	26	6.3	70
3	1.2	14	7.5	83

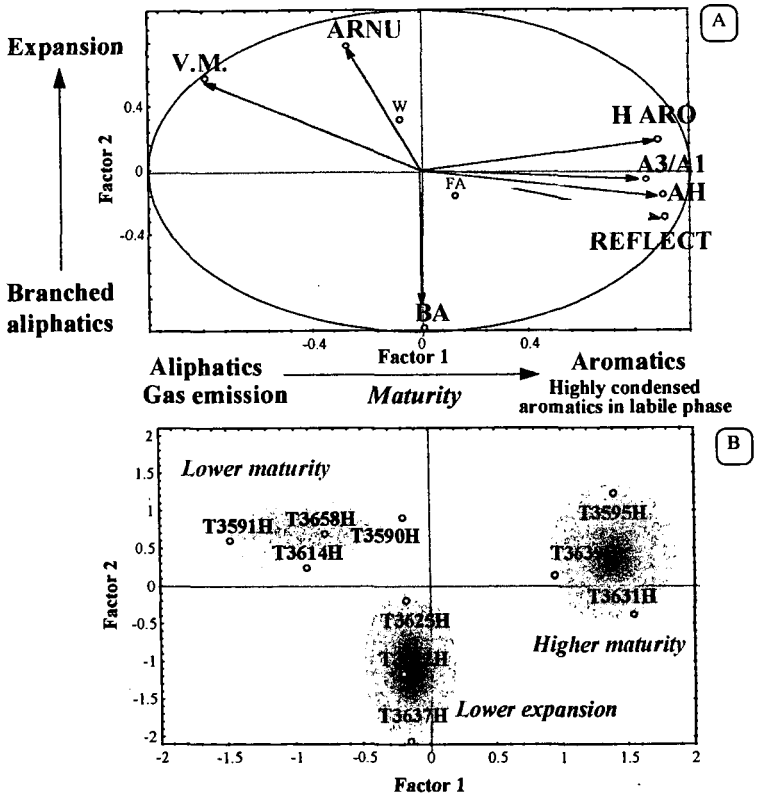

Figure 1 : First PCA performed from 9 variables (spectroscopic indices, petrography and plastic properties) and 10 wet coking coals. This PCA explains 87% of the total variance with 3 factors. This figure shows the 2 first Principal Components (PC) and visualizes the main chemical and physical characteristics of wet coals. A/ R-mode factor analysis : initial variables. B/ Q-mode factor analysis : coking coals.

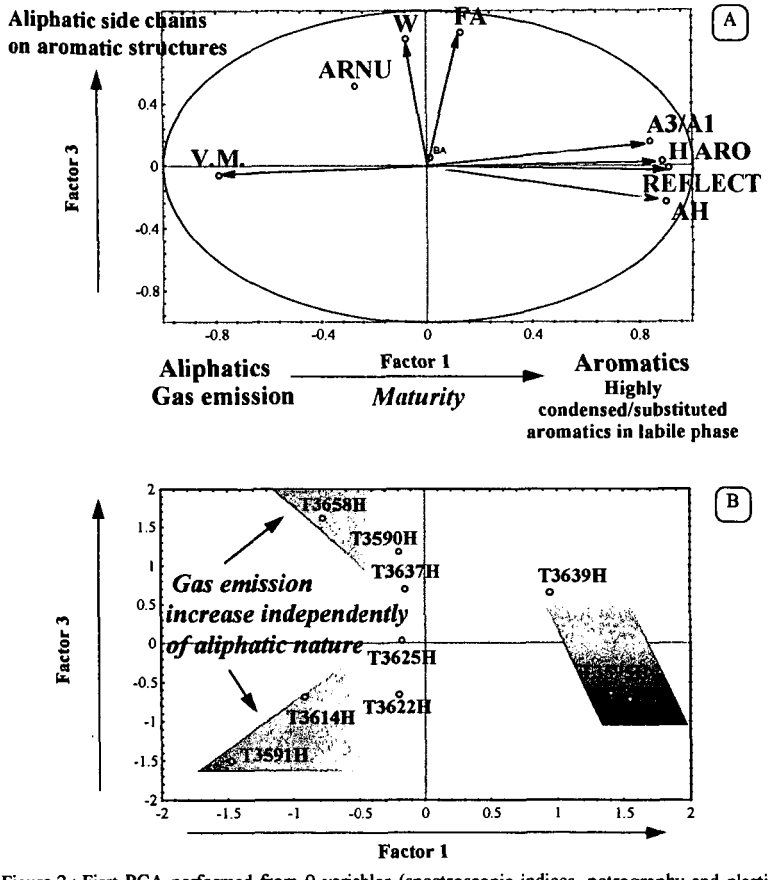

Figure 2 : First PCA performed from 9 variables (spectroscopic indices, petrography and plastic properties) and 10 wet coking coals. This PCA explains 87% of the total variance with 3 factors. This figure shows the 2nd and the 3rd Principal Components (PC). A/ R-mode factor analysis : initial variables. B/ Q-mode factor analysis : coking coals.

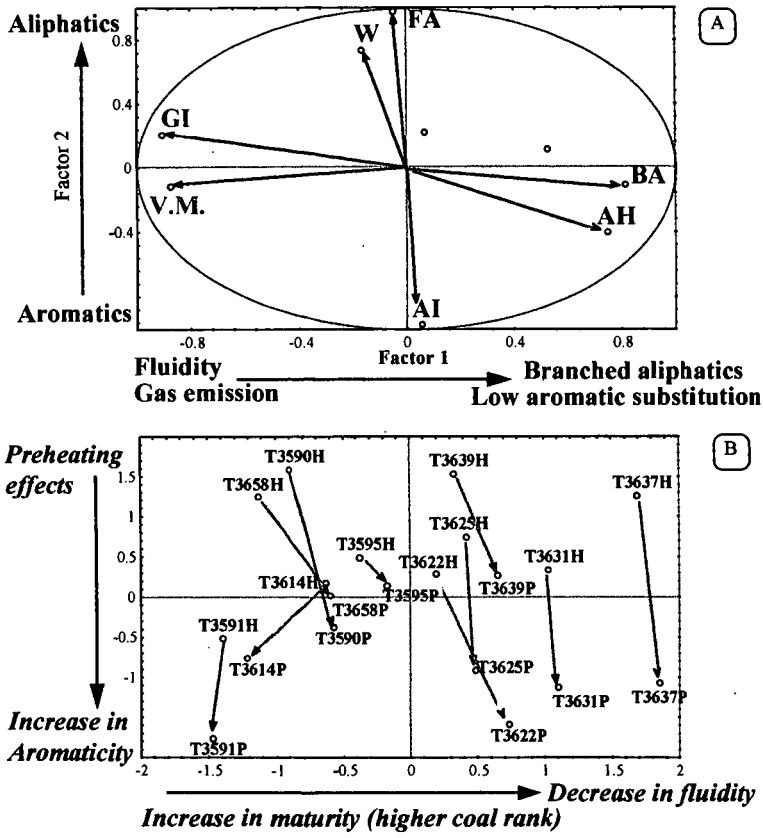

Figure 3 : Comparison between plastic property and structural characteristics changes during preheating. Second PCA performed from 9 variables (spectroscopic indices, petrography and plastic properties) and 20 (wet and preheated) coking coals. This PCA explains 83% of the total variance with 3 factors. This figure shows the 1st and the 2nd Principal Components (PC). A/ R-mode factor analysis : initial variables. B/ Q-mode factor analysis : coking coals.

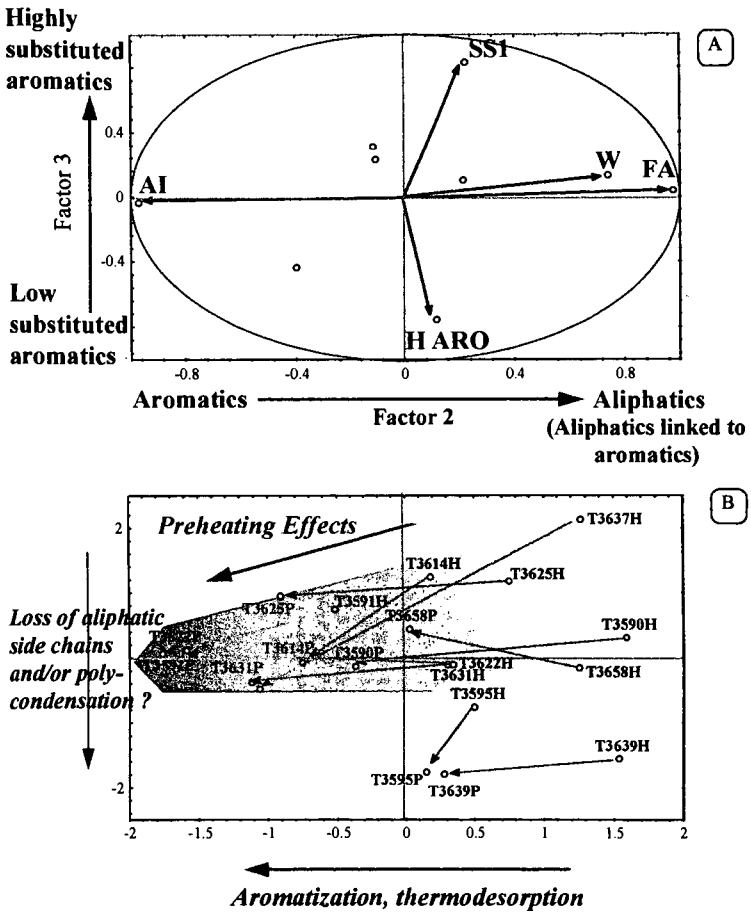

Figure 4 : Aromatic changes during preheating. Second PCA performed from 9 variables (spectroscopic indices, petrography and plastic properties) and 20 (wet and preheated) coking coals. This PCA explains 83% of the total variance with 3 factors. This figure shows the 2nd and the 3rd Principal Components (PC). A/ R-mode factor analysis : initial variables. B/ Q-mode factor analysis : coking coals.

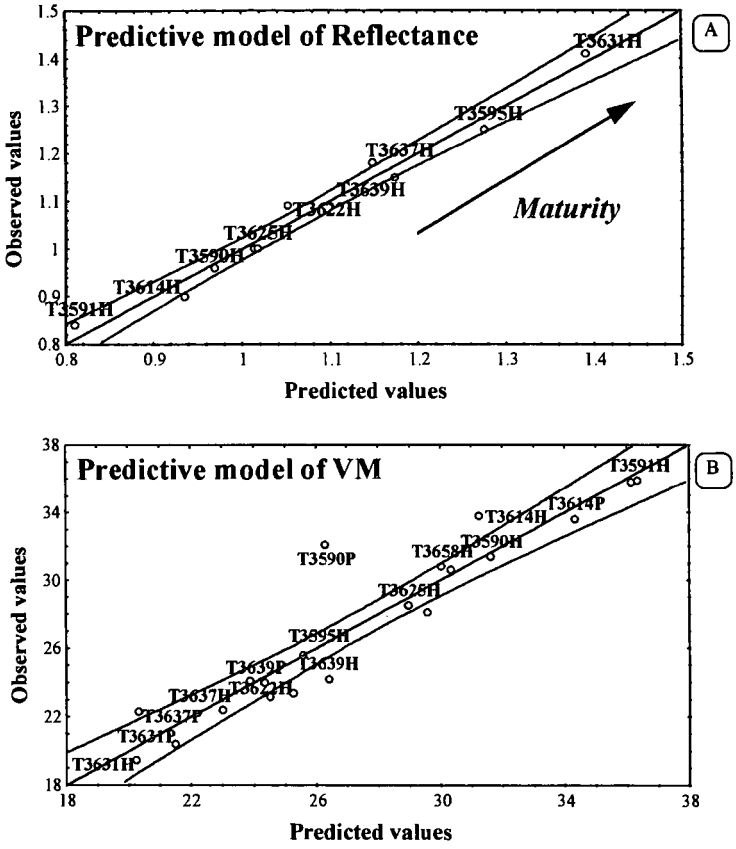

Figure 5 : Prediction of the petrography properties of the coking coals by Multivariate Linear Regression (MLR) A/ Predictive model of Reflectance from wet coal data (3 indices, 10 coals, Adjusted $R^2 = 0.96$, $F(3,6)=79$, $p<0.00003$, Std. Error of estimate: 0.03). B/ Predictive model of Volatile Matter Amount (VM) from wet and preheated coal data (4 indices, 20 coals, Adjusted $R^2 = 0.85$, $F(4,15)=28$, $p<0.00000$, Std. Error of estimate: 2).

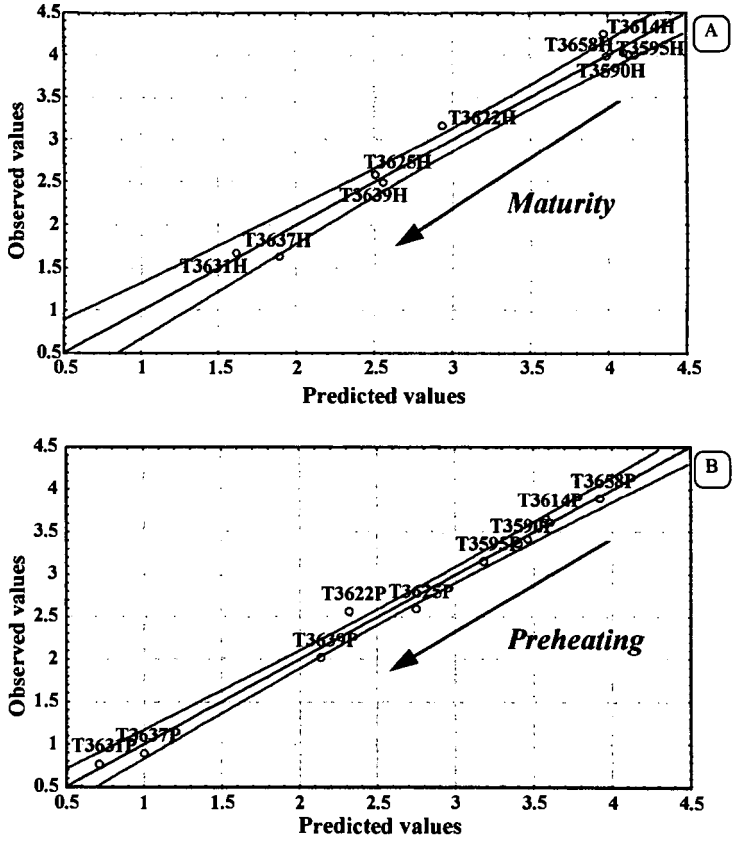

Figure 6 : Prediction of the plastic properties of the coking coals by Multivariate Linear Regression (MLR) A/ Predictive model of Gieseler Index (GI from wet coal data (4 indices, 10 coals, Adjusted R^2 = 0.95, F(5,4)=44, p<0.0004, Std. Error of estimate: 0.2). B/ Predictive model of GI from preheated coal data (5 indices, 10 coals, Adjusted R^2 = 0.97, F(5,4)=70, p<0.0006, Std. Error of estimate: 0.2).

EVALUATION OF ORGANIC MATTER REACTIVITY DURING PYROLYSIS BY *MICRO-FTIR TECHNIQUES.*

O. Ruau, P. Landais, R. Michels and E. Langlois

CNRS-CREGU, BP 23, 54501 Vandoeuvre lès Nancy Cedex, France.

Keywords: FTIR microspectroscopy, Organic matter, Polar compounds.

INTRODUCTION

The understanding of the processes occuring, as well as reacting mechanisms taking place during organic matter maturation and oil generation is of major importance in order to develop models to be used in petrolem exploration. The artificial maturation of organic matter performed in laboratory allows to reduce the duration of experiments and to control the reacting medium components (water, polar compounds, gas, generated hydrocarbons).

Infrared spectroscopy is a well adapted technique for the characterization of organic matter as far as it provides information on the chemical composition (aliphatic, aromatic and oxygenated bearing functions) and functionnal distribution (hydroxyls, carbonyls, carboxyls, ethers, etc.). Coupling an infrared spectrometer with an adapted microscope and using a diamond anvil compression cell allows to facilitate the sample preparation, to improve the quality of the recorded spectra and to use quantitatively the data obtained from the solid residues. In this study, the reactivity of solid residues and polar compounds related to several artificial maturation series has been investigated thanks to these new transmission micro-FTIR techniques.

ANALYTICAL

Samples: The samples used in this study are polars and solid residues from (i) confined pyrolysis series of an immature vitrinite rich coal from the Mahakam delta[1], (ii) confined and hydrous pyrolysis of Woodford shale[2], (iii) confined pyrolysis of Kimmeridge Clay[3].

Transmission Infrared microspectroscopy: The sample preparation protocols of the solid residues and the polar compounds have been previously described in Ruau et al.[4] (1996). The micro FTIR analysis were performed on a Nicolet System 800 coupled with a Nic-Plan microscope which was fitted with a 250 µm narrow band MCT detector cooled to 77K. The standard analytical conditions were X 15 infrared objective, 40-60 µm diameter infrared spot, 32 to 128 scans, spectral resolution of 4cm^{-1}, gain = 4.

Flash pyrolysis - Gas chromatography - Mass spectrometry (Py-GC-MS): Solid residues and polar compounds have been investigated by Py-GC-MS using a CDS 2000 pyrolyser coupled with a HP 5890AII chromatogram and a HP 5972A mass spectrometer. Flash pyrolysis was performed at 620°C for 20 s.

RESULTS AND DISCUSSION

Reactivity of the chloroform extracted solid residue. A detailed inspection of the transmission micro-infrared spectra of the solid residues recorded thanks to the diamond anvil compression cell reveals the presence of interference fringes between 1900 and 2800 cm^{-1} that were used for the sample thickness determination[4]. Thus the band integrations were normalized to a common sample thickness (e.g. 30 µm). This operation allowed the intensity variations of a given band to be directly investigated. The variations of the ν aromatic C-H (3000-3100 cm^{-1}), ν aliphatic C-H (2800-3000 cm^{-1}) and ν C=O (1650-1800 cm^{-1}) normalized to a sample thickness of 30 µm are reported in figure 1.

This figure shows that the removal of the C=O functions and aliphatic moieties follows a rather linear trend while the increase of aromatic CH is rather exponential. Special care was also adressed to the distribution of C=O bearing functions. The results show that the 1650 cm^{-}

' band assigned to conjugated C=O first increases during maturation untill 320°C and then decreases. This observation strongly suggests a functional rearrangement within the C=O groups during the maturation. This type of approach facilitates the survey of the chemical modifications the solid residues may undergo during maturation.

Transmission micro-FTIR was applied for the characterization of the fractions issued from other maturation series and particularly to successive pyrolysis-extraction experiments[5]. The results showed that the behavior of the kerogen and the polar fractions (asphaltenes and resins) strongly depends on the presence (or absence) in the reacting medium of polars, hydrocarbons, and generated water. Furthermore, a specific reactivity of polars was clearly evidenced.

Reactivity of the polar compounds. Spectra of the polar compounds can be recorded on the same micro-FTIR system than that used for the solid residues. Then, a comparison of the chemical composition of these fractions as well as their specific evolution along the maturation profile can be made. Spectra reported on figure 2 evidence major differences between the solid and the polar compounds. Generally, the solid residue spectra show more intense bands related to aromatic groups (C=C and aromatic CH), while the spectra of the polar compounds exhibit marked aliphatic CH as well as OH and C=O bands.

Data extracted from the integration of polar compounds and solid residue micro-infrared spectra provide the chemical evolution of each fraction during the artificial maturation. If the solid residue react as previously described with a removal of aliphatic moieties and oxygenated bearing functions, the polar compounds behaviour is somewhat different. The evolution of the aliphaticity of the resins suggests that resins may be considered as the kerogen relay for the hydrocarbon generation. On the other hand, it is shown that asphaltenes undergo an oxidation contemporaneous to the removal of the generated water and to the production of hydrocarbons. These results suggest that asphaltenes are implied in complex and specific reactions during maturation that should be taken into account for the modelisation of the hydrocarbon generation process.

Combined use of micro FTIR and Py-GC-MS techniques. Micro-FTIR results were also compared to PyGCMS data obtained on the solid residues and the polar fractions. This approach provides a molecular insight that is particularly suitable for the elucidation of problems related to organic matter reactivity. Parameters obtained by these two different approaches allow the same process to be evidenced by two ways. The aromatization of the solid residue during the artificial maturation can be depicted by the increase of the ratio aromatic compounds/sum of the compounds (Py-GC-MS) as well as the ratio aromatic CH/ Sum of the integrated bands (μ-IRTF) (Figure 3). On the other hand, these two techniques can be used in a complementary way to explain for example the evolution the methyl/methylenes distribution of the aliphatic fraction of the asphaltenes.

CONCLUSIONS

Transmission infrared microspectroscopy appears as an improved routine technique to rapidly record high quality spectra of organic matter. The sample preparation as well as the amounts of studied material can be significantly reduced. The quality of the micro-infrared spectra facilitates the qualitative overview of the gross chemical variations occuring during laboratory simulated maturation of organic matter. Thanks to the diamond anvil compression cell, the micro-infrared spectra of solid residues can be used in a quantitative way in order to follow the chemical evolution of organic matter during maturation. The versatility of the micro-FTIR technique allows the characterization of the polar compounds of the same maturation serie. Then the specific reactivity of each fraction can be underlined. Coupling this technique with the PyGCMS provides converging and/or complementary informations on the chemical composition of the studied samples as well as their reactivity.

REFERENCES

1 Landais P. and Gérard L. *Int. J. Coal Geol.* **1996**, 30, 4, 285.

2 Michels R., Landais P., Torkelson B.E. and Philp R.P. *Geochim. Cosmochim. Acta.* **1995**, *59*, 1589-1604.

3 Michels R., Langlois E., Ruau O., Mansuy L., Elie M. and Landais P. *Energy and Fuels.* **1996**, *10*, 39.

4 Ruau O., Landais P. and Gardette J.L. *Fuel*, **1996** Accepeted.

5 Mansuy L., Landais P. and Ruau O. *Energy and Fuels.* **1995**, *9*, 691.

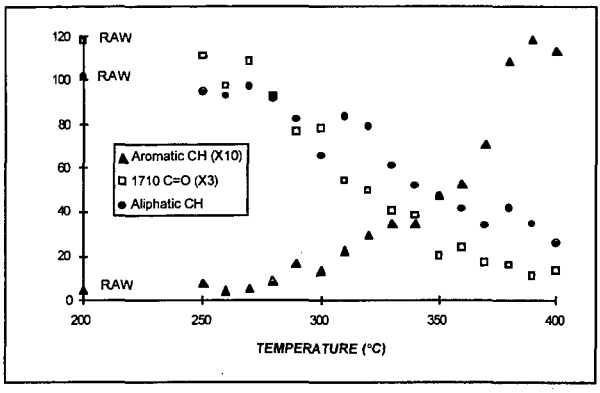

Figure 1 : Evolution of aliphatic C-H (2800-3000 cm^{-1}) integrated area, aromatic C-H (3000-3100 cm^{-1}) integrated area (X 10) and C=O (1710 cm^{-1}) integrated area (X 3), both normalized to a sample thickness of 30 µm, with increasing pyrolysis temperature (Confined pyrolysis of a Mahakam coal).

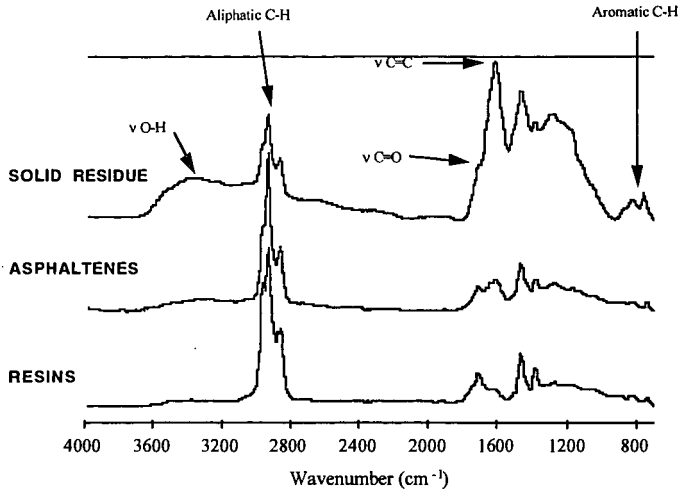

Figure 2 : Comparison between asphaltenes, resins and solid residue obtained by the confined pyrolysis of a Mahakam coal (250°C, 24 h).

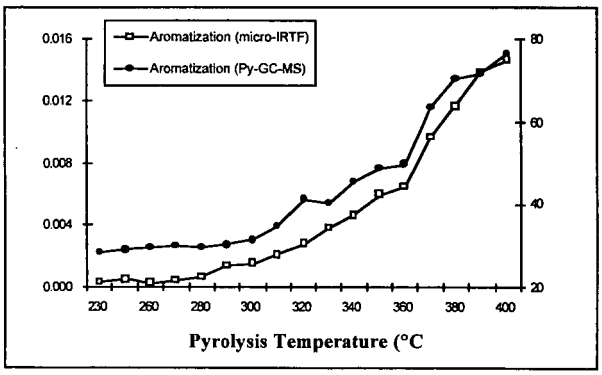

Figure 3 : Aromatization of the solid residue along the artificial maturation evidenced by micro-IRTF and Py-GC-MS data (Mahakam coal).